Sulfated vanadia-based and titania-based catalysts for selective oxidation of methanol to dimethoxymethane (DMM)

Hongying Zhao

N° d'ordre : 92-2010 Année 2010

THESE DE L'UNIVERSITE DE LYON

Délivrée par

L'UNIVERSITE CLAUDE BERNARD LYON 1

ECOLE DOCTORALE DE CHIMIE

Pour l'obtention du DIPLOME DE DOCTORAT

(arrêté du 7 août 2006)

Spécialité : chimie

Présentée et soutenue publiquement le 28 Juin 2010

par

Hongying ZHAO

TITRE: **Etude de catalyseurs à base d'oxyde de titane et d'oxyde de vanadium sulfatés pour l'oxydation sélective du méthanol en diméthoxyméthane (DMM)**

(TITLE: **Sulfated vanadia-based and titania-based catalysts for selective oxidation of methanol to dimethoxymethane (DMM)**)

Directeur de thèse: Mme Aline AUROUX

JURY:	M. J.M. LANCELIN	Président
	Mme. A.AUROUX	Directeur de thèse
	Mme. S. BENNICI	Co-encadrant
	M. M.A. BANARES	Rapporteur
	M. J.C. VEDRINE	Rapporteur
	M. J. SHEN	Examinateur
	Mme. V. RAKIC	Examinateur

UNIVERSITE CLAUDE BERNARD - LYON 1

Président de l'Université	**M. le Professeur L. Collet**
Vice-président du Conseil Scientifique	M. le Professeur J-F. Mornex
Vice-président du Conseil d'Administration	M. le Professeur G. Annat
Vice-président du Conseil des Etudes et de la Vie Universitaire	M. le Professeur D. Simon
Secrétaire Général	M. G. Gay

COMPOSANTES SANTE

Faculté de Médecine Lyon Est – Claude Bernard	Directeur : M. le Professeur J. Etienne
Faculté de Médecine Lyon Sud – Charles Mérieux	Directeur : M. le Professeur F-N. Gilly
UFR d'Odontologie	Directeur : M. le Professeur D. Bourgeois
Institut des Sciences Pharmaceutiques et Biologiques	Directeur : M. le Professeur F. Locher
Institut des Sciences et Techniques de Réadaptation	Directeur : M. le Professeur Y. Matillon
Département de Biologie Humaine	Directeur : M. le Professeur P. Farge

COMPOSANTES ET DEPARTEMENTS DE SCIENCES ET TECHNOLOGIE

Faculté des Sciences et Technologies	Directeur : M. le Professeur F. Gieres
Département Biologie	Directeur : M. le Professeur C. Gautier
Département Chimie Biochimie	Directeur : Mme le Professeur H. Parrot
Département GEP	Directeur : M. N. Siauve
Département Informatique	Directeur : M. le Professeur S. Akkouche
Département Mathématiques	Directeur : M. le Professeur A. Goldman
Département Mécanique	Directeur : M. le Professeur H. Ben Hadid
Département Physique	Directeur : Mme S. Fleck
Département Sciences de la Terre	Directeur : M. le Professeur P. Hantzpergue
UFR Sciences et Techniques des Activités Physiques et Sportives	Directeur : M. C. Collignon
Observatoire de Lyon	Directeur : M. B. Guiderdoni
Ecole Polytechnique Universitaire de Lyon 1	Directeur : M. le Professeur J. Lieto
Institut Universitaire de Technologie de Lyon 1	Directeur : M. le Professeur C. Coulet
Institut de Science Financière et d'Assurance	Directeur : M. le Professeur J-C. Augros
Institut Universitaire de Formation des Maîtres	Directeur : M R. Bernard

“Nothing in life is to be feared. It is only to be understood.”

- Marie Curie

Acknowledgements

This work has been accomplished from September 2007 to June 2010, carrying out most of the research work in Institut de Recherches sur la Catalyse et l'Environnement de Lyon (IRCELYON) and another four months in Nanjing University. I am grateful to Mr. Michel Lacroix, directeur de IRCELYON, for welcoming me in IRCELYON during my Ph.D.

First and foremost I want to thank my advisor Mme. Aline Auroux, directeur de recherche, in IRCELYON, leader of clean and renewable energies group. She has taught me how good research can be done. She has shown me different ways to approach a research problem and the need to be persistent to accomplish any goal. I appreciate all her contributions of time, ideas, and guidance to make my Ph.D experience fruitful. I am also thankful for the excellent example she has provided as a successful women chemist and professor.

I also gratefully acknowledge Professor Jianyi Shen, chairman of chemistry department in Nanjing University, who gave me the first view of the research and led me into the word of catalysis chemistry. His broad-mindedness and professional qualities helped me for the whole thesis.

I gratefully thank Dr. Simona Bennici who shared her valuable knowledge, experience and technical expertise with me during the experiments as well as valuable discussions.

I gratefully thank Prof. M.A. Bañares from Instituto de Catálisis y Petroleoquímica, Prof. J.M. Lancelin from Université Lyon 1, Prof. V. Rakic from University of Belgrade, Prof. J. Shen from Nanjing Univeristy and Prof. J.C. Védrine from Université Paris VI for accepting to refer and judge this manuscript as members of my Ph.D. jury.

I must also express my deepest gratitude and thanks to all the facilities at IRCELYON for the convenient scientific and technical services for analysis of my samples, particularly to:

Acknowledgements

Mr. Swamy Prakash, for so much help and valuable discussions in using the FTIR apparatus.

Mrs. Laurence Massin, for XPS measurements and her valuable experience and discussions.

Mrs. Marlène Daniel, who taught me the operating of Raman spectroscopy apparatus and gave me much guidance about this technique.

Mr. Mimoun Aouine and Mrs. Laurence Burel, who provided SEM and TEM analysis helping me a lot for studying the morphology properties of my samples.

Thanks also to Dr. Georgeta Postole, who provided me with constant advice and encouragements as well as valuable experiences and discussions.

I had a real pleasure to work with my colleagues who were in Energy Group at IRCELYON in France during my stay: Reem Kourieh, Dusan Stosic, Adrien Mekki-Berrada, Hao Yu and Emil Obeid. Let me say "Thank you" to all of you for your continually unselfish help and all the happy time working together.

I also owe my earnest gratitude to all my friends both in France and in China who gave me their help and encouragement.

I also wish to express my thanks to Chemistry Department of Nanjing University in China, providing the catalytic test for all the samples studied in this work.

I gratefully acknowledge the China Scholarship Council. Without its financial support provided for my PhD studies, I could not achieve this work.

Last, but not least, I would like to thank my family for all their love and encouragement. For my parents and my grandmother who raised me with a love of science and supported me unconditionally in all my pursuits.

Contents

List of Publications

The results of this thesis have been published or submitted to publication in several international journals which are listed below:

I. J. Liu, Q. Sun, Y, Fu, **H. Zhao**, A. Auroux, J. Shen, "Preparation of mesoporous V–Ce–Ti–O for the selective oxidation of methanol to dimethoxymethane", Catalysis Letters 126 (2008) 155–163.

II. **H. Zhao**, S. Bennici, J. Shen, A. Auroux, "The influence of the preparation method on the structural, acidic and redox properties of V_2O_5–TiO_2/SO_4^{2-} catalysts", Applied Catalysis A: General 356 (2009) 121–128.

III. **H. Zhao**, S. Bennici, J. Shen, A. Auroux, "Surface and catalytic properties of V_2O_5–TiO_2/SO_4^{2-} catalysts for the oxidation of methanol prepared by various methods", Journal of Molecular Catalysis A: Chemical 309 (2009) 28–34.

IV. **H. Zhao**, S. Bennici, J. Shen, A. Auroux, "Calorimetric study of the acidic character of V_2O_5–TiO_2/SO_4^{2-} catalysts used in methanol oxidation to dimethoxymethane", Journal of Thermal Analysis and Calorimetry 99 (2010) 843–847.

V. **H. Zhao**, S. Bennici, J. Cai, J. Shen, A. Auroux, "Effect of vanadia loading on the acidic, redox and catalytic properties of V_2O_5–TiO_2 and V_2O_5–TiO_2/SO_4^{2-} catalysts for partial oxidation of methanol", Catalysis Today 152 (2010) 70–77.

VI. **H. Zhao**, S. Bennici, J. Shen, A. Auroux, "Nature of surface sites of V_2O_5–TiO_2/SO_4^{2-} catalysts and reactivity in selective oxidation of methanol to DMM", Journal of Catalysis 272 (2010) 176–189.

VII. **H. Zhao**, S. Bennici, J. Shen, A. Auroux, "Influence of the metal oxide support on the surface and catalytic properties of sulfated mixed vanadia catalysts for selective oxidation of methanol", Submitted to Journal of Catalysis.

VIII. **H. Zhao**, S. Bennici, J. Shen, A. Auroux, "Influence of the host oxide of sulfated-titania catalysts on partial oxidation methanol reaction", Applied Catalysis A: General, under revison.

List of Communications

I. Conference of Yugoslav Materials Science Society (YUCOMAT), 08–12th Sep., 2008: Herceg Novi, Montenegro, "Influence of the preparation method on the properties of V_2O_5–TiO_2/SO_4^{2-} catalysts", **H. Zhao**, S. Bennici, J. Shen, A. Auroux, *Oral presentation*.

II. 9th European Meeting on Environmental Chemistry (EMEC–9), 3–6th Dec., 2008: Girona, Spain, "Improved V_2O_5–TiO_2/SO_4^{2-} catalysts for the selective oxidation of methanol to dimethoxymethane", S. Bennici, **H. Zhao**, J. Shen, A. Auroux, *Oral presentation*.

III. 6th world congress on Catalysis by Acids and Bases (ABC–6), 10–14th May, 2009: Genova, Italy, "Acidity and catalytic properties of V_2O_5–TiO_2/SO_4^{2-} catalysts prepared by various methods", **H. Zhao**, S. Bennici, J. Shen, A. Auroux, *Oral presentation*.

IV. 6th world congress on Oxidation Catalysis (6WCOC), 5–10th July, 2009: Lille, France, "Selective oxidation of methanol to dimethoxymethane over V_2O_5–TiO_2/SO_4^{2-} catalysts prepared by various methods", **H. Zhao**, S. Bennici, J. Shen, A. Auroux, *Poster*.

V. 9th Mediterranean Conference on Calorimetry and Thermal Analysis, 15–18th June, 2009: Marseille, France, "Calorimetric study of the acidic character of sulfated vanadia-titania catalysts used in methanol oxidation to dimethoxymethane", **H. Zhao**, S. Bennici, J. Shen, A. Auroux, *Poster*.

1. Background and Introduction

My PhD work is related to the topic “Clean Energy”

Climate change is one of the greatest environmental challenges of our time, with the potential to alter all aspects of human life. A significant factor in climate change is the emissions that are released into the atmosphere by human activity. One of these processes is the burning of fuels to create energy for vehicles. The emissions from burning fossil fuels contribute significantly to global warming and poor air quality. Therefore, these environmental problems argue for the development and introduction of fuel-cell vehicles (FCVs) [1,2]. Fuel cell vehicles (FCVs) have the potential to significantly reduce the dependence on foreign oil and to lower harmful emissions that cause climate change. FCVs run on hydrogen rather than on gasoline and therefore emit nearly no harmful tailpipe emissions.

One of the key techniques to do so is the development of mobile hydrogen sources for fuel cells [3,4]. Hydrogen is one of the most promising energy carriers for the future. At present, steam reforming of natural gas and light oil fractions is widely used in industry to produce hydrogen [5,6]. However, heavy reliance on fossil fuels can cause the similar environmental problems as conventional vehicles: emission of air pollutants and greenhouse gases, acidic rain, depletion of natural resources, and so on. Consequently, the production of hydrogen from alternative resources has attracted considerable interest. One convenient method could be the on-board reforming of methanol to hydrogen [7,8], but the high toxicity of methanol is a too big restriction for a broad application. Compared to methanol, dimethoxymethane (DMM) is a preferring material for steam forming process to produce H_2. It has the advantage of high content of hydrogen, extremely low toxicity, environmentally benign. Furthermore, it is a liquid and easy for storage and transportation at ambient conditions. Steam reforming of DMM consists of the hydrolysis of DMM to methanol and formaldehyde, which are further reformed to produce H_2 and CO_2.

$$CH_3OCH_2OCH_3 + H_2O \rightarrow 2CH_3OH + CH_2O \qquad (1)$$

$$CH_3OH + H_2O \rightarrow 3H_2 + CO_2 \quad (2)$$

$$CH_2O + H_2O \rightarrow 2H_2 + CO_2 \quad (3)$$

The overall reaction can then be expressed as,

$$CH_3OCH_2OCH_3 + 4H_2O \rightarrow 8H_2 + 3CO_2 \quad (4)$$

Taken together, DMM might be used as a fuel to be reformed to produce H_2 for fuel cells. Thus, the synthesis of DMM and the improvement of DMM producing are studied in this work.

Industrially, DMM is produced by a two-stage process: methanol oxidation to formaldehyde on silver or ferric molybdate catalysts and dehydrative condensation of the formaldehyde with methanol in the presence of liquid and solid acids [9,10]. So a one-stage heterogeneous reaction process has economical and environmental benefits in the production of DMM. It has been reported in the literature that DMM can be also synthesized by the direct oxidation of methanol on crystalline $SbRe_2O_6$ [11], Re/γ–Fe_2O_3 [12], heteropolyacids [13], RuO_x/SiO_2 [14], Cu–ZSM–5 [15], and V_2O_5–TiO_2 [16,17]. Irrespective to the catalytic system, all the studies suggest that the selective oxidation of methanol to DMM may involve two steps: (1) oxidation of methanol to formaldehyde on redox sites and (2) condensation of formaldehyde produced with additional methanol to DMM on acidic sites. Therefore, bi-functional catalysts with both acidic and redox properties are required for this reaction:

$$CH_3OH + 1/2\ O_2 \rightarrow CH_2O + H_2O \quad (5)$$

$$2CH_3OH + CH_2O \rightarrow CH_3OCH_2OCH_3 + H_2O \quad (6)$$

The overall reaction can then be expressed as,

$$3CH_3OH + 1/2O_2 \rightarrow CH_3OCH_2OCH_3 + 2H_2O \quad (7)$$

The mechanism of catalytic methanol oxidation was summarized by Tatibouët [18]. The first reaction step is the formation of methoxy groups by dissociative adsorption of methanol on dual acid-base site formed by an accessible cation and a surface oxygen ion. The further transformation of adsorbed methoxy group will depend on the acid strength of the adsorbing site, and on the nature of the active

centers in close proximity. The basic or nucleophilic character of oxygen species close to the methoxy group will lead to the break of a C–H bond, while weak acid sites will favor the desorption of the reaction products. According to this scheme, the selective formation of formaldehyde will require both weak acid and basic sites to limit the H abstraction and to prevent a too strong adsorption of formaldehyde, respectively. Strong acid sites prolong the residence time of formaldehyde species to form dioxymethylene species, able to react with methanol to form DMM. If both acid and basic sites are stronger than those needed for DMM formation, dioxymethylene species will be oxidized into formate species which quickly react with methanol to form methyl formate or are further oxidized to COx. If only strong acid sites are present, only dimethyl ether is formed. The formation of these different products can be summarized on an acid-base strength diagram (Fig.1.1). Indeed, as both acidic and redox sites are needed to oxidize methanol to DMM, bi-functional catalysts should be the most active systems.

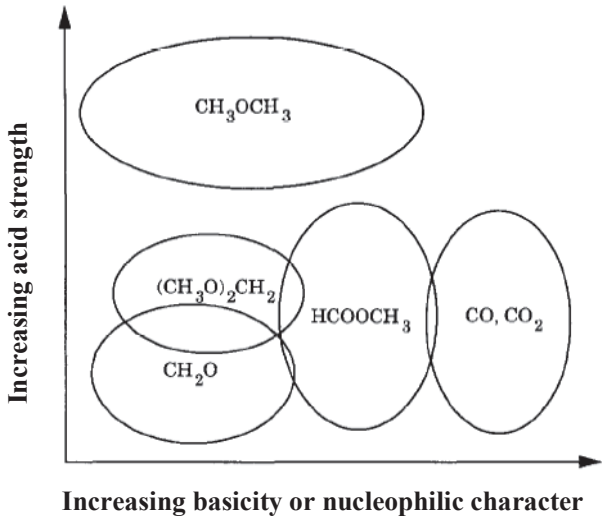

Fig.1.1 Schematic representation of the main reaction products as a function of the acidic-basic character of active sites [from ref.18].

Supported V_2O_5 catalysts are usually used in this reaction of methanol oxidation [18,19]. Moreover, it has been shown that the addition of SO_4^{2-} species to TiO_2 generates strong acidic sites at high temperature and can lead to high activity [20].

Amiridis et al. [21] have also reported that, on vanadia–titania catalysts, the gaseous SO_2 contained in the feed gas system could participate in the formation of surface sulfate species which strongly interact with vanadia and then improve the catalytic surface reactivity. Further, it has recently been reported that [22,23] the selective oxidation of methanol to DMM over V_2O_5–TiO_2 (VTi) catalysts can be improved by doping VTi catalysts with SO_4^{2-} ions, suggesting that the surface acidity of the catalysts could be greatly enhanced by the addition of SO_4^{2-}. Therefore in order to verify this proposal, we prepared various kinds of sulfated vanadia-titania, sulfated binary vanadia-based oxides and sulfated binary titania-based oxides, which were used to DMM synthesis via selective oxidation of methanol.

To summarize, the objective of this work was to study:

(1) Design and preparation of various series of sulfated vanadia-titania catalysts by co-precipitation, sol-gel, impregnation, mechanical grinding to investigate how both the preparation method and the sulfate content impact the acidic and redox properties and finally influence the DMM synthesis. The obtained materials were thoroughly characterized by complementary physico-chemical techniques (BET, ICP, XRD, FTIR, Raman, XPS, TGA, O_2 chemisorption, redox cycles (TPR1/TPO/TPR2)). NH_3 adsorption calorimetry and pyridine adsorption FTIR were used to investigate the acidic properties. Isopropanol (IPA) probe reaction with the presence of O_2 was employed to provide information about the surface acidity and redox properties simultaneously.

(2) Since co-precipitation was by far the best preparation method in terms of maximizing the surface area and the mesoporosity, sulfated vanadia-titania catalysts were prepared by co-precipitation and calcined at different temperatures in order to fix the right amount of surface residual sulfate (with or without washing with deionized water) during the calcination step and to develop active surface structure most appropriate for DMM synthesis. The catalysts were thoroughly characterized by BET, XRD, ICP, XPS, SEM, TEM, Raman spectroscopy, TPR. Ammonia adsorption

microcalorimetry and pyridine adsorption FTIR were used to investigate in detail the acidity of catalysts. The factors limiting the activity and selectivity were evaluated by selective oxidation of methanol reaction to DMM.

(3) High surface area 25%V_2O_5–M_xO_y–SO_4^{2-} (M= Ti, Zr, Al or Ce) catalysts were prepared by co-precipitation and impregnation methods. The central theme in this research was to understand how the different guest metal oxides could influence the acidic, redox and catalytic properties of these catalysts. Moreover, the influence of the host metal oxide on the types of surface VO_x and sulfate species was also investigated. The structural properties were characterized by BET, XRD, ICP, XPS and Raman spectroscopies. The redox properties were investigated by TPR/MS technique, while the acidic properties were studied by ammonia adsorption calorimetry and simultaneous ammonia TPD–MS–TG–DSC measurements. The surface properties will be correlated to the catalytic activity.

(4) Since the products of partial oxidation of methanol reaction are strongly related with the proportion of acidic and redox sites of catalysts, 25%M_xO_y–TiO_2–SO_4^{2-} (M= Cr, Mn, Fe, Co or Mo) mixed metal oxides with high surface area were also evaluated by this reaction. The catalysts were prepared by co-precipitation and thoroughly characterized by BET, XRD, ICP, XPS, SEM, TEM, Raman spectroscopy, TPR–MS and ammonia adsorption calorimetry measurements. Methanol oxidation reaction was employed to provide information about the surface acidity and redox properties simultaneously.

2. Experimental Description

The following chapter describes the catalysts preparation and experimental techniques used in this work.

2.1 Catalyst preparation

2.1.1 Sulfated vanadia-titania (V_2O_5–TiO_2/SO_4^{2-}) catalysts prepared by various methods

Different synthesis routes were followed for obtaining four series of catalysts, each one composed of three samples differing as to the calcination temperature. The theoretical amount of vanadium pentoxide was fixed at 25wt% whatever the preparation method used.

2.1.1.1 Preparation by co-precipitation

High surface area vanadia-titania-sulfate catalysts (denoted by VTiS) were prepared by a co-precipitation method. 4 g of V_2O_5–TiO_2/SO_4^{2-} sample were prepared starting from 2.5 g of $VOSO_4 \cdot xH_2O$ and 9.2 g of $TiOSO_4 \cdot xH_2SO_4 \cdot xH_2O$. At first, the precursors were dissolved in 400 mL of deionized water, forming a solution (S1) containing vanadium and titanium while 20 mL of a 28 wt% $NH_3 \cdot H_2O$ solution was placed in an ice bath. Then S1 was slowly dropped into the $NH_3 \cdot H_2O$ solution under vigorous stirring in the ice bath, and a brown precipitate formed immediately. This precipitate was first aged for 1 h at room temperature and then filtered. The filtered cake was redispersed by stirring into a mixture containing 1-butanol to form homogeneous slurry. Finally the slurry was transferred to a beaker which was placed in an oil bath to remove the solvent. At the temperature of 367 K (azeotropic point of the water-butanol system), water and part of 1-butanol in the slurry were distilled, and then at 391 K (boiling point of 1-butanol), the residual 1-butanol was further removed. The VTiS–1, VTiS–2 and VTiS–3 samples were prepared in this way, and then calcined in air for 5 h at 673, 723 and 773 K, respectively (see Table 1).

2.1.1.2 Preparation by co-precipitation with 1wt% poly-ethylene-glycol (PEG–400)

PEG-doped VTiS particles were synthesized by adding an amount of 1wt% of PEG–400 into diluted $NH_3.H_2O$ solution, followed by the same process as above. The VTiS–4, VTiS–5 and VTiS–6 samples were prepared in this way, with calcination temperatures of 673, 723 and 773 K, respectively. PEG is known to improve the physical properties of the sample in terms of surface area and structure and it also carries the role of reducing agent [24] (see Table 1).

2.1.1.3 Preparation by sol-gel method

The synthesis of mixed vanadia oxide (V_2O_5/TiO_2) was carried out using an organic mixture containing vanadyl acetylacetonate and titanium (IV) isopropoxide in propanol-2-ol as solvent. A homogeneous gel was obtained by hydrolysis and precipitation after addition of water to this mixture. The amount of water added corresponded to a volume ratio $[H_2O]/[Ti(OR)_4]$ equal to 2. To obtain sulfated oxides, sulfuric acid was added to the organic mixture, according to a molar ratio nS/nTi=0.25. Next, the gels were filtered, and then dried for 12 h at 373 K. Finally, the catalysts were obtained after calcination in air for 12 h. This longer time of calcination compared to the other series of samples was justified by preliminary TG–DTG experiments which have shown that decomposition of sol-gel precursors required a slightly higher temperature and more time than the other precursors. The VTiS–7, VTiS–8 and VTiS–9 samples were prepared in this way, with calcination temperatures of 673, 723 and 773 K, respectively (see Table 1).

2.1.1.4 Preparation by mechanical grinding

$V_2O_5–SO_4^{2-}/TiO_2$ catalysts were also prepared by mechanical grinding in an agate mortar using TiO_2 (313 $m^2 \cdot g^{-1}$ after calcination at 723 K, Millennium* G5) and $VOSO_4.xH_2O$ in definite proportions corresponding to the theoretical amount of 25 wt% V_2O_5, and then calcined in air for 5 h. The VTiS–10, VTiS–11 and VTiS–12

samples were prepared in this way, using calcination temperatures of 673, 723 and 773 K, respectively. However it should be noticed that the parent commercial TiO_2 already contained some sulfates (0.17 wt% S) (see Table 1).

2.1.2 Vanadia-titania (V_2O_5–TiO_2) and sulfated vanadia-titania (V_2O_5–TiO_2/SO_4^{2-}) catalysts with different vanadia contents by impregnation

Vanadium oxide systems with different V_2O_5 contents (denoted by VTi) supported on commercial TiO_2 (Millennium* G5, uncalcined) were prepared by incipient wetness impregnation, using ammonia vanadate (NH_4VO_3) as metal precursor and oxalic acid as complexing agent ($NH_4VO_3/C_2O_2H_2$ molar ratio=1/2). After being kept at room temperature for 12 h to ensure their stabilization, the resulting solids were dried at 373K overnight and then calcined in air at 673K for 6 h. Pure TiO_2 catalyst, used as reference, was also calcined at 673 K in air for 6 h.

The sulfated vanadia-titania catalysts (denoted by VTiS) were prepared by incipient wetness impregnation of 1 g of above mentioned vanadia-titania catalysts with an aqueous solution containing the theoretical percentage of $(NH_4)_2SO_4$ to achieve 5 wt% SO_4^{2-} (1.7 wt% S). The resulting solids were then dried at 373 K overnight and calcined at 673 K in air for 6 h (see Table 2).

2.1.3 Sulfated vanadia-titania (V_2O_5–TiO_2–SO_4^{2-}) catalysts prepared by co-precipitation and calcined at different temperatures

5 g of V_2O_5–TiO_2/SO_4^{2-} catalysts (25 wt% V_2O_5) were prepared by a co-precipitation method [25] with 3.2 g of $VOSO_4 \cdot xH_2O$ and 11.5 g of $TiOSO_4 \cdot xH_2SO_4 \cdot xH_2O$ as precursors, and 25 mL 28 wt% $NH_3.H_2O$ solution as precipitant. Samples VTiS–573, VTiS–623, VTiS–673, VTiS–673 and VTiS–723 were prepared in this way, and then calcined in air for 5 h at 573, 623, 673, 723 and 773 K, respectively. Additionally, samples VTiSw50–673 and VTiSw300–673 were prepared by the same procedure of co-precipitation, washed with respectively 50 and

300 mL deionized water while filtering the precipitate and then calcined at given temperature of 673 K in air for 5 h (see Table 2).

2.1.4 V_2O_5–M_xO_y and V_2O_5–M_xO_y–SO_4^{2-} (M=Ti, Zr, Al or Ce) catalysts

The theoretical amount of vanadium pentoxide was fixed at 25 wt% whatever the host metal oxide was.

2.1.4.1 Prepared in two steps: co-precipitation of mixed oxides followed by sulphate impregnation

Vanadia-based bimetallic oxides (denoted by VM(c1); M=Ti, Zr, Al or Ce) were prepared by modifying a previous reported co-precipitation method [25]. The vanadia, titania, zirconia, alumina and ceria precursors were $VOCl_3$, $TiCl_4$, $ZrOCl_2$, $Al(NO_3)_3$ and $Ce(NO_3)_3$, respectively. Briefly, $VOCl_3$ was dissolved into deionized water (1mL $VOCl_3$ in 250 mL H_2O) mixed with 5-8 mL diluted HNO_3 (38 wt% HNO_3) with vigorous stirring to form a vanadium-containing solution (S1). The oxide support precursor was dissolved into a limited amount of deionized water to form the metal ion containing solution (S2), while $TiCl_4$ was dissolved in C_2H_5OH (1 mL $TiCl_4$ in 30 mL C_2H_5OH) in an ice bath. S2 was slowly dropped into S1 with continuous stirring to form a mixed solution (S3). Then S3 solution was slowly dropped into diluted $NH_3.H_2O$ placed in an ice bath to form the precipitate. The precipitate was first aged for 1 h at room temperature, then filtered, washed several times with deionized water until free from chloride ions, and the filtrate cake dried as reported in [25]. The samples were all calcined at 673 K in air for 5 h, except for sample VAl(c1) which calcination temperature was increased up to 773 K for a better decomposition of the precursor.

The sulfated vanadia-based bimetallic oxides (denoted by VMS(c1-i); M=Ti, Zr, Al or Ce) were prepared by incipient wetness impregnation of the above mentioned supported-vanadia catalysts with an aqueous solution containing the given percentage

of $(NH_4)SO_4$ to achieve a theoretical amount of 5 wt% SO_4^{2-} (1.7 wt% S). The resulting solids were then dried at 373 K overnight and then calcined at 673 K in air for 5 h (see Table 3).

2.1.4.2 Prepared directly by co-precipitation from sulfated precursors

Sulfated vanadia-based bimetallic oxides (denoted by VMS(c2); M=Ti, Zr, Al or Ce) were also prepared by co-precipitation. The precursors were $VOSO_4$, $TiOSO_4$, $Zr(SO_4)_2$, $Al_2(SO_4)_3$ and $Ce(SO_4)_2$, respectively. The details of the preparation method have been previously described in [25]. Specially, $Ce(SO_4)_2$ was dissolved in deionized water and then the pH was adjusted to around zero by adding dilute HNO_3 (38 wt% HNO_3) in order to complete the dissolution. Then the aqueous solution of $VOSO_4$ was added dropwise to $Ce(SO_4)_2$ solution with vigorous stirring to form a mixed aqueous solution for precipitation with ammonia. At last, the samples were all calcined at 673 K in air for 5 h, except sample VAlS(c2) which calcination temperature was increased to 773 K (see Table 3).

2.1.5 M_xO_y/TiO_2–SO_4^{2-} (M=Cr, Mn, Fe, Co or Mo*) catalysts*

The theoretical amount of each metal oxide (CrO_x, Mn_2O_3, Fe_2O_3, Co_3O_4 and MoO_3) was fixed at 25 wt%.

Sulfated binary titania-based oxides (denoted by MTiS; M=Cr, Mn, Fe, Co or Mo) were prepared by a previous reported co-precipitation method [25]. In order to obtain the similar content of sulfate for each sample, the same titania precursor was used for all samples: $TiOSO_4{\cdot}xH_2SO_4{\cdot}xH_2O$. The other precursors were $Cr(NO_3)_3{\cdot}9H_2O$, $Fe(NO_3)_3{\cdot}9H_2O$, $Co(NO_3)_2{\cdot}6H_2O$, $Mn(NO_3)_2{\cdot}xH_2O$, $(NH_4)_6Mo_7O_{24}{\cdot}4H_2O$. The details of the preparation method have been previously described in [25]. Specially for sample MoO_3/TiO_2-SO_4^{2-}, theoretical required amount of $(NH_4)_6Mo_7O_{24}{\cdot}4H_2O$ was dissolved into a limited amount of deionized water and then added to filtrated precipitate cake containing Ti. At last the mixed cake

containing Mo and Ti was dried as reported in [25]. All the samples were calcined at a given temperature of 673 K in air for 5 h (see Table 4).

2.2 Catalyst characterization

Different techniques were used to characterize the physico-chemical properties of the catalysts which are listed as the following:

The surface areas and pore sizes were measured by nitrogen adsorption at 77 K on a Micromeritics 2010 apparatus after heat pretreatment under vacuum for 3 h at a temperature 100 K lower than the calcination temperature.

The X-ray diffraction (XRD) measurements were carried out on a Bruker D5005 powder diffractometer scanning from 3° to 80° (2θ) at a rate of 0.02 degree s^{-1} using a Cu Kα radiation (λ=0.15418nm) source. The applied voltage and current were 50 kV and 35 mA, respectively.

Elemental analysis was performed using ICP optical emission spectroscopy (ICP–OES) with an ACTIVA spectrometer from Horiba JOBIN YVON.

The X-ray photoelectron spectra were measured on a KRATOS AXIS Ultra DLD spectrometer equipped with a hemispherical electron analyzer and an Al anode (Al Kα=1486.6 eV) powered at 150 W, a pass energy of 20 eV, and a hybrid lens mode. The detection area analyzed was 700×300 μm. Charge neutralization was required for all samples. The peaks were referenced to the C–(C, H) components of the C1s band at 284.6 eV. Shirley background subtraction and peak fitting to theoretical Gaussian-Lorentzian functions were performed using an XPS processing program (vision 2.2.6 KRATOS). The residual pressure in the spectrometer chamber was 5×10^{-7} Pa during data acquisition.

Scanning electron microscopy (SEM) was performed using a Philips 5800 SEM electron microscrope. The samples were deposited onto scotch carbon and metallized by sputtering. A gold film ensures a good conductivity for the observation.

2. Experimental Description

The recording of transmission electron micrographs was carried out using a JEOL 2010 equipment operating at 200 kV with a high resolution pole piece and an energy dispersive X-ray spectrometer (EDS) (Link Isis from Oxford Instruments). The samples were dispersed in ethanol using a sonicator and a drop of the suspension was dripped onto a carbon film supported on a copper grid and then ethanol was evaporated. EDS study was carried out using a probe size of 15 nm to analyze borders and centers of the particles and the small particles. Standard deviations were evaluated for atomic ratio from at least 10 analyses.

Raman spectroscopy measurements were performed using a LabRAM HR (Jobin Yvon) spectrometer. The excitation was provided by the 514.5 nm line of an Ar^+ ion laser (Spectra physics) employing a laser power of 100 μW. The laser beam was focused through microscope objective lenses (×100) down to a 1 μm spot on the sample.

The skeletal FTIR and pyridine adsorption FTIR spectra were recorded at room temperature with a Bruker Vector 22 FTIR spectrophotometer (DTGS detector) operating in the 4000–400 cm^{-1} range, with a resolution of 2 cm^{-1} and 100 acquisition scans. In each skeletal FTIR experiment, 2 mg of sample was mixed with 198 mg of KBr. In each pyridine adsorption FTIR measurement, the self-supporting wafer (10–30 mg, 18 mm diameter) was first activated in situ at a temperature 100 K lower than the calcination temperature in oxygen flow for 14 h, then evacuated at the same temperature for 2 h and then exposed to pyridine (Air Liquide, 99.8%, vapor pressure 3.3 kPa) at room temperature for 5 min. The desorption was carried out by evacuation for 30 min each at room temperature, 373 K, 473 K and 573 K, respectively . The spectra were recorded at room temperature after adsorption and desorption at each temperature (see scheme Fig.2.2.1).

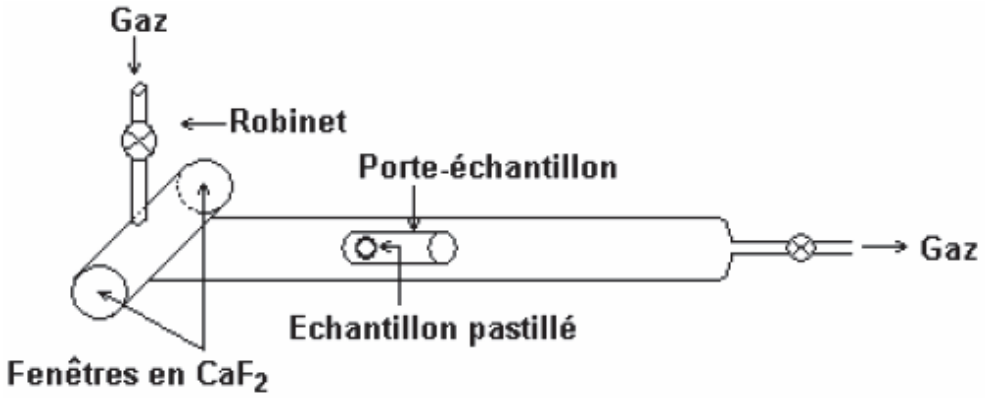

Fig.2.2.1 Scheme of the in-situ cell for adsorption FTIR (IRCELYON)

The microcalorimetric studies of ammonia adsorption were performed at 423 K in a heat flow calorimeter (C80 from Setaram) linked to a conventional volumetric apparatus equipped with a Barocel capacitance manometer for pressure measurements. Ammonia used for measurements (Air Liquide, purity > 99.9%) was purified by successive freeze-pump-thaw cycles. About 100 mg of sample was pretreated in a quartz cell under evacuation overnight at a temperature 100 K lower than the calcination temperature. The differential heats of adsorption were measured as a function of coverage by repeatedly introducing small doses of ammonia gas onto the catalyst until an equilibrium pressure of about 66 Pa was reached. The sample was then outgassed for 30 min at the same temperature, and a second adsorption was performed at 423 K until an equilibrium pressure of about 27 Pa was attained in order to calculate the irreversibly chemisorbed amount of ammonia at this pressure (see scheme Fig.2.2.2) [26,27].

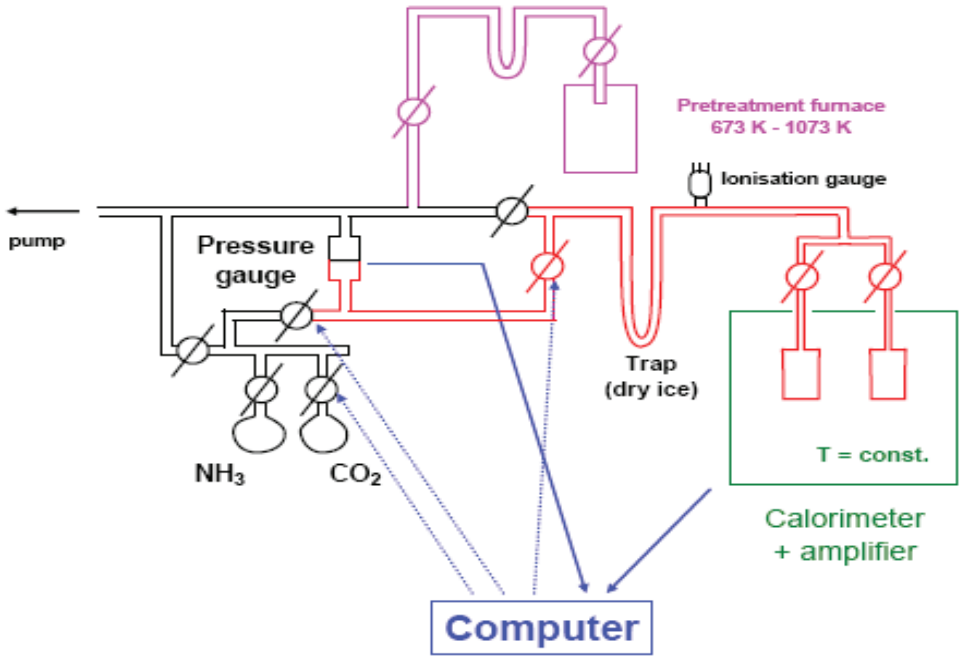

Fig.2.2.2. Scheme of adsorption microcalorimetry system (IRCELYON)

Temperature-programmed desorption (TPD) of ammonia was performed on a Setaram TG–DSC 111 device coupled with a mass spectrometer (Thermostar, Pfeiffer) as a detector. A capillary-coupling system was used. The TPD experiments were carried out in the range 298–923 K under helium flow as the carrier gas (10 mL min^{-1}). For each experiment, about 20 mg of sample with ammonia absorbed in previous microcalorimetric experiments was used. Initially, the samples were purged with helium at room temperature for 15 min and then heated with 5 K min^{-1} up to 373 K. The temperature was kept constant at 373 K for 30 min and then was linearly increased up to 923 K with same ramp of 5 K min^{-1}. During this temperature increase, the mass spectrometer was set at m/e=15 in order to avoid the interference of m/e peaks of water fragmentation. For sulfate desorption, the gas phase composition was analyzed by setting the mass spectrometer m/e=64 for SO_2 (see scheme Fig.2.2.3).

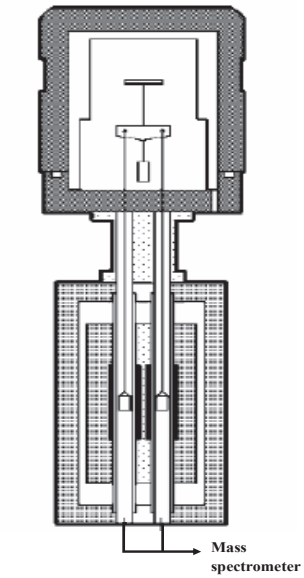

Fig.2.2.3. Scheme of TG–DSC 111–MS system

Redox cycles (TPR1/TPO/TPR2), carried out in sequences consisting of a first temperature programmed reduction (TPR) on the oxidized sample (TPR1), a temperature programmed oxidation (TPO), and a second temperature programmed reduction (TPR2), were performed using a TPD/R/O-1100 instrument (ThermoFisher). Prior to the TPR1 run, the fresh sample was treated in a stream of O_2/He (0.998% v/v, flowing at 20 mL min^{-1}), ramping the temperature at 10 K min^{-1} from RT to a temperature 100 K lower than the calcination temperature and maintaining it for 60 min, and then cooled to 313 K. The TPR1 measurement was carried out using H_2/Ar (4.98% v/v) as reducing gas mixture, flowing at 20 mL min^{-1}. The heating rate was 10 K min^{-1} from 313 K to 1073 K (or 1223 K for bulk metal oxides). The TPO run was carried out on the reduced sample (after TPR1) cooled at 313K in N_2 flow. After a purge with Ar (20 mL min^{-1}), the oxidizing gas mixture composed of O_2/He (0.998 % v/v) flowed at 20 mL min^{-1} through the sample from 313 to 1073 K. The oxidized sample was further reduced during the TPR2 run, under the same experimental conditions as TPR1 described above, up to a final temperature of 1223K. The H_2 or O_2 consumption was detected by a thermal conductivity detector (TCD). The sample size used was adjusted in order to have around 69 μmol of metal oxide independently of the loading of the oxides. This allowed us to maintain a K value of 100 s. The

characteristic number, K, can be defined to facilitate the selection of appropriate operating parameters; a fixed K value between 60 and 140 s guarantees optimal conditions to obtain good TPR/TPO profiles [28,29]. The peak areas were calibrated with given H_2/Ar (4.98% v/v) and O_2/He (0.998% v/v) mixture injections for TPR and TPO, respectively.

Gases evolving from the TPR reactor were analyzed by a mass spectrometer (Omnistar, Pfeiffer) by a heated capillary. The signals for m/e=34 (H_2S) and 64 (SO_2) were recorded.

2.3 Catalytic reactions

The reaction of isopropanol conversion was used to characterize the surface acidity. This probe reaction was carried out in a fixed-bed glass tube reactor. About 100 mg of sample was loaded for each reaction. Isopropanol was introduced onto the catalyst by bubbling air through a glass saturator filled with isopropanol maintained at 295K. Isopropanol and reaction products were analyzed by an online gas chromatograph (GC), using a polyethylene glycol (PEG) 20M packed column connected to a Flame Ionization Detector (FID). Prior to the test, each catalyst was pretreated by heating in air at the same temperature as that used for calcination for 1 h and then cooled in the air flow to the reaction temperature.

The oxidation of methanol was carried out in a fixed-bed micro-reactor made of glass with an inner diameter of 6 mm. The methanol was introduced into the reaction zone by bubbling O_2/N_2 (1/5) through a glass saturator filled with methanol (99.9%) maintained at 278 K. In each test, 0.2 g of catalyst was loaded, and the gas hourly space velocity (GHSV) was 11400 mL g^{-1} h^{-1}. The feed composition was maintained as methanol:O_2:N_2=1:3:15 (v/v). The tail gas out of the reactor was analyzed by an on-line GC equipped with an FID detector and a thermal conductivity detector (TCD). The column used was PORAPAK N for the separation of methanol, DMM and other organic compounds. The gas lines were kept at 373 K to prevent condensation of the

reactant and products. The reaction was carried out at atmospheric pressure. Prior to the test, the samples were pretreated in the same way as for the isopropanol conversion reaction [23].

3. List of Catalysts

Table 1 Sulfated vanadia-titania catalysts used in this work

Catalyst	Component	Preparation method	Precursors	Calcination Temp.[b] (K)	Publication
VTiS-1	25%V_2O_5−TiO_2−SO_4^{2-}	co-precipitation	$VOSO_4 \cdot xH_2O$, $TiOSO_4 \cdot xH_2SO_4 \cdot xH_2O$	673	II
VTiS-2	25%V_2O_5−TiO_2−SO_4^{2-}	co-precipitation	$VOSO_4 \cdot xH_2O$, $TiOSO_4 \cdot xH_2SO_4 \cdot xH_2O$	723	II, II, IV
VTiS-3	25%V_2O_5−TiO_2−SO_4^{2-}	co-precipitation	$VOSO_4 \cdot xH_2O$, $TiOSO_4 \cdot xH_2SO_4 \cdot xH_2O$	773	II
VTiS-4	25%V_2O_5−TiO_2−SO_4^{2-}	co-precipitation modified with PEG-400 [a]	$VOSO_4 \cdot xH_2O$, $TiOSO_4 \cdot xH_2SO_4 \cdot xH_2O$	673	II
VTiS-5	25%V_2O_5−TiO_2−SO_4^{2-}	co-precipitation modified with PEG-400 [a]	$VOSO_4 \cdot xH_2O$, $TiOSO_4 \cdot xH_2SO_4 \cdot xH_2O$	723	II, II, IV
VTiS-6	25%V_2O_5−TiO_2−SO_4^{2-}	co-precipitation modified with PEG-400 [a]	$VOSO_4 \cdot xH_2O$, $TiOSO_4 \cdot xH_2SO_4 \cdot xH_2O$	773	II
VTiS-7	25%V_2O_5−TiO_2−SO_4^{2-}	sol-gel	$VO(C_5H_7O_2)_2$, $Ti[OCH(CH_3)_2]_4$	673	II
VTiS-8	25%V_2O_5−TiO_2−SO_4^{2-}	sol-gel	$VO(C_5H_7O_2)_2$, $Ti[OCH(CH_3)_2]_4$	723	II, II, IV
VTiS-9	25%V_2O_5−TiO_2−SO_4^{2-}	sol-gel	$VO(C_5H_7O_2)_2$, $Ti[OCH(CH_3)_2]_4$	773	II
VTiS-10	25%V_2O_5−TiO_2−SO_4^{2-}	mechanical grinding	$VOSO_4 \cdot xH_2O$, $TiOSO_4 \cdot xH_2SO_4 \cdot xH_2O$	673	II
VTiS-11	25%V_2O_5−TiO_2−SO_4^{2-}	mechanical grinding	$VOSO_4 \cdot xH_2O$, $TiOSO_4 \cdot xH_2SO_4 \cdot xH_2O$	723	II, II, IV
VTiS-12	25%V_2O_5−TiO_2−SO_4^{2-}	mechanical grinding	$VOSO_4 \cdot xH_2O$, $TiOSO_4 \cdot xH_2SO_4 \cdot xH_2O$	773	II

[a] PEG-400: Polyethylene glycol 400; [b] All catalysts were calcined in air

Table 2 Sulfated vanadia-titania catalysts used in this work

Catalyst	Component	Preparation method	Precursors	Calcination Temp.[b] (K)	Publication
5VTi	$5\%V_2O_5{-}TiO_2$	impregnation	NH_4VO_3, TiO_2 (Millennium* G5)[a]	673	V
5VTiS	$5\%V_2O_5{-}TiO_2/SO_4^{2-}$	impregnation	NH_4VO_3, TiO_2 (Millennium* G5)[a], $(NH_4)_2SO_4$	673	V
15VTi	$15\%V_2O_5{-}TiO_2$	impregnation	NH_4VO_3, TiO_2 (Millennium* G5)[a]	673	V
15VTiS	$15\%V_2O_5{-}TiO_2/SO_4^{2-}$	impregnation	NH_4VO_3, TiO_2 (Millennium* G5)[a], $(NH_4)_2SO_4$	673	V
25VTi	$25\%V_2O_5{-}TiO_2$	impregnation	NH_4VO_3, TiO_2 (Millennium* G5)[a]	673	V
25VTiS	$25\%V_2O_5{-}TiO_2/SO_4^{2-}$	impregnation	NH_4VO_3, TiO_2 (Millennium* G5)[a], $(NH_4)_2SO_4$	673	V
VTiS-573	$25\%V_2O_5{-}TiO_2{-}SO_4^{2-}$	co-precipitation	$VOSO_4{\cdot}xH_2O$, $TiOSO_4{\cdot}xH_2SO_4{\cdot}xH_2O$	573	IV, VI
VTiS-623	$25\%V_2O_5{-}TiO_2{-}SO_4^{2-}$	co-precipitation	$VOSO_4{\cdot}xH_2O$, $TiOSO_4{\cdot}xH_2SO_4{\cdot}xH_2O$	623	IV, VI
VTiS-673	$25\%V_2O_5{-}TiO_2{-}SO_4^{2-}$	co-precipitation, washing	$VOSO_4{\cdot}xH_2O$, $TiOSO_4{\cdot}xH_2SO_4{\cdot}xH_2O$	673	IV, VI
VTiSw50-673	$25\%V_2O_5{-}TiO_2{-}SO_4^{2-}$	co-precipitation, washing	$VOSO_4{\cdot}xH_2O$, $TiOSO_4{\cdot}xH_2SO_4{\cdot}xH_2O$	673	IV, VI
VTiSw300-673	$25\%V_2O_5{-}TiO_2{-}SO_4^{2-}$	co-precipitation	$VOSO_4{\cdot}xH_2O$, $TiOSO_4{\cdot}xH_2SO_4{\cdot}xH_2O$	673	IV, VI
VTiS-723	$25\%V_2O_5{-}TiO_2{-}SO_4^{2--}$	co-precipitation	$VOSO_4{\cdot}xH_2O$, $TiOSO_4{\cdot}xH_2SO_4{\cdot}xH_2O$	723	IV, VI
VTiS-773	$25\%V_2O_5{-}TiO_2{-}SO_4^{2-}$	co-precipitation	$VOSO_4{\cdot}xH_2O$, $TiOSO_4{\cdot}xH_2SO_4{\cdot}xH_2O$	773	IV, VI

[a] TiO_2 (Millennium* G5): uncalcined; [b] All catalysts were calcined in air

3. List of Catalysts

Table 3 V_2O_5–M_xO_y–SO_4^{2-} (M=Ti, Zr, Al or Ce) catalysts used in this work

Catalyst	Component	Preparation method	Precursors	Calcination Temp.[a] (K)	Publication
VTi(c1)	25%V_2O_5–TiO_2	co-precipitation	$VOCl_3$, $TiCl_4$	673	VII
VTiS(c1-i)	25%V_2O_5–TiO_2/SO_4^{2-}	co-precipitation and impregnation	$VOCl_3$, $TiCl_4$, $(NH_4)_2SO_4$	673	VII
VTiS(c2)	25%V_2O_5–TiO_2–SO_4^{2-}	co-precipitation	$VOSO_4 \cdot xH_2O$, $TiOSO_4$·aq	673	VII
VZr(c1)	25%V_2O_5–ZrO_2	co-precipitation	$VOCl_3$, $ZrOCl_2 \cdot 8H_2O$	673	VII
VZrS(c1-i)	25%V_2O_5–ZrO_2/SO_4^{2}	co-precipitation and impregnation	$VOCl_3$, $ZrOCl_2 \cdot 8H_2O$, $(NH_4)_2SO_4$	673	VII
VZrS(c2)	25%V_2O_5–ZrO_2–SO_4^{2}	co-precipitation	$VOSO_4 \cdot xH_2O$, $Zr(SO_4)_2 \cdot xH_2O$	673	VII
VAl(c1)	25%V_2O_5–Al_2O_3	co-precipitation	$VOCl_3$, $Al(NO_3)_3 \cdot 9H_2O$	773	VII
VAlS(c1-i)	25%V_2O_5–Al_2O_3/SO_4^{2-}	co-precipitation and impregnation	$VOCl_3$, $Al(NO_3)_3 \cdot 9H_2O$, $(NH_4)_2SO_4$	673	VII
VAlS(c2)	25%V_2O_5–Al_2O_3–SO_4^{2-}	co-precipitation	$VOSO_4 \cdot xH_2O$, $Al_2(SO_4)_3 \cdot xH_2O$	773	VII
VCe(c1)	25%V_2O_5–CeO_2	co-precipitation	$VOCl_3$, $Ce(NO_3)_3 \cdot 6H_2O$	673	VIII
VCeS(c1-i)	25%V_2O_5–CeO_2/SO_4^{2}	co-precipitation and impregnation	$VOCl_3$, $Ce(NO_3)_3 \cdot 6H_2O$, $(NH_4)_2SO_4$	673	VII
VCeS(c2)	25%V_2O_5–CeO_2–SO_4^{2}	co-precipitation	$VOSO_4 \cdot xH_2O$, $Al_2(SO_4)_3 \cdot xH_2O$	673	VII

[a] All catalysts were calcined in air

3. List of Catalysts

Table 4 M_xO_y−TiO2−SO_4^{2-} (M=Cr, Mn, Fe, Co or Mo) catalysts used in this work

Catalyst	Component	Preparation method	Precursors	Calcination Temp.[a] (K)	Publication
25CrTiS	25%CrO_x−TiO_2−SO_4^{2-}	co-precipitation	$Cr(NO_3)_3.9H_2O$, $TiOSO_4{\cdot}xH_2SO_4{\cdot}xH_2O$	673	VIII
25MnTiS	25%Mn_2O_3−TiO_2−SO_4^{2-}	co-precipitation	$Mn(NO_3)_2.xH_2O$, $TiOSO_4{\cdot}xH_2SO_4{\cdot}xH_2O$	673	VIII
25FeTiS	25%Fe_2O_3−TiO_2−SO_4^{2-}	co-precipitation	$Fe(NO_3)_3.9H_2O$, $TiOSO_4{\cdot}xH_2SO_4{\cdot}xH_2O$	673	VIII
25CoTiS	25%Co_3O4−TiO_2−SO_4^{2-}	co-precipitation	$Co(NO_3)_2.6H_2O$, $TiOSO_4{\cdot}xH_2SO_4{\cdot}xH_2O$	673	VIII
25MoTiS	25%MoO_3−TiO_2−SO_4^{2-}	co-precipitation and impregnation	$(NH_4)_6Mo_7O_{24}.4H_2O$, $TiOSO_4{\cdot}xH_2SO_4{\cdot}xH_2O$	673	VIII
TiS	TiO_2−SO_4^{2-}	co-precipitation	$TiOSO_4{\cdot}xH_2SO_4{\cdot}xH_2O$	673	VIII

[a] All catalysts were calcined in air

References

[1] B.D. Mcnicol, D.A.J. Rand, K.R. Williams, J. Power Sources 100 (2001) 47−59.
[2] P.K. Cheekatamarla, C.M. Finnerty, J. Power Sources 160 (2006) 490−499.
[3] J.C. Amphlett, K.A.M. Creber, J.M. Davis, R.F. Mann, B.A. Peppley, D.M. Stokes, Int. J. Hydrogen Energy 19 (1994) 131.
[4] L.Carrette, K.A. Friedrich, U. Stimming, ChemPhysChem 1 (2000) 162.
[5] A.D. Qi, S.D. Wang, G.Z. Fu, C.J. Ni, D.Y. Wu, Appl. Catal. Catal. A 281 (2005) 233−236.
[6] J.C. Amphlett, M.J. Evans, R.A. Jones, R.F. Mann, R.D. Weir, Can. J. Chem. Eng. 59 (1981) 720.
[7] B. Emonts, J.B. Hansen, S.L. Jorgensen, B. Hohlein, R. Peters, J. Power Sources 71 (1998) 288−293.
[8] J.P. Shen, C.S. Song, Catal. Today 77 (2002) 89−98.
[9] H. Friedrich, W. Neugebauer, US Patent 3 843 562 (1974).
[10] S. Satoh, Y. Tanigawa, US Patent 6 379 507 (2002).
[11] Y. Yuan, H. Liu, H. Imoto, T. Shido, Y. Iwasawa, J. Catal. 195 (2000) 51−61.
[12] Y. Yuan, Y. Iwasawa, J. Phys. Chem. B 106 (2002) 4441−4449.
[13] H. Liu, N. Bayat, E. Iglesia, Angew. Chem. Int. Ed. 42 (2003) 5072−5075.
[14] H. Liu, E. Iglesia, J. Phys. Chem. B 109 (2005) 2155−2163.
[15] Y. Zhang, I.J. Drake, D.N. Briggs, A.T. Bell, J. Catal. 244 (2006) 219−229.
[16] G. Busca, J. Lamotte, J.C. Lavalley, V. Lorenzelli, J. Am. Chem. Soc. 109 (1987) 5197.
[17] G. Busca, Catal Today 27 (1996) 457−496.
[18] J.M. Tatibouët, Appl. Catal. A 148 (1997) 213−252.
[19] P. Forzatti, K. Fujimoto, M. Miyauchi, H. Tominaga, Appl. Catal A 157 (1997) 387−408.
[20] G.T. Went, L.J. Leu, A.T. Bell, J. Catal. 134 (1992) 479−491.
[21] M.D. Amiridis, I.E. Wachs, G. Deo, J.M. Jehng, D.S. Kim, J. Catal. 161 (1996) 247−253.
[22] S. Royer, X. Sécordel, M. Brandhorst, F. Dumeignil, S. Cristol, C. Dujardin, M. Capron, E. Payen, J.L. Dubois, Chem. Commun., 7 (2008) 865−867.
[23] Y. Fu, J. Shen, Chem. Commun., 21 (2007) 2172−2174.
[24] L. Kong, Z. Liu, M. Shao, Q.Xie, W. Yu, Y. Qian, J. Solid State Chem. 177 (2004) 690.
[25] H. Zhao, S. Bennici, J. Shen, A. Auroux, Appl. Catal. A 356 (2009) 121−128.
[26] A. Auroux, Top. Catal. 4 (1997) 71−89.
[27] A. Auroux, Top. Catal. 19 (2002) 205−213.
[28] P. Malet, A. Caballero, J. Chem. Soc., Faraday Trans. I 84 (1988) 2369−2375.
[29] D.A.M. Monti, A. Baiker, J. Catal. 83 (1983) 323−335.

4. Published Results

Publication I

Catal Lett (2008) 126:155–163
DOI 10.1007/s10562-008-9598-y

Preparation of Mesoporous V–Ce–Ti–O for the Selective Oxidation of Methanol to Dimethoxymethane

Jingwei Liu · Qing Sun · Yuchuan Fu · Hongying Zhao · Aline Auroux · Jianyi Shen

Received: 30 April 2008 / Accepted: 22 July 2008 / Published online: 5 September 2008

Abstract Mesoporous V–Ce–Ti–O oxides were synthesized through the combination of sol–gel and hydrothermal methods and were characterized by different techniques. N_2 adsorption showed that the mesoporous oxides with 0–20 wt.% V_2O_5 possessed the surface areas of about 160 $m^2\ g^{-1}$ with narrow pore size distribution centered around 4–5 nm. Vanadium species were highly dispersed in the samples, as confirmed by the wide angle XRD and Raman spectroscopy. The surface acidity of the materials was determined by the microcalorimetric adsorption of NH_3. Temperature programmed reduction and O_2 chemisorption were used to probe the redox property of the materials. It was found that the mesoporous V–Ce–Ti–O possessed bifunctional characters of acidic and redox properties that catalyzed the oxidation of methanol to dimethoxymethane (DMM). These bifunctional characters were further enhanced by the addition of V_2O_5 and SO_4^{2-} onto V–Ce–Ti–O simultaneously. Such supported catalysts exhibited excellent performance for the selective oxidation of methanol to DMM. Specifically, 72% conversion of methanol with 85% selectivity to DMM was achieved at 423 K over a SO_4^{2-}–V_2O_5/V–Ce–Ti–O catalyst.

J. Liu · Q. Sun · Y. Fu · H. Zhao · J. Shen (✉)
Lab of Mesoscopic Chemistry, School of Chemistry and Chemical Engineering, Nanjing University, Nanjing 210093, China
e-mail: jyshen@nju.edu.cn

H. Zhao · A. Auroux
Institut de Recherches sur la Catalyse et l'Environnement de Lyon, UMR 5256, CNRS-Université Lyon 1, 2 Avenue Albert Einstein, 69626 Villeurbanne Cedex, France

Keywords Mesoporous V–Ce–Ti–O · Surface acidity · Surface redox property · Oxidation of methanol · Synthesis of dimethoxymethane

1 Introduction

V_2O_5/TiO_2 catalysts are extensively studied in various reactions such as selective oxidation of methanol to formaldehyde [1] and methyl formate [2], selective oxidation of aromatic compounds to aromatic aldehydes [3], selective oxidation of olefins to phthalic anhydride [4], ammoxidation of aromatic hydrocarbons [5] and selective catalytic reduction of NO_X [6]. It is generally true that the V_2O_5/TiO_2 with higher surface areas may work better since more vanadia species could be dispersed on the surface to act as active sites [7]. However, TiO_2 usually exhibits a moderate surface area of about 50 $m^2\ g^{-1}$ (e.g., Degussa P25) [1, 2]. Although mesoporous titanium oxides may provide a higher surface area to support more VO_x species, these materials were usually not thermally stable [8]. The surface areas of these materials might be greatly decreased upon the calcination at temperatures higher than 673 K. Doping with rare earth elements was proved to be an effective way to enhance the thermal stability of mesoporous materials [9, 10], in which cerium was recently reported as an excellent dopant in mesoporous titania [9]. In addition, cerium is known as an essential component for three-way catalysts (TWC) due to its oxygen storage capability. It also plays positive synergetic roles in some catalytic systems [11]. Therefore, Ce doped mesoporous titania might be used as supports for a variety of oxidation reactions.

Among the aforementioned reactions, the oxidation of methanol has been widely used as a probe reaction to

characterize the activity of oxide catalysts and to correlate the structures and surface acidic and redox properties [12]. It has been reported that methanol could be converted to dimethyl ether (DME) on acidic surface, to formaldehyde (FA) and methyl formate (MF) on oxidative surface, and to dimethoxymethane (DMM) on acidic and oxidative bifunctional surfaces [12].

In this work, mesoporous V–Ce–Ti–O materials were first synthesized through the combination of sol–gel and hydrothermal methods, and were characterized by X-ray diffraction (XRD), N_2 adsorption, transmission electron microscopy (TEM), O_2 chemisorption, laser Raman spectroscopy (LRS), temperature programmed reduction (TPR), and microcalorimetric adsorption of ammonia. The surface redox and acidic properties of the V–Ce–Ti–O could be enhanced by the addition of V_2O_5 and SO_4^{2-}. These materials were tested for the selective oxidation of methanol to DMM.

2 Experimental

2.1 Preparation of Samples

Mesoporous Ce–Ti–O has been synthesized by Yue and Gao [9]. In this work, mesoporous V–Ce–Ti–O materials were synthesized via the combination of sol–gel and conventional hydrothermal methods. In a typical procedure, 5.48 g P123 (triblock copolymer pluronic) and 0.89 g $CeCl_3 \cdot 7H_2O$ were dissolved in 25 mL absolute ethanol, and then 16.10 g titanium butoxide (TBOT) was added under vigorous stirring. Desired amounts of V_2O_5 were added into a mixed solution of 17.8 mL ethanol and 30% H_2O_2 under constant stirring, until V_2O_5 was completely dissolved. The molar ratio of V_2O_5/H_2O_2 was 0.22. Then, the solution containing vanadium was added dropwise into the solution containing titanium precursor at room temperature. The mixed solution formed was clear at first, and then became a gel in 10 min. A sample 20V–Ti–O without cerium cations was also prepared for comparison. A precipitate (no gel) was formed without the presence of cerium cations. The gel (or precipitate) together with 70 mL distilled water was subsequently transferred into a Teflon-lined autoclave and kept at 393 K for 24 h. Afterwards, the gel (or precipitate) was filtered, washed with deionized water and ethanol and dried at room temperature for 12 h. The samples were then calcined at 673 K for 5 h in air (temperature ramped at 1 K min^{-1}). The samples Ce–Ti–O, 10V–Ce–Ti–O, 20V–Ce–Ti–O, 40V–Ce–Ti–O and 20V–Ti–O prepared this way contained about 0, 10, 20, 40 and 20% V_2O_5 (wt.%), respectively.

The V_2O_5/V–Ce–Ti–O, SO_4^{2-}/V–Ce–Ti–O and SO_4^{2-}–V_2O_5/V–Ce–Ti–O samples were prepared by using the incipient wetness impregnation method. Specifically, for each preparation, a known amount of above mentioned V–Ce–Ti–O oxide was added into the aqueous solution containing the desired amount of vanadium oxalate and/or $Ti(SO_4)_2$ and stirred. After being kept at room temperature overnight, the impregnated samples were dried at 373 K and then calcined in air at 673 K for 5 h.

2.2 Characterization

Low angle and wide angle powder X-ray diffraction patterns were collected on the Philips X'Pert Pro diffractometer using Ni-filtered Cu Kα radiation ($\lambda = 0.15418$ nm), operated at 40 kV and 40 mA. Nitrogen adsorption–desorption isotherms were measured at liquid nitrogen temperature using a Micromeritics ASAP 2020. Prior to a measurement, the sample was degassed to 10^{-3} Torr at 573 K for 4 h. Pore size distribution and pore volume were calculated by the BJH method according to the desorption isotherm branch. Elemental analysis was performed on an ARL-9800 X-ray fluorescence spectrometer. TEM images were obtained from a JEOL JEM 2100 transmission electronic microscope with an accelerating voltage of 200 kV. The samples were dispersed in ethanol under ultrasonic conditions and deposited onto copper grids coated with ultrathin carbon films. Laser Raman spectra were acquired on a Renishaw inVia Raman microscope with the 514.5 nm line of an Ar ion laser as the excitation source of about 2 mW. Spectra were recorded with 1 cm^{-1} resolution and 20 scans.

The dispersion of vanadium species was measured by using the high temperature oxygen chemisorption method (HTOC). About 0.1–0.2 g sample was reduced in flowing H_2 (40 mL min^{-1}) at 640 K for 2 h, and evacuated at the same temperature for 0.5 h. Oxygen uptake was measured at 640 K.

Microcalorimetric adsorption of ammonia was performed at 423 K by using a Tian-Calvet type heat flux Setaram C80 calorimeter. The calorimeter was connected to a volumetric system equipped with a Baratron capacitance manometer for the pressure measurement and gas handling. About 0.1 g sample was pretreated in 500 Torr O_2 at 573 K for 1 h, followed by evacuation at the same temperature for 1 h. The probe molecule ammonia was purified with the successive freeze-pump-thaw cycles.

TPR measurements were carried out in a continuous mode using a U-type quartz micro-reactor (3.5 mm inner diameter). A sample of about 50 mg was contacted with a H_2:N_2 mixture (5.13% volume of H_2 in N_2) at a total flow rate of 40 mL min^{-1}. The sample was heated at a rate of 10 K min^{-1} from room temperature to 1250 K. The hydrogen consumption was monitored using a thermal conductivity detector (TCD).

2.3 Catalytic Reactions

The reaction of selective oxidation of methanol was carried out at atmospheric pressure in a fixed-bed micro-reactor (glass) with an inner diameter of 6 mm. Methanol was introduced into the reaction zone by bubbling O_2/N_2 (1/5) through a glass saturator filled with methanol (99.9%) maintained at 278 K. In each test, 0.2 g of catalyst was loaded, and the gas hourly space velocity (GHSV) was 11400 mL g^{-1} h^{-1}. The feed composition was maintained as methanol: O_2:N_2 = 1:3:15 (v/v). Methanol, DMM, formaldehyde and other organic compounds were analyzed by using a GC equipped with FID and TCD detectors connected to Porapak N columns. CO and CO_2 were detected by using another GC with a TCD connected to a TDX-01 column. The gas lines were kept at 373 K to prevent condensation of reactants and products.

3 Results and Discussion

3.1 Structure Characterization

Figure 1 presents the low angle XRD patterns of V–Ce–Ti–O samples. Only a single broad peak was observed for the samples with the content of V_2O_5 lower than 20%, indicating the mesostructure that lacked of long range order [13–15]. The intensity of this peak decreased gradually with the increase of V_2O_5 content, suggesting the increased disordered structures of the samples.

Figure 2 shows the wide angle XRD patterns for the V–Ce–Ti–O oxides. The diffraction peaks due to anatase were observed for all the samples. No other diffraction peaks were observed for the V–Ce–Ti–O samples with 0–20% of V_2O_5,

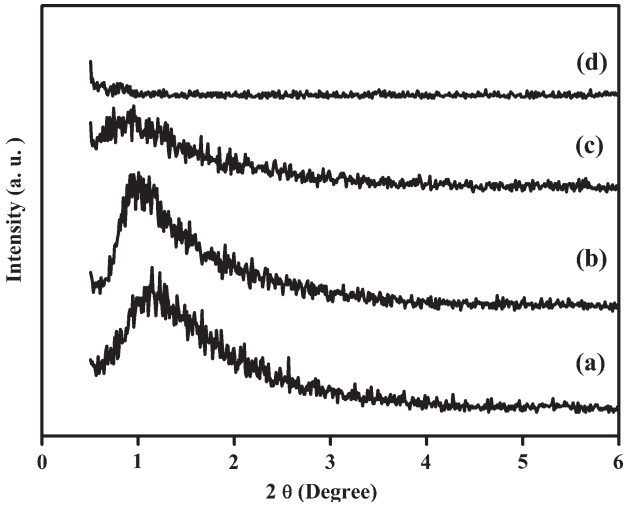

Fig. 1 Low angle XRD patterns of (**a**) Ce–Ti–O, (**b**) 10V–Ce–Ti–O, (**c**) 20V–Ce–Ti–O and (**d**) 40V–Ce–Ti–O

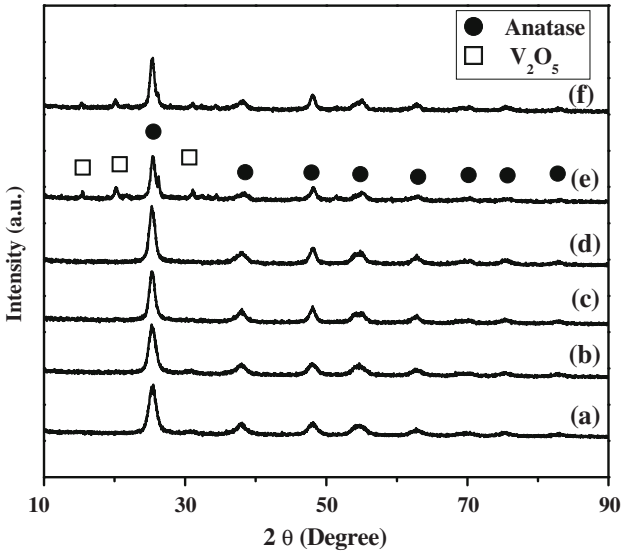

Fig. 2 Wide angle XRD patterns of (**a**) Ce–Ti–O, (**b**) 10V–Ce–Ti–O, (**c**) 10V/10V–Ce–Ti–O, (**d**) 20V–Ce–Ti–O, (**e**) 20V–Ti–O and (**f**) 40V–Ce–Ti–O

indicating that vanadia and ceria species were highly dispersed in the oxides. In the sample with 40% V_2O_5, weak diffraction peaks of crystalline V_2O_5 appeared, suggesting the occurrence of agglomeration of vanadia species. Crystalline V_2O_5 was also observed for the 20V–Ti–O without the presence of cerium. The 10V–Ce–Ti–O was used to support additional 10% V_2O_5, and the resulted 10V/10V–Ce–Ti–O displayed only the diffraction peaks of anatase, indicating the highly dispersed V_2O_5 on the surface of 10V–Ce–Ti–O. Figure 3 shows the nitrogen adsorption–desorption isotherms and corresponding BJH pore size distributions for the V–Ce–Ti–O oxides. The surface areas and pore parameters are summarized in Table 1. All the oxides prepared exhibited typical IV nitrogen isotherms, characteristic of mesoporous materials, according to the IUPAC classification [16]. Narrow pore size distributions were derived from the hysteresis loops as seen in the inserts of Fig. 3. The surface area, average pore size and pore volume for the Ce–Ti–O were found to be 160 m^2 g^{-1}, 5.2 nm and 0.3 cm^3 g^{-1}, respectively. With the incorporation of less than 20% V_2O_5, the surface areas of the formed V–Ce–Ti–O oxides changed little, while pore sizes and pore volumes decreased apparently. Further increase of V_2O_5 to 40% led to the significantly decreased surface area (62 m^2 g^{-1}) and increased pore size (12.7 nm). The surface area of the 20V–Ti–O (91 m^2 g^{-1}) was much lower than that of the corresponding 20V–Ce–Ti–O (159 m^2 g^{-1}), suggesting that cerium might play an important role in maintaining the thermal stability of the V–Ce–Ti–O oxides. Such effect of cerium was also reported by Radwan et al. [17]. Addition of 10% V_2O_5 on the 10V–Ce–Ti–O decreased the surface areas to about 130 m^2 g^{-1} and increased the pore sizes to about 7 nm. Simultaneous addition of V_2O_5 and SO_4^{2-} resulted in a

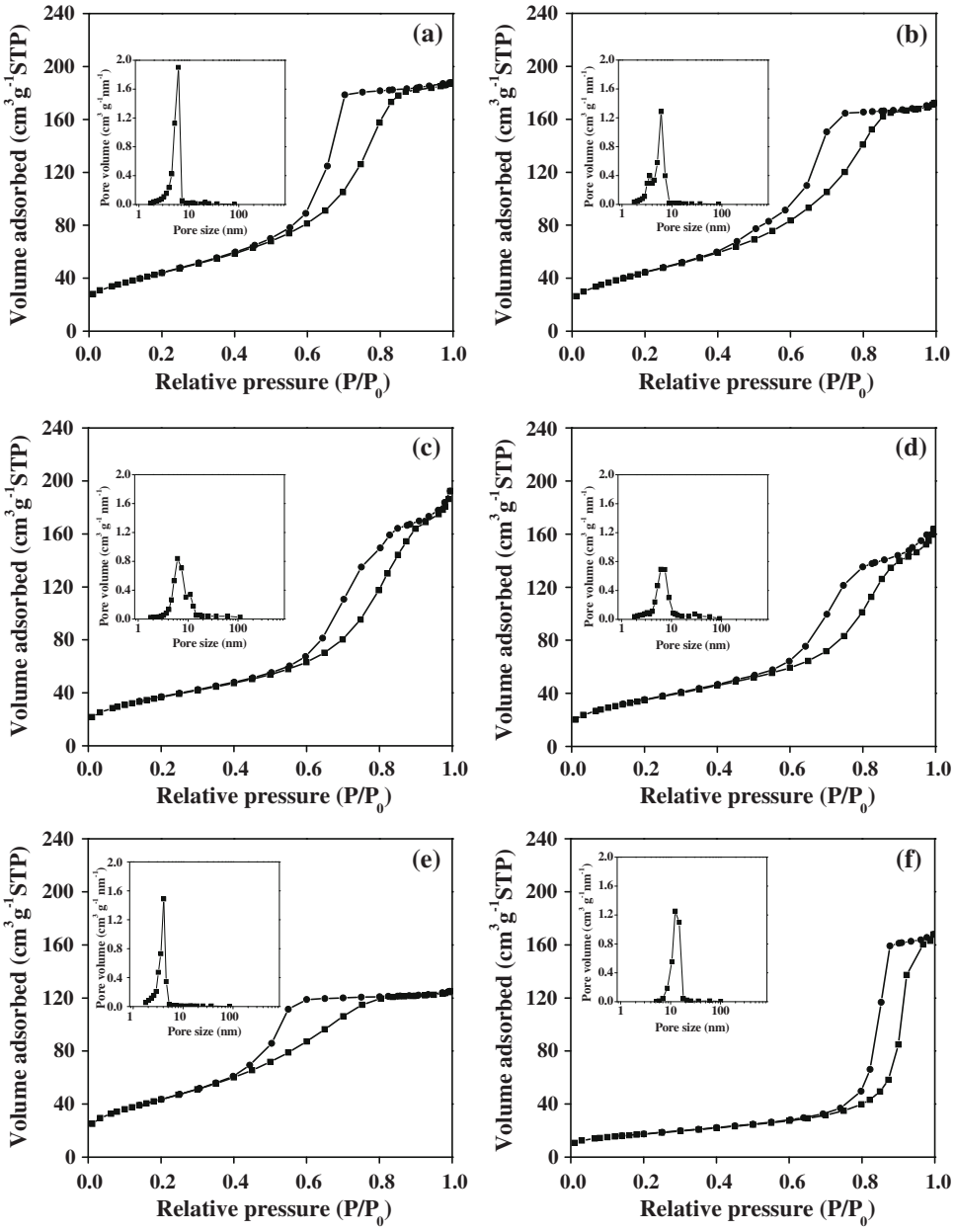

Fig. 3 Nitrogen adsorption–desorption isotherms and pore size distributions for (**a**) Ce–Ti–O, (**b**) 10V–Ce–Ti–O, (**c**) 10V/10V–Ce–Ti–O, (**d**) $5SO_4^{2-}$–10V/10V–Ce–Ti–O, (**e**) 20V–Ce–Ti–O and (**f**) 40V–Ce–Ti–O

Table 1 Surface areas, pore parameters and O_2 uptakes for the V–Ce–Ti–O samples

Sample	S_{BET} (m^2 g^{-1})	Pore size (nm)	Pore volume (cm^3 g^{-1})	O_2 uptake (μmol g^{-1})	V density calculated (V nm^{-2})
Ce–Ti–O	160	5.2	0.30	6	–
10V–Ce–Ti–O	162	5.0	0.27	534	4.0
20V–Ce–Ti–O	159	3.6	0.20	990	7.4
20V–Ti–O	91	8.4	0.31	861	11.3
40V–Ce–Ti–O	62	12.7	0.26	1516	29.4
10V/10V–Ce–Ti–O	134	7.2	0.30	870	7.8
$5SO_4^{2-}$–10V/10V–Ce–Ti–O	128	7.4	0.26	894	8.4

sample $5SO_4^{2-}$–10V/10V–Ce–Ti–O with the similar surface area and pore size as the 10V/10V–Ce–Ti–O.

The TEM images of 10V–Ce–Ti–O, 10V/10V–Ce–Ti–O and $5SO_4^{2-}$–10V/10V–Ce–Ti–O are shown in Fig. 4. No long range ordered structures were observed for the samples. Small particles (around 7 nm) with uniform size distribution were clearly seen for the 10V–Ce–Ti–O. Addition of 10% V_2O_5 only and simultaneous addition of 10% V_2O_5 and 5% SO_4^{2-} increased the particle size to about 10 nm. The mesoporosity of the V–Ce–Ti–O oxides was mainly due to the inter-particle voids.

The Raman spectra of the V–Ce–Ti–O oxides are presented in Fig. 5. It is well known that the bands around 149, 199, 408, 528 and 645 cm^{-1} are characteristic of anatase, whereas the bands around 144, 148, 611 cm^{-1} are ascribed to rutile phase [18]. Thus, all the V–Ce–Ti–O oxides studied in this work exhibited typical Raman features of anatase. No rutile phase was observed. Bulk CeO_2 usually exhibits a strong band at 460 cm^{-1} due to the F_{2g} Raman active mode characteristic of fluorite-structured materials [19]. The absence of the Raman line due to CeO_2 for all the V–Ce–Ti–O samples indicated the highly dispersed Ce^{4+} cations in the lattice of the samples, similar to the system of Ce–Ti–Cu–O oxides [20]. Additional Raman features around 800–1200 cm^{-1} observed are due to the different surface vanadia species. Only the Raman signals due to highly dispersed vanadia species were observed for the samples with V_2O_5 less than 40%. Specifically, the bands around 1024–1030 cm^{-1} could be assigned to isolated monomeric (or oligomeric) terminal V=O species [21], while the bands around 940 cm^{-1} and 830 cm^{-1} are characteristic of polymeric V–O–V species [22] and octahedral decavanadate species $V_{10}O_{28}$ [5, 23] (or isolated VO_4^{3-} tetrahedral structure [24]), respectively. When V_2O_5 reached 40%, a clear band at 999 cm^{-1} corresponding to V=O symmetric stretching vibration of crystalline V_2O_5 was discerned, indicating the formation of crystalline V_2O_5. Addition of 10% V_2O_5 onto the 10V–Ce–Ti–O did not result in new Raman features as compared with those of 10V–Ce–Ti–O, suggesting again that the additional V_2O_5 was highly dispersed on the 10V–Ce–Ti–O, in accordance with XRD results. In addition, the modification of SO_4^{2-} on the 10V/10V–Ce–Ti–O did not influence the dispersion of vanadia species (spectrum not shown).

3.2 Surface Redox and Acidic Properties

The adsorption of O_2 has been used to evaluate the dispersion of supported V_2O_5 [25–27]. Parekh and Weller [25, 26] proposed a low temperature oxygen adsorption method (LTOC) while Oyama et al. suggested a high temperature oxygen adsorption method (HTOC) [27].

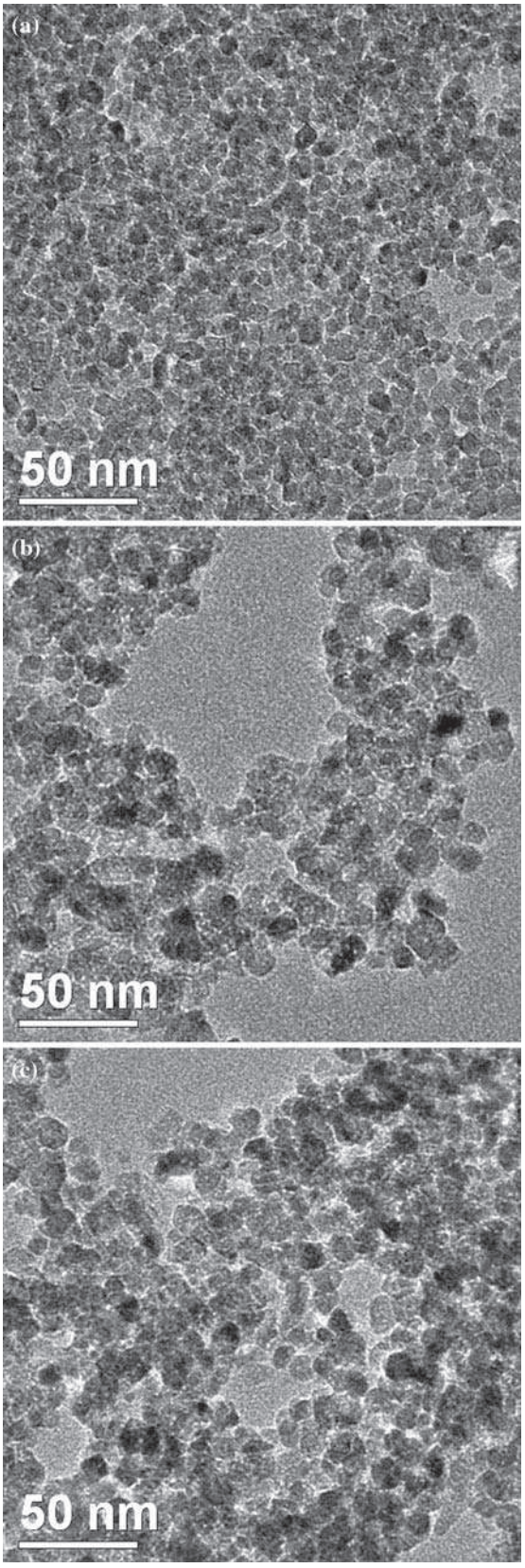

Fig. 4 Transmission electron microscopy (TEM) images of (**a**) 10V–Ce–Ti–O, (**b**) 10V/10V–Ce–Ti–O and (**c**) $5SO_4^{2-}$–10V/10V–Ce–Ti–O

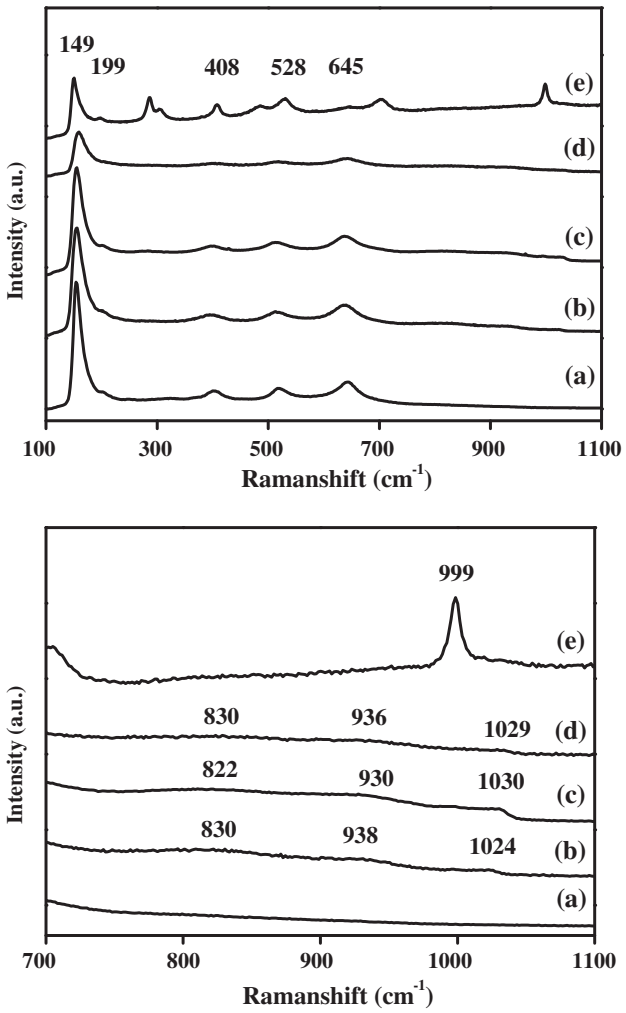

Fig. 5 Raman spectra of (**a**) Ce–Ti–O, (**b**) 10V–Ce–Ti–O, (**c**) 10V/10V–Ce–Ti–O, (**d**) 20V–Ce–Ti–O and (**e**) 40V–Ce–Ti–O

It was suggested that the HTOC might exert less possibility of bulk reduction and sintering [28], and we used the technique to estimate roughly the dispersion of vanadium species. In this technique, the samples were first reduced in H_2 at 640 K, at which only surface vanadium species were supposedly reduced [27]. O_2 adsorption was then performed at 640 K to titrate the number of reduced vanadium cations on the surface with the ratio of O/V = 1.

Table 1 gives the O_2 uptakes and corresponding V densities for the different V–Ce–Ti–O oxides. It is seen that the Ce–Ti–O did not seem to adsorb O_2 (6 μmol g^{-1} only), indicating that little species could be reduced in the sample (or non-redox). The incorporation of vanadium species increased the O_2 uptakes. Since the Ce–Ti–O almost did not adsorb O_2, O_2 was mainly adsorbed on vanadium species in the V–Ce–Ti–O samples. Wachs [29] reported that the theoretical density for the monolayerly dispersed vanadium species on TiO_2 was 7.9 V nm^{-2}. Since the 10V–Ce–Ti–O possessed 9.6% V_2O_5 (measured by XRF, see Table 2) and the surface area of 162 m^2 g^{-1}, the density of vanadium species was calculated to be 3.9 V nm^{-2}, lower than the monolayer capacity. The surface density of vanadium as titrated by O_2 adsorption for the sample was 4.0 V nm^{-2}, almost same as the amount of vanadium contained in the sample. This implied that all the vanadium species in the 10V–Ce–Ti–O sample were titrated by the O_2 adsorption at 640 K. Similarly, the 20V–Ce–Ti–O and 10V/10V–Ce–Ti–O contained vanadium species of 7.5 and 9.0 V nm^{-2}, according to their surface areas in Table 1 and the contents of V_2O_5 in Table 2. The titrated surface densities of vanadium in the two samples were 7.4 and 7.8 V nm^{-2}, respectively, suggesting again that the O_2 adsorption at 640 K titrated most of the vanadium species in the samples. The content of V_2O_5 in the 40V–Ce–Ti–O was not measured. Supposing it contained 40% V_2O_5 with the surface area of 62 m^2 g^{-1}, the density of vanadium was calculated to be 42.7 V nm^{-2}. The surface density of vanadium for this sample as titrated by O_2 adsorption was 29.8 V nm^{-2}, much greater than the monolayer dispersion capacity (7.9 V nm^{-2}), indicating that the HTOC technique did titrate sublayers of vanadia species. Without the presence of Ce, the 20V–Ti–O exhibited lower surface

Table 2 Selective oxidation of methanol over different catalysts at 423 K

Catalyst	Content[a] (wt.%)			Conv. (%)	Selectivity (%)			
	Ce	V_2O_5	SO_4^{2-}		DMM[b]	FA[b]	MF[b]	DME[b]
Ce–Ti–O	1.6	–	–	0.9	0	0	0	100
10V–Ce–Ti–O	1.5	9.6	–	12	62	22	16	0
20V–Ce–Ti–O	1.1	18.0	–	31	26	22	51	1
20V–Ti–O	–	–	–	22	48	40	11	1
2.5SO_4^{2-}/20V–Ce–Ti–O	1.0	17.8	2.5	40	91	1	7	1
10V/10V–Ce–Ti–O	1.3	18.2	–	29	52	18	29	1
5SO_4^{2-}–10V/10V–Ce–Ti–O	1.3	17.7	5.5	72	85	0	14	1

[a] The contents of Ce, V_2O_5 and SO_4^{2-} were measured by XRF

[b] DMM = dimethoxymethane; FA = formaldehyde; DME = dimethyl ether; MF = methyl formate

area as compared to the 20V–Ce–Ti–O, leading to the lower O_2 uptake and lower dispersion of vanadium species.

Temperature programmed reduction (TPR) is a technique usually used to characterize the reducibility of various metal oxides or supported catalysts. Figure 6 shows the TPR profiles of different V–Ce–Ti–O samples. No TPR peaks were observed for the Ce–Ti–O, indicating the non-redox feature of the sample, consistent with the result of O_2 adsorption. Two TPR peaks can be seen for the 10V–Ce–Ti–O around 775 and 797 K, which might be ascribed to the reduction of monomeric and polymeric surface VO_x species from V^{5+} to V^{3+} [30, 31]. These two peaks shifted to higher temperatures with the increase of vanadia content. Addition of 10% V_2O_5 on the 10V–Ce–Ti–O did not seem to change the TPR profile, but increased the peak intensities. Bulk V_2O_5 displayed a completely different reduction feature, which has been discussed thoroughly before [32]. The significantly lower reduction temperatures for the V–Ce–Ti–O than for bulk V_2O_5 suggested the enhanced reducibility (or redox ability) of the V–Ce–Ti–O samples.

Microcalorimetric adsorption of ammonia has been used to determine the number, strength and strength distribution of surface acidities [33]. Differential heats versus coverage for NH_3 adsorption on the V–Ce–Ti–O samples are depicted in Fig. 7. The Ce–Ti–O exhibited the initial adsorption heat of 151 kJ mol^{-1} with NH_3 saturation coverage of 2.6 μmol m^{-2}. The incorporation of V into the Ce–Ti–O enhanced the surface acidity since both the initial heat and saturation coverage of NH_3 increased. Specifically, the initial heat and ammonia coverage increased to 183 kJ mol^{-1} and 4 μmol m^{-2}, respectively, for the 10V–Ce–Ti–O. Addition of SO_4^{2-} into V–Ce–Ti–O also increased the surface acidity. For example, addition of 2.5% SO_4^{2-} into the 20V–Ce–Ti–O increased the initial heat from 158 to 173 kJ mol^{-1} and the saturation coverage of ammonia from 3.5 to 4.4 μmol m^{-2}. However, when more SO_4^{2-} (5.5%) was added into the 10V/10V–Ce–Ti–O, much lower initial heat (15 kJ mol^{-1}) was measured, due to the endothermic interaction of ammonia with polymerized surface sulfates. Similar phenomenon was also reported by Desmartin-Chomel et al. for the sulfated titania, and the existence of polymerized sulfate species were observed by FTIR [34]. Thus, the initial heat of ammonia adsorption for the samples with high contents of SO_4^{2-} cannot be used as an indication of strength of surface acidity. However, it is clear that the density of acid sites as determined by the adsorption of ammonia was significantly higher for the 5% SO_4^{2-}–10V/10V–Ce–Ti–O (4.6 μmol m^{-2}) than for the 10V/10V–Ce–Ti–O (3.9 μmol m^{-2}). The sample SO_4^{2-}/20V–Ce–Ti–O with 2.5% SO_4^{2-} did not show the decreased initial heat. This might be an indication that no polymerized surface sulfates were formed in the $2.5SO_4^{2-}$/20V–Ce–Ti–O [34].

Infrared spectroscopy for ammonia adsorption is a frequently used tool to probe the surface acidity (Brønsted and Lewis sites). The FTIR spectra of adsorbed NH_3 for the V–Ce–Ti–O samples are presented in Fig. 8. The Ce–Ti–O

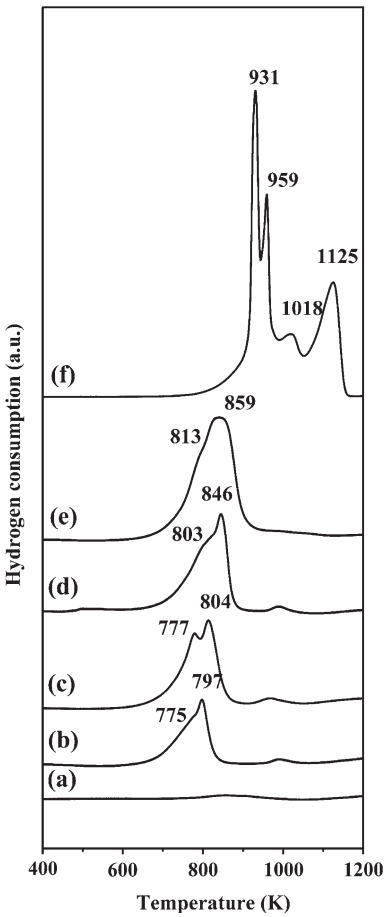

Fig. 6 TPR profiles of (**a**) Ce–Ti–O, (**b**) 10V–Ce–Ti–O, (**c**) 10V/10V–Ce–Ti–O, (**d**) 20V–Ce–Ti–O, (**e**) 40V–Ce–Ti–O and (**f**) V_2O_5

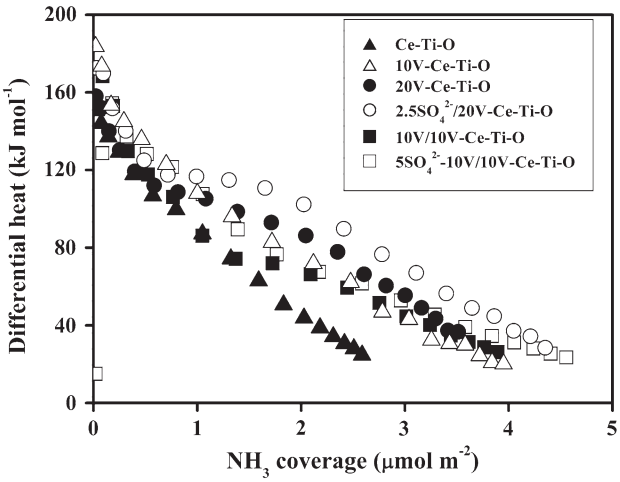

Fig. 7 Differential heat versus coverage for NH_3 adsorption at 423 K over the V–Ce–Ti–O catalysts

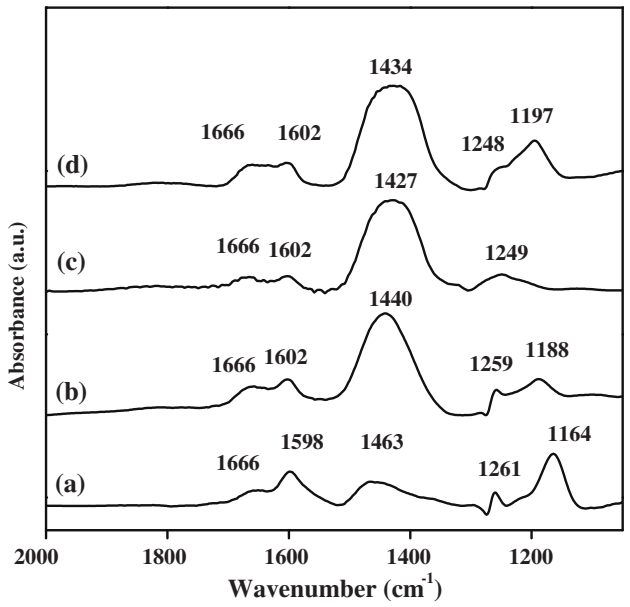

Fig. 8 FTIR spectra for NH_3 adsorption on (**a**) Ce–Ti–O, (**b**) 10V–Ce–Ti–O, (**c**) 10V/10V–Ce–Ti–O and (**d**) $5SO_4^{2-}$–10V/10V–Ce–Ti–O collected at room temperature

exhibited the bands at 1598, 1261 and 1164 cm^{-1}, belonging to NH_3 coordinately adsorbed on Lewis acid sites [34]. The bands at 1666 and 1463 cm^{-1} were related to the adsorbed NH_3 on Brønsted acid sites [34]. Figure 8 shows that the Ce–Ti–O possessed mainly Lewis acidity with only weak Brønsted acidity. The incorporation of 10% V_2O_5 into Ce–Ti–O greatly enhanced the Brønsted acidity, as illustrated by the increased intensity around 1440 cm^{-1}. The enhanced surface Brønsted acidity might be created by the hydroxyl groups on the vanadia species in the 10V–Ce–Ti–O. The Lewis acidity with the band around 1164–1188 cm^{-1} due to the surface of Ce–Ti–O was still seen in the 10V–Ce–Ti–O. This band disappeared when additional 10% V_2O_5 was added into the 10V–Ce–Ti–O, probably due to the covering of Ce–Ti–O surface by dispersed V_2O_5. The band around 1249 cm^{-1} could be ascribed to the Lewis sites on the surface of dispersed V_2O_5. Further addition of 5% SO_4^{2-} on the 10V–Ce–Ti–O did not seem to increase the surface Brønsted acidity. In stead, a band around 1197 cm^{-1} appeared, which was owing to the Lewis acidic sites generated upon the addition of sulfate. The generation of Lewis acid sites due to the addition of sulfate on TiO_2 has been reported elsewhere [34].

3.3 Selective Oxidation of Methanol to Dimethoxymethane

Methanol and its derivatives have been widely studied due to their industrial importance [12]. In addition, the catalytic oxidation of methanol is a convenient structure-sensitive reaction, which has been widely used to characterize the surfaces of metal oxides for their acid/base and redox properties [12, 35]. The results for the conversion of methanol over the Ce–Ti–O and V–Ce–Ti–O catalysts under oxidative atmosphere were given in Table 2.

The data in Table 2 showed that the conversion of methanol was very low (0.9%) over the Ce–Ti–O at 423 K. The only product was DME. This is due to that the Ce–Ti–O was lack of redox property, as evidenced by the results of O_2 adsorption and TPR. Incorporation of V into Ce–Ti–O drastically improved the activity of selective oxidation of methanol. For example, the conversion of methanol on the 10V–Ce–Ti–O was 12% with DMM as the main product (62%). The increased activity and selectivity to DMM were due to the enhanced surface acidic and redox properties of the V–Ce–Ti–O. The 20V–Ce–Ti–O sample exhibited higher methanol conversion and higher selectivity to MF than the 10V–Ce–Ti–O. The 20V–Ti–O exhibited lower methanol conversion than the 20V–Ce–Ti–O and produced more formaldehyde. Addition of 2.5% SO_4^{2-} into the 20V–Ce–Ti–O increased the conversion of methanol from 31 to 40% and the selectivity to DMM from 26 to 91%, owing to the enhanced surface acidity. It has been reported that the selective oxidation of methanol to DMM might involve two steps: (1) oxidation of methanol to formaldehyde on redox sites and (2) condensation of formaldehyde produced with additional methanol to DMM on acidic sites. Thus, the strengths of surface acidity and redox ability of a catalyst were two important aspects in determining the selective oxidation of methanol to DMM [36–40].

Addition of V_2O_5 and SO_4^{2-} onto V–Ce–Ti–O enhanced further the surface redox and acidic properties. For example, the addition of 10% V_2O_5 onto 10V–Ce–Ti–O increased the conversion of methanol from 12 to 29% and the selectivity to MF from 16 to 29%, due to the enhanced surface redox ability. Further addition of 5.5% SO_4^{2-} increased the conversion of methanol from 29 to 72% and the selectivity to DMM from 52 to 85%, owing to the enhanced surface acidity. The selectivity of DMM was quite high (85%) over the SO_4^{2-}–10V/10V–Ce–Ti–O, even at high conversion of methanol (72%). This result appears promising for the industrial application. Thus, we demonstrated in this work that the mesoporous V–Ce–Ti–O oxides could act as the appropriate supports for V_2O_5 and SO_4^{2-} to achieve the excellent performance for the selective oxidation of methanol to DMM.

4 Conclusion

Mesoporous V–Ce–Ti–O materials were successfully synthesized via a combination of sol–gel and hydrothermal methods, which possessed the surface areas of about 160 $m^2\ g^{-1}$ and pore sizes of about 4–5 nm. Such

materials exhibited weak surface acidity and redox ability that could be significantly enhanced by the addition of V_2O_5 and SO_4^{2-} simultaneously on the surface, leading to the bi-functional catalysts with strong acidic and redox characters that favored the selective oxidation of methanol to dimethoxymethane. Specifically, the 5% SO_4^{2-}–10% V/10% V–Ce–Ti–O exhibited the excellent performance for the selective oxidation of methanol to DMM. The conversion of methanol reached 72% over the 5% SO_4^{2-}–10% V/10% V–Ce–Ti–O with 85% selectivity to DMM at 423 K.

Acknowledgment We acknowledge the financial supports from NSFC (20673055) and MSTC (2004DFB02900 and 2005CB221400).

References

1. Roozeboom F, Cordingley PD, Gellings PJ (1981) J Catal 68:464
2. Elmi AS, Tronconi E, Cristiani C, Gomez Martin JP, Forzatti P, Busca G (1989) Ind Eng Chem Res 28:387
3. Maurya SK, Patil P, Umbarkar SB, Gurjar MK, Dongare M, Rudiger S, Kemnitz E (2005) J Mol Catal A 234:51
4. Cavani F, Cortelli C, Frattini A, Panzacchi B, Ravaglia V, Trifiro F, Fumagalli C, Leanza R, Mazzoni G (2006) Catal Today 118:298
5. Sanati M, Andersson A (1990) J Mol Catal 59:233
6. Mutin PH, Popa AF, Vioux A, Delahay G, Coq B (2006) Appl Catal B 69:49
7. Shyue JJ, De Guire MR (2005) J Am Chem Soc 127:12736
8. Yang P, Zhao D, Margolese DI, Chmelka BF, Stucky GD (1998) Nature 396:152
9. Yue Y, Gao Z (2000) Chem Commun 1755
10. Severin KG, Abdel-Fattah TM, Pinnavaia TJ (1998) Chem Commun 1471
11. Terribile D, Llorca J, Boaro M, de Leitenburg C, Dolcetti G, Trovarelli A (1998) Chem Commun 1897
12. Tatibouet JM (1997) Appl Catal A 148:213
13. Luo H, Wang C, Yan Y (2003) Chem Mater 15:3841
14. Kartini I, Menzies D, Blake D, da Costa JCD, Meredith P, Riches JD, Lu GQ (2004) J Mater Chem 14:2917
15. Khushalani D, Ozin GA, Kuperman A (1999) J Mater Chem 9:1491
16. Gregg SJ, Sing KS (1982) Adsorption, surface area and porosity. Academic Press, New York
17. Radwan NRE, Fagal GA, El-Shobaky GA (2001) Colloids Surf A 178:277
18. Kosmulski M (2002) Adv Colloid Interface Sci 99:255
19. Reddy BM, Khan A, Yamada Y, Kobayashi T, Loridant S, Volta JC (2003) J Phys Chem B 107:5162
20. Francisco MSP, Mastelaro VR, Nascente PAP, Florentino AO (2001) J Phys Chem B 105:10515
21. Machej T, Haber J, Turek AM, Wachs IE (1991) Appl Catal 70:115
22. Zhao C, Wachs IE (2006) Catal Today 118:332
23. Went GT, Oyama ST, Bell AT (1990) J Phys Chem 94:4240
24. Went GT, Leu LJ, Bell AT (1992) J Catal 134:479
25. Roozeboom F, Mittelmeijer-Hazeleger MC, Moulijn JA, Medema J, De Beer VHJ, Gellings PJ (1980) J Phys Chem 84:2783
26. Parekh BS, Weller SW (1977) J Catal 47:100
27. Oyama ST, Went GT, Lewis KB, Bell AT, Somorjai GA (1989) J Phys Chem 93:6786
28. Arena F, Frusteri F, Parmaliana A (1999) Appl Catal A 176:189
29. Wachs IE (1996) Catal Today 27:437
30. Besselmann S, Freitag C, Hinrichsen O, Muhler M (2001) Phys Chem Chem Phys 3:4633
31. Poelman H, Sels BF, Olea M, Eufinger K, Paul JS, Moens B, Sack I, Balcaen V, Bertinchamps F, Gaigneaux EM, Jacobs PA, Marin GB, Poelman D, De Gryse R (2007) J Catal 245:156
32. Bosch H, Kip BJ, Ommen JGv, Gellings PJ (1984) J Chem Soc Faraday Trans 180:2479
33. Auroux A (1997) Top Catal 4:71
34. Desmartin-Chomel A, Flores JL, Bourane A, Clacens JM, Figueras F, Delahay G, Fendler AG, Lehaut-Burnouf C (2006) J Phys Chem B 110:858
35. Badlani M, Wachs IE (2001) Catal Lett 75:137
36. Sun Q, Fu Y, Liu J, Auroux A, Shen J (2008) Appl Catal A 334:26
37. Fu Y, Shen J (2007) Chem Commun 2172
38. Liu H, Bayat N, Iglesia E (2003) Angew Chem Int Ed 42:5072
39. YuanY, Shido T, Iwasawa Y (2000) Chem Commun 1421
40. Royer S, Sécordel X, Brandhorst M, Dumeignil F, Cristol S, Dujardin C, Capron M, Payen E, Dubois J (2008) Chem Commun 865

Publication II

Applied Catalysis A: General 356 (2009) 121–128

Contents lists available at ScienceDirect

Applied Catalysis A: General

journal homepage: www.elsevier.com/locate/apcata

The influence of the preparation method on the structural, acidic and redox properties of V_2O_5-TiO_2/SO_4^{2-} catalysts

H. Zhao [a,b], S. Bennici [a], J. Shen [b], A. Auroux [a,*]

[a] Université Lyon 1, CNRS, UMR 5256, IRCELYON, Institut de recherches sur la catalyse et l'environnement de Lyon, 2 avenue Albert Einstein, F-69626 Villeurbanne, France
[b] Laboratory of Mesoscopic Chemistry, School of Chemistry and Chemical Engineering, Nanjing University, Nanjing 210093, China

ARTICLE INFO

Article history:
Received 23 September 2008
Received in revised form 6 December 2008
Accepted 23 December 2008
Available online 6 January 2009

Keywords:
V_2O_5-TiO_2/SO_4^{2-}
Co-precipitation
Sol–gel
Mechanical grinding
Structural properties
Redox properties
Isopropanol conversion

ABSTRACT

The introduction of sulfates into vanadia-titania catalysts and the influence of the preparation method on the properties of the sulfated samples have been studied. Series of V_2O_5-TiO_2/SO_4^{2-} (VTiS) catalysts were prepared by co-precipitation, sol–gel and mechanical grinding methods and calcined at different temperatures. Their structural properties were characterized by X-ray diffraction (XRD), Fourier transform infrared spectroscopy (FT-IR), thermogravimetric analysis (TGA) and X-ray photoelectron spectroscopy (XPS). Co-precipitation was by far the best preparation method in terms of maximizing the surface area and the mesoporosity. Temperature-programmed reduction (TPR) revealed that only the vanadia species were reducible. The results from XRD and FT-IR showed that V_2O_5 was well dispersed on the surface of TiO_2. XPS showed that the surface vanadium oxide was composed of stoichiometric V_2O_4 and V_2O_5, as well as V_2O_3 species especially for the samples prepared by mechanical grinding. Meanwhile, titanium was present in its fully oxidized state in all the VTiS samples, and the sulfur-containing species presented an oxidation state of +6. The reaction of isopropanol (IPA) conversion in air was used to characterize the surface acid/base and redox properties. The higher activity for the IPA conversion over the VTiS catalysts as compared to TiO_2 was possibly due to the generation of redox sites upon the addition of V_2O_5. Moreover, the surface acidic properties were enhanced and the redox properties weakened upon addition of SO_4^{2-} species.

1. Introduction

V_2O_5-TiO_2 catalysts are commonly used for a number of industrially important reactions, including the selective oxidation of *o*-xylene to phthalic anhydride [1–5], the selective catalytic reduction (SCR) of NO_x [6–10], the selective oxidation of alkanes [11–14], the ammoxidation of hydrocarbons [12–15], the selective oxidation of toluene to benzaldehyde and benzoic acid [16,17], the selective oxidation of methanol to formaldehyde [18] and methyl formate [19], and the selective oxidation of ethanol to acetaldehyde [20]. Extensive studies have been devoted to such catalysts regarding the dispersion, surface structure, oxidation states and reducibility of the supported vanadia species under different conditions, and these properties have been correlated to the performance in selective oxidation reactions. Excellent summaries about these studies can be found in refs. [21–26]. Moreover, it has been shown that the addition of SO_4^{2-} species to TiO_2 generates strong acidic sites at high temperature and can lead to high activity in the SCR reaction [27]. This effect is especially strong in the case of SO_4^{2-}/TiO_2 catalysts, which show higher activity than V_2O_5 based catalysts at high temperature [28]. Chen and Yang [29,30] have reported that the addition of SO_2 increased the NO removal activity of V_2O_5/TiO_2 due to the formation of surface sulfate species enhancing the surface acidity of catalyst. Amiridis et al. [7] have also reported that, on vanadia-titania catalysts, the gaseous SO_2 contained in the feed gas system could participate in the formation of surface sulfate species which strongly interact with vanadia and then improve the catalytic surface reactivity. Furthermore, it has recently been reported that TiO_2-supported V_2O_5 catalysts modified by SO_4^{2-} ions possess a better activity in the selective catalytic reduction of NO_x [31,32], suggesting that the surface acidity of the catalysts could be greatly enhanced by the addition of SO_4^{2-}. Moreover, in the SCR reaction, it is certain that both the acidity and the redox properties of the catalysts are controlling factors of the reactivity [30,32].

Supported vanadium oxide catalysts can be prepared by several methods, such as impregnation, co-precipitation, liquid-phase grafting and chemical vapour deposition [33]. The principal techniques of catalyst preparation involve two stages: the first stage is dispersion and is achieved by impregnation, grafting, or co-precipitation, while the second stage is calcination. Although the synthesis of V_2O_5/TiO_2 systems has been extensively studied, the

* Corresponding author. Fax: +33 472445399.
E-mail address: aline.auroux@ircelyon.univ-lyon1.fr (A. Auroux).

0926-860X/$ – see front matter © 2008 Elsevier B.V. All rights reserved.
doi:10.1016/j.apcata.2008.12.037

Table 1
Chemical analysis, X-ray photoelectronic spectroscopy analysis, BET surface area, average pore radius, and pore volume of the samples.

Sample	Preparation method	Calcination temperature (K)	CA (wt.%)			XPS (wt.%)			S_{BET} ($m^2\ g^{-1}$)	Average pore diameter (nm)	Pore volume ($ml\ g^{-1}$)
			V	Ti	S	V	Ti	S			
VTiS-1	Co-precipitation	673	12.56	40.72	1.45	14.2	37.2	1.5	250	12.6	0.911
VTiS-2		723	13.37	43.84	<0.3	17.7	35.7	0.3	105	20.7	0.644
VTiS-3		773	13.59	43.96	<0.3	17.6	36.6	–	58	n.d.	n.d.
VTiS-4	Co-precipitation with 1 wt.% PEG	673	12.45	41.37	2.49	14.1	35.9	2.7	243	10.4	0.794
VTiS-5		723	13.38	45.11	<0.3	18.2	36.2	–	74	22.7	0.556
VTiS-6		773	13.67	44.23	<0.3	18.1	36.5	–	51	n.d.	n.d.
VTiS-7	Sol–gel	673	9.65	39.50	5.67	35.2	13.6	1.5	7	n.d.	n.d.
VTiS-8		723	11.4	44.83	1.35	19.1	26.1	5.0	43	12.7	0.153
VTiS-9		773	12.29	46.90	<0.3	24.4	27.5	0.3	32	n.d.	n.d.
VTiS-10	Mechanical grinding	673	14.39	31.02	8.19	2.5	39.7	5.7	145	n.d.	n.d.
VTiS-11		723	12.43	34.59	6.51	3.7	42.5	4.4	132	7.3	0.290
VTiS-12		773	15.27	39.10	1.37	3.1	44.4	4.0	117	n.d.	n.d.
TiO_2	Millenium	723	–	–	0.17	–	–	0.2	313	4.6	0.37

n.d.: not determined.

introduction of sulfates into vanadia-titania catalysts and the influence of the method of preparation on the properties of sulfated V_2O_5/TiO_2 have received little attention. Thus, in the present work, we study the influence of the preparation method and the effect of the calcination temperature on the properties of VTiS catalysts, focusing especially on the structural and redox properties.

V_2O_5-TiO_2/SO_4^{2-} catalysts were prepared by co-precipitation, co-precipitation with 1 wt.% PEG-400 (poly-ethylene-glycol-400), sol–gel, and mechanical grinding methods. The textural properties and the crystalline structure of the materials were studied by using BET, X-ray diffraction (XRD), and FT-IR techniques, while the redox properties were measured by using TPR. Moreover, the samples were also tested in the isopropanol (IPA) conversion probe reaction and the results analyzed in relation with the addition of SO_4^{2-}.

2. Experimental

2.1. Catalyst preparation

Different synthesis routes were followed for obtaining four groups of catalysts, each one composed of three samples differing as to the calcination temperature.

The theoretical amount of vanadium pentoxide was fixed at 25 wt.% whatever the preparation method used.

2.1.1. Preparation by co-precipitation

High surface area vanadia-titania-sulfate catalysts (denoted by VTiS) were prepared by a co-precipitation method. 4 g of V_2O_5-TiO_2/SO_4^{2-} sample were prepared starting from 2.5 g of $VOSO_4{\cdot}xH_2O$ and 9.2 g of $TiOSO_4{\cdot}xH_2SO_4{\cdot}xH_2O$. At first, the precursors were dissolved in 400 mL of deionized water, forming a solution (S1) containing vanadium and titanium while 20 mL of a 28 wt.% $NH_3{\cdot}H_2O$ solution were placed in an ice bath. Then S1 was slowly dropped into the $NH_3{\cdot}H_2O$ solution under vigorous stirring in the ice bath, and a brown precipitate formed immediately. This precipitate was first aged for 1 h at room temperature and then filtered. The filtered cake was redispersed by stirring into a mixture containing 1-butanol to form a homogeneous slurry. Finally the slurry was transferred to a beaker which was placed in an oil bath to remove the solvent. At the temperature of 367 K (azeotropic point of the water–butanol system), water and part of 1-butanol in the slurry were distilled, and then at 391 K (boiling point of 1-butanol), the residual 1-butanol was further removed. The VTiS-1, VTiS-2 and VTiS-3 samples were prepared in this way, and then calcined in air for 5 h at 673, 723 and 773 K, respectively (Table 1).

2.1.2. Preparation by co-precipitation with 1 wt.% PEG-400

PEG-doped VTiS particles were synthesized by adding an amount of 1 wt.% of PEG-400 into diluted $NH_3{\cdot}H_2O$ solution, followed by the same process as above. The VTiS-4, VTiS-5 and VTiS-6 samples were prepared in this way, with calcination temperatures of 673, 723 and 773 K, respectively (Table 1). PEG is known to improve the physical properties of the sample in terms of surface area and structure and it also carries the role of reducing agent [34].

2.1.3. Preparation by sol–gel method

The synthesis of mixed vanadia oxide (V_2O_5/TiO_2) was carried out using an organic mixture containing vanadyl acetylacetonate and titanium (IV) isopropoxide in propanol-2-ol as solvent. A homogeneous gel was obtained by hydrolysis and precipitation after addition of water to this mixture. The amount of water added corresponded to a volume ratio $[H_2O]/[Ti(OR)_4]$ equal to 2. To obtain sulfated oxides, sulfuric acid was added to the organic mixture, according to a molar ratio nS/nTi = 0.25. Next, the gels were filtered, and then dried for 12 h at 373 K. Finally, the catalysts were obtained after calcination in air for 12 h. This longer time of calcination compared to the other series of samples was justified by preliminary TG–DTG experiments which have shown that decomposition of sol–gel precursors required a slightly higher temperature and more time than the other precursors. The VTiS-7, VTiS-8 and VTiS-9 samples were prepared in this way, with calcination temperatures of 673, 723 and 773 K, respectively (Table 1).

2.1.4. Preparation by mechanical grinding

V_2O_5-SO_4^{2-}/TiO_2 catalysts were also prepared by mechanical grinding in an agate mortar using TiO_2 (313 $m^2\ g^{-1}$ after calcinations at 723 K, Millennium* G5) and $VOSO_4{\cdot}xH_2O$ in definite proportions corresponding to the theoretical amount of 25 wt.% V_2O_5, and then calcined in air for 5 h. The VTiS-10, VTiS-11 and VTiS-12 samples were prepared in this way, using calcination temperatures of 673, 723 and 773 K, respectively (Table 1). However, it should be noticed that the parent commercial TiO_2 already contains some sulfates (0.17 wt.% S).

2.2. Catalyst characterization

Elemental analysis was performed using ICP atomic emission spectroscopy (ICP–AES) with a flame PerkinElmer M1100 spectrometer.

The surface areas and pore sizes were measured by nitrogen adsorption at 77 K on a Micromeritics 2010 apparatus after heat pretreatment under vacuum for 3 h at a temperature 50 K lower than the calcination temperature.

The X-ray diffraction (XRD) measurements were carried out on a Bruker D5005 powder diffractometer scanning from 3° to 80° (2θ) at a rate of 0.02° s^{-1} using a Cu Kα radiation (λ = 0.15418 nm) source. The applied voltage and current were 50 kV and 35 mA, respectively.

The thermogravimetric analyses (TGA) were performed on a SETARAM Labsys instrument in the 303–1073 K temperature range, with a heating rate of 5 K min^{-1}, under nitrogen flow.

The X-ray photoelectron spectra (XPS) were measured on a KRATOS AXIS Ultra DLD spectrometer equipped with a hemispherical electron analyzer and an Al anode (Al Kα = 1486.6 eV) powered at 150 W, a pass energy of 20 eV, and a hybrid lens mode. The detection area analyzed was 700 μm × 300 μm. Charge neutralization was required for all samples. The peaks were referenced to the C–(C, H) components of the C 1s band at 284.6 eV. Shirley background subtraction and peak fitting to theoretical Gaussian–Lorentzian functions were performed using an XPS processing program (vision 2.2.6 KRATOS). The residual pressure in the spectrometer chamber was 5×10^{-9} mbar during data acquisition.

The skeletal FT-IR spectra were recorded at room temperature with a Bruker Vector 22 FTIR spectrophotometer (DTGS detector) operating in the 4000–400 cm^{-1} range, with a resolution of 2 cm^{-1} and 100 acquisition scans. In each experiment, 2 mg of sample were mixed with 198 mg of KBr.

H_2-TPR measurements were carried out in a continuous mode using a U-type quartz microreactor (16 mm diameter). 50 mg of the calcined samples were first pretreated in situ for 1 h at 673 K (1 K min^{-1}) in air flow. After cooling and a step of purge of the lines in Ar flow, an H_2:Ar mixture (H_2:Ar volume ratio of 1% and total flow of 20 mL min^{-1}) was sent through the sample while increasing the temperature up to 1073 K with a rate of 5 K min^{-1}. The hydrogen consumption was monitored using a DelsiNermag (DN) 11 thermal conductivity detector (TCD).

The reaction of isopropanol conversion was used to characterize the surface acidity. This probe reaction was carried out in a fixed-bed glass tube reactor. About 100 mg of sample were loaded for each reaction. Isopropanol was introduced onto the catalyst by bubbling air through a glass saturator filled with isopropanol maintained at 295 K. Isopropanol and reaction products were analyzed by an online gas chromatograph, using a PEG 20M packed column connected to a Flame Ionization Detector (FID). Each catalyst was pretreated by heating air at the same calcination temperature for 1 h and then cooled in the same flow to the reaction temperature.

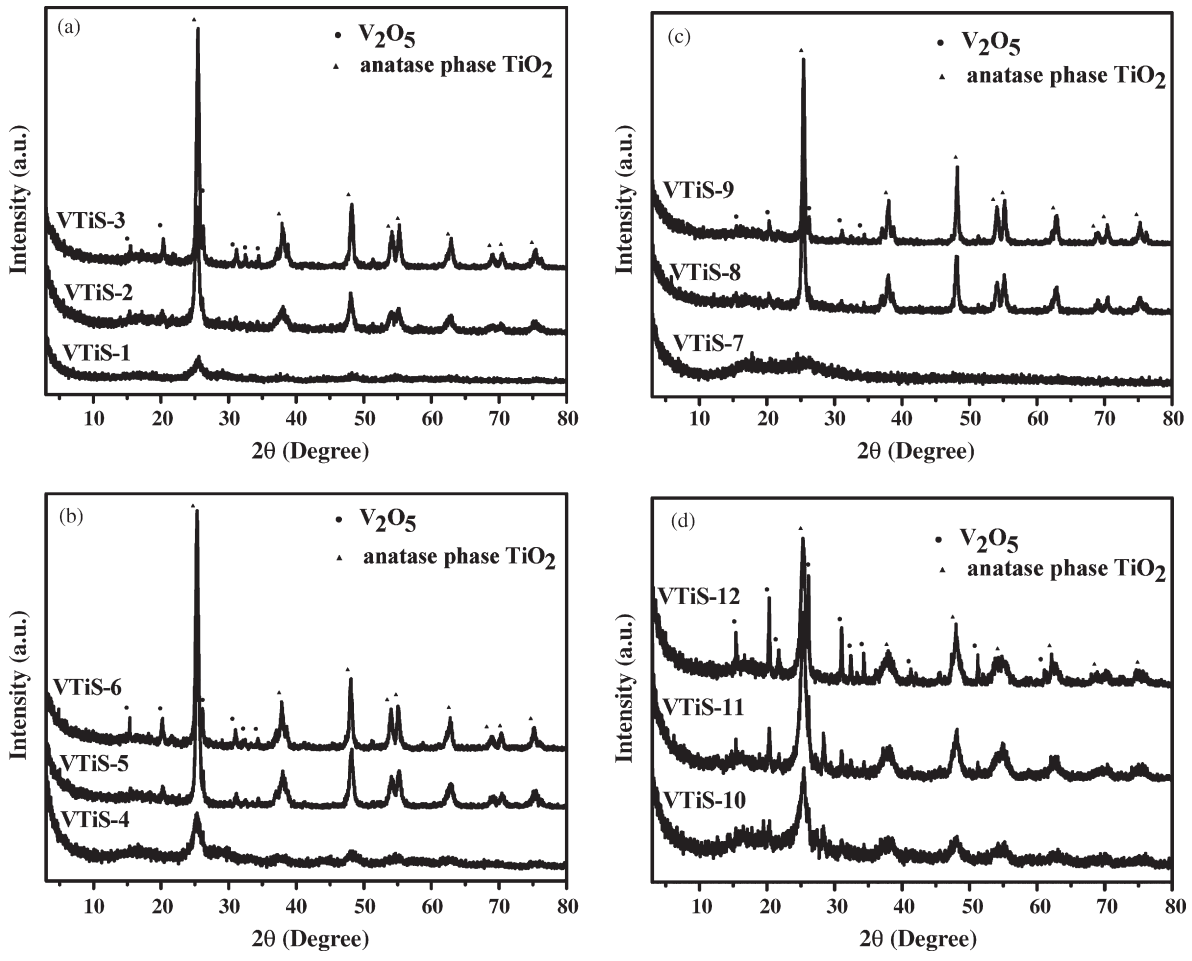

Fig. 1. X-ray diffraction (XRD) patterns for VTiS catalysts prepared by different methods: (a) co-precipitation, (b) co-precipitation with 1 wt.% PEG-400, (c) sol–gel and (d) mechanical grinding.

3. Results and discussion

3.1. Surface structure

The results of bulk (chemical analysis) and surface (XPS) analysis, as well as surface area and porosity data for all the samples, are given in Table 1. Depending on the preparation method and calcination temperature, the sulfur wt.% varied greatly and remained difficult to control. The sulfur content was observed to be higher for sol–gel and mechanical grinding than for co-precipitation method and in any case it decreased with increasing calcination temperature. The chemical analysis (CA) results can be compared to the surface analysis obtained from XPS measurements. Sol–gel samples are noticeably enriched in vanadia species at their surface compared to the co-precipitated samples (Table 1) probably due to a segregation of vanadia on the surface. On the contrary, the samples prepared by mechanical grinding display much less vanadia species at their surface than expected from chemical analysis. The sample area analyzed by XPS and the particle size certainly play an important role in this observation and stem for the heterogeneity of these samples.

The XRD patterns of all VTiS samples are presented in Fig. 1. It can be seen from the figure that typical diffraction peaks characteristic of anatase TiO_2 are observed for all VTiS samples except for VTiS-7, indicating that calcination at 673 K in air for 12 h is not sufficient to obtain the crystalline anatase phase. VTiS-1 and VTiS-4 samples are poorly crystallized and contain amorphous TiO_2. The intensities of the peaks due to anatase TiO_2 increased with increasing calcination temperature. A weakly crystalline vanadia phase appeared only when the calcination temperature reached 773 K, indicating that vanadium oxide was present in a highly dispersed manner. It also appears that sulfate ions delay the crystallization and the sintering upon calcination, since sulfate-free oxides are more crystalline than sulfated ones [32]. Very similar XRD diffraction lines were observed for the co-precipitated VTiS samples doped or not with 1 wt.% PEG-400, but the intensities of the peaks were stronger for the former, which suggests the agglomeration of TiO_2 and V_2O_5 particles upon the addition of 1 wt.% PEG-400.

Table 2 lists the average sizes of the TiO_2 particles as determined by the Debye–Scherrer formula from the XRD data, and found to be around 12 nm for VTiS-2 and VTiS-5, 21 and 9 nm for VTiS-8 and VTiS-11, respectively, which samples were all calcined at the same temperature of 723 K. The crystal size increased with increasing calcination temperature, suggesting the agglomeration of TiO_2 particles, in consistence with the surface area data given in Table 1.

The influence of the preparation method on the thermal properties of the 673 K calcined samples was investigated by thermal analysis; the results are illustrated in Fig. 2a and b for samples VTiS-1 and VTiS-7, respectively. A significant weight loss beginning at 700 K and corresponding to a DTG peak maximum around 755–760 K was observed for both samples, temperature at which the decomposition of water and organic ligands is already completed. This phenomenon is attributed to the decomposition of sulfate species present in the solid and is confirmed by the very low amount of sulfur remaining in samples VTiS-2 and VTiS-3. Besides, for sample VTiS-7 in addition to a little shift of this peak to a higher decomposition temperature a shoulder in the region between 770 and 820 K, centered at 780 K was observed corresponding to a subsequent decomposition of the remaining sulfur species. Moreover, a further small weight loss was observed in the temperature range of 873–990 K, which is related to the oxygen loss from vanadium(V) oxide species to vanadium(IV) oxide species, as already reported by several authors [35,36]. This transformation is stronger for VTiS-1 sample than for VTiS-7 according to the higher vanadia content. Very similar TG–DTG curves to VTiS-1 were observed for VTiS-4 and VTiS-10 samples.

Table 2
Calculated average size of TiO_2 particles in the VTiS catalysts prepared at various calcination temperatures by different preparation methods.

Sample	Calcination temperature (K)	FWHM (°)	Average size (nm)
VTiS-1	673	1.23	7
VTiS-2	723	0.67	12
VTiS-3	773	0.44	19
VTiS-4	673	1.09	7
VTiS-5	723	0.61	13
VTiS-6	773	0.43	18
VTiS-7	673	–	–
VTiS-8	723	0.39	21
VTiS-9	773	0.34	24
VTiS-10	673	0.90	9
VTiS-11	723	0.89	9
VTiS-12	773	0.78	10

The VTiS-1 sample, prepared by co-precipitation and calcined at 673 K in air flow for 5 h, displays the largest surface area of 250 $m^2\ g^{-1}$. Moreover, it was found that increasing the calcination temperature decreased the surface area, down to the lowest value at 773 K (58 $m^2\ g^{-1}$) for the same series of samples. Adding PEG did not change significantly the surface area of the co-precipitated samples. Indeed no benefit was gained upon PEG addition. Comparatively, samples prepared by the sol–gel method displayed lower surface area. Generally, in sol–gel methodology the proton concentration plays an important role and may be was too high upon addition of sulfuric acid to obtain larger surface areas. In addition, the very low surface area of sample VTiS-7 calcined at 673 K could be explained by an incomplete solvent removal during the gel-drying step and/or an incomplete decomposition of the sol–gel precursor at this temperature. A minimum calcination temperature of 723 K was needed to form the V_2O_5-TiO_2-SO_4^{2-} catalyst. Samples prepared by mechanical grinding maintained a relatively high surface area at high temperature.

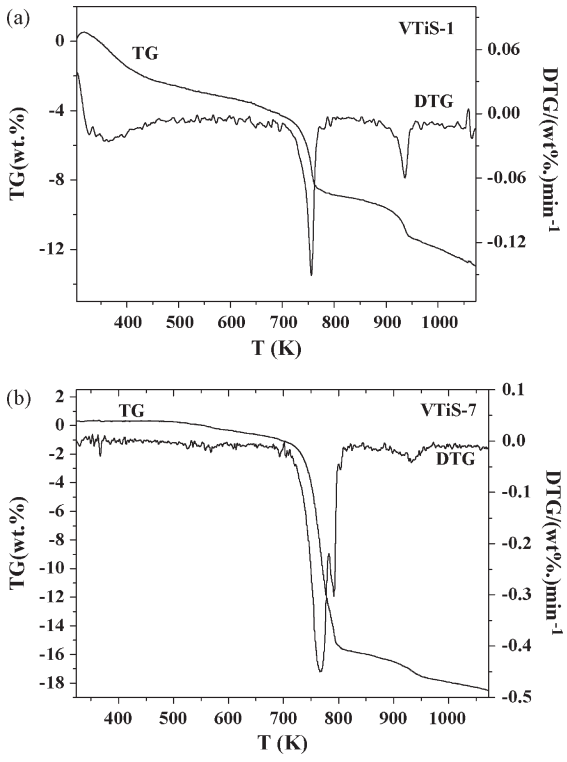

Fig. 2. TG and DTG curves of the calcined (a) VTiS-1 and (b) VTiS-7 catalysts.

Table 3
Binding energies and V/Ti atomic ratios (surface and bulk composition) of the VTiS catalysts.

Sample	Calcination temperature (K)	Binding energy (eV)					(V/Ti)[d]	(V/Ti)[e]
		V $2p_{3/2}$			Ti $2p_{3/2}$	S $2p_{1/2}$		
VTiS-1	673		516.5 (19%)[b]	517.6 (81%)[c]	459.0	169.0	0.36	0.29
VTiS-2	723		516.5 (21%)[b]	517.7 (79%)[c]	459.0	169.3	0.47	0.29
VTiS-3	773		516.3 (21%)[b]	517.7 (79%)[c]	459.0	–	0.46	0.29
VTiS-4	673		516.4 (29%)[b]	517.6 (71%)[c]	459.0	169.0	0.37	0.28
VTiS-5	723		516.4 (20%)[b]	517.7 (80%)[c]	459.1	–	0.47	0.28
VTiS-6	773		516.6 (21%)[b]	517.6 (79%)[c]	459.1	–	0.47	0.29
VTiS-7	673		516.3 (12%)[b]	517.5 (88%)[c]	459.0	169.1	2.5	0.23
VTiS-8	723		516.5 (9%)[b]	517.7 (91%)[c]	459.0	168.9	0.71	0.24
VTiS-9	773		516.4 (11%)[b]	517.6 (89%)[c]	459.0	169.0	0.83	0.25
VTiS-10	673	515.7 (13%)[a]	517.0 (73%)[b]	518.0 (14%)[c]	459.4	169.1	0.06	0.44
VTiS-11	723	515.7 (12%)[a]	516.9 (73%)[b]	518.0 (15%)[c]	459.2	169.1	0.08	0.34
VTiS-12	773	515.7 (13%)[a]	516.9 (81%)[b]	518.0 (6%)[c]	459.3	169.0	0.06	0.37

[a] Binding energies (BEs) between 515.7 and 515.8 eV correspond to V^{3+} in V_2O_3.
[b] Binding energies (BEs) between 516.3 and 517.0 eV correspond to V^{4+} in V_2O_4.
[c] Binding energies (BEs) between 517.5 and 518.0 eV correspond to V^{5+} in V_2O_5.
[d] Surface atomic ratio determined by XPS.
[e] Bulk atomic ratio determined by chemical analysis (for comparison).

The catalysts as well as the TiO_2 support present nitrogen adsorption–desorption isotherms of type IV with H1 or H3 hysteresis loops, according to the IUPAC classification [37], characteristic of mesoporous materials. The average pore diameters and pore volumes of the samples calcined at 723 K are summarized in Table 1. The surface area and pore volume for VTiS-2 were found to be 105 $m^2\ g^{-1}$, and 0.644 $cm^3\ g^{-1}$, respectively, slightly higher than those of VTiS-5, calcined at the same temperature (see Table 1) which could be explained by the agglomeration of TiO_2 and V_2O_5 particles with the addition of 1 wt.% PEG-400. VTiS-8 prepared by sol–gel method exhibited a considerably decreased pore volume of about 0.153 $cm^3\ g^{-1}$ (due to the change in the crystallographic phase as shown by the XRD results), while the average pore size increased very slightly. Finally, the average pore size and pore volume for VTiS-11 were 7.3 nm, and 0.290 $cm^3\ g^{-1}$, respectively.

Information about the relative amounts and dispersion of vanadia and sulfate species as well as indications about the oxidation state of vanadium in the catalysts were acquired by XPS. The C 1s peak at 284.6 eV was used as an internal standard for the calibration of binding energies. The binding energy (BE) references of the V $2p_{3/2}$ line used to identify the vanadium oxide phases in the catalysts were calculated based on the data in refs. [38,39]. Andersson [38] has reported the V $2p_{3/2}$ line position for several vanadium oxides by standardizing the spectra to the O 1s signal at 529.6 eV. Since in this study the O 1s peak is centered at around 530.4 eV, i.e. allows a shift of ≈0.8 eV in V $2p_{3/2}$ signal toward higher BEs, the reference V $2p_{3/2}$ peak position for V_2O_5, V_6O_{13}, V_2O_4 and V_2O_3 could be fixed around 517.5, 517.1, 516.4 and 515.8 eV, respectively.

For all samples, Table 3 presents the binding energies of the V $2p_{3/2}$, Ti $2p_{3/2}$, and S $2p_{1/2}$ lines as well as the V/Ti atomic ratios from XPS measurements and chemical analysis. Moreover, Table 4 reports the relative components from the decomposition of the O 1s line. As example the V 2p, Ti 2p, and S 2p XPS spectra for VTiS-4 sample are presented in Fig. 3a–c, respectively. Besides the V 2p XPS spectrum of VTiS-10 catalyst is given in Fig. 4 for comparison. Only two peaks related to the presence of V^{5+} and V^{4+} could be detected for the VTiS-4 sample, centered at 517.6 and 516.4 eV, respectively, while the presence of three oxidation states for ViTS-10 was established by V $2p_{3/2}$ peaks centered at 518.0, 517.0 and 515.7 eV characteristic of V^{5+}, V^{4+}, and V^{3+} species, respectively [40–42]. No differences were detected among the various samples for the Ti and S XPS peaks.

The observed values of the V $2p_{3/2}$ line revealed that the surface of catalysts prepared by co-precipitation, co-precipitation with PEG and sol–gel, the pentavalent, fully oxidized state of vanadia was predominant. The sol–gel samples presented about 10% V^{4+} species while the co-precipitated samples were slightly more reduced, presenting contributions of ≈20% V^{4+}. The formation of V^{4+} species may be due to the exposure of the catalysts to X-radiation under ultra-high vacuum (UHV) operating conditions.

Samples prepared by mechanical grinding showed a totally different repartition of vanadia species. The main contribution (>70%) corresponded to V^{4+} species; a slight displacement toward higher BEs (+0.4 eV) and the presence of ≈12% V^{3+} were observed,

Table 4
Binding energies and O 1s concentration (in atomic %) for the different oxygen species ($TiO_2 + V_2O_5$, –OH, and $–SO_4^{2-}$) present on the VTiS catalyst surfaces.

Sample	Calcination temperature (K)	Binding energy (eV) of O 1s		
		TiO_2 and V_2O_5	–OH	SO_4^{2-}
VTiS-1	673	530.4 (78%)	531.7 (15%)	532.4 (7%)
VTiS-2	723	530.4 (90%)	531.7 (10%)	–
VTiS-3	773	530.3 (85%)	531.5 (15%)	–
VTiS-4	673	530.4 (73%)	531.4 (10%)	532.2 (16%)
VTiS-5	723	530.4 (89%)	531.5 (11%)	–
VTiS-6	773	530.4 (84%)	531.5 (16%)	–
VTiS-7	673	530.3 (79%)	531.5 (15%)	532.5 (6%)
VTiS-8	723	530.3 (62%)	531.6 (22%)	532.3 (16%)
VTiS-9	773	530.3 (88%)	531.5 (12%)	–
VTiS-10	673	530.5 (62%)	–	532.1 (38%)
VTiS-11	723	530.4 (67%)	–	532.0 (33%)
VTiS-12	773	530.4 (71%)	–	532.1 (29%)

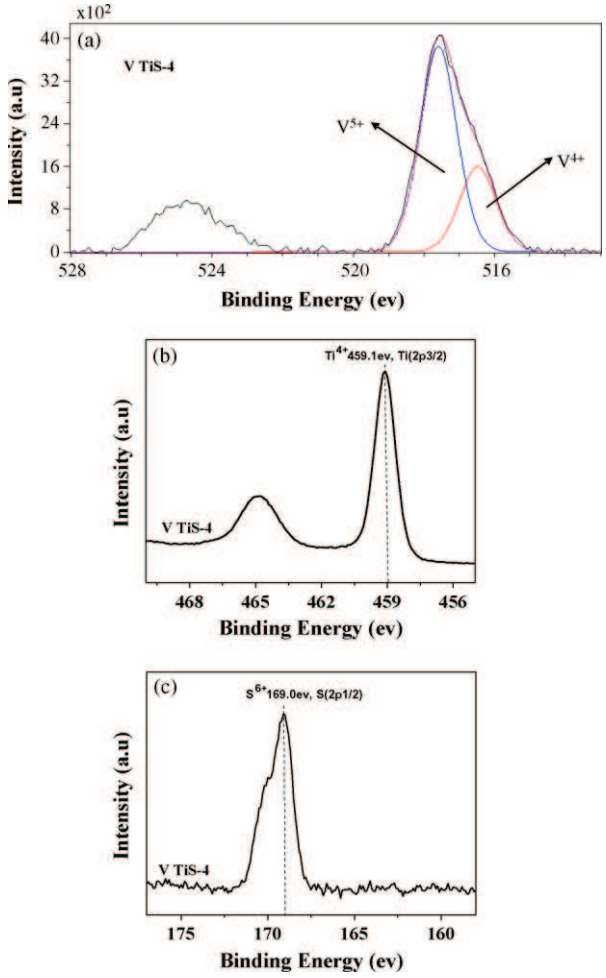

Fig. 3. (a) V 2p, (b) Ti 2p, and (c) S 2p XPS spectra for the calcined VTiS-4 sample.

indicating that a large amount of sulfate could favor the reduction of V(V) to V(IV) and even to V(III). As seen in Table 2, the BE position of the Ti $2p_{3/2}$ line was at 459.0 ± 0.1 eV (value of pure TiO_2 is ≈458.8 eV [43]. This position was maintained for all samples, with the exception of mechanical grinding catalysts, whose value had shifted to 459.3 eV.

Binding energies of 169.0 eV were measured for the S 2p line. According to the literature data [44], these binding energy values are typical of sulfur in the S^{6+} oxidation state on the catalyst surface, as in Na_2SO_4 or $Fe_2(SO_4)_3$. The peaks at 161–162.8 eV assigned to sulfide and at 164 eV assigned to elemental sulfur were not observed. The S^{6+} species might be present in the form of bidentate sulfate on the surface of TiO_2, either chelating or

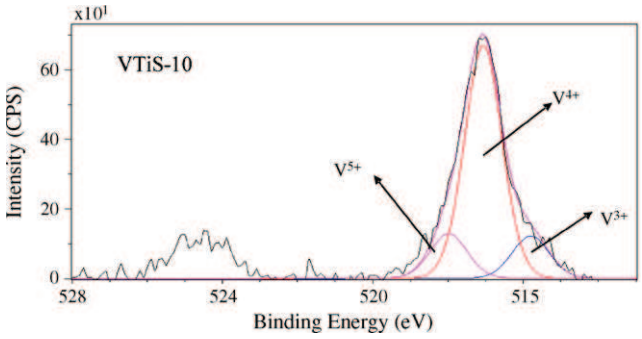

Fig. 4. V 2p XPS spectra for the calcined VTiS-10 sample.

bridging, as proposed in the literature [45]. The results of chemical analysis and X-ray photoelectron spectra for the S element showed that the S content decreased rapidly with increasing calcination temperature. The S content in the VTiS samples calcined at 773 K was very low (S < 0.3 wt.%), beyond the detection capacity of CA, suggesting that most of the sulfate ions might have decomposed during calcination of the VTiS catalysts at this high temperature and as confirmed by TG analysis.

The XPS spectra of the O 1s line were identical and could be divided into three bands centered at 530.4 eV (vanadium and titanium bonded oxygen; both vanadia and titania are thought to contribute in the formation of this band), 531.5 eV (Ti–OH contribution [46], and ≈532.2 eV (sulfate contribution).

This latter contribution was not observed for samples calcined at high temperature (773 K) except for those prepared by mechanical grinding which display a large amount of sulfur.

As can be noted in Table 3, the surface V/Ti ratios are higher for samples prepared by the sol–gel method, which is an indication that vanadium is more heterogeneously distributed and preferentially located on the external surface of the particles. Besides, the very low surface V/Ti atomic ratio of samples prepared by mechanical grinding should be only indicative of the very high heterogeneity of these samples.

3.2. Infrared analysis

The skeletal IR spectra of samples calcined at 723 K (and sample VTS-12) are reported in Fig. 5. It can be seen that water molecules were incorporated, as evidenced by the two intense peaks centered at 3440 and 1624 cm^{-1}, which are characteristic of the stretching vibrations of O–H and the bending vibrations of H–O–H, respectively. This indicates that a number of hydrogen bonds were formed between the hydroxyl groups on the surface of the samples and adsorbed water molecules. Thus, it appears that the samples contained a number of surface hydroxyl groups, although the VTiS samples had been calcined at 723 K. This observation was confirmed by the XPS analysis of the O 1s band (Table 4). Appropriate surface hydroxyl groups may be the active sites of the catalysts, although superfluous surface hydroxyl groups can have an adverse effect on catalytic activity [47,48]. The band at 1029 cm^{-1} can be assigned to the stretching mode of the $(V{=}O)^{3+}$ double bond [49,50]. In addition, for VTiS-11, two bands at 1090 and 1135 cm^{-1} can be observed and attributed to surface vibrations of water molecules causing deformations of TiO_6 octahedra surrounding surface Ti atoms [51,52]. This spectrum

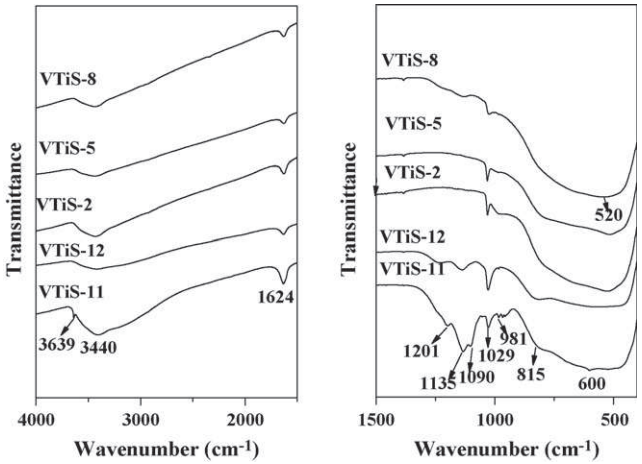

Fig. 5. FT-IR skeletal spectra of VTiS catalysts in the high frequency (4000–1500 cm^{-1}) and low frequency (1500–400 cm^{-1}) regions (2 mg sample in 198 mg KBr).

also shows a band at 1201 cm^{-1} ascribed to the asymmetric stretching mode of S–O linkages [53], confirming the incorporation of sulfur species into the titania structure. In particular, there are three weak peaks at 981 cm^{-1} characteristic of free SO_4^{2-} on the titania surface, with peak positions matching the literature data [54]. Furthermore, the symmetry of the sulfate ions on the TiO_2 surface should be C 3v, and their configuration could be unidentate –Ti–SO_4 [30]. For VTiS-12, the intensity of the bands at 1201 and 981 cm^{-1} decreased, which suggests that the amount of free SO_4^{2-} decreased with increasing calcination temperature. In addition, the spectrum of VTiS-12 shows that the 1090 cm^{-1} band disappeared and the intensity of the band at 1135 cm^{-1} decreased, indicating the decomposition of the water molecules adsorbed on the surface due to the increased calcination temperature.

It is worth noticing that no OH groups were detected by XPS analysis under high vacuum (Table 4), thus confirming that only molecular water was adsorbed on the mechanical grinding samples.

In the low frequency region, the appearance of large broad bands in the 500–900 cm^{-1} range with maxima at 600 cm^{-1} or at 530 cm^{-1} is probably characteristic of Ti–O–Ti anatase structure or of vanadate species in the interlayer spaces [55].

3.3. Redox properties

TPR is frequently used to study the redox properties of metal oxide catalysts. Normalized TPR spectra of the VTiS catalysts calcined at 723 K are presented in Fig. 6, which shows the H_2 consumption (a.u.) as a function of the temperature. The TPR profile of pure TiO_2 is given for comparison. The temperature of maximum reduction (T_M) and the consumption of dihydrogen ($\mu mol\ g^{-1}$) are presented in Table 5.

For TiO_2 support, only a very weak H_2 consumption peak around 830 K was observed, which might be due to a slight reduction of the surface Ti species. This indicates the low reducibility of TiO_2.

It is supposed generally that at lower temperature, the surface species (probably the tetracoordinated V species) would be reduced, whereas at higher temperature the more polymeric or bulk-like vanadium oxide would be reduced [56]. In this H_2-TPR study it was not possible to distinguish the different VO_x surface species possibly present because only one reduction peak was observed for all the catalysts. However, the elevated reduction temperature of VTiS-11 could indicate the presence of bulk-like V_2O_5 crystallites.

As can be seen in Fig. 6, only one peak of reduction, appearing around 862 K, was obtained for VTiS-2, VTiS-5 and VTiS-8,

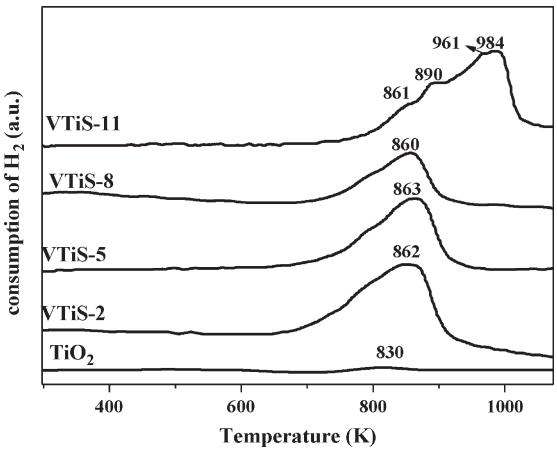

Fig. 6. TPR profiles of the VTiS catalysts.

Table 5
Reducibility of the catalysts as revealed by the H_2-TPR measurements.

Catalyst	T_M[a] (K)	H_2 consumption ($\mu mol\ g^{-1}$)
VTiS-11	861, 890, 961	3420
VTiS-8	860	1311
VTiS-5	863	2320
VTiS-2	862	2724
TiO_2	830	–

[a] Maximum temperature of the TPR peaks.

probably due to the reduction of highly polymeric vanadia or crystalline vanadia species. For VTiS-11 prepared by mechanical grinding, the intensity of this peak increased and the temperature of the maximum of the peak (T_{max}) shifted to higher values (984 K). Moreover, a reduction peak of crystalline V_2O_5 is visible around 961 K for VTiS-11, similar to that observed for bulk V_2O_5 [57,58], in agreement with the XRD results. Namely, bulk V_2O_5 is known to give rise to TPR peaks located at 910, 932, 971, 1044 and 1102 K, corresponding to intermediate oxides in the transformation of V_2O_5 to V_2O_3, which has been discussed thoroughly in the literature [57]. Additionally, the H_2 consumptions ($\mu mol\ g^{-1}$) were found to vary in the order VTiS-11 > VTiS-2 > VTiS-5 > VTiS-8, suggesting that the reduction extents of these catalysts varied in the same order.

3.4. Isopropanol probe reaction

It is well known that isopropanol undergoes dehydration reactions to produce propylene (PPE) and diisopropyl ether (DIPE) on acid sites, while it undergoes a dehydrogenation reaction to acetone (ACE) on basic sites in inert atmosphere. In addition, IPA can also be oxidatively dehydrogenated to ACE in an oxidative atmosphere, which can be used to probe the surface redox properties. Thus, the conversion of IPA and selectivities to PPE, DIPE and ACE in air can be used to characterize the surface acidic and redox properties.

Table 6 presents the results for the probe reaction of IPA conversion in air at 393 K on VTiS samples calcined at 723 K and TiO_2 as a reference. It can be seen that TiO_2 mainly produced the dehydration products (PPE and DIPE) with a total selectivity of 98%, suggesting the acidic character and lack of redox activity of TiO_2 in good agreement with the results from TPR. Addition of 25 wt.% V_2O_5 apparently created a large amount of redox sites since the oxidative product ACE was produced with a high selectivity (77% and 79% for VTiS-2 and VTiS-5, respectively, in which samples display very low amounts of sulfur species). The addition of significant quantities of sulfate ions (samples VTiS-8 and VTiS-11) seemed to increase the amounts of dehydration products (PPE and DIPE), while there was less of the oxidation product (ACE) although the difference was not large for sample VTiS-8. Therefore, the surface acidic properties might be enhanced and the redox properties weakened upon the addition of sulfate ions.

Table 6
Catalytic activities of TiO_2 and VTiS catalysts in the isopropanol probe reaction at 393 K in air.

Sample	Conversion of IPA (%)	Selectivity (%)		
		PPE	ACE	DIPE
VTiS-2	9	9	77	14
VTiS-5	8	9	79	12
VTiS-8	5	13	71	16
VTiS-11	7	23	37	40
TiO_2	6	28	2	70

IPA, isopropanol; PPE, propylene; DIPE, diisopropyl ether; ACE, acetone.

4. Conclusions

V_2O_5-TiO_2/SO_4^{2-} catalysts were prepared by co-precipitation, co-precipitation with 1 wt.% PEG-400, sol–gel and mechanical grinding methods. This investigation has demonstrated the existence of important differences between the catalysts prepared by different preparation methods. The XRD and skeletal IR results suggest that vanadia species were well dispersed up to a calcination temperature of 773 K. The XPS results indicate that the Ti and S species present in the catalysts were all in fully oxidized states, while surface V species were mainly about 80–90% V^{5+} and about 10–20% V^{4+}, with additionally 6–15% V^{3+} in the samples prepared by mechanical grinding. The presence of V^{3+} was related to the higher concentration of SO_4^{2-} ions, which can facilitate the reduction of vanadium oxide once the catalysts are exposed to high vacuum and the XPS electron beam. TPR results show that the reducibilities varied in the order VTiS-11 > VTiS-2 > VTiS-5 > VTiS-8. To sum up, the structural and redox properties of V_2O_5-TiO_2/SO_4^{2-} catalysts were influenced by the preparation method and the concentration of sulfate ions. It should be possible to control the concentration of SO_4^{2-} by choosing the right preparation route and proper calcination temperature, and therefore to tune the acidic and redox properties of such catalysts.

Acknowledgements

The authors are thankful to the scientific services of IRCELYON, for providing chemical analysis, XRD and XPS measurements.

Hongying Zhao gratefully acknowledges the China Scholarship Council for the financial support of her PhD grant.

Financial supports from NSFC (20673055), MSTC (2005CB221400 and 2004DFB02900) and Jiangsu Province, China (BG2006031) are acknowledged.

References

[1] M. Wainwright, N. Foster, Catal. Rev. Sci. Eng. 19 (1979) 211.
[2] V. Nikolov, D. Klissurski, A. Anastasov, Catal. Rev. Sci. Eng. 33 (1991) 319.
[3] C.R. Dias, M.F. Portela, M.A. Banares, M. Galan-Fereres, M. Lopez-Granados, M.A. Pena, J.L.G. Fierro, Appl. Catal. A 224 (2002) 141.
[4] A.I. Anastatov, Chem. Eng. Sci. 58 (2003) 89.
[5] J.N. Papageorgiou, G.F. Froment, Chem. Eng. Sci. 51 (1996) 2091.
[6] L. Lietti, J. Svachula, P. Forzatti, G. Busca, G. Ramis, F. Bregani, Catal. Today 17 (1993) 131.
[7] M.D. Amiridis, I.E. Wachs, G. Deo, J.-M. Jehng, D.S. Kim, J. Catal. 161 (1996) 247.
[8] L. Casagrand, L. Lietti, I. Nova, P. Forzatti, A. Baiber, Appl. Catal. B 22 (1999) 247.
[9] O. Zegaoui, C. Hoang-Van, M. Karroua, Appl. Catal. B 9 (1996) 211.
[10] M.A. Reiche, E. Ortelli, A. Baiker, Appl. Catal. B: Environ. 23 (1999) 187.
[11] B. Grzybowska-Swierkosz, Appl. Catal. A 157 (1997) 263.
[12] K.V. Narayana, A. Venugopal, K.S. Rama Rao, S. Khaja Masthan, V. Venkat Rao, P. Kanta Rao, Appl. Catal. A 167 (1998) 11.
[13] C.R. Dias, M.F. Portela, G.C. Bond, J. Catal. 157 (1995) 344.
[14] M.A. Banares, Catal. Today 51 (1999) 319.
[15] G. Centi, Appl. Catal. A 147 (1996) 267.
[16] D.A. Bulushev, L. Kiwi-Minsker, V.I. Zaikovskii, A. Renken, J. Catal. 193 (2000) 145.
[17] H. Ge, G.W. Chen, Q. Yuan, et al. Chem. Eng. J. 127 (2007) 39.
[18] F. Roozeboom, P.D. Cordingley, P.J. Gellings, J. Catal. 68 (1981) 464.
[19] P. Forzatti, E. Tronconi, G. Busca, P. Tittarelli, Catal. Today 1 (1987) 209.
[20] N.E. Quaranta, J. Soria, V.C. Corberan, J.L.G. Fierro, J. Catal. 171 (1997) 1.
[21] B. Grzybowska, Catal. Today 1 (1987) 341.
[22] G.C. Bond, S.F. Tahir, Appl. Catal. 71 (1991) 1.
[23] I.E. Wachs, B.M. Weckhuysen, Appl. Catal. A 157 (1997) 67.
[24] S. Albonetti, G. Baldi, A. Barzanti, A.L. Costa, J. Epoupa Mengou, F. Trifirò, A. Vaccari, Appl. Catal. A 325 (2007) 309.
[25] P.H. Ha, R.P. Maddigapu, K.A. Pullur, J.K. Lee, H.S. Jung, Appl. Catal. B 78 (2008) 301.
[26] C.E. Hetrick, J. Lichtemberger, M.D. Amiridis, Appl. Catal. B 77 (2008) 255.
[27] G.T. Went, L.J. Leu, A.T. Bell, J. Catal. 134 (1992) 479.
[28] V.I. Marshneva, E.M. Slavinskaya, O.V. Kalinkina, G.V. Odegova, E.M. Moroz, G.V. Lavrova, A.N. Salanov, J. Catal. 155 (1995) 171.
[29] J.P. Chen, R.T. Yang, J. Catal. 125 (1990) 411.
[30] J.P. Chen, R.T. Yang, J. Catal. 139 (1993) 277.
[31] S.M. Jung, P. Grange, Appl. Catal. B 36 (2002) 207.
[32] L. Baraket, A. Ghorbel, P. Grange, Appl. Catal. B 72 (2007) 37.
[33] G.C. Bond, Appl. Catal. A: Gen. 157 (1997) 91.
[34] L. Kong, Z. Liu, M. Shao, Q. Xie, W. Yu, Y. Qian, J. Solid State Chem. 177 (2004) 690.
[35] D.J. Cole, C.F. Cullis, D.J. Hucknall, J. Chem. Soc., Faraday Trans. 72 (1) (1976) 2185.
[36] G. Oliveri, G. Ramis, G. Busca, V.S. Escribano, J. Mater. Chem. 12 (1993) 1239.
[37] S.J. Gregg, K.S. Sing, Adsorption, Surface Area, and Porosity, Academic Press, New York, 1982.
[38] S.L.T. Andersson, J. Chem. Soc. Faraday Trans. I 75 (1979) 1356.
[39] J.A. Odriozola, J. Soria, G.A. Somorjai, H. Heinemann, J.F. Garcia de la Banda, M. Lopez Granados, J.C. Conesa, J. Phys. Chem. 95 (1991) 240.
[40] J.P. Nogier, M. Delamar, Catal. Today 20 (1994) 109.
[41] M. Demeter, M. Neumann, W. Reichelt, Surf. Sci. 41 (2000) 454.
[42] A.-C. Dupuis, M. Abu Haija, B. Richter, H. Kuhlenbeck, H.-J. Freund, Surf. Sci. 539 (2003) 99.
[43] J. Keranen, C. Guimon, E.I. Iiskola, A. Auroux, L. Niinisto, Catal. Today 78 (2003) 149.
[44] M.H. Kim, I.-S. Nam, Y.G. Kim, J. Catal. 179 (1998) 350.
[45] D. Fraenkel, Ind. Eng. Chem. Res. 36 (1997) 52.
[46] C. Guimon, A. Gervasini, A. Auroux, J. Phys. Chem. B 105 (2001) 10316.
[47] M. El-Maazawi, A.N. Finken, A.B. Nair, J. Catal. 191 (2000) 138.
[48] J.G. Yu, Rare Met. 23 (2004) 289.
[49] L.D. Frederickson, D.M. Hausen, Anal. Chem. 35 (1963) 818.
[50] H. Zhang, W. Zhong, X. Duan, X. Fu, J. Catal. 129 (1991) 426.
[51] M.A. Fox, M.T. Dulay, Chem. Rev. 93 (1993) 341.
[52] M. Koranne, J. Goodwin, G. Marcelin, J. Catal. 148 (1994) 369.
[53] D. Stoilona, M. Gergiev, D. Marinova, Vib. Spectrosc. 39 (2005) 46.
[54] T. Yamaguchi, Appl. Catal. 61 (1990) 1.
[55] G. Carja, G. Delahay, Appl. Catal. B 47 (2004) 59.
[56] M.M. Monhamed, M.M. Al-Esaimi, J. Mol. Catal. A: Chem. 255 (2006) 53.
[57] S. Besselmann, C. Freitag, O. Hinrichsen, M. Muhler, Phys. Chem. Chem. Phys. 3 (2001) 4633.
[58] Q. Sun, Y. Fu, J. Liu, A. Auroux, J. Shen, Appl. Catal. A 334 (2008) 26.

Publication III

Journal of Molecular Catalysis A: Chemical 309 (2009) 28–34

Contents lists available at ScienceDirect

Journal of Molecular Catalysis A: Chemical

journal homepage: www.elsevier.com/locate/molcata

Surface and catalytic properties of V_2O_5–TiO_2/SO_4^{2-} catalysts for the oxidation of methanol prepared by various methods

H. Zhao [a,b], S. Bennici [a], J. Shen [b], A. Auroux [a,*]

[a] Université Lyon 1, CNRS, UMR 5256, Institut de recherches sur la catalyse et l'environnement de Lyon (IRCELYON), 2 avenue Albert Einstein, F-69626 Villeurbanne, France
[b] Laboratory of Mesoscopic Chemistry, School of Chemistry and Chemical Engineering, Nanjing University, Nanjing 210093, China

ARTICLE INFO

Article history:
Received 19 January 2009
Received in revised form 21 April 2009
Accepted 21 April 2009
Available online 3 May 2009

Keywords:
V_2O_5–TiO_2/SO_4^{2-}
Adsorption microcalorimetry
Acidity
Methanol selective oxidation
Dimethoxymethane

ABSTRACT

The influence of the preparation method on the surface and catalytic properties of sulfated vanadia–titania catalysts has been studied. V_2O_5–TiO_2/SO_4^{2-} (VTiS) catalysts with 25 wt% V_2O_5 and 0.2–6.5 wt% S were prepared by co-precipitation, sol–gel and mechanical grinding methods and calcined at 723 K in air. The structural properties were characterized by O_2 chemisorption and laser Raman spectroscopy (LRS). The surface acidity was determined by the techniques of NH_3 adsorption microcalorimetry and pyridine adsorption infrared spectroscopy (FT-IR). Catalytic tests of oxidation of methanol to dimethoxymethane (DMM) were performed at atmospheric pressure in a fixed-bed micro-reactor. The Raman spectra revealed that vanadia existed in the form of a crystalline V_2O_5 phase. The results of ammonia adsorption of microcalorimetry showed a much lower heat of adsorption for samples with high content of SO_4^{2-}. Meanwhile, pyridine adsorption of FT-IR showed that both Lewis and Brønsted acid sites were present on the surface of all VTiS catalysts. The catalytic performance was also influenced by the preparation methods. VTiS-CP catalyst, prepared by co-precipitation, exhibited the highest DMM yield with a DMM selectivity of 86% for 61% methanol conversion at 423 K.

1. Introduction

During the last 20 years, numerous papers [1–7] have been devoted to the development of selective catalysts for the partial oxidation of methanol, with important industrial applications as a target. V_2O_5–TiO_2 (VTi) catalysts are recognized as suitable systems for the partial oxidation of methanol [1–3], and recent publications [4,5] show that the selective oxidation of methanol to dimethoxymethane (DMM) over V_2O_5–TiO_2 catalysts can be improved by doping VTi catalysts with SO_4^{2-} ions. In the reaction of methanol oxidation, DMM has usually been regarded as a by-product and has not been extensively studied. DMM has an extremely low toxicity and can be used as an excellent solvent in pharmaceutical and perfume industries, as a reagent in organic synthesis [8], and as an intermediate for the production of concentrated formaldehyde [9]. Importantly, it has been also recently reported that DMM can be effectively steam-reformed to produce H_2 for fuel cells [10]. Generally DMM is produced by condensation of formaldehyde with methanol over acidic catalysts [11]. Furthermore, methanol is one of the most important chemical intermediates used in the chemical industry, and the oxidation of methanol has been widely used as a probe reaction to characterize the activity of oxide catalysts [12–14] interpreted in terms of both structural and chemical (acidic and redox) properties.

It is well known that the acidity of solid catalysts is an important factor that determines their applications as industrial catalysts, and, consequently, many of their catalytic properties can be directly related to their acidity [15]. Adsorption microcalorimetry can be used to determine the distribution of heats of adsorption as well as the "acidity spectrum" of a catalyst surface. Previous results in the literature [15,16] have also shown that heats of ammonia adsorption can be taken into account for characterizing the surface of acid catalysts and correlated with their activity and selectivity in a variety of reactions. This motivated the use of ammonia adsorption microcalorimetry and pyridine adsorption FT-IR in conjunction with catalytic performance tests to investigate the influence of the preparation method on the surface and catalytic properties of V_2O_5–TiO_2/SO_4^{2-} catalysts.

The surface structure and vanadium dispersion were studied by Raman spectroscopy and O_2 chemisorption, respectively. Ammonia adsorption calorimetry was used to determine the number and strength of the surface acid sites of the V_2O_5–TiO_2/SO_4^{2-} (VTiS) catalysts, while the nature of the acid sites present on the catalysts was determined by pyridine adsorption FT-IR. The catalytic reaction of selective oxidation of methanol to DMM over V_2O_5–TiO_2/SO_4^{2-} catalysts was tested and the results analyzed in relation with the preparation methods.

* Corresponding author. Fax: +33 472445399.
E-mail address: aline.auroux@ircelyon.univ-lyon1.fr (A. Auroux).

1381-1169/$ – see front matter © 2009 Elsevier B.V. All rights reserved.
doi:10.1016/j.molcata.2009.04.011

2. Experimental

2.1. Catalyst preparation

In this work, four samples with the same theoretical amount of vanadia loading (25 wt%) were prepared by using different procedures, namely co-precipitation (sample VTiS-CP), co-precipitation with 1% polyethylene glycol (VTiS-CPEG), sol–gel (VTiS-SG) and mechanical grinding (VTiS-MG). The precursors were respectively $VOSO_4$ and $TiOSO_4$ for VTiS-CP and VTiS-CPEG, vanadyl acetylacetonate and titanium isopropoxide plus sulfuric acid for VTiS-SG, TiO_2 and $VOSO_4$ for VTiS-MG. The samples were all calcined at 723 K in air for 5 h, except sample VTiS-SG for which the calcination time was increased up to 12 h for a better decomposition of the precursors.

The details of the preparation methods have been previously described in [17].

2.2. Catalyst characterization

Raman spectroscopy measurements were performed using a LabRAM HR (Jobin Yvon) spectrometer. The excitation was provided by the 514.5 nm line of an Ar^+ ion laser (Spectra Physics) employing a laser power of 100 μW. The laser beam was focused through microscope objective lenses (100×) down to a 1 μm spot on the sample.

The dispersion of the vanadium species was measured on a Micromeritics 2010 apparatus by using the high temperature oxygen chemisorption (HTOC) method [18]. The samples were reduced in purified H_2 flow (154 mL min^{-1}) at 640 K for 2 h followed by evacuation at the same temperature for 4 h, and then oxygen uptake was measured at the same temperature.

The pyridine adsorption infrared spectra were recorded with a Bruker Vector 22 FT-IR spectrophotometer (DTGS detector), in the 4000–400 cm^{-1} range, with a resolution of 2 cm^{-1} and using 100 scans. The self-supporting wafer (10–30 mg, 18 mm diameter) was first activated in situ at 573 K in oxygen flow for 14 h, then evacuated at the same temperature for 2 h and then exposed to pyridine (Air Liquide, 99.8%, vapor pressure 3.3 kPa) at room temperature for 5 min. The desorption was carried out by evacuation for 30 min each at room temperature, 373 K, 473 K and 573 K. The spectra were recorded at room temperature after adsorption and desorption at each temperature.

The microcalorimetric studies of ammonia adsorption were performed at 423 K in a heat flow calorimeter (C80 from Setaram) linked to a conventional volumetric apparatus equipped with a Barocel capacitance manometer for pressure measurements. The ammonia used for the measurements (Air Liquide, purity >99.9%) was purified by successive freeze–pump–thaw cycles. About 100 mg of sample was pretreated in a quartz cell under evacuation overnight at 623 K. The differential heats of adsorption were measured as a function of coverage by repeatedly introducing small doses of ammonia gas onto the catalyst until an equilibrium pressure of about 66 Pa was reached. The sample was then outgassed for 30 min at the same temperature, and a second adsorption was performed at 423 K until an equilibrium pressure of about 27 Pa was attained in order to calculate the irreversibly chemisorbed amount of ammonia at this pressure.

2.3. Catalytic reaction

The oxidation of methanol was carried out in a fixed-bed microreactor made of glass with an inner diameter of 6 mm. The methanol was introduced into the reaction zone by bubbling O_2/N_2 (1/5) through a glass saturator filled with methanol (99.9%) maintained at 278 K. In each test, 0.2 g of catalyst was loaded, and the gas hourly space velocity (GHSV) was 11,400 ml g^{-1} h^{-1}. The feed composition was kept constant at methanol:O_2:N_2 = 1:3:15 (v/v). The tail gas out of the reactor was analyzed by an on-line GC equipped with an FID detector and a TCD detector. The column used was PORAPAK N for the separation of methanol, DMM and other organic compounds. The gas lines were kept at 373 K to prevent condensation of the reactant and products. The reaction was carried out at atmospheric pressure.

3. Results and discussion

The samples are listed in Table 1 together with their surface areas and chemical compositions. As can be seen, the vanadia loadings were close to the theoretical one (25 wt%) but the sulfur amount varied greatly with the preparation method.

3.1. Surface structures

Oxygen adsorption can be used to evaluate the dispersion of a metal oxide on the surface of a support. Parekh and Weller [19,20] proposed a low temperature oxygen chemisorption (LTOC) method while Oyama et al. [18] suggested a HTOC method. Prereducing the samples at the same temperature as that used to measure oxygen uptakes (640 K) seems to prevent bulk reduction and leads to more reliable dispersion values [18,21]. Therefore, this method was adopted for the measurements of vanadium dispersion in this work.

The surface oxygen atom densities were calculated starting from the oxygen uptakes (determined by O_2 chemisorption) and the BET surface areas (determined by N_2 adsorption at 77 K), and are reported in Table 1. The total number of vanadium sites on each sample (expressed as the number of V atoms per unit surface area) was calculated starting from the metal content determined by chemical analysis and is also reported as comparison in Table 1. Wachs et al. reported that the theoretical density for the monolayer dispersion of vanadia on TiO_2 is 7.9×10^{18} V m^{-2} [22]. From the total vanadium loadings presented in Table 1 it can be noticed that all samples display loadings higher than the monolayer capacity, thus confirming the existence of a crystalline V_2O_5 phase in our samples as determined by Raman analysis (see next paragraph) and XRD [17].

The oxygen site density values were 8.6×10^{18}, 17.6×10^{18}, 24.1×10^{18} and 3.2×10^{18} m^{-2} for VTiS-CP, VTiS-CPEG, VTiS-SG and VTiS-MG, respectively.

Unfortunately, the oxygen atom site densities were higher than the average density of V=O groups on the low-index planes of V_2O_5 (5.0×10^{18} atom m^{-2}) [18], indicating that the HTOC technique did titrate some bulk V_2O_5, making it impossible to calculate the real dispersion of vanadium. Indeed, this technique is better suited for the study of samples prepared by impregnation or atomic layer deposition. However, the determination of the oxygen site density makes it possible to compare the surface properties of the different samples independently of their specific surface area.

The surface structure of vanadia and titania species on the VTiS catalysts was examined by Raman spectroscopy, from 1600 to 200 cm^{-1}, as shown in Fig. 1. It has been generally recognized that the Raman bands at 1030 and 900–100 cm^{-1} represent terminal V=O bonds in monomeric vanadyl and polymeric vanadate species, respectively [23–25]. Crystalline V_2O_5 displays Raman bands around 996, 703, 530, 483, 406, 306 and 285 cm^{-1} [26,27]. It is important to note that there were some yellow particles among the white particles of sample VTiS-MG; thus, the VTiS-MG catalyst is not homogeneous, and consequently both types of particles were analyzed. As can be seen in Fig. 1, all the catalysts exhibited typical Raman features of crystalline V_2O_5 with bands around 1002, 710, 535, 489, 412, 310 and 291 cm^{-1}. The formation of crystalline V_2O_5 on the catalyst surface has also been observed by XRD [17]. It can be

Table 1
Chemical analysis, BET surface areas, oxygen uptakes, and oxygen atom site density on the surface of V_2O_5–TiO_2/SO_4^{2-} catalysts.

Catalyst	CA (wt%)			S_{BET} ($m^2\,g^{-1}$)	O_2 uptake ($mmol\,g^{-1}$)[a]	Total loading ($\times10^{18}\,V\,m^{-2}$)[b]	O site density ($\times10^{18}\,atom\,m^{-2}$)[c]
	V	Ti	S				
VTiS-CP	13.4	43.8	0.2	105	0.75	15.1	8.6
VTiS-CPEG	13.4	45.1	0.2	74	1.08	21.4	17.6
VTiS-SG	11.4	44.8	1.4	43	0.86	31.3	24.1
VTiS-MG	12.4	34.6	6.5	132	0.35	11.1	3.2

[a] Reduction of samples by H_2 and O_2 adsorption were both performed at 640 K.
[b] Supposing that all the vanadium atoms are located on the surface.
[c] Supposing that each surface V adsorbs an oxygen atom.

also seen that strong Raman bands due to the covalent character of Ti–O bonds [22] appeared at 650, 528 and 408 cm^{-1} for all the VTiS catalysts except for VTiS-MG-yellow particles, suggesting that these yellow particles were mostly composed of vanadia. It was reported in the literature [28] that the sulfate species present on sulfated V_2O_5/TiO_2 samples display a characteristic band around 1370 cm^{-1} in the Raman spectra due to terminal S=O bonds. However, this band was not observed for our VTiS catalysts, even though surface sulfate species were detected by IR for the VTiS-MG catalyst [17].

3.2. Surface acidity

Ammonia adsorption microcalorimetry measurements were carried out to determine the number, strength and strength distribution of the surface acid sites of catalysts [15,29]. The results of the microcalorimetric measurements were used to complement the acidity study by FT-IR, and were correlated with the catalytic activity. The surface acidity was thus determined in terms of number of acid sites and sites strength. The results are presented in Figs. 2–4 and Table 2. Figs. 2 and 3 represent the differential heats and integral heats of NH_3 adsorption vs. coverage, respectively. As the samples displayed quite different surface areas (see Table 1) the adsorbed volumes have been expressed in μmol NH_3 per m^2 of catalyst.

The initial heats of ammonia adsorption observed on co-precipitated VTiS samples doped or not with 1 wt% PEG-400 were similar. The initial heats of NH_3 adsorption were 209 and 196 kJ mol^{-1} for the VTiS-CP and VTiS-CPEG samples, respectively (see Table 2), which indicates that these two samples are quite acidic, in agreement with the results from Hammett titration [30]. As can be seen in Fig. 2, low initial heats of adsorption were observed for the VTiS-SG and VTiS-MG samples, containing high content of sulfur. The low heat values recorded for the first four ammonia increments (which were totally consumed by the sample) were followed by an increase to higher heats of adsorption,

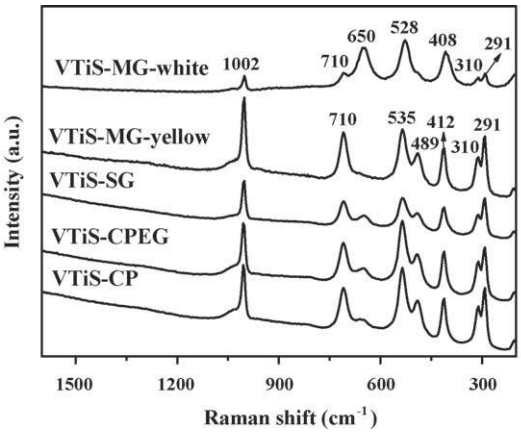

Fig. 1. Raman spectra of VTiS catalysts.

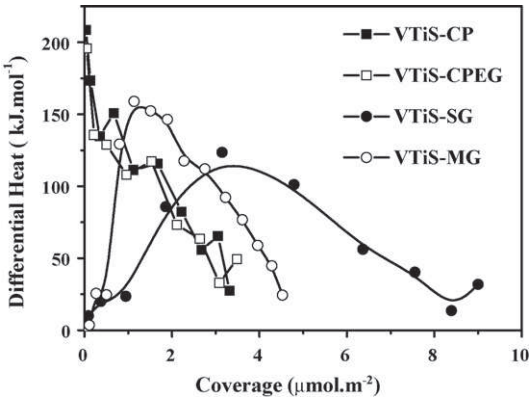

Fig. 2. Differential heat vs. coverage (in μmol m^{-2} of catalyst) for NH_3 adsorption at 423 K over VTiS catalysts.

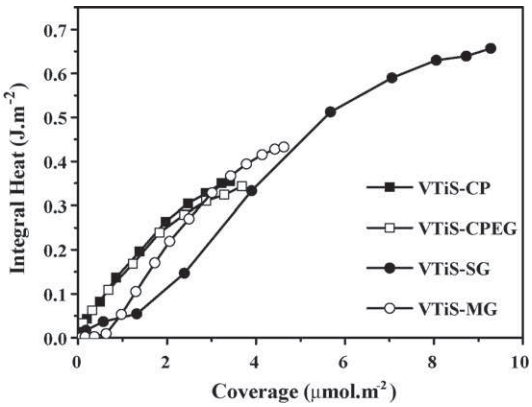

Fig. 3. Integral heat vs. coverage (in μmol m^{-2} of catalyst) for NH_3 adsorption at 423 K over VTiS catalysts.

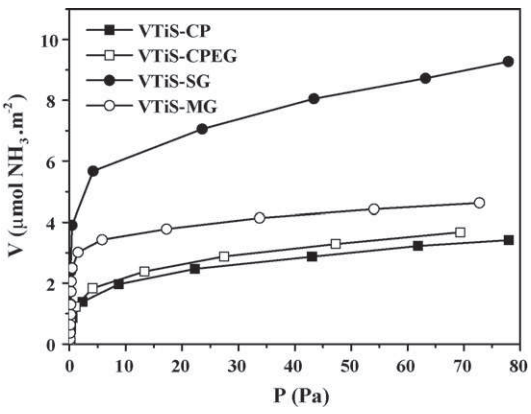

Fig. 4. Volumetric isotherms of NH_3 adsorption at 423 K for the VTiS catalysts.

Table 2
Total and irreversible adsorption of ammonia at a pressure of 27 Pa and an adsorption temperature of 423 K.

Sample	V_{tot}[a] (27 Pa) (μmol g^{-1})	V_{tot}[a] (27 Pa) (μmol m^{-2})	V_{irr}[b] (μmol g^{-1})	V_{irr}[b] (μmol m^{-2})	Q_{init}[c] (kJ mol^{-1})	Q_{int}[d] (27 Pa) (J g^{-1})
VTiS-CP	243	2.3	123	1.2	209	32
VTiS-CPEG	193	2.6	77	1.1	196	23
VTiS-SG	281	6.5	216	5.0	3	26
VTiS-MG	503	3.8	392	3.0	10	54

[a] Total amount of NH_3 retained as determined at 27 Pa of equilibrium pressure.
[b] "Irreversible" amount of NH_3 retained as determined from the difference between the amounts adsorbed in the first and second adsorptions at 27 Pa.
[c] Heat evolved from the first NH_3 dose.
[d] Total heat evolved at 27 Pa of NH_3 equilibrium pressure upon NH_3 adsorption.

corresponding to what is normally expected for a strong acid. This strange phenomenon can only be interpreted by the combination of two phenomena, endothermic and exothermic, respectively, thus inducing a lower initial heat. The very strong acid sites due to sulfate ions are supposed to create either a strong or dissociative chemisorption. It has been reported in the literature [16,31] that the first doses of NH_3 could dissociate at the surface (endothermic phenomenon) with the formation of OH species, evidenced by NH_3 adsorption infrared spectroscopy [31]. The lower heats of adsorption are then attributed to the contribution of NH_3 dissociation to the differential heat of adsorption. Another explanation could be the formation of ammonium sulfate (however this last possibility implies a transformation that is too exothermic [32], making it unlikely) or more probably ammonium sulfite. This particular behavior observed for samples containing a relatively high amount of sulfur made it difficult to appreciate the initial heats of adsorption of the sulfated oxides. As this phenomenon was scarcely observed by adsorption calorimetry for sulfated zirconias it is supposed to imply a special type of sulfur species on the catalyst surface, which could involve the support type and/or the preparation method. For co-precipitated catalysts with or without 1 wt% PEG-400, which contain a much lower amount of sulfur species, the heats of NH_3 adsorption gradually decreased with NH_3 coverage, revealing the heterogeneous strength distribution of these catalysts. Fig. 4, which represents the ammonia adsorption isotherms, did not reflect this particular behavior of samples VTiS-SG and VTiS-MG, thus confirming that these two samples are more acidic due to their higher sulfate species content.

As shown in Fig. 3, ammonia adsorption integral heat curves for VTiS-CP and VTiS-CPEG catalysts can be approximately viewed as sections of parabolas, and the highest parabola should correspond to the sample on which the titration of the largest amount of strong sites occurred [33]. The coverage being reported per unit of surface area (instead of g of catalyst) the two curves are very close and confirm the similar acidic behavior of the samples prepared by co-precipitation. The curves, for VTiS-SG and VTiS-MG samples, display a plateau in the low coverage region for the first four NH_3 doses, which can be associated to the strange phenomenon of very low initial differential heats of adsorption for these two samples. Therefore the parabolic sections of the curves are shifted to higher coverages.

The quantitative results of NH_3 adsorption are summarized in Table 2. The total amount of ammonia adsorbed at an equilibrium pressure of 27 Pa (V_{tot}) and the amount irreversibly adsorbed at the same pressure (V_{irr}) are indicative of the total number of acid sites on the surface of the sample and the amount of strong acid sites, respectively. Reported in μmol g^{-1}, both V_{tot} and V_{irr} varied in the order of VTiS-MG > VTiS-SG > VTiS-CP > VTiS-CPEG, greatly influenced by the preparation method and consequently by the sulfur amount. When V_{tot} and V_{irr} are expressed per unit surface area, the total and strong surface acid sites densities for the VTiS-CP and VTiS-CPEG samples are similar, while the VTiS-SG sample possesses more total and strong surface acid sites than VTiS-MG, which confirms the role played by the surface area in the determination of the acidity of solids (see Table 2 and Fig. 2). The data in Table 2 clearly indicate that most of the adsorbed ammonia is strongly chemisorbed on samples VTiS-SG and VTiS-MG, while the co-precipitated samples display a large part of physisorption.

IR spectroscopy of pyridine adsorption on supported vanadium oxide surfaces has been examined widely in the literature [34–37], as it can be used to distinguish between the different types of surface acid sites in the catalysts.

Fig. 5(A)–(D) present the IR spectra of pyridine adsorption on VTiS catalysts, after desorption at different temperatures: (a) 298 K, (b) 373 K, (c) 473 K, and (d) 573 K. All the spectra reported in Fig. 5 were obtained by subtracting the spectrum of the fresh catalyst (without pyridine adsorption at room temperature) from those obtained after pyridine adsorption. The same adsorption bands characteristic of pyridine on Lewis and Brønsted acid sites were observed for all VTiS catalysts, and no significant shift in the peak frequency positions was observed as a function of the preparation method. The bands at 1609, 1575, 1487 and 1448 cm^{-1} have been assigned to the 8a, 8b, 19a and 19b vibrational modes of pyridine coordinated to Lewis acid sites [34,36]. The bands at 1638 (v8a), 1575 (v8b), 1487 (v19a) and 1537 cm^{-1} (v19b) correspond to pyridinium ions bonded to Brønsted acid sites. The bands around 1487 (v19a) and 1575 cm^{-1} (v8b) are associated simultaneously to both Brønsted and Lewis acid sites. In addition to these peaks, at a desorption temperature of 298 K, the IR spectra of the catalysts show a peak at 1437 cm^{-1} corresponding to physisorbed pyridine. It has been reported in the literature [38] that pure V_2O_5 presents low Brønsted and Lewis acidities, while TiO_2 exhibits strong Brønsted and Lewis acidities according to the relative intensities of the bands around 1536 and 1446 cm^{-1}.

Two Lewis and Brønsted acid site peaks at ~1448 and 1537 cm^{-1}, respectively, were used to compare the acidity, i.e. the number and strength of the acid sites of the different catalysts. The absolute concentration of surface acid sites determined in this manner is subject to a ~10% error, as estimated in the literature [39,40]. However, reliable and valuable information can be obtained on a relative scale, when comparing the acidity in a series of catalysts [40].

Fig. 6 shows the integrated intensities of these two bands estimated by band-separation techniques of the spectra for VTiS catalysts. A quantitative comparison of the acid site populations of the samples can be performed by calculating the area under the LPy and BPy peaks [34,41,42]. Because of the possibility of physical re-adsorption on the surface with increasing evacuation temperatures, it is reasonable to compare the acid site populations at an evacuation temperature higher than 400 K. Therefore, the concentration of Brønsted and Lewis acid sites varied in the order of VTiS-MG > VTiS-CP > VTiS-CPEG > VTiS-SG, which indicates that the mechanical mixing sample which comes from the simple addition of titania and vanadyl sulfate is more acidic than the other samples, thus confirming the calorimetric results.

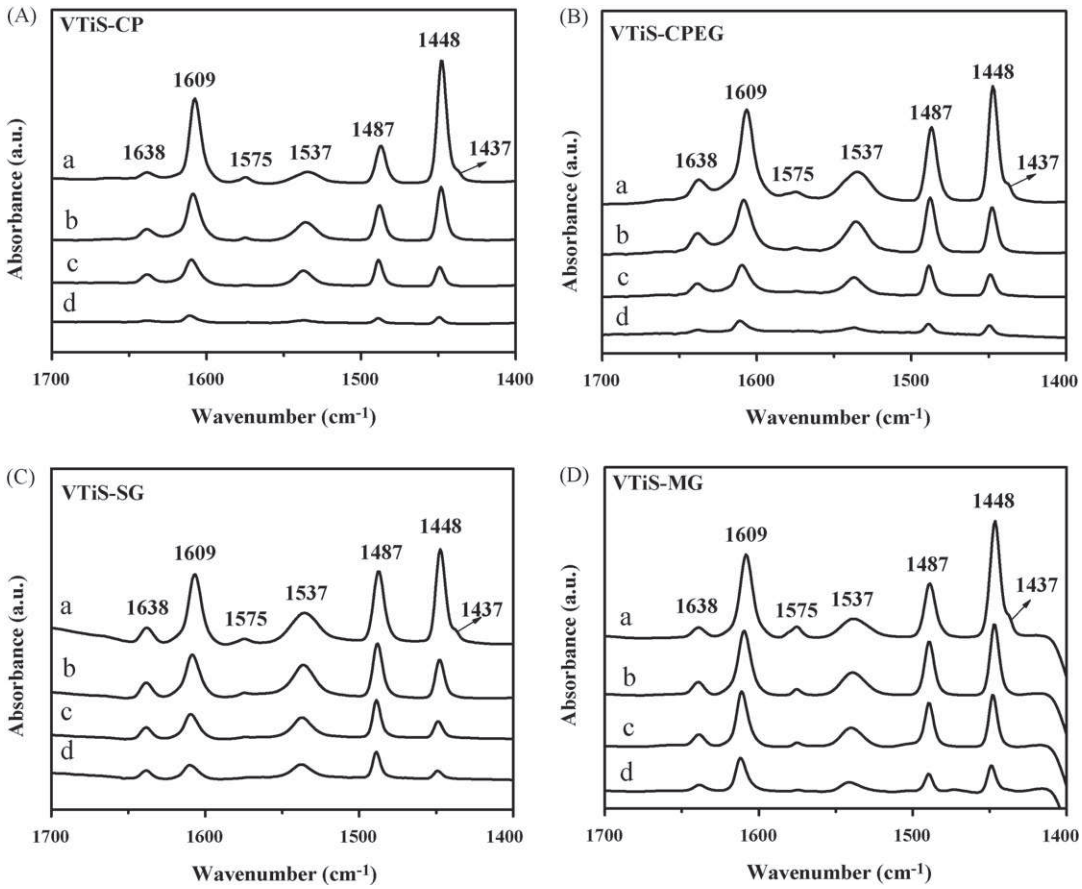

Fig. 5. FT-IR spectra for pyridine adsorption and desorption on (A) VTiS-CP, (B) VTiS-CPEG, (C) VTiS-SG and (D) VTiS-MG catalysts at different temperatures: (a) 298 K, (b) 373 K, (c) 473 K and (d) 573 K.

3.3. Methanol oxidation reaction

Methanol and its derivatives have been widely studied due to their industrial importance. In addition, the catalytic oxidation of methanol is a convenient structure-sensitive reaction. The distribution of products reflects the nature of the surface active sites: methanol is converted to formaldehyde (FA) and methyl formate (MF) on redox sites, to dimethyl ether (DME) on acidic sites, and to DMM on acidic and redox bi-functional sites [12,13]. Hence, the conversion of methanol can also be used to evaluate the surface acidic and redox properties of VTiS catalysts. The results are shown in Table 3 and Fig. 7.

The VTiS-CP catalyst, prepared by the co-precipitation method, showed the highest methanol conversion to DMM, but a drastic decrease in selectivity was observed for reaction temperatures higher than 423 K. In addition, the distribution of products on VTiS-

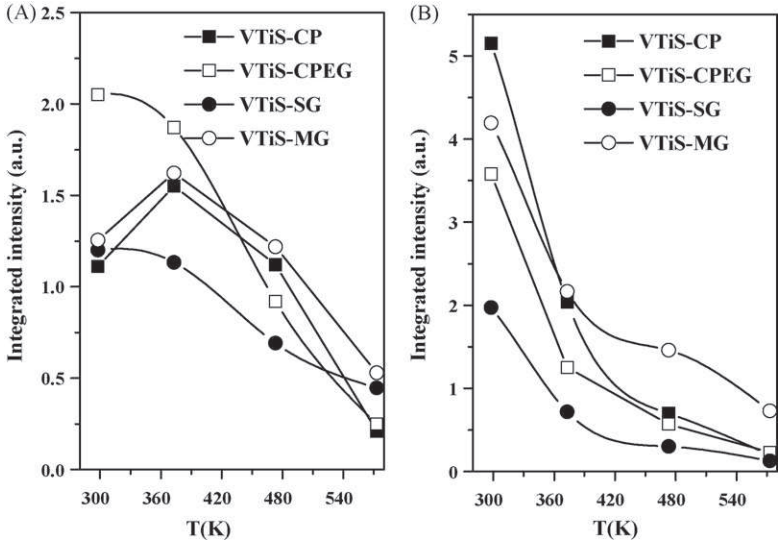

Fig. 6. Integrated intensity of BPy and LPy bands as a function of temperature on VTiS catalysts. (A) BPy band (1537 cm^{-1}); (B) LPy band (1448 cm^{-1}).

Table 3
Catalytic activities of the VTiS catalysts in the methanol oxidation reaction.

Sample	Temp. (K)	Methanol conversion (%)	Selectivity (%)				
			DMM	FA	MF	DME	CO_x
VTiS-CP	393	13	98	0	1	1	0
	403	24	96	0	3	1	0
	413	42	93	0	6	1	0
	423	61	86	1	12	1	0
	433	72	40	13	46	1	0
	443	87	1	6	74	2	17
VTiS-CPEG	393	10	98	0	1	1	0
	403	17	96	0	3	1	0
	413	23	83	9	7	1	0
	423	28	56	26	17	1	0
	433	37	24	38	37	1	0
	443	76	1	10	73	1	15
VTiS-SG	393	7	96	0	1	3	0
	403	12	97	0	2	1	0
	413	19	96	0	3	1	0
	423	33	93	0	6	1	0
	433	47	89	0	10	1	0
	443	65	72	2	25	1	0
VTiS-MG	393	2	93	0	0	7	0
	403	4	93	0	0	7	0
	413	8	91	2	0	7	0
	423	15	90	2	1	7	0
	433	21	88	3	1	8	0
	443	33	84	3	3	10	0

DMM: dimethoxymethane; FA: formaldehyde; MF: methyl formate; DME: dimethyl ether; CO_x: CO_2 (or CO).

CP catalyst indicates that the surface acidity was strong enough to catalyze the reaction of methanol to DMM, without producing a large amount of FA and MF as oxidation products (see Table 3). The catalytic performance of the VTiS-CPEG sample was similar to that of VTiS-CP, with a slightly lower activity and selectivity to DMM (at 423 K, VTiS-CP: conversion = 61%, S_{DMM} = 86%, vs. VTiS-CPEG: conversion = 28%, S_{DMM} = 56%). This can be attributed to a decreased reducibility and surface acidity upon addition of 1 wt% PEG-400. For samples prepared by sol–gel and mechanical grinding, a different behavior was observed. In fact, even increasing the reaction temperature up to 443 K, no formic acid (FA) production could be observed, and a very high selectivity towards DMM (72 and 84% respectively for VTIS-SG and VTIS-MG) was maintained. These results can be related to the higher percentage of SO_4^{2-} present on these two samples, which can both inhibit the activity of the redox sites (connected to FA production) and/or prevent the deactivation of the acidic sites even at high reaction temperature [4].

Furthermore, the selectivity to DME (usually created on strong acid sites) over the VTiS-MG catalyst prepared by mechanical grinding was higher and increased with increasing reaction temperatures. Of all catalysts studied in this work, the VTiS-CP sample was found to be the most effective in the selective oxidation of methanol to DMM with 61% conversion of methanol and 86% selectivity to DMM, probably due to the presence of the highest amount of vanadia surface species and an appropriate content of SO_4^{2-}.

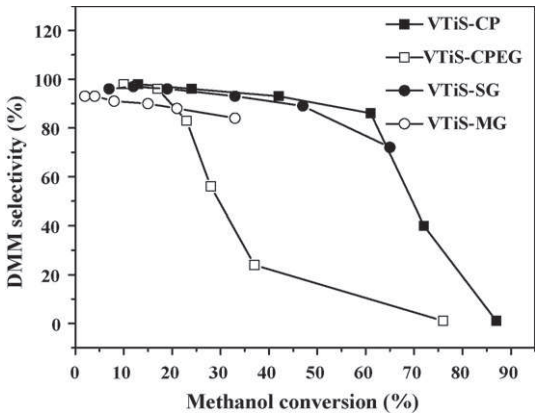

Fig. 7. DMM selectivity vs. methanol conversion over VTiS catalysts.

4. Conclusion

As expected, the surface and catalytic properties of V_2O_5–TiO_2/SO_4^{2-} catalysts were greatly influenced by different preparation methods. Crystallites of V_2O_5 were detected for all samples by Raman spectroscopy. Moreover, Raman spectroscopy also suggested that the sample prepared by mechanical grinding was not homogeneous. The ammonia adsorption calorimetric study showed the special behavior of NH_3 dissociation at the surface of some samples, those containing a high content of sulfur. However, pyridine adsorption FT-IR did not show an obvious difference of surface acidity between the samples, and indicated the coexistence of both Lewis and Brønsted acid sites for all VTiS catalysts studied in this work. The co-precipitated catalyst VTiS-CP was found to exhibit the best performance for the selective oxidation of methanol to DMM. Specifically, the conversion of methanol could be as high as 61% over VTiS-CP, with a high DMM selectivity of 86% at 423 K. Meanwhile, catalytic methanol oxidation was also successfully used to investigate the quantities of surface active sites. In conclusion, the acidic and catalytic properties were affected on one hand by the preparation method and on the other hand by the SO_4^{2-} content.

Acknowledgements

The authors are thankful to the scientific services of IRCELYON and in particular to P. Mascunan, for providing O_2 chemisorption and Raman measurements.

Hongying Zhao gratefully acknowledges the China Scholarship Council for the financial support of her PhD grant. Financial

supports from NSFC (20673055), MSTC (2005CB221400 and 2004DFB02900) and Jiangsu Province, China (BG2006031) are acknowledged.

References

[1] F. Roozeboom, P.D. Cordingley, P.J. Gellings, J. Catal. 68 (1981) 464–472.
[2] P. Forzatti, E. Tronconi, G. Busca, P. Tittarelli, Catal. Today 1 (1987) 209–218.
[3] A. Baiker, D. Monti, J. Catal. 91 (1985) 361–365.
[4] S. Royer, X. Sécordel, M. Brandhorst, F. Dumeignil, S. Cristol, C. Dujardin, M. Capron, E. Payen, J.-L. Dubois, Chem. Commun. 7 (2008) 865–867.
[5] Y. Fu, J. Shen, Chem. Commun. 21 (2007) 2172–2174.
[6] S. Damyanova, M.L. Cubeiro, J.L.G. Fierro, J. Mol. Catal. A: Chem. 142 (1999) 85–100.
[7] C.R. Anthony, L. Mcelwee-White, J. Mol. Catal. A: Chem. 227 (2005) 113–117.
[8] K. Fuji, S. Nakano, E. Fujita, Synthesis 4 (1975) 276–277.
[9] J. Masamoto, T. Iwaisako, M. Chohno, M. Kawamura, J. Ohtake, K. Matsuzaki, J. Appl. Polym. Sci. 50 (1993) 1299–1305.
[10] Q. Sun, A. Auroux, J. Shen, J. Catal. 244 (2006) 1–9.
[11] S. Satoh, Y. Tanigawa, US Patent 6,379,507 (2002).
[12] J.M. Tatibouët, Appl. Catal. A 148 (1997) 213–252.
[13] M. Badlani, I.E. Wachs, Catal. Lett. 75 (2001) 137–149.
[14] L.E. Briand, Met. Oxides: Chem. Appl. 108 (2006) 353–390.
[15] A. Auroux, Top. Catal. 4 (1997) 71–89.
[16] F. Belkhadem, J.-M. Clacens, A. Bengueddach, F. Figueras, Appl. Catal. A 298 (2006) 188–193.
[17] H. Zhao, S. Bennici, J. Shen, A. Auroux, Appl. Catal. A 356 (2009) 121–128.
[18] S.T. Oyama, G.T. Went, K.B. Lewis, A.T. Bell, G.A. Somorjai, J. Phys. Chem. 93 (1989) 6786–6790.
[19] B.S. Parekh, S.W. Weller, J. Catal. 47 (1977) 100–108.
[20] S.W. Weller, Acc. Chem. Res. 16 (1983) 101–106.
[21] B.M. Reddy, B. Manohar, E.P. Reddy, Langmuir 9 (1993) 1781–1785.
[22] I.E. Wachs, Catal. Today 27 (1996) 437–455.
[23] G.T. Went, L.J. Leu, A.T. Bell, J. Catal. 134 (1992) 479–491.
[24] M.D. Amiridis, I.E. Wachs, G. Deo, J.M. Jehng, D.S. Kim, J. Catal. 161 (1996) 247–253.
[25] G.T. Went, L.J. Leu, R.R. Rosin, A.T. Bell, J. Catal. 134 (1992) 492–505.
[26] I.R. Beattie, T.R. Gilson, J. Chem. Soc. A (1969) 2322–2327.
[27] F. Roozeboom, M.C. Mittelmeijer-Hazeleger, J.A. Moulijn, J. Medema, V.H.J. De Beer, P.J. Gellings, J. Phys. Chem. 84 (1980) 2783–2791.
[28] J.P. Dunn, J.M. Jehng, D.S. Kim, L.E. Briand, H.G. Stenger, I.E. Wachs, J. Phys. Chem. B 102 (1998) 6212–6218.
[29] J. Keränen, A. Auroux, S. Ek-Härkönen, L. Niinistö, Thermochim. Acta 379 (2001) 233–239.
[30] K. Tanabe, Mater. Chem. Phys. 17 (1987) 217–225.
[31] A. Desmartin-Chomel, J.L. Flores, A. Bourane, J.-M. Clacens, F. Figueras, G. Delahay, A. Giroir Fendler, C. Lehaut-Burnouf, J. Phys. Chem. B 110 (2006) 858–863.
[32] A. Gervasini, J. Fenyvesi, A. Auroux, Langmuir 12 (1996) 5356–5364.
[33] A. Gervasini, A. Auroux, J. Phys. Chem. 97 (1993) 2628–2639.
[34] F. Hatayama, T. Ohno, T. Maruoka, T. Ono, H. Miyata, J. Chem. Soc., Faraday Trans. 87 (1991) 2629–2633.
[35] T. Blasco, A. Galli, J.M. López Nieto, F. Trifiró, J. Catal. 169 (1997) 203–211.
[36] J. Keränen, A. Auroux, S. Ek, L. Niinistö, Appl. Catal. A 228 (2002) 213–225.
[37] J. Datka, A.M. Turek, J.M. Jehng, I.E. Wachs, J. Catal. 135 (1992) 186–199.
[38] Q. Sun, Y. Fu, J. Liu, A. Auroux, J. Shen, Appl. Catal. A 334 (2008) 26–34.
[39] M. Amiridis, R. Duevel, I. Wachs, Appl. Catal. B 20 (1999) 111–122.
[40] T. Barzetti, E. Selli, D. Moscotti, L. Forni, J. Chem. Soc., Faraday Trans. 92 (1996) 1401–1407.
[41] H. Miyata, K. Fujii, S. Inui, Y. Kubokawa, Appl. Spectrosc. 40 (1986) 1177–1180.
[42] H. Miyata, Y. Nakagawa, S. Miyagawa, Y. Kubokawa, J. Chem. Soc., Faraday Trans. 1 (84) (1988) 2129–2134.

Publication IV

J Therm Anal Calorim (2010) 99:843–847
DOI 10.1007/s10973-009-0499-0

Calorimetric study of the acidic character of V_2O_5–TiO_2/SO_4^{2-} catalysts used in methanol oxidation to dimethoxymethane

H. Zhao · S. Bennici · J. Shen · A. Auroux

MEDICTA2009 Conference

Abstract The surface acidic properties of sulfated vanadia–titania catalysts prepared by various methods were investigated by adsorption microcalorimetry, using ammonia as probe molecule. The acidic characteristics of the samples were shown to be strongly affected by the preparation method, calcination temperature, and sulfur content. The samples prepared by sol–gel and mechanical grinding exhibited higher acidity than co-precipitated samples. Moreover, increasing the calcination temperature of co-precipitated samples resulted in a decrease in surface area from 402 to 57 $m^2\ g^{-1}$ and sulfur content from around 4 to 0.2 mass%, but up to a certain point generated a stronger acidity. The optimal calcination temperature appeared to be around 673 K.

Keywords Acidity · Calorimetry · Dimethoxymethane · Methanol selective oxidation · V_2O_5–TiO_2/SO_4^{2-}

Introduction

Vanadia–titania catalysts can be found in wide applications, such as the methanol selective oxidation to formaldehyde [1] and methyl formate [2], and the selective oxidation of ethanol to acetaldehyde [3]. In addition, sulfated vanadia–titania catalysts are starting to have new applications in the partial oxidation of methanol to dimethoxymethane (DMM) [4, 5], which can undergo further steam reforming to produce hydrogen.

The knowledge of the number and strength of the sites existing at the surface of a catalyst is of paramount interest, as the first step in any catalytic reaction is the adsorption and the subsequent activation of the reactant molecules. Adsorption microcalorimetry [6, 7] is a useful technique to describe, in detail, the quantitative and energetic features of surface sites. It allows, if properly arranged, the simultaneous determination of the adsorbed amounts of a suitable probe molecule and of the heat evolved at increasing surface coverage.

Although, we have previously reported the influence of the preparation method on the surface properties of some sulfated vanadia-titania catalysts calcined at a given temperature of 723 K [4, 8], the purpose of this article is to study in detail the influence of the calcination temperature and washing with deionized water on the surface acidity of V_2O_5–TiO_2/SO_4^{2-} catalysts prepared by different methods. Results about the physicochemical characteristics of the samples and their acidity as studied by ammonia adsorption microcalorimetry are presented.

Experimental

Samples with the same theoretical amount of vanadia loading (25 mass%) were prepared using different procedures, namely co-precipitation (samples named VTiS–CP), co-precipitation with 1-mass% polyethylene glycol (VTiS–CPEG), sol-gel (VTiS–SG), and mechanical grinding (VTiS–MG). The precursors were $VOSO_4$ and $TiOSO_4$ for VTiS–CP and VTiS–CPEG, respectively, vanadyl

H. Zhao · S. Bennici · A. Auroux (✉)
Université Lyon 1, CNRS, UMR 5256, IRCELYON, Institut de recherches sur la catalyse et l'environnement de Lyon, 2 avenue Albert Einstein, 69626 Villeurbanne, France
e-mail: aline.auroux@ircelyon.univ-lyon1.fr

H. Zhao · J. Shen
Laboratory of Mesoscopic Chemistry, School of Chemistry and Chemical Engineering, Nanjing University, 210093 Nanjing, China

acetylacetonate and titanium isopropoxide plus sulfuric acid for VTiS–SG, TiO_2 and $VOSO_4$ for VTiS–MG.

In this study, the samples VTiS–CP-723, VTiS–CPEG-723, and VTiS–MG-723 were prepared by the corresponding procedures cited above and calcined at 723 K in air for 5 h, except sample VTiS–SG-723 for which the calcination time was increased up to 12 h for a better decomposition of the organic precursors.

The VTiS–CP-573, VTiS–CP-623, VTiS–CP-673, and VTiS–CP-773 samples were prepared by co-precipitation and calcined in air for 5 h at 573, 623, 673, and 773 K, respectively. Moreover, the samples VTiSw50–CP-673 and VTiSw300–CP-673 were prepared by co-precipitation, washed, respectively, with 50 and 300 mL deionized water and then calcined at 673 K in air for 5 h.

The details of the preparation methods have been previously described in [4].

Elemental analysis was performed using ICP atomic emission spectroscopy (AES–ICP) with a flame PerkinElmer M1100 spectrometer. The BET surface areas were measured using nitrogen adsorption at 77 K on a Micromeritics 2010 apparatus.

The microcalorimetric studies of ammonia adsorption were performed at 423 K in a heat-flow calorimeter (C80 from Setaram) linked to a conventional volumetric apparatus equipped with a Barocel capacitance manometer for pressure measurements. Before each experiment the samples were outgassed overnight at a temperature of 100 K lower than the calcination temperature. After a first adsorption, performed by repeatedly adding successive amounts of NH_3 onto the sample until an equilibrium pressure of about 67 Pa was reached, the sample was evacuated for 30 min, to remove the weakly adsorbed NH_3, and a second adsorption was performed to determine the amount of ammonia irreversibly adsorbed.

Results and discussion

The results of bulk analysis (chemical analysis) as well as surface area for all the VTiS samples are given in Table 1. Depending on the preparation method and calcination temperature, the sulfur mass% varied greatly and remained difficult to control. The sulfur content was observed to be higher for samples prepared by sol–gel and mechanical grinding than by co-precipitation method. Meanwhile for co-precipitated samples, the sulfur concentration decreased with increasing the calcination temperature and by washing with deionized water, thus suggesting that the sulfur species did not seem to be tightly anchored to vanadia species or support surface. Additionally, the way the sulfur species anchored to the support surface was strongly affected by the preparation method, leading to different surface acidities. Furthermore, sample VTiS–CP-573 displayed a high surface area of 402 $m^2\ g^{-1}$. With increasing the calcination temperature, the surface area decreased, down to the lowest value at 773 K (57 $m^2\ g^{-1}$). Washing with deionized water did not significantly change the surface area of the same series samples. In addition, comparing samples prepared by different methods and calcined at 723 K, it was found that adding PEG did not influence the surface area of the co-precipitated samples and indeed no benefit was gained

Table 1 Chemical analysis, BET surface areas, ammonia adsorption data from microcalorimetry measurements at 423 K

Catalyst	CA/mass%			S_{BET}/$m^2\ g^{-1}$	V^a_{tot}/μmol g^{-1}	V^a_{tot}/μmol m^{-2}	V^b_{irr}/μmol g^{-1}	V^b_{irr}/μmol m^{-2}	Q^c_{int}/J g^{-1}
	V	Ti	S						
VTiS–CP-723	13.4	43.8	0.2	105	243	2.3	123	1.2	32
VTiS–CPEG-723	13.4	45.1	0.2	74	193	2.6	77	1.1	23
VTiS–SG-723	11.4	44.8	1.4	43	281	6.5	216	5.0	26
VTiS–MG-723	12.4	34.6	6.5	132	503	3.8	392	3.0	54
VTiS–CP-573	10.4	33.9	3.2	402	578	1.4	264	0.7	61
VTiS–CP-623	10.9	34.7	4.0	368	591	1.6	358	1.0	70
VTiS–CP-673	12.6	41.0	2.6	287	608	2.1	374	1.3	69
VTiS–CP-723	13.4	43.8	0.2	105	243	2.3	123	1.2	32
VTiS–CP-773	13.4	44.4	0.2	57	163	2.9	69	1.2	16
VTiSw50–CP-673	13.1	39.9	0.8	290	568	2.0	319	1.1	69
VTiSw300–CP-673	12.6	41.6	0.2	289	551	1.9	275	1.0	63

[a] Total amount of NH_3 retained as determined at 27 Pa of equilibrium pressure

[b] "Irreversible" amount of NH_3 retained as determined from the difference between the amounts adsorbed in the first and second adsorptions at 27 Pa

[c] Total heat evolved at 27 Pa of NH_3 equilibrium pressure upon NH_3 adsorption

upon PEG addition. It was also found that sample VTiS–SG-723, prepared by sol–gel method, displayed the lowest surface area of 43 $m^2\ g^{-1}$.

Ammonia adsorption microcalorimetry measurements were carried out to determine the number, strength, and strength distribution of the surface acid sites of catalysts [9, 10]. The surface acidity was thus determined in terms of number of acid sites and sites strength. The results are presented in Figs. 1 and 2 and Table 1. Figure 1a–c represents the differential heats of adsorption versus coverage of ammonia, while Fig. 2a–c gives the volumetric isotherms of NH_3 adsorption.

As shown in Fig. 1a, the initial heats of ammonia adsorption observed on co-precipitated VTiS samples doped or not with 1-mass% PEG–400 were similar, around 200 kJ mol^{-1}, which indicates that these two samples are quite acidic, in agreement with the results from Hammett titration [11]. However, very low initial heats of adsorption were observed for the VTiS–SG-723 and VTiS–MG-723 samples, containing high content of sulfur. The low heat

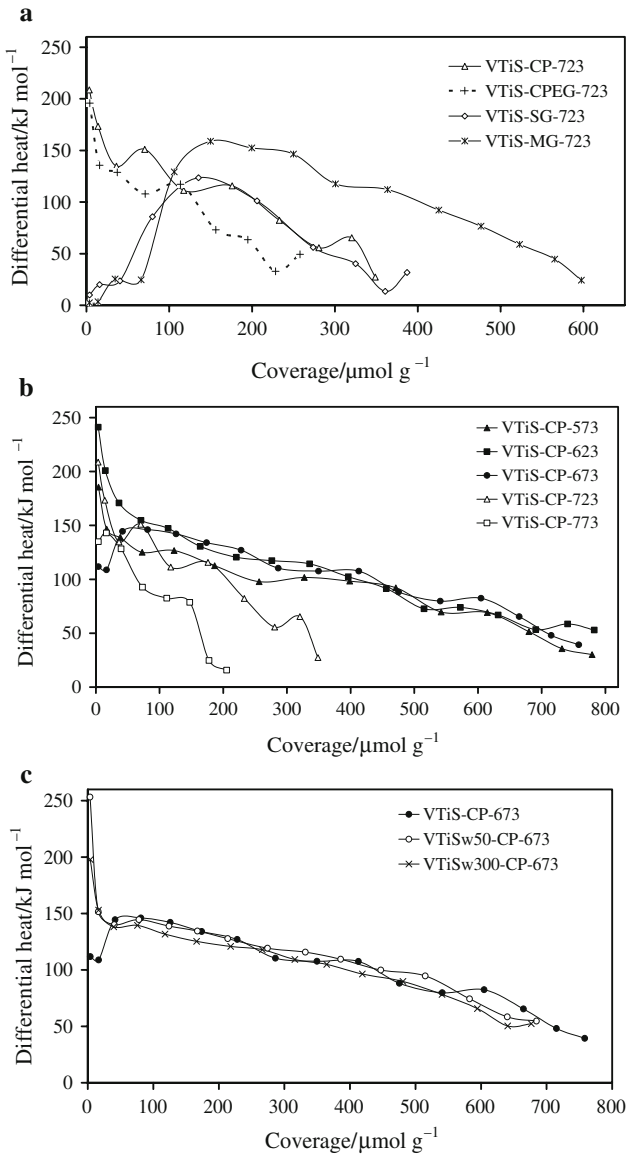

Fig. 1 Differential heat versus coverage (in μmol g^{-1} of catalyst) for NH_3 adsorption at 423 K over VTiS catalysts **a** VTiS catalysts prepared by different methods and calcined at 723 K, **b** VTiS catalysts prepared by co-precipitation and calcined at various temperatures, **c** VTiS catalysts prepared by co-precipitation, washed with different amount of deionized water and then calcined at 673 K

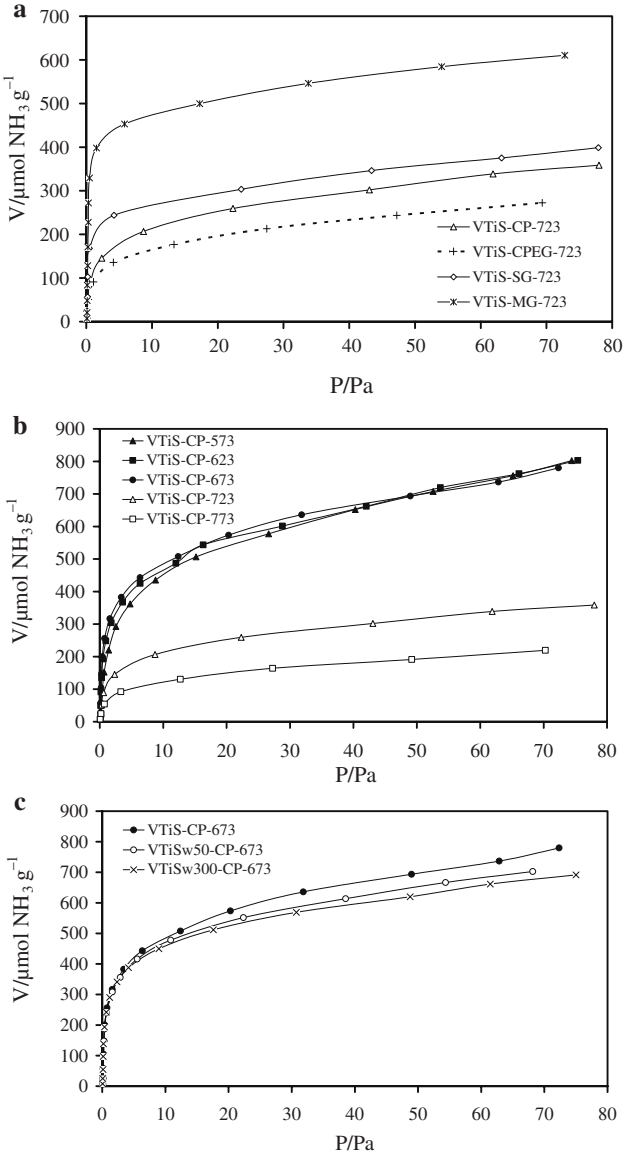

Fig. 2 Volumetric isotherms of NH_3 adsorption at 423 K for VTiS catalysts **a** VTiS catalysts prepared by different methods and calcined at 723 K, **b** VTiS catalysts prepared by co-precipitation and calcined at various temperatures, **c** VTiS catalysts prepared by co-precipitation, washed with different amount of deionized water and then calcined at 673 K

values recorded for the first four ammonia increments (which were totally consumed by the sample) were followed by an increase to higher heats of adsorption, corresponding to what is normally expected for a strong acid. This strange phenomenon can only be interpreted by the combination of two phenomena, endothermic and exothermic, thus inducing a lower initial heat. The very strong acid sites due to sulfate ions are supposed to create either a strong or a dissociative chemisorption. It has been reported in the literature [12] that the first doses of NH_3 could dissociate at the surface (endothermic phenomenon) with the formation of OH species, evidenced by NH_3 adsorption infrared spectroscopy [12]. The low heats of adsorption are then attributed to the contribution of NH_3 dissociation to the differential heat of adsorption. Another explanation could be probably the formation of ammonium sulfite [13]. This particular behavior observed for samples containing a relatively high amount of sulfur made it difficult to appreciate the initial heats of adsorption of the sulfated oxides. As this phenomenon was scarcely observed by adsorption calorimetry for sulfated zirconias it is supposed to imply a special type of sulfur species on the catalyst surface, which could involve the support type and/or the preparation method. For co-precipitated catalysts with or without 1-mass% PEG–400, which contain a much lower amount of sulfur species, the heats of NH_3 adsorption gradually decreased with NH_3 coverage, revealing the heterogeneous strength distribution of these catalysts. Figure 2a, which represents the ammonia adsorption isotherms, did not reflect the particular behavior of samples VTiS–SG-723 and VTiS–MG-723, thus confirming that these two samples chemisorbed more ammonia and were more acidic due to their higher sulfate species content.

In Fig. 1b are shown the differential heats of adsorption versus ammonia coverage on samples prepared by co-precipitation and calcined at different temperatures (system VTiS–CP). Relatively, low initial heat of adsorption was obtained for sample VTiS–CP-673. However, it is noteworthy that no low initial heats were observed for VTiS–CP-573 and VTiS–CP-623 samples which contained a higher sulfur concentration than sample VTiS–CP-673 thus confirming the role played by the calcination temperature in the determination of the sulfate-type species on the catalyst surface. In order to determine how the sulfur concentration could influence the acidity of VTiS catalysts, NH_3 adsorption microcalorimetry experiments were also performed on the VTiSw catalysts, washed with deionized water and then calcined at 673 K. After washing with different amounts of deionized water, the content of sulfur (chemical analysis) drastically decreased from 2.58 mass% (VTiS–CP-673) to 0.75 mass% (VTiSw50–CP-673) and even to <0.1 mass% (VTiSw300–CP-673). As can be seen in Fig. 1c, the low initial heat of adsorption previously observed for sample VTiS–CP-673 disappeared for the washed catalysts at low ammonia coverage (<40 μmol g^{-1}). Beyond this value, the profiles of the three curves are similar, characteristic of vanadia–titania mixed oxides. This phenomenon could suggest that only a high concentration of sulfur species can modify significantly the relatively strong acidity of VTi catalysts prepared by co-precipitation.

The quantitative results of NH_3 adsorption are summarized in Table 1. The total amount of adsorbed ammonia at an equilibrium pressure of 27 Pa (V_{tot}) and the amount irreversibly adsorbed at the same pressure (V_{irr}) are indicative of the total number of acid sites and amount of strong acid sites on the surface of the sample, respectively. For samples prepared by different methods and calcined at 723 K, both V_{tot} and V_{irr}, reported in μmol g^{-1}, varied in the order of VTiS–MG-723 > VTiS–SG-723 > VTiS–CP-723 > VTiS–CPEG-723, greatly influenced by the preparation method and consequently by the sulfur amount. In addition, the adsorption isotherms for these samples (Fig. 2a) varied in the same order with a maximum uptake of 360, 270, 400, and 610 μmol g^{-1} for VTiS–CP-723, VTiS–CPEG-723, VTiS–SG-723, and VTiS–MG-723, respectively. For co-precipitated samples calcined at different temperatures, the maximum uptake values of V_{tot} and V_{irr} were obtained for sample VTiS–CP-673, calcined at 673 K. The maximal ammonia uptake was analogous for all the samples except for VTiS–CP-723 and VTiS–CP-773 samples (see Fig. 2b and c), due to their drastic decrease in surface area. Furthermore, the total and strong surface acid sites densities of co-precipitated samples (Table 1) increased with increasing calcination temperature up to a maximum at 673 K (sample VTiS–CP-673), despite a slight decrease in surface area and sulfur content when compared to samples VTiS–CP-573 and -623 respectively. Interestingly, it was the only co-precipitated sample displaying low initial heats of adsorption. Above 673 K a drastic decrease of the number of acid sites was observed. The data in Table 1 clearly indicate that most of the adsorbed ammonia is strongly chemisorbed on samples VTiS–SG-723 and VTiS–MG-723, while all the co-precipitated series samples display a large part of physisorption.

Conclusions

V_2O_5–TiO_2/SO_4^{2-} catalysts were prepared by co-precipitation, co-precipitation with 1-mass% PEG–400, sol–gel, and mechanical grinding methods. The investigation has demonstrated the existence of differences in surface acidity between catalysts prepared by various methods, calcined at different temperature and more or less washed with deionized water. Co-precipitation method was by far the best preparation method in terms of maximizing the surface area

and 673 K was the optimal calcination temperature in terms of maximizing the total acidity. The ammonia adsorption calorimetric study showed the special behavior of NH_3 dissociation at the surface of samples VTiS–SG-723, VTiS–MG-723, and to a small extent VTiS–CP-673. Meanwhile, the data from calorimetric study performed on the washed catalysts (system VTiSw) indicated that a high concentration of sulfur affected only the very strong acidity of VTiS catalysts. For co-precipitated samples, the strongest acidity found for sample VTiS–CP-673 cannot be associated to the sulfur content which was smaller for this sample than for VTiS–CP-573 and VTiS–CP-623 samples, but to the sulfate-type species on the catalyst surface. To sum up, the acidic properties of VTiS samples were affected by the preparation method and calcination temperature as well as by the type of sulfur species present on the surface.

Acknowledgements The authors are thankful to the scientific services of IRCELYON. Hongying Zhao gratefully acknowledges the China Scholarship Council for the financial support of her PhD grant. Financial supports from NSFC (20673055) and MSTC (2005CB 221400 and 2004DFB02900) are acknowledged.

References

1. Roozeboom F, Cordingley PD, Gellings PJ. Vanadium oxide monolayer catalysts: the vapor-phase oxidation of methanol. J Catal. 1981;68:464–72.
2. Forzatti P, Tronconi E, Busca G, Tittarelli P. Oxidation of methanol to methyl formate over V-Ti oxide catalysts. Catal Today. 1987;1:209–18.
3. Quaranta NE, Soria J, Cortes Corberan V, Fierro JLG. Selective oxidation of ethanol to acetaldehyde on $V_2O_5/TiO_2/SiO_2$ catalysts: effect of TiO_2-coating of the silica support. J Catal. 1997;171:1–13.
4. Zhao H, Bennici S, Shen J, Auroux A. The influence of the preparation method on the structural, acidic and redox properties of V_2O_5-TiO_2/SO_4^{2-} catalysts. Appl Catal A General. 2009;356:121–8.
5. Sun Q, Fu Y, Liu J, Auroux A, Shen J. Structural, acidic and redox properties of V_2O_5-TiO_2-SO_4^{2-} catalysts. Appl Catal A General. 2008;334:26–34.
6. Zou H, Li M, Shen J, Auroux A. Surface acidity of supported vanadia catalysts. J Therm Anal Calorim. 2003;72:209–21.
7. Bennici S, Auroux A. Thermal analysis and calorimetric methods. In: Jackson SD, Hargreaves SJ, editors. Metal oxide catalysis. Wiley-VCH Verlg: GmbH & Co; 2009. p. 391–442.
8. Zhao H, Bennici S, Shen J, Auroux A. Surface and catalytic properties of V_2O_5-TiO_2/SO_4^{2-} catalysts for the selective oxidation of methanol prepared by various methods. J Mol Catal A Chem. 2009;309:28–34.
9. Auroux A. Acidity characterization by microcalorimetry and relationship with reactivity. Top Catal. 1997;4:71–89.
10. Keränen J, Auroux A, Ek-Härkönen S, Niinistö L. Calorimetric measurements of the acidity of supported vanadium oxides prepared by ALE and impregnation. Thermochim Acta. 2001;379:233–9.
11. Tanabe K. Niobic acid as an unusual acidic solid material. Mater Chem Phys. 1987;17:217–25.
12. Desmartin-Chomel A, Flores JL, Bourane A, Clacens JM, Figueras F, Delahay G, et al. Calorimetric and FTIR study of the acid properties of sulfated titanias. J Phys Chem B. 2006;110:858–63.
13. Gervasini A, Fenyvesi J, Auroux A. Microcalorimetric study of the acidic character of modified metal oxide surfaces. Influence of the loading amount on alumina, magnesia, and silica. Langmuir. 1996;12:5356–64.

Publication V

Catalysis Today 152 (2010) 70–77

Contents lists available at ScienceDirect

Catalysis Today

journal homepage: www.elsevier.com/locate/cattod

Effect of vanadia loading on the acidic, redox and catalytic properties of V_2O_5–TiO_2 and V_2O_5–TiO_2/SO_4^{2-} catalysts for partial oxidation of methanol

H. Zhao [a,b], S. Bennici [a], J. Cai [b], J. Shen [b], A. Auroux [a,*]

[a] Université Lyon 1, CNRS, UMR 5256, IRCELYON, Institut de recherches sur la catalyse et l'environnement de Lyon, 2 avenue Albert Einstein, F-69626 Villeurbanne, France
[b] Laboratory of Mesoscopic Chemistry, School of Chemistry and Chemical Engineering, Nanjing University, Nanjing 210093, China

ARTICLE INFO

Article history:
Available online 5 September 2009

Keywords:
V_2O_5–TiO_2
V_2O_5–TiO_2/SO_4^{2-}
Adsorption microcalorimetry
Acidic and redox properties
Methanol oxidation

ABSTRACT

V_2O_5/TiO_2 and V_2O_5/TiO_2–SO_4^{2-} catalysts with various vanadia loadings (5, 15 and 25 wt% V_2O_5) were prepared by successive incipient wetness impregnations and the effect of doping with SO_4^{2-} was studied. The catalysts were characterized by XRD, BET, XPS, Raman spectroscopy, redox cycles (TPR1/TPO/TPR2), ammonia adsorption microcalorimetry and tested in the selective oxidation of methanol to dimethoxymethane (DMM). The Raman spectra revealed the formation of crystalline V_2O_5 particles when the vanadia coverage was higher than 15 wt%. Redox cycles revealed that the monomeric vanadia species were easier to reduce but more difficult to oxidize than the polymeric and crystalline species. The supported vanadia species were found to be composed of stoichiometric V_2O_4 and V_2O_5, as shown by XPS. The ammonia adsorption microcalorimetric study evidenced acid sites with adsorption heats $Q_{diff} > 110$ kJ mol^{-1}, in amounts which increased upon the addition of SO_4^{2-} but decreased with increasing vanadia loading. Furthermore, the results of the methanol oxidation reaction suggest that the addition of SO_4^{2-} on highly dispersed supported vanadia catalysts promoted the catalytic activity.

1. Introduction

Supported vanadium systems, mainly on TiO_2 support, are among the most widely studied catalysts for the partial oxidation of methanol [1–6], which is known to proceed via dissociative chemisorption to form surface V-OCH_3 and support –OH intermediates [7,8]. Thus the nature and the surface area of the support as well as the structure of the vanadium species are all key factors in the formation of active surface species [9]. According to spectroscopic investigations, isolated monomeric vanadyl species, polymeric vanadia species and V_2O_5 crystallites may coexist on the titania support, their relative abundances being related to the vanadia content [10–13].

It is well known that the surface acidity exerts an important role in the partial oxidation of methanol, and it has been shown that the addition of SO_4^{2-} species to TiO_2 generates strong acidic sites at high temperature and can lead to high activity in the selective catalytic reduction (SCR) reaction [14]. Amiridis et al. [15] and Dunn et al. [16] have also reported that, on vanadia–titania catalysts, the gaseous SO_2 contained in the feed gas system could participate in the formation of surface sulfate species which strongly interact with vanadia and then improve the catalytic surface reactivity. Moreover, recent articles [17,18] show that the addition of the proper concentration of SO_4^{2-} to TiO_2 (anatase)-supported vanadium oxide can improve the catalytic activity in the selective oxidation of methanol to dimethoxymethane (DMM), which can undergo further steam reforming to produce hydrogen. Thus, it is very important to study the acidity of these solids in terms of the nature, amount, strength and strength distribution of their surface sites, from the fundamental and applicative points of view. Adsorption microcalorimetry of a basic probe molecule is a useful technique to describe, in detail, the quantitative and energetic features of the surface sites [19,20], and we have applied it to measure the acidity of the catalysts studied in this work.

Considering that most commercial titanias are sulfated to some extent due to the usual preparation procedure involving a sulfate, we investigated the influence of vanadia content in the presence of a very small amount of sulfate species (0.2–0.7 wt% S) in the reaction of selective oxidation of methanol to DMM. Moreover, in order to examine the role of sulfate species, sulfated vanadia–titania catalysts (1.1–1.8 wt% S) were prepared. Thus, this paper presents a study of the acidic and redox properties of V_2O_5–TiO_2 and V_2O_5–TiO_2/SO_4^{2-} catalysts with different amounts of vanadia and sulfate. The samples were fully characterized by XRD, BET, XPS and TPR/TPO. In addition, Raman spectroscopy was used to provide complementary information about the nature of the surface vanadium oxide species present in titania-supported vanadia

* Corresponding author. Fax: +33 472445399.
E-mail address: aline.auroux@ircelyon.univ-lyon1.fr (A. Auroux).

0920-5861/$ – see front matter © 2009 Elsevier B.V. All rights reserved.
doi:10.1016/j.cattod.2009.08.005

catalysts. A tentative correlation with the activity in partial oxidation of methanol was established.

2. Experimental

2.1. Catalyst preparation

Vanadium oxide systems with different V_2O_5 contents (denoted by VTi) supported on commercial TiO_2 (Millennium* G5, uncalcined) were prepared by incipient wetness impregnation, using ammonia vanadate (NH_4VO_3) as metal precursor and oxalic acid as complexing agent ($NH_4VO_3/C_2O_2H_2$ molar ratio = 1/2). After being kept at room temperature for 12 h to ensure their stabilization, the resulting solids were dried at 373 K overnight and then calcined in air at 673 K for 6 h. Pure TiO_2 catalyst, used as reference, was also calcined at 673 K in air for 6 h.

The sulfated vanadia–titania catalysts (denoted by VTiS) were prepared by incipient wetness impregnation of 1 g of above mentioned vanadia–titania catalysts with an aqueous solution containing the theoretical percentage of $(NH_4)_2SO_4$ to achieve 5 wt% SO_4^{2-} (1.7 wt% S). The resulting solids were then dried at 373 K overnight and calcined at 673 K in air for 6 h.

2.2. Catalyst characterization

Elemental analysis was performed using ICP atomic emission spectroscopy (ICP-AES) with a flame PerkinElmer M1100 spectrometer.

The surface areas, pore volumes and pore sizes were measured by nitrogen adsorption at 77 K on a Micromeritics 2010 apparatus after heat pretreatment under vacuum for 3 h at a temperature of 623 K.

The X-ray diffraction (XRD) measurements were carried out on a Bruker D5005 powder diffractometer scanning from 3° to 80° (2θ) at a rate of 0.02° s^{-1} using a Cu Kα radiation (λ = 0.15418 nm) source. The applied voltage and current were 50 kV and 35 mA, respectively.

The X-ray photoelectron spectra (XPS) were measured on a KRATOS AXIS Ultra DLD spectrometer equipped with a hemispherical electron analyzer and an Al anode (Al Kα = 1486.6 eV) powered at 150 W, a pass energy of 20 eV, and a hybrid lens mode. The detection area analyzed was 700 μm × 300 μm. Charge neutralization was required for all samples. The peaks were referenced to the C–(C, H) components of the C 1s band at 284.6 eV. Shirley background subtraction and peak fitting to theoretical Gaussian–Lorentzian functions were performed using an XPS processing program (Vision 2.2.6 KRATOS). The residual pressure in the spectrometer chamber was 5×10^{-9} mbar during data acquisition.

Raman spectroscopy measurements were performed using a LabRAM HR (Jobin Yvon) spectrometer. The excitation was provided by the 514.5 nm line of an Ar^+ ion laser (Spectra physics) employing a laser power of 100 μW. The laser beam was focused through microscope objective lenses (100×) down to a 1 μm spot on the sample.

Redox cycles (TPR1/TPO/TPR2), carried out in sequences consisting of a first temperature-programmed reduction (TPR) on the oxidized sample (TPR1), a temperature-programmed oxidation (TPO), and a second temperature-programmed reduction (TPR2), were performed using a TPD/R/O-1100 instrument (ThermoFisher). Prior to the TPR1 run, the fresh sample was treated in a stream of O_2/He (0.998% v/v, flowing at 20 mL min^{-1}), ramping the temperature at 10 K min^{-1} from RT to 623 K and maintaining it for 60 min, and then cooled to 313 K. The TPR1 measurement was carried out using H_2/Ar (4.98% v/v) as reducing gas mixture, flowing at 20 mL min^{-1}. The heating rate was 10 K min^{-1} from 313 K to 1073 K for VTi and VTiS systems and up to 1223 K for bulk V_2O_5. The TPO run was carried out on the reduced sample (after TPR1) cooled at 313 K in N_2 flow. After a purge with Ar (20 mL min^{-1}), the oxidizing gas mixture composed of O_2/He (0.998% v/v) flowed at 20 mL min^{-1} through the sample from 313 to 1073 K. The oxidized sample was further reduced during the TPR2 run, under the same experimental conditions as TPR1 described above, up to a final temperature of 1223 K for VTi and VTiS systems. The H_2 or O_2 consumption was detected by a thermal conductivity detector (TCD). The sample size used was adjusted in order to have around 69 μmol of V_2O_5 independently of the vanadia loading of the sample. This allowed us to maintain a K value of 100 s. The characteristic number, K, can be defined to facilitate the selection of appropriate operating parameters; a fixed K value between 60 and 140 s guarantees optimal conditions to obtain good TPR/TPO profiles [21,22]. The peak areas were calibrated with given H_2/Ar (4.98% v/v) and O_2/He (0.998% v/v) mixture injections for TPR and TPO, respectively.

The microcalorimetric studies of ammonia adsorption were performed at 423 K in a heat flow calorimeter (C80 from Setaram) linked to a conventional volumetric apparatus equipped with a Barocel capacitance manometer for pressure measurements. The ammonia used for measurements (Air Liquide, purity > 99.9%) was purified by successive freeze–pump–thaw cycles. About 100 mg of sample was pretreated in a quartz cell under evacuation overnight at 623 K. The differential heats of adsorption were measured as a function of coverage by repeatedly introducing small doses of ammonia gas onto the catalyst until an equilibrium pressure of about 66 Pa was reached. The sample was then outgassed for 30 min at the same temperature, and a second adsorption was performed at 423 K until an equilibrium pressure of about 27 Pa was attained in order to calculate the irreversibly chemisorbed amount of ammonia at this pressure.

2.3. Catalytic reaction

The oxidation of methanol was carried out in a fixed-bed microreactor made of glass with an inner diameter of 6 mm. The methanol was introduced into the reaction zone by bubbling O_2/N_2 (1/5) through a glass saturator filled with methanol (99.9%) maintained at 278 K. In each test, about 200 mg of catalyst was loaded, and the gas hourly space velocity (GHSV) was 11,400 mL g^{-1} h^{-1}. The feed composition was maintained as methanol:O_2:N_2 = 1:3:15 (v/v). The tail gas out of the reactor was analyzed by an on-line GC equipped with an FID detector and a TCD detector. The column used was PORAPAK N for the separation of methanol, DMM and other organic compounds. The gas lines were kept at 373 K to prevent condensation of the reactant and products. The reaction was carried out at atmospheric pressure.

3. Results and discussion

3.1. Structure properties

The X-ray diffraction patterns of the VTi and VTiS catalysts are shown in Fig. 1. The typical diffraction peaks characteristic of anatase TiO_2 were observed for all the catalysts. No crystalline vanadia phase appeared even for a V_2O_5 content close to 25 wt%, indicating that vanadium oxide was present in a highly dispersed manner. However, the presence of V_2O_5 crystallites with size less than 4 nm, which is beyond the detection capacity of the powder XRD technique, cannot be excluded. In addition, as shown in Fig. 1, the addition of SO_4^{2-} did not affect the dispersion of VTi catalysts.

The results of bulk (chemical analysis) and surface (XPS) analysis, the surface and bulk V/Ti ratios as well as the BET surface areas are listed in Table 1. TiO_2 possessed a high surface area of

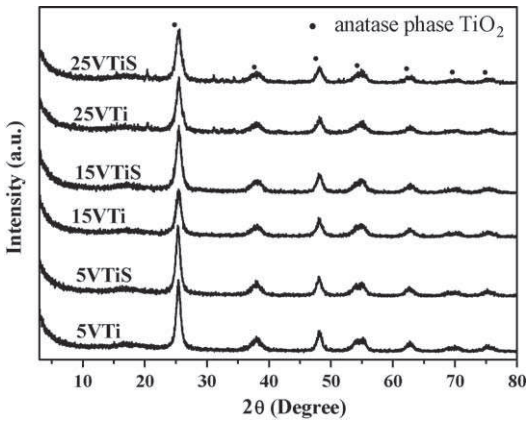

Fig. 1. X-ray diffraction (XRD) patterns of VTi and VTiS catalysts.

209 $m^2 g^{-1}$. Generally, in V_2O_5–TiO_2 systems the surface area continually decreases with increasing V_2O_5 content. In this work, the surface areas of the catalysts containing 5 and 15 wt% V_2O_5 were maintained around 200 $m^2 g^{-1}$ and then decreased to 165 $m^2 g^{-1}$ when the V_2O_5 content reached 25 wt%. In addition, the surface areas of the VTi catalysts also decreased upon addition of SO_4^{2-}. Similar pore volumes (0.26–0.38 $cm^3 g^{-1}$) and average pore sizes (5.7–6.4 nm) were obtained for all catalysts. As presented in Table 1, the commercial TiO_2 support in the supported vanadia catalyst was already sulfated with 0.2–0.7 wt% S, and the sulfur concentration in the VTiS systems slightly decreased from 1.76 wt% (5VTiS) to 1.11 wt% (25VTiS) with increasing vanadia loading. However, the surface and bulk V/Ti ratios were similar for all the catalysts, indicating that the vanadium was homogeneously distributed on the surface of TiO_2 support.

Table 2 presents the binding energies (BE) of V $2p_{3/2}$, O 1s, Ti $2p_{3/2}$ and S $2p_{1/2}$ lines and the relative components from the decomposition of V $2p_{3/2}$ and O 1s lines. The binding energy references [23,24] of the V $2p_{3/2}$ line for V_2O_5 and V_2O_4 are around 517.5 and 516.4 eV, respectively. As seen in Table 2, all the catalysts exhibited about 20% V^{4+} species, except the 5VTi and 5VTiS samples which were more reduced, presenting a contribution of ~50% V^{4+}. This difference observed at low vanadia loading indicates that a high dispersion of vanadium oxide could favor the reduction of V(V) to V(IV) upon exposure to X-radiation under ultra-high vacuum operating conditions. The BE position of the Ti $3p_{3/2}$ line was around 459.0 ± 1 eV and maintained for all the catalysts, suggesting the presence of Ti^{4+} of TiO_2 [25]. The XPS spectra of the S 2p line displayed the same band centered at 169.0 eV, which is typical of sulfur in the S^{6+} oxidation state and in the form of bidentate sulfate (SO_4^{2-}) species on the surface of TiO_2 [26,27].

In a previous paper [28] we have already reported that the O 1s spectra can be decomposed into three peaks to gain information about the O 1s components, which are the lattice oxygen of the TiO_2 + V_2O_5 oxides, the bridged oxygen of surface hydroxyl groups (Ti–OH) and the oxygen of sulfates (SO_4^{2-}) respectively. We obtained the same results in this work for all VTi and VTiS samples.

The surface structure of vanadia and titania species on the VTiS catalysts was examined by Raman spectroscopy, from 1600 to 200 cm^{-1}, as shown in Fig. 2. Previous studies by Wachs et al. [10–13,29,30] have already shown that, depending on the vanadia loading, two types of surface vanadia species and microcrystalline phase V_2O_5 particles can be present on the surface of V_2O_5–TiO_2 catalysts. Under hydrated conditions and at low surface coverage a broad Raman band at ~940 cm^{-1} is present, corresponding to the distorted tetrahedral vanadia species in polymeric metavanadate compounds. This band quickly shifts to ~994 cm^{-1} as the vanadia loading is increased, which is due to microcrystalline V_2O_5 [13,29]. The Raman spectra of the catalysts prepared for this work were in agreement with the observations reported in the literature.

For the present catalysts, broad Raman bands at 947 and 807 cm^{-1} assigned to polymerized vanadia species were detected for the submonolayer coverage [10] corresponding to approximately 5 wt% vanadia, regardless of whether SO_4^{2-} was added.

Table 1
Chemical analysis, X-ray photoelectronic spectroscopy analysis, V/Ti atomic ratios for surface and bulk composition and BET surface area of the samples.

Sample	S_{BET} ($m^2 g^{-1}$)	C.A. (wt%)			XPS (wt%)			V/Ti (surface atomic ratio)	V/Ti (bulk atomic ratio)
		V	Ti	S	V	Ti	S		
5VTi	197	2.82	50.42	0.62	4.45	48.43	0.53	0.09	0.06
5VTiS	174	2.74	50.13	1.76	3.40	46.41	3.33	0.07	0.05
15VTi	206	7.73	48.48	0.18	8.34	45.71	0.65	0.17	0.16
15VTiS	178	8.05	47.02	1.41	7.75	43.78	2.50	0.17	0.15
25VTi	165	14.45	40.77	0.68	18.98	36.32	Traces	0.5	0.4
25VTiS	134	13.82	38.87	1.11	14.69	36.75	1.84	0.38	0.4
TiO_2	209	–	–	<0.2	–	–	<0.2	–	–

Table 2
Binding energies and concentration (in atomic %) of the different oxygen (TiO_2 + V_2O_5, –OH, and –SO_4^{2-}) and vanadia species present on the surface of VTi and VTiS catalysts.

Sample	Binding energy (ev)						
	V $2p_{3/2}$		O 1s			Ti $2p_{3/2}$	S $2p_{1/2}$
	V_2O_4	V_2O_5	TiO_2 and V_2O_5	–OH	SO_4^{2-}		
5VTi	516.0 (53%)	17.0 (47%)	29.8 (81%)	30.9 (12%)	531.9 (7%)	458.6	168.5
5VTiS	516.1 (52%)	17.1 (47%)	530.0 (72%)	531.1 (11%)	531.9 (17%)	458.8	168.7
15VTi	516.4 (21%)	517.7 (79%)	530.3 (82%)	531.0 (9%)	532.0 (9%)	459.1	168.9
15VTiS	516.4 (19%)	517.6 (81%)	530.4 (74%)	531.1 (9%)	532.1 (17%)	459.0	168.8
25VTi	516.2 (17%)	517.4 (83%)	530.2 (87%)	531.3 (13%)	–	459.0	169.0
25VTiS	516.3 (16%)	517.5 (84%)	530.1 (77%)	531.3 (12%)	531.9 (11%)	459.0	169.0

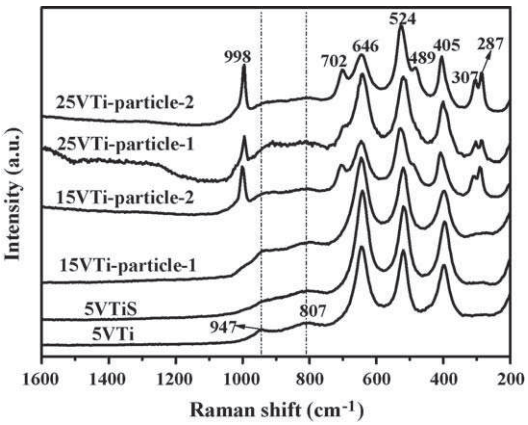

Fig. 2. Raman spectra of VTi and VTiS catalysts.

Upon increasing the vanadia loading up to 15 wt%, the catalyst became heterogeneous, and consequently both types of particles were analyzed. 15VTi-particle-1 exhibited the Raman bands due to polymeric vanadate species, similar to those of sample 5VTi, while 15VTi-particle-2 gave rise to strong Raman bands typical of crystalline V_2O_5 around 998, 702, 524, 489, 425, 307 and 287 cm^{-1}. The catalyst with 25 wt% vanadia content is also rather heterogeneous, as shown by 25VTi-particle-1 and 25VTi-particle-2, but the major Raman band at 998 cm^{-1} due to crystalline V_2O_5 could be detected on both types of particles.

3.2. Redox cycles with temperature-programmed reduction and oxidation

The reversibility in a redox cycle of the VO_x species of the studied VTi and VTiS catalysts was investigated by TPR and oxidation analysis (TPR1/TPO/TPR2 cycle). Table 3 summarizes the most important results, in terms of maximum temperatures (T_{m1} and T_{m2}) of the reduction and oxidation peaks and of the integrated H_2 and O_2 consumptions. Fig. 3 shows the reduction and oxidation profiles of all the studied catalysts.

Table 3
Redox behavior of the VTi and VTiS catalysts from TPR/TPO experiments.

Sample	Experiment	The maximum temperatures of peaks		Reduction *or* oxidation
		Peak 1 (T_{m1})	Peak 2 (T_{m2})	(μmol H_2 g_v^{-1}) *or* (μmol O_2 g_v^{-1})
5VTi	TPR1	749	976	29,043
	TPO	829	–	9,468
	TPR2	873	n.d.[a]	20,248
5VTiS	TPR1	813	993	48,759
	TPO	838	–	8,905
	TPR2	853	n.d.[a]	19,964
15VTi	TPR1	730, 774	944	28,616
	TPO	777	–	10,065
	TPR2	916	n.d.[a]	20,272
15VTiS	TPR1	753, 784	945	32,932
	TPO	775	878	10,075
	TPR2	1015	n.d.[a]	21,193
25VTi	TPR1	749, 797	928	24,394
	TPO	775	924	9,433
	TPR2	931	1084	19,702
25VTiS	TPR1	752, 802	930	27,236
	TPO	773	921	8,813
	TPR2	929	n.d.[a]	21,845
Pure V_2O_5	TPR1	938, 974	1110, 1195	22,096
	TPO	779	935	10,379
	TPR2	978, 1015	n.d.[a]	23,513

[a] Not determined.

3.2.1. Temperature-programmed reduction in H_2

When reducing bulk V_2O_5 in the temperature range from RT up to 1223 K, four peaks were observed, located at 938, 974, 1110 and 1195 K, respectively. The first peak should be assigned to the formation of V_6O_{13}, the second to VO_2, and with the completion of hydrogen consumption V_2O_3 is reached [31]. For the VTi and VTiS systems, conventional TPR runs were carried out up to 1073 K only to study the reducibility of the vanadia species. More than one reduction peak was observed, indicating the presence of several types of oxygen-containing vanadium species on the TiO_2 surface. In addition, considering that different vanadia species such as monomeric, polymeric and crystalline VO_x species may coexist at the surface of the studied catalysts, the peaks do not necessarily represent different steps of reduction of the same species but should rather be considered to result from a superposition of reduction steps of several different species [29]. Referring to the literature [32], the maximum temperature of reduction peaks (T_{m1}) in the low-temperature region (<900 K) indicates the presence of monomeric VO_x species ($T_{m1} \leq 770$ K) and polymeric VO_x species ($T_{m2} = 774$–813 K) in the VTi and VTiS systems (Table 3).

From a comparison of the TPR profiles of the VTi samples, T_{m1} of reduction peaks was found to be shifted to higher values with increasing V_2O_5 content, indicating that more polymeric vanadia species might be formed, as confirmed by Raman spectroscopy measurements. Additionally, the addition of SO_4^{2-} might inhibit the reduction of vanadia, since the reduction peak maxima shifted to higher temperatures for samples with low V_2O_5 content, possibly due to an increased proportion of polymeric vanadia species upon re-calcination, or due to the formation of the sulfate species "crowding" the vanadyl species together and leading to more polymerization [15].

For example, an increase of 60 K was observed for the T_{m1} value of sample 5VTiS compared to sample 5VTi (5VTi: $T_{m1} = 749$ K; 5VTiS: $T_{m1} = 813$ K). When the V_2O_5 content was increased to 15 wt%, this peak ($T_{m1} = 784$ K) acquired a shoulder at lower temperature (753 K), indicating that insoluble vanadium species became heterogeneous, which was consistent with the Raman spectra showing that sample 15VTi contained both polymeric VO_x and microcrystalline V_2O_5 particles. When the V_2O_5 content reached 25 wt%, a similar TPR behavior was detected with sample 25VTi (see Table 3).

Furthermore, considering the rather different amounts of reducible VO_x species in VTi and VTiS systems, the H_2 consumption has been expressed as μmol H_2 per gram of vanadium (μmol g_v^{-1}). Obviously, the H_2 consumption continually decreased with increasing V_2O_5 content, possibly due to the formation of highly polymeric VO_x species. However, the H_2 consumption increased with the introduction of SO_4^{2-}, thus indicating the reduction of SO_4^{2-} ions [33].

3.2.2. Temperature-programmed oxidation after TPR with O_2

The reoxidation behavior of the catalysts starting from the V^{3+} oxidation state obtained after TPR1 was analyzed by TPO. The TPO profiles are shown in Fig. 3(a) and (b) TPO. The TPO profiles of bulk V_2O_5 exhibit two separate peaks ($T_{m1} = 779$ K and $T_{m2} = 935$ K). Hence, oxidation occurs at lower temperature than reduction with hydrogen. The TPO profiles resemble more or less the TPR profiles viewed from higher to lower temperature. This suggests that the transitions observed in the TPR experiments are reversed in the TPO experiments. Thus, for bulk V_2O_5, the peak at 779 K corresponds to the transition of V_2O_3 to VO_2, and the second peak at 935 K to the formation of V_2O_5. For VTi and VTiS systems,

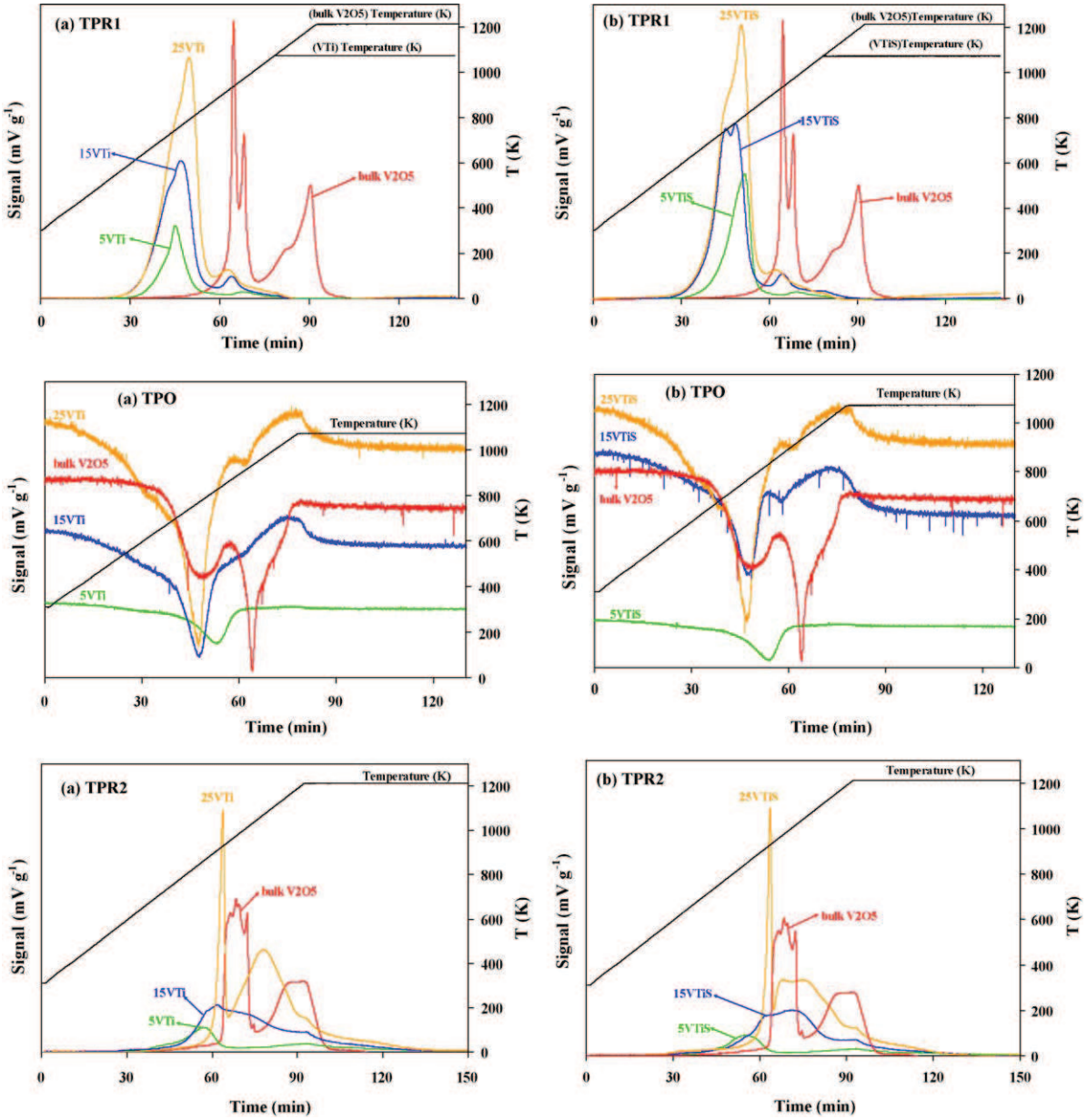

Fig. 3. Redox cycles of (a) VTi catalysts, (b) VTiS catalysts and bulk V_2O_5. Profiles of reduction (TPR1, TPR2) and oxidation (TPO) as a function of temperature and time (10 K min^{-1}) (bulk V_2O_5, red; 5VTi and 5VTiS, green; 15VTi and 15VTiS, blue; 25VTi and 25VTiS, orange). All spectra were magnified (5×) except bulk V_2O_5. (For interpretation of the references to colour in this figure legend, the reader is referred to the web version of the article.)

Table 4
Ammonia adsorption data from microcalorimetry measurements at 423 K.

Sample	V_{tot}[a] (27 Pa) (μmol g^{-1})	V_{tot}[a] (27 Pa) (μmol m^{-2})	V_{irr}[b] (μmol g^{-1})	V_{irr}[b] (μmol m^{-2})	Q_{init}[c] (kJ mol^{-1})
5VTi	498	2.5	291	1.5	194
5VTiS	486	2.8	316	1.8	219
15VTi	483	2.3	275	1.3	210
15VTiS	514	2.9	335	1.9	231
25VTi	425	2.6	213	1.3	220
25VTiS	406	3.0	243	1.8	145
TiO_2	517	2.5	279	1.3	210

[a] Total amount of NH_3 retained as determined at 27 Pa of equilibrium pressure.
[b] "Irreversible" amount of NH_3 retained as determined from the difference between the amounts adsorbed in the first and second adsorptions at 27 Pa.
[c] Heat evolved from the first NH_3 dose.

Table 5
Catalytic activities of the VTi and VTiS catalysts in the methanol oxidation reaction.

Sample	Temp. (K)	Con. of methanol (%)	Selectivity (%)				
			DMM	FA	MF	DME	CO_x
5VTi	403	6	88	6	6	0	0
	413	9	74	8	17	0	0
	423	12	59	12	28	0	0
	433	21	30	13	57	0	0
	453	41	9	20	59	1	11
5VTiS	403	12	87	0	0	13	0
	413	19	85	0	0	15	0
	423	28	77	3	1	19	0
	433	32	47	10	32	12	0
	453	71	6	16	19	23	36
15VTi	403	22	90	3	7	0	0
	413	37	59	6	34	1	0
	423	51	28	12	58	1	1
	433	84	0	6	13	0	81
15VTiS	403	22	94	1	2	2	0
	413	36	84	2	11	3	0
	423	52	53	5	39	3	0
	433	86	1	7	12	2	77
25VTi	403	31	93	2	4	0	0
	413	49	74	7	19	1	0
	423	67	24	17	58	1	0
	433	92	0	2	35	2	61
25VTiS	403	25	95	2	1	2	0
	413	36	85	7	7	1	0
	423	58	54	13	31	2	0
	433	92	0	1	37	5	56

DMM: dimethoxymethane, FA: formaldehyde, MF: methyl formate, DME: dimethyl ether, CO_x: CO_2 (or CO).

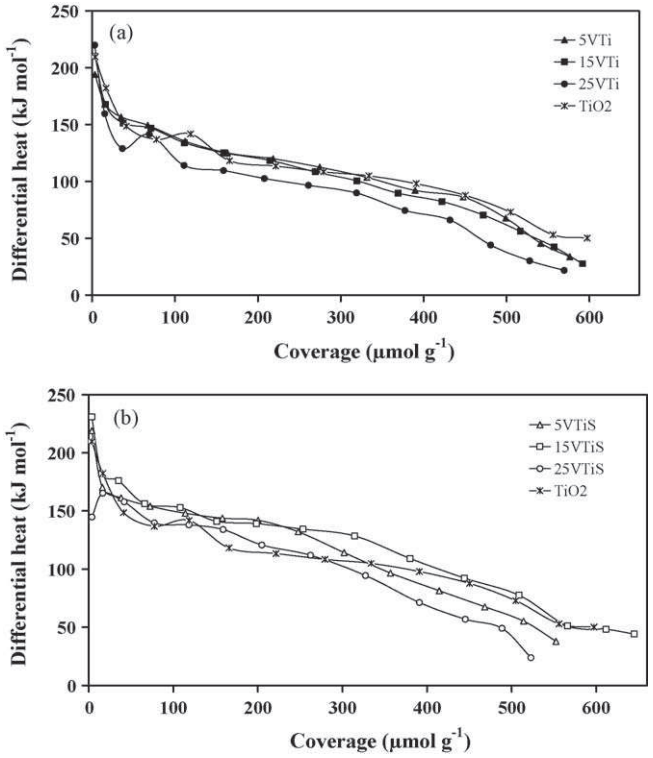

Fig. 4. Differential heat versus coverage (in μmol g^{-1} of catalyst) for NH_3 adsorption at 423 K over (a) VTi and (b) VTiS catalysts.

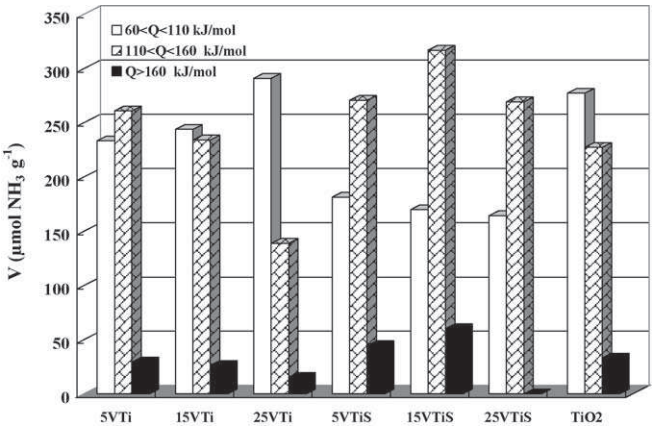

Fig. 5. Acidity spectra of the VTi and VTiS catalysts.

the same transitions that were observed in TPR are also seen in TPO, being inversely related. Compared to bulk V_2O_5, the supported vanadia catalysts (VTi and VTiS) are not only easier to reduce but also easier to reoxidize, indicating that the support promotes both reduction and reoxidation. From a comparison of TPR1 and TPO profiles, it appears that the polymeric or crystalline vanadia species present on the TiO_2 support are the easiest to reoxidize but most difficult to reduce, whereas highly dispersed vanadia species present on TiO_2 are the easiest to reduce but the most difficult to reoxidize. This is in agreement with the results obtained by Majunke and Baerns [34].

3.2.3. Temperature-programmed reduction after TPO with H_2

A second reduction analysis (TPR2) was performed on the samples freshly reoxidized by TPO. Fig. 3(a) and (b) TPR2 comparatively present the collected reduction profiles. As shown in this figure, part of the vanadia species were not reduced at the temperature of 1223 K, and the remaining part necessitated a much higher temperature to be reduced, which made it difficult to reach the maximum of the reduction peak and the stoichiometric consumption of hydrogen. In all cases, the positions and shapes of the peaks of the TPR2 profiles were different from those of TPR1; the TPR2 profiles showed a shift toward higher temperatures than TPR1. The lack of overlap between TPR1 and TPR2 suggested a mobility of the vanadia species leading to more aggregated vanadia phase [35]. The newly created vanadia species were more crystalline, especially for the sample with 25 wt% V_2O_5 which presented the highest reduction temperatures.

3.3. Acidity properties

The acidity of the catalysts was determined by ammonia adsorption microcalorimetry [20]. Table 4 presents the initial heats of adsorption (denoted by Q_{init}) and the amount of ammonia adsorbed under an equilibrium pressure of 27 Pa. Fig. 4 displays the differential heats of ammonia adsorption as a function of coverage for the VTi and VTiS catalysts and pure TiO_2 support, while Fig. 5 shows the acid site strength distribution of the catalysts which gives the number of sites of a given strength.

The initial heat of ammonia adsorption on TiO_2 was found to be about 210 kJ mol^{-1}, suggesting that the TiO_2 support used in this work is strongly acidic. The addition of V_2O_5 did not change significantly the initial heat, while the addition of SO_4^{2-} slightly increased the initial heat except for the 25VTiS sample. Additionally, the amount of irreversibly absorbed ammonia (V_{irr}), corresponding to strong chemisorption, decreased with increasing V_2O_5 content, but the strong acid site densities became similar when V_{irr} was expressed per unit surface area, which reveals that the decrease of the number of acid sites can be attributed to the

decrease of surface area. Nevertheless, the number and the density of strong acid sites (see V_{irr}) increased upon the addition of SO_4^{2-}.

We have shown in previous studies [28] on sulfated vanadia–titania prepared by sol–gel that the first doses of ammonia were fully adsorbed with very low heats evolved, thus inducing very low initial differential heats of adsorption. This observation was explained by a combination of both an endothermic effect such as NH_3 dissociation [36] or the formation of ammonium sulfite [37] and the exothermic adsorption; however, such an effect was not observed in the present study, or only to a very low extent on sample 25 VTiS. Moreover, the heat of NH_3 adsorption gradually decreased with NH_3 coverage for all the studied catalysts, suggesting a heterogeneous strength distribution of these catalysts, as shown in Fig. 4.

Fig. 5 shows the acid site strength distributions of all the catalysts. For the VTi samples, the populations of strong acid sites ($Q_{diff} > 160$ kJ mol^{-1}) and medium acid sites ($110 < Q_{diff} < 160$ kJ mol^{-1}) decreased with increasing amount of V_2O_5, while the amount of weak acid sites with $60 < Q_{diff} < 110$ kJ mol^{-1} increased. For the VTiS samples, it is clear that the strong and medium acid sites increased upon the addition of SO_4^{2-} even if the low initial heats of adsorption made it difficult to calculate the number of strong acid sites for sample 25VTiS.

3.4. Selective oxidation of methanol

The selective oxidation of methanol to dimethoxymethane (DMM) may involve two steps: (1) oxidation of methanol to formaldehyde on redox sites and (2) condensation of formaldehyde produced with additional methanol to form DMM on acidic sites. Thus, bifunctional catalysts with redox and acidic characters are required for the reaction. In addition, the relative strengths of surface acidity and redox ability of a catalyst may be important in determining reaction pathways as well as selectivity to DMM.

In this work, the conversion of methanol increased with increasing V_2O_5 content, due to enhanced redox properties. This behavior supported the results of the TPR1 measurements, in which the H_2 consumption (expressed as μmol H_2 per gram of catalyst and not per g of V) increased with the vanadia loading. Meanwhile, the selectivity to DMM increased slightly upon the addition of SO_4^{2-} due to the enhanced acidity (see Table 5). Nevertheless, samples 15VTiS and 25VTiS possessed similar catalytic behaviors even as the vanadia content increased from 15 to 25 wt%. Many researchers claim that amorphous monomeric VO_x species with terminal V=O bonds are the most active species for reactant adsorption and C–H bond breaking, particularly when compared to crystalline V_2O_5 [38–41]. As evidenced by Raman spectroscopy, crystalline V_2O_5 species are present on sample 15VTi, and even more crystalline V_2O_5 particles were detected for sample 25VTi. The formation of crystalline V_2O_5 species with increasing vanadia loading would also be applicable to the polymeric vanadia species in the VTiS systems, as evidenced by TPR measurements.

Among all the VTi and VTiS catalysts, sample 25VTiS showed the highest yield at the reaction temperature of 423 K, with 58% methanol conversion and 54% DMM selectivity. Fu and Shen [17] have already reported positive effects upon the addition of different sulfates to the V_2O_5/TiO_2 system for the selective oxidation of methanol to DMM. They mention good results over $Ti(SO_4)_2$-modified V_2O_5/TiO_2 catalysts ($S_{BET} = 82$ m^2 g^{-1}; V_2O_5% = 10 wt%; S% = 0.2 wt%) with DMM selectivities of 89–92% for 48–60% methanol conversions. It seems that the enhanced DMM selectivity is strongly affected not simply by the addition of SO_4^{2-}, but also by the nature of the sulfate-carrier–vanadia interaction, the amount of exposed carrier surface, the vanadia loading, and the catalyst surface area. In addition, when sulfated species ($(NH_4)_2SO_4$) were added to the VTi system, the conversion of methanol obviously increased for sample 5VTiS and the selectivity to DME (created on strong acid sites) too, which suggests that the addition of SO_4^{2-} on a "monolayer-type" vanadia–titania catalyst easily improves both the redox (confirmed by TPR experiments) and surface acidity properties. Thus, these results indicate that monomeric and polymeric vanadia, as opposed to crystalline V_2O_5, are the most reactive species in methanol oxidation, a model reaction for V_2O_5/TiO_2 catalysts.

4. Conclusion

A series of V_2O_5–TiO_2 (VTi) catalysts were prepared by incipient wetness impregnation and modified with SO_4^{2-} species. Raman spectroscopy suggested that microcrystalline V_2O_5 particles started to be formed for sample 15VTi. Moreover, the Raman spectra also suggested that the samples with higher vanadia loadings were not homogeneous. XPS showed that titanium and sulfur were present in their fully oxidized states for all the VTi and VTiS catalysts, while the state of vanadium was composed of stoichiometric pentavalent and tetravalent V. The maxima of the reduction peaks in TPR1 profiles indicated the presence of isolated monomeric vanadia species ($T_{m1} \leq 770$ K) and polymeric vanadia species ($T_{m1} = 774$–813 K) on the support surface. The monomeric species are more easily reduced but more difficult to oxidize than the polymeric and crystalline species. The ammonia adsorption calorimetry study showed that the number of acid sites with $Q_{diff} > 110$ kJ mol^{-1} was obviously increased upon the addition of SO_4^{2-}. The best catalytic behavior in this work was obtained on sample 25VTiS with, 58% DMM selectivity for 58% methanol conversion at 423 K. Consequently, the acidic and redox properties were related with the vanadia content and the addition of sulfate species, which finally affected the catalytic behavior of the methanol oxidation to dimethoxymethane.

Acknowledgements

The authors are thankful to the scientific services of IRCELYON, in particular to Laurence Massin for providing XPS measurements and to Marlène Daniel for providing Raman spectroscopy measurements.

Hongying Zhao gratefully acknowledges the China Scholarship Council for the financial support of her PhD grant.

Financial supports from NSFC (20673055) and MSTC (2005CB221400 and 2004DFB02900) are acknowledged.

References

[1] P. Forzatti, E. Tronconi, G. Busca, P. Tittarelli, Catal. Today 1 (1987) 209–218.
[2] F. Roozeboom, P.D. Cordingley, P.J. Gellings, J. Catal. 68 (1981) 464–472.
[3] A. Baiker, D. Monti, J. Catal. 91 (1985) 361–365.
[4] G.C. Bond, S.F. Tahir, Appl. Catal. 71 (1991) 1–31.
[5] P. Forzatti, E. Tronconi, A.S. Elmi, G. Busca, Appl. Catal. A: Gen. 157 (1997) 387–408.
[6] Q. Wang, R.J. Madix, Surf. Sci. 496 (2002) 51–63.
[7] A. Khodakov, B. Olthof, A.T. Bell, E. Iglesia, J. Catal. 181 (1999) 205–216.
[8] G. Busca, J. Mol. Catal. 50 (1989) 241–249.
[9] M.A. Banares, M.V. Martinez-Huerta, X. Gao, J.L.G. Fierro, I.E. Wachs, Catal. Today 61 (2000) 295–301.
[10] I.E. Wachs, Catal. Today 27 (1996) 437–455.
[11] I.E. Wachs, B.M. Weckhuysen, Appl. Catal. A: Gen. 157 (1997) 67–90.
[12] G. Deo, I.E. Wachs, J. Haber, Crit. Rev. Surf. Chem. 4 (1994) 141–187.
[13] I.E. Wachs, G. Deo, B.M. Weckhuysen, A. Andreini, M.A. Vuurman, M. De Boer, M.D. Amiridis, J. Catal. 161 (1996) 211–221.
[14] S.M. Jung, P. Grange, Catal. Today 59 (2000) 305–312.
[15] M.D. Amiridis, I.E. Wachs, G.D. Deo, J.M. Jehng, D.S. Kim, J. Catal. 161 (1996) 247–253.
[16] J.P. Dunn, H.G. Stenger Jr., I.E. Wachs, J. Catal. 181 (1999) 233–243.
[17] Y. Fu, J. Shen, Chem. Commun. 21 (2007) 2172–2174.
[18] S. Royer, X. Sécordel, M. Brandhorst, F. Dumeignil, S. Cristol, C. Dujardin, M. Capron, E. Payen, J.-L. Dubois, Chem. Commun. 7 (2008) 865–867.

[19] N. Cardona-Martinez, J.A. Dumesic, Adv. Catal. 38 (1992) 149–244.
[20] A. Auroux, Top. Catal. 4 (1997) 71–89.
[21] P. Malet, A. Caballero, J. Chem. Soc., Faraday Trans. I 84 (1988) 2369–2375.
[22] D.A.M. Monti, A. Baiker, J. Catal. 83 (1983) 323–335.
[23] S.L.T. Andersson, J. Chem. Soc., Faraday Trans. I 75 (1979) 1356–1370.
[24] J.A. Odriozola, J. Soria, G.A. Somorjai, H. Heinemann, J.F. Garcia de la Banda, M. Lopez Granados, J.C. Conesa, J. Phys. Chem. 95 (1991) 240–246.
[25] J. Keränen, C. Guimon, E. Iiskola, A. Auroux, L. Niinistö, Catal. Today 78 (2003) 149–157.
[26] M.H. Kim, I.-S. Nam, Y.G. Kim, J. Catal. 179 (1998) 350–360.
[27] D. Fraenkel, Ind. Eng. Chem. Res. 36 (1997) 52–59.
[28] H. Zhao, S. Bennici, J. Shen, A. Auroux, Appl. Catal. A: Gen. 356 (2009) 121–128.
[29] G.T. Went, L.-J. Leu, A.T. Bell, J. Catal. 134 (1992) 479–491.
[30] I.E. Wachs, J. Catal. 124 (1990) 570–573.
[31] S. Besselmann, C. Freitag, O. Hinrichsen, M. Muhler, Phys. Chem. Chem. Phys. 3 (2001) 4633–4638.
[32] G.Y. Popova, T.V. Andrushkevich, E.V. Semionova, Y.A. Chesalov, L.S. Dovlitova, V.A. Rogov, V.N. Parmon, J. Mol. Catal. A: Chem. 283 (2008) 146–152.
[33] B.Q. Xu, W.M.H. Sachtler, J. Catal. 167 (1997) 224–233.
[34] F. Majunke, M. Baerns, Catal. Today 20 (1994) 53–60.
[35] S. Bennici, A. Auroux, in: D. Jackson, J. Hargreaves (Eds.), Metal Oxide Catalysis, vol. 1, Wiley-VCH, 2009, pp. 391–436.
[36] A. Desmartin-Chomel, J.L. Flores, A. Bourane, J.M. Clacens, F. Figueras, G. Delahay, A. Giroir Fendler, C. Lehaut-Burnouf, J. Phys. Chem. B 110 (2006) 858–863.
[37] A. Gervasini, J. Fenyvesi, A. Auroux, Langmuir 12 (1996) 5356–5364.
[38] J.C. Vedrine (Ed.), EUROCAT oxide Catal. Today 20 (1994).
[39] G.C. Bond, J. Chem. Technol. Biotechnol. 68 (1997) 6–13.
[40] C.R. Dias, M.F. Portela, G.C. Bond, J. Catal. 157 (1995) 344–352.
[41] G. Centi, Appl. Catal. A: Gen. 147 (1996) 267–298.

Publication VI

Journal of Catalysis 272 (2010) 176–189

Contents lists available at ScienceDirect

Journal of Catalysis

journal homepage: www.elsevier.com/locate/jcat

Nature of surface sites of V_2O_5—TiO_2/SO_4^{2-} catalysts and reactivity in selective oxidation of methanol to dimethoxymethane

Hongying Zhao [a,b], Simona Bennici [a], Jianyi Shen [b], Aline Auroux [a,*]

[a] Université Lyon 1, CNRS, UMR 5256, Ircelyon, Institut de Recherches sur la Catalyse et l'environnement de Lyon, 2 Avenue Albert Einstein, F-69626 Villeurbanne, France
[b] Laboratory of Mesoscopic Chemistry, School of Chemistry and Chemical Engineering, Nanjing University, Nanjing 210093, China

ARTICLE INFO

Article history:
Received 29 October 2009
Revised 24 February 2010
Accepted 25 February 2010
Available online 3 April 2010

Keywords:
V_2O_5—TiO_2/SO_4^{2-}
TPR
Pyridine FTIR
Ammonia adsorption calorimetry
Methanol selective oxidation
Dimethoxymethane

ABSTRACT

The selective oxidation of methanol to dimethoxymethane (DMM) over sulfated vanadia–titania catalysts, prepared by co-precipitation and calcined at different temperatures, was studied in the 393–473 K interval under steady state conditions. The catalysts were characterized by X-ray diffraction (XRD), Brunauer–Emmett–Teller isotherms (BET), inductively coupled plasma optical emission spectroscopy (ICP–OES), X-ray photoelectron spectroscopy (XPS), scanning electron microscopy (SEM), transmission electron microscopy (TEM), Fourier transform infrared spectroscopy (FTIR), and Raman spectroscopy. The redox and acidic properties were examined using temperature programmed reduction (TPR), isopropanol probe reaction, ammonia adsorption calorimetry, and pyridine adsorption FTIR techniques. As evidenced by pyridine adsorption FTIR, some Brönsted acid sites transformed to Lewis sites upon removal of sulfate species by washing the samples with deionized water. A high sulfur content increased the number of Brönsted acid sites but reduced their strength. The best catalyst revealed the presence of amorphous polymeric VO_x species with terminal V=O bonds, and both redox and Brönsted acid sites, resulting from an adequate balance between the calcination temperature and the sulfate concentration. These are the key parameters for optimizing the DMM production.

1. Introduction

Dimethoxymethane (DMM) is especially interesting for industrial applications [1–4], since it is suitable as fuel additive with a high chemical stability, as solvent in the perfume industry and as reagent in organic syntheses. Industrially, DMM is produced by a two-stage process: methanol oxidation to formaldehyde on silver and ferric molybdate catalysts and dehydrative condensation of the formaldehyde with methanol in the presence of liquid and solid acids [3,4]. Thus, a one-stage heterogeneous reaction process has economical and environmental benefits in the production of DMM, where three methanol molecules are incorporated into one DMM molecule ($3CH_3OH + 1/2O_2 \rightarrow CH_2(OCH_3)_2 + 2H_2O$). It has been reported in the literature that DMM can be also synthesized by the direct oxidation of methanol on crystalline $SbRe_2O_6$ [5], $Re/\gamma\text{-}Fe_2O_3$ [6], heteropolyacids [7], RuO_x/SiO_2 [8], Cu–ZSM-5 [9], and V_2O_5/TiO_2–$Ti(SO_4)_2$ [10].

Irrespective to the catalytic system, all the studies suggest a dual mechanism involving redox and acidic sites (Brönsted in case of Keggin structures [3,11], or Lewis for Re-based catalysts [6]). Additionally, Wachs indicated that the surface Brönsted acid sites can facilitate oxidation reactions requiring the participation of dual redox-acid sites [12]. Achieving an adequate balance between the two kinds of active sites is thus a crucial prerequisite for optimal DMM production.

Furthermore, the contributions of different VO_x species to the catalytic performance have been debated for some time in previous studies [13–24]. Many researchers claim that amorphous monomeric VO_x species with terminal V=O bonds are the most active species for reactant adsorption and C–H bond breaking compared to crystalline V_2O_5 [13–15]. Grzybowska-Swierkosz [16] pointed out the necessary participation of both monomeric and polymeric species. Tatibouët [17,18] proposed that a surface site constituted by a vanadyl V=O double bond standing up and a near "oxygen vacancy" constituted by the sixth coordination of a vanadium (vanadyl down) could be the most appropriate for DMM formation. In contrast, Gervasini et al. [19] found higher catalytic activity for polymeric rather than for monomeric VO_x species in partial oxidation of o-xylene to phthalic anhydride (PA), and Van Hengstum et al. [20] reported that vanadia multilayers and/or crystallites did not affect the selective oxidation of toluene. Weckhuysen et al. [21] stated that the V–O-support bond is important in methanol oxidation, a model reaction for V_2O_5/TiO_2 catalyst. Moreover, density functional theory (DFT) has demonstrated that the oxygen atom in the V–O–Ti bond is the most reactive toward atomic hydrogen adsorption, the limiting step of the oxidation reaction, because of the high stability of terminal V=O bonds [22]. Wachs

* Corresponding author. Fax: +33 472445399.
E-mail address: aline.auroux@ircelyon.univ-lyon1.fr (A. Auroux).

0021-9517/$ - see front matter © 2010 Elsevier Inc. All rights reserved.
doi:10.1016/j.jcat.2010.02.028

and Weckhuysen [23], on the other hand, stressed the critical role of bridging oxygen in V–O-support as mentioned also by Bulushev et al. [24].

We have recently studied the reactivity of sulfated vanadia–titania catalysts prepared by various methods to selectively catalyze methanol oxidation to DMM [25]. These previous results [25,26] investigated how both the preparation method and the sulfate content impacted the DMM synthesis. In this work, the challenge lied in: (1) fixing the right amount of surface residual sulfate (with or without washing with deionized water) during the calcination step in order to tune the acidity of the coprecipitated V_2O_5—TiO_2/SO_4^{2-} catalysts and (2) developing active surface structure most appropriate for DMM synthesis during the calcination process. The VTiS samples were characterized by X-ray diffraction (XRD), Brunauer–Emmett–Teller isotherms (BET), inductively coupled plasma optical emission spectroscopy (ICP–OES), X-ray photoelectron spectroscopy (XPS), scanning electron microscopy (SEM), transmission electron microscopy (TEM), Fourier transform infrared spectroscopy (FTIR), Raman spectroscopy, ammonia adsorption calorimetry, and pyridine adsorption FTIR. This study reports, in detail, the effects of surface structure, nature, and strength of active acidic sites on the performance of the selective oxidation of methanol to DMM.

2. Experimental

2.1. Catalyst preparation

Five gram of V_2O_5—TiO_2/SO_4^{2-} catalysts were prepared by a co-precipitation method [27] with 3.2 g of $VOSO_4 \times H_2O$ and 11.5 g of $TiOSO_4 \times H_2SO_4 \times H_2O$ as precursors, and 25 mL 28 wt.% $NH_3{\cdot}H_2O$ solution as precipitant. Samples VTiS-573, VTiS-623, VTiS-673, VTiS-673, and VTiS-723 were prepared in this way, and then calcined in air for 5 h at 573, 623, 673, 723, and 773 K, respectively. Additionally, samples VTiSw50-673 and VTiSw300-673 were prepared by the same procedure of co-precipitation, washed with, respectively, 50 and 300 mL deionized water while filtering the precipitate and then calcined at given temperature of 673 K in air for 5 h.

2.2. Catalyst characterization

Elemental analysis was performed using ICP optical emission spectroscopy (ICP–OES) with an ACTIVA spectrometer from Horiba JOBIN YVON.

The surface areas and pore sizes were measured by nitrogen adsorption at 77 K on a Micromeritics 2010 apparatus after heat pretreatment under vacuum for 3 h at a temperature 100 K lower than the calcination temperature.

The X-ray diffraction (XRD) measurements were carried out on a Bruker D5005 powder diffractometer scanning from 3° to 80° (2θ) at a rate of 0.02 degree s^{-1} using a Cu Kα radiation (λ = 0.15418 nm) source. The applied voltage and current were 50 kV and 35 mA, respectively.

The X-ray photoelectron spectra were measured on a KRATOS AXIS Ultra DLD spectrometer equipped with a hemispherical electron analyzer and an Al anode (Al Kα = 1486.6 eV) powered at 150 W, a pass energy of 20 eV, and a hybrid lens mode. The detection area analyzed was 700 μm × 300 μm. Charge neutralization was required for all samples. The peaks were referenced to the C–(C, H) components of the C1s band at 284.6 eV. Shirley background subtraction and peak fitting to theoretical Gaussian–Lorentzian functions were performed using an XPS processing program (vision 2.2.6 KRATOS). The residual pressure in the spectrometer chamber was 5×10^{-9} mbar during data acquisition.

Scanning electron microscopy (SEM) was performed using a Philips 5800 SEM electron microscope. The samples were deposited onto scotch carbon and metallized by sputtering. A gold film ensures a good conductivity for the observation.

The recording of transmission electron micrographs was carried out using a JEOL 2010 equipment operating at 200 kV with a high resolution pole piece and an energy dispersive X-ray spectrometer (EDS) (Link Isis from Oxford Instruments). The samples were dispersed in ethanol using a sonicator and a drop of the suspension was dripped onto a carbon film supported on a copper grid and then ethanol was evaporated. EDS study was carried out using a probe size of 15 nm to analyze borders and centers of the particles and the small particles. Standard deviations were evaluated for atomic ratio from at least 10 analyzes.

Raman spectroscopy measurements were performed using a LabRAM HR (Jobin Yvon) spectrometer. The excitation was provided by the 514.5 nm line of an Ar^+ ion laser (Spectra physics) employing a laser power of 100 μW. The laser beam was focused through microscope objective lenses (100×) down to a 1-μm spot on the sample.

H_2-TPR measurements were performed using a TPD/R/O-1100 instrument (ThermoFisher). Prior to the TPR run, the fresh sample was treated in a stream of O_2/He (0.998% v/v, flowing at 20 mL min^{-1}), ramping the temperature at 10 K min^{-1} from RT to a temperature 100 K lower than the calcination temperature and maintaining it for 60 min, and then cooled to 313 K. The TPR measurement was carried out using H_2/Ar (4.98% v/v) as reducing gas mixture, flowing at 20 mL min^{-1}. The heating rate was 10 K min^{-1} from 313 K to 1073 K. The H_2 consumption was detected by a thermal conductivity detector (TCD). The sample size used was adjusted in order to have around 69 μmol of V_2O_5 independently of the vanadia loading of the sample. This allowed us to maintain a *K* value of 100 s. (The characteristic number, *K*, can be used to facilitate the selection of appropriate operating parameters; a fixed *K* value between 60 and 140 s guarantees optimal conditions to obtain good TPR profiles [28,29].) The TPR peak areas were calibrated with given H_2/Ar (4.98% v/v) mixture injections.

The skeletal FTIR and pyridine adsorption FTIR spectra were recorded at room temperature with a Bruker Vector 22 FTIR spectrophotometer (DTGS detector) operating in the 4000–400 cm^{-1} range, with a resolution of 2 cm^{-1} and 100 acquisition scans. In each skeletal FTIR experiment, 2 mg of sample was mixed with 198 mg of KBr. In each pyridine adsorption FTIR measurement, the self-supporting wafer (10–30 mg, 18 mm diameter) was first activated in situ at a temperature 100 K lower than the calcination temperature in oxygen flow for 14 h, then evacuated at the same temperature for 2 h and then exposed to pyridine (air liquid, 99.8%, vapor pressure 3.3 kPa) at room temperature for 5 min. The desorption was carried out by evacuation for 30 min each at room temperature, 373 K, 473 K, and 573 K, respectively. The spectra were recorded at room temperature after adsorption and desorption at each temperature.

The microcalorimetric studies of ammonia adsorption were performed at 423 K in a heat flow calorimeter (C80 from Setaram) linked to a conventional volumetric apparatus equipped with a Barocel capacitance manometer for pressure measurements. Ammonia used for measurements (air liquid, purity > 99.9%) was purified by successive freeze–pump–thaw cycles. About 100 mg of sample was pretreated in a quartz cell under evacuation overnight at a temperature 100 K lower than the calcination temperature. The differential heats of adsorption were measured as a function of coverage by repeatedly introducing small doses of ammonia gas onto the catalyst until an equilibrium pressure of about 66 Pa was reached. The sample was then outgassed for 30 min at the same temperature, and a second adsorption was performed at 423 K until an equilibrium pressure of about 27 Pa was

attained in order to calculate the irreversibly chemisorbed amount of ammonia at this pressure.

2.3. Catalytic reactions

The reaction of isopropanol conversion was used to characterize the surface acidity. This probe reaction was carried out in a fixed-bed glass tube reactor. About 100 mg of sample was loaded for each reaction. Isopropanol was introduced onto the catalyst by bubbling air through a glass saturator filled with isopropanol maintained at 295 K. Isopropanol and reaction products were analyzed by an online gas chromatograph (GC), using a polyethylene glycol (PEG) 20 M packed column connected to a Flame Ionization Detector (FID). Prior to the test, each catalyst was pretreated by heating in air at the same temperature as that used for calcination for 1 h and then cooled in the air flow to the reaction temperature.

The oxidation of methanol was carried out in a fixed-bed microreactor made of glass with an inner diameter of 6 mm. The methanol was introduced into the reaction zone by bubbling O_2/N_2 (1/5) through a glass saturator filled with methanol (99.9%) maintained at 278 K. In each test, 0.2 g of catalyst was loaded, and the gas hourly space velocity (GHSV) was 11,400 mL g^{-1} h^{-1}. The feed composition was maintained as methanol:O_2:N_2 = 1:3:15 (v/v). The tail gas out of the reactor was analyzed by an online GC equipped with an FID detector and a thermal conductivity detector (TCD). The column used was PORAPAK N for the separation of methanol, DMM, and other organic compounds. The gas lines were kept at 373 K to prevent condensation of the reactant and products. The reaction was carried out at atmospheric pressure. Prior to the test, the samples were pretreated in the same way as for the isopropanol conversion reaction.

3. Results and discussion

3.1. Surface structures

The XRD patterns of the VTiS catalysts are presented in Fig. 1. It can be seen from the figure that typical diffraction peaks characteristic of anatase TiO_2 were observed for all VTiS catalysts. In particular, the VTiS-573 and VTiS-623 samples exhibited broader diffraction patterns indicating the much more amorphous nature of their TiO_2 species. The intensity of the peaks due to anatase TiO_2 increased with increasing calcination temperature, indicating agglomeration of TiO_2 particles. Crystalline V_2O_5 was detected only for samples calcined at 723 and 773 K, suggesting that vanadium oxide was present in a highly dispersed manner at low calcination temperature. In addition, the average sizes of V_2O_5 and TiO_2 particles as determined by the Debye–Scherrer formula from the XRD data are presented in Table 1. Upon increasing the calcination temperature, the titania particle size increased from 1 nm (VTiS-573) to 4 nm (VTiS-673), and then increased to 15 nm (VTiS-723) and 18 nm (VTiS-773). The average sizes of crystalline V_2O_5 were found to be 18 nm for VTiS-723 and 22 nm for VTiS-773, indicating the aggregation of particles.

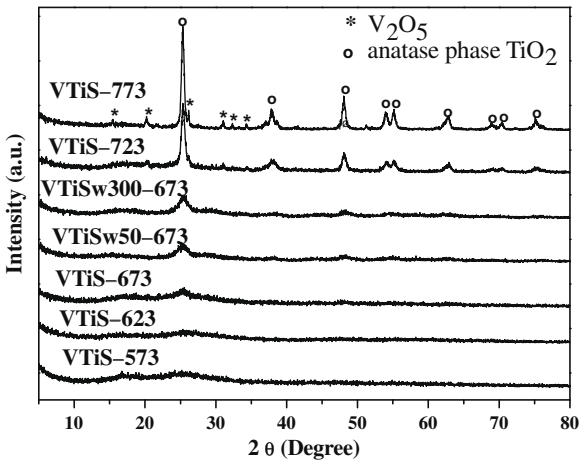

Fig. 1. X-ray diffraction (XRD) patterns of VTiS and VTiSw catalysts.

The BET surface area, porosity data, bulk (ICP) and surface (XPS) analysis for all studied VTiS catalysts are given in Table 1. The surface areas continuously decreased from 402 to 57 m^2 g^{-1} along with the average pore size which increased from 8.1 to 31.7 nm with increasing calcination temperature. The structure of VTiS catalysts did not change after washing with deionized water. The concentration of sulfur and nitrogen decreased drastically with increasing calcination temperature (especially for $T_{cal.} \geqslant 723$ K) and/or washing with deionized water, suggesting that the sulfur species were not tightly anchored to the support surface.

Table 2 lists the binding energies of $V2p_{3/2}$, O1s, $S2p_{1/2}$, and N1s and relative components from the decomposition of the O1s and $V2p_{3/2}$ lines. The reference $V2p_{3/2}$ peak positions for V_2O_5 and V_2O_4 are around 517.5 and 516.4 eV, respectively [30,31]. The full oxidation state (+5) of vanadia was predominant at catalyst surface. The formation of 20–30% V^{4+} species may be due to the exposure of the catalysts to X-radiation under ultra-high vacuum (UHV) operating conditions.

As seen in Table 2, the O1s spectra were identical and can be divided into three peaks respectively at ~530.4 eV (lattice oxygen of TiO_2 + V_2O_5 oxides contribution), ~513.2 eV (–OH contribution), and ~532.0 eV (sulfate oxygen contribution). The trend of sulfate oxygen content varied with the concentration of sulfur as shown by ICP and XPS, suggesting that the sulfur compound exists in the SO_4^{2-} form. The N1s line at binding energy around 400.0–401.2 eV may be due to an uncompleted decomposition at 553 K of ammonium salts formed during the preparation method [31]. In addition, the $S2p_{1/2}$ line at the binding energy of about 169.0 eV is typical of sulfur in S^{6+} oxidation state, such as in Na_2SO_4 or $Fe_2(SO_4)_3$ [32,33].

The surface structure of vanadia and titania species present on the VTiS catalysts was examined by Raman spectra, from 1500 to 200 cm^{-1}, as shown in Fig. 2. No Raman band was observed for VTiS-573 and VTiS-623 samples, possibly due to the presence of highly amorphous VO_x species on the surface. Since the BET surface area of catalysts decreased with increasing calcination temperature, polymeric vanadate species could have developed on the catalyst surface. The pronounced Raman bands at 1034 cm^{-1} assigned to terminal V=O bond and at 943 cm^{-1} due to V–O–V linkage for polymeric vanadate species were detected for samples calcined at 673 K [34–36]. As reported in the literature [37], the presence of surface sulfate species slightly perturbs the molecular structure of the surface vanadia species by broadening the 1034 cm^{-1} Raman band. In addition, there is a possibility of cleavage of the V–O–V bridge at high total sulfates amount, favoring the formation of $VO_2(SO_4)_2^{3-}$ species, which are more stable and having higher molecular symmetry [38]. In Fig. 2, the intensity of the band at 943 cm^{-1} decreased after washing the samples with deionized water thus indicating an overlapping of the SO_4^{2-} symmetrical stretch band in $VO_2(SO_4)_2^{3-}$ with the V–O–V band at 943 cm^{-1} [39]. Furthermore, crystalline V_2O_5 was formed when the calcination temperature reached 723 K (V_2O_5 has Raman bands around 996, 703, 530, 483, 406, 306, and 285 cm^{-1}) [40,41]. The bands at 642, 516, and 404 cm^{-1} are corresponding to Ti–O groups [42].

FTIR compared with Raman spectroscopy provides complementary information about the nature of surface metal oxide species. The skeletal FTIR spectra of VTiS samples are reported in Fig. 3a,

Table 1
Chemical analysis, X-ray photoelectron spectroscopy analysis, surface area and porosity data of the samples and calculated average size of V_2O_5 and TiO_2 particles.

Sample	C.A. (wt.%)			XPS (wt.%)				S_{BET} (m^2/g)	Average pore diameter (nm)	Pore volume (ml g^{-1})	Particle average size (nm)	
	V	Ti	S	V	Ti	S	N				V_2O_5	TiO_2
VTiS-573	10.4	33.9	3.2	11.2	31.6	5.0	2.9	402	8.1	0.8	–	1
VTiS-623	10.9	34.7	4.0	11.3	32.6	4.7	2.2	368	9.4	0.9	–	2
VTiS-673	12.6	41.0	2.6	12.3	34.7	3.7	1.7	287	11.3	0.9	–	4
VTiSw50-673	13.1	39.9	0.8	15.3	36.5	1.1	–	290	10.7	0.9	–	5
VTiSw300-673	12.6	41.6	<0.1	15.7	37.6	–	–	289	13.3	1.1	–	6
VTiS-723	12.8	43.0	0.7	14.8	37.7	2.5	1.0	100	24.1	0.6	18	15
VTiS-773	13.4	44.4	<0.1	12.2	41.0	–	0.6	57	31.7	0.5	22	18

Table 2
Binding energies of surface species and concentration (in atomic %) of different oxygen ($TiO_2 + V_2O_5$, –OH and SO_4^{2-}) and vanadia species present on the surface of the VTiS catalysts.

Sample	Binding energy (eV)						
	V2$p_{3/2}$		O1s			S2$p_{1/2}$	N1s
	V_2O_4	V_2O_5	$TiO_2 + V_2O_5$	–OH	SO_4^{2-}		
VTiS-573	516.6(25%)	517.6(75%)	530.4(54%)	531.1(7%)	532.0(39%)	168.9	401.0
VTiS-623	516.5(22%)	517.6(78%)	530.4(54%)	531.2(12%)	532.1(34%)	169.0	401.2
VTiS-673	516.4(22%)	517.7(78%)	530.4(63%)	531.1(7%)	532.0(30%)	169.9	400.2
VTiSw50-673	516.4(28%)	517.5(72%)	530.3(79%)	531.4(12%)	532.2(9%)	168.8	–
VTiSw300-673	516.2(30%)	517.4(70%)	530.2(88%)	531.4(12%)	–	–	–
VTiS-723	516.5(18%)	517.7(82%)	530.3(65%)	531.0(20%)	532.1(14%)	168.9	400.3
VTiS-773	516.2(19%)	517.4(81%)	530.1(88%)	530.9(12%)	–	–	400.1

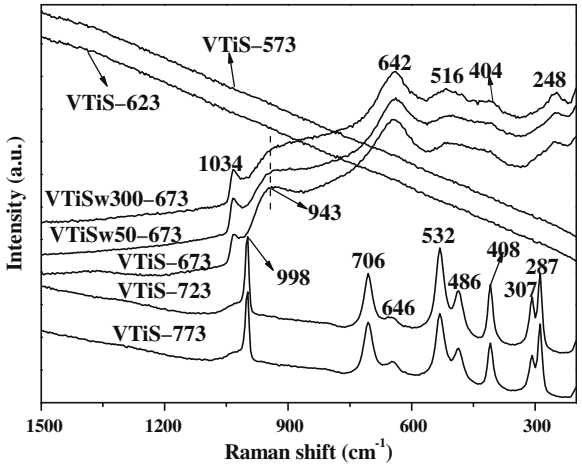

Fig. 2. Raman spectra of VTiS and VTiSw catalysts.

and the spectrum of pure TiO_2 (Millennium* G5, uncalcined) containing 0.17 wt.% sulfur (analyzed by ICP) is given for comparison. The two bands at 3430 and 1628 cm^{-1} attributed to hydrogen bonded O–H groups and H–O–H groups, respectively, were observed for all samples, and confirmed by XPS analysis of the O1s band (see Table 2). It suggests that the samples contained a certain number of surface hydroxyl groups, although some samples were calcined as high as 773 K. For pure TiO_2 as reference, other four bands at 1402, 1126, and 1051 cm^{-1} were observed; the first band was assigned to the asymmetric stretching mode of SO_2 in covalent sulfate species ($(TiO)_2SO_2$) [43,44], while the latter two originated from surface vibrations incorporating water molecules causing deformation of the surface TiO_6 octahedra surrounding surface Ti atoms [45]. For VTiS catalysts, bands at 1402, 1135, and 1050 cm^{-1} are depicted in addition to a small band at 1201 cm^{-1}. It appears that the addition of vanadia modified the spectrum obtained for TiO_2 in doing some changes such as shifting the bands at 1126, 1051 cm^{-1}, respectively, into 1135, 1060 cm^{-1} and the appearance of a new band at 1201 cm^{-1}. This indeed suggests that a strong interaction could occur between vanadia, titania, and sulfate species. The weak band at 1201 cm^{-1} could be ascribed to the asymmetric stretching mode of S–O linkages in the form of $(VO)_2SO_2$ [44], due to the migration of vanadium ions into the TiO_2–SO_4^{2-} vacant positions, but more extensive tests are required to prove this definitively. The intensities of the 1201 and 1402 cm^{-1} bands of VTiS catalysts decreased even vanished with increasing calcination temperature, as shown in Fig. 3a, which is in harmony with the XPS and ICP investigations for sulfate concentration. Inversely, a sharp band at 1030 cm^{-1} assigned to the V=O stretching vibration mode of crystalline V_2O_5 appeared when the calcination temperature reached 723 K. A large band in the range of 500–900 cm^{-1} centered at 647 cm^{-1} is probably characteristic of Ti–O–Ti anatase structure or due to vanadate species in the interlayer spaces.

Fig. 3b displays the spectra of washed VTiSw catalysts. The intensity of the band at 1201 cm^{-1} ascribed above to sulfated species decreased by washing with water, accordingly to the foregoing ICP and XPS results that the sulfate concentration drastically decreased by washing. In addition, the intensity of the band at 1135 cm^{-1} characteristic of incorporated water molecules interacting with Ti^{4+} also decreased, thus indicating that the sulfate species may impact this weak interaction by polarizing the H–O–H bond.

Fig. 3c displays the spectra of the same catalysts before (fresh VTiS–$T_{cal.}$) and after (used VTiS–$T_{cal.}$) catalytic test of methanol conversion. It can be seen that the intensity of the bands assigned to surface hydroxyl groups (at ~3430, 1628, 1135 and 1060 cm^{-1}) and the bands corresponding to sulfate species (at ~1402 and 1201 cm^{-1}) decreased after the catalytic reaction. However, the band at 1030 cm^{-1} due to V=O bonds of crystalline V_2O_5 remained the same in terms of position and intensity before and after catalytic reaction. This reflected to some extent that appropriate surface groups ($-OH + SO_4^{2-}$) may be the active sites of the catalysts, but superfluous ones can have an adverse effect on catalytic activity.

The morphology of the VTiS catalysts has been examined by electron microscopy as shown in Figs. 4 and 5. The image of

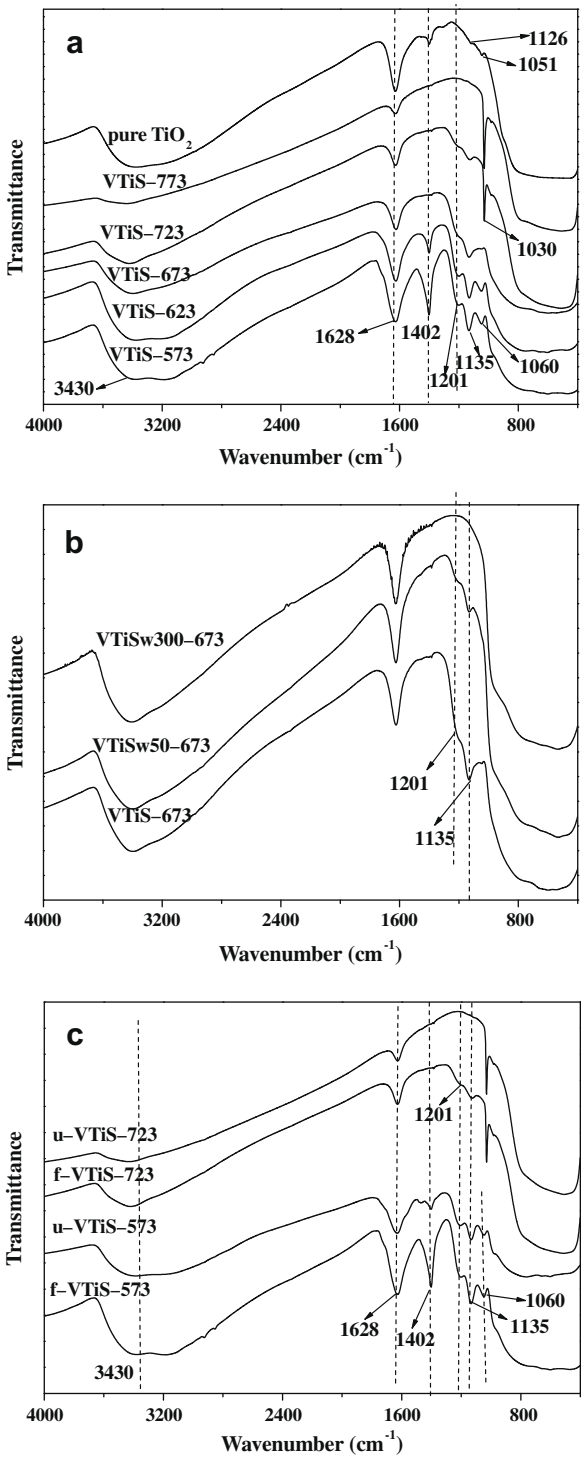

Fig. 3. FTIR skeletal spectra of: (a) VTiS catalysts and (b) VTiSw catalysts (c) catalysts before (fresh VTiS–$T_{cal.}$) and after (used VTiS–$T_{cal.}$) catalytic test of methanol conversion.

VTiS-573, presented in Fig. 4a, shows cauliflower-shaped species, which are constituted of small particles. Increasing the calcination temperature would result progressively in a loss of structure, i.e., decreased BET surface area and pore volume and increased pore diameter. Thus, for sample calcined at 623 K, the appearance of plate-shaped species was observed due to the aggregation of sample particles (shown in Fig. 4b), implying lower porosity. This phenomenon is more evident at the higher calcination temperature of 673 K as shown in Fig. 4c. Upon increasing the calcination temperature from 673 K to 723 K, an apparent change in morphology was observed for sample VTiS-723 (Fig. 4d) with the formation of needle-like crystalline particles on the surface. Moreover, the aggregation of needle-like particles was observed for sample VTiS-773 when raising the calcination temperature up to 773 K (Fig. 5a). As example, the morphology of VTiS-773 is shown in Fig. 5, which gives mainly morphological information with magnification varying from 1000× (Fig. 5a) to 20,000× (Fig. 5c). Besides the already known cauliflower-shaped species, the existence of needle-like crystals was detected on the surface of cauliflower-shaped particles (Fig. 5b and c) [46]. The morphology of VTiS-773 was deeply analyzed by TEM, and its composition (EDS) is also given, as shown in Fig. 6. The white needles are composed mainly of vanadia, while the darker part composed of numerous platelet-like particles is constituted of titania, indicating that needle-like crystals were growing away from the titania support surface. In addition, the TiO_2 particles present on samples VTiS-723 and VTiS-773 displayed irregular platelet-like shapes with dimensions of approximately 22 nm × 16 nm (obtained by TEM), which is consistent with the calculated particle size of TiO_2 shown in Table 1. However, the dimension of the needle-like vanadia crystallites was difficult to estimate from TEM analysis.

3.2. Surface acidity

3.2.1. Ammonia adsorption calorimetry study

Surface acidity, determined by ammonia adsorption calorimetry [47], expressed in terms of initial adsorption heat (denoted by Q_{init}) and amounts of ammonia adsorbed under an equilibrium pressure of 27 Pa, is shown in Table 3. The differential heats of adsorption vs. ammonia uptake (expressed in μmol NH_3 $m^{-2}_{catalyst}$) on VTiS and VTiSw catalysts are presented in Fig. 7a and b, respectively. The acid site strength distributions of the same catalysts, providing the number of sites of a given strength, are displayed in Fig. 8.

As can be seen in Fig. 7a, samples VTiS-573 and VTiS-623 exhibited quite strong acidic properties since the initial heats were 185 and 241 kJ mol^{-1}, respectively. Considering the experimental error involved in measuring the initial heat of adsorption, the initial heat slightly decreased, except for sample VTiS-673, with increasing calcination temperature. The surfaces of these catalysts appeared as heterogeneous with a continuous decrease of the energy as a function of the ammonia coverage. A particular behavior was however observed for sample VTiS-673 with low initial heats, which increased with coverage. This behavior was already reported in a previous paper [25] for sulfated vanadia–titania catalysts prepared by sol–gel and chemical grinding. This strange phenomenon was explained by a combination of both an endothermic effect such as NH_3 dissociation [48] or formation of ammonium sulfite [49] and the exothermic adsorption. However, such an effect with a lower extent was only observed for sample VTiS-673 and not for VTiS-573 and VTiS-623 samples, which contained higher sulfate concentrations. This observation indicates that the appearance of low initial heat might be related to the nature and strength of sulfate-carrier interactions created by appropriate calcination temperature.

In order to determine how the sulfate concentration impacts the surface acidity on VTiS catalysts, the acidity behavior of VTiS-673 catalyst with 2.58 wt.% sulfur (ICP) was compared with VTiSw catalysts washed with different amounts of deionized water before calcination at the same temperature of 673 K (Fig. 7b). The removal of sulfate from surface eliminated the low initial heat of adsorption previously obtained for the VTiS-673 catalyst at low ammonia uptake (<0.13 μmol m^{-2}). Beyond this value, the profiles of the three curves are similar, characteristic of vanadia–titania catalysts. This observation indicates that a high concentration of sulfur species

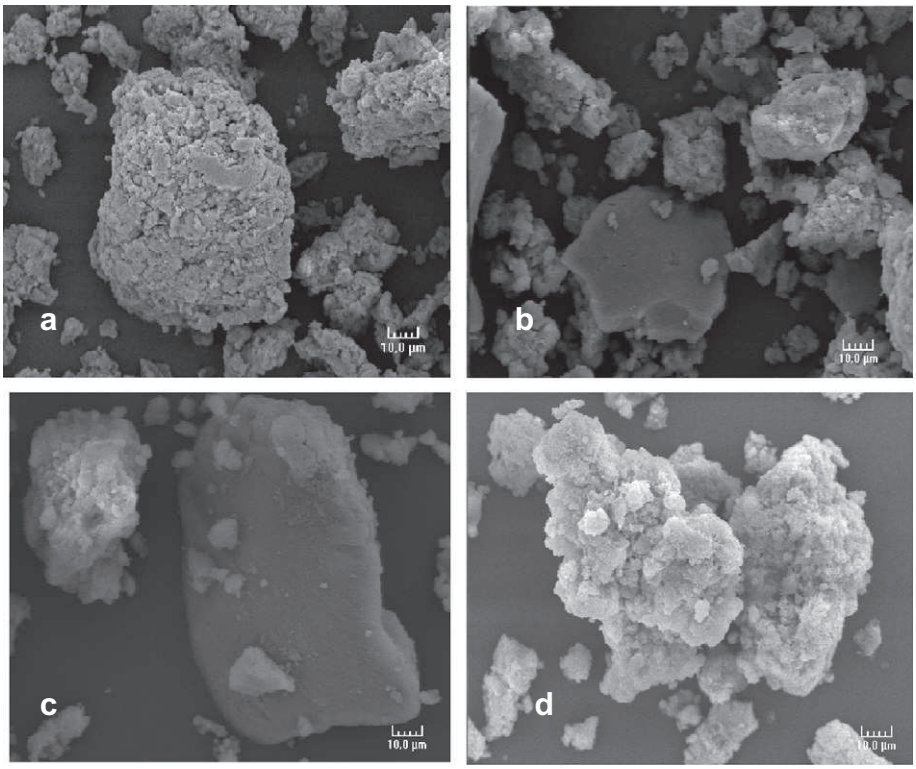

Fig. 4. SEM images of: (a) VTiS-573, (b) VTiS-623, (c) VTiS-673, and (d) VTiS-723 catalysts at the magnification of 1000×.

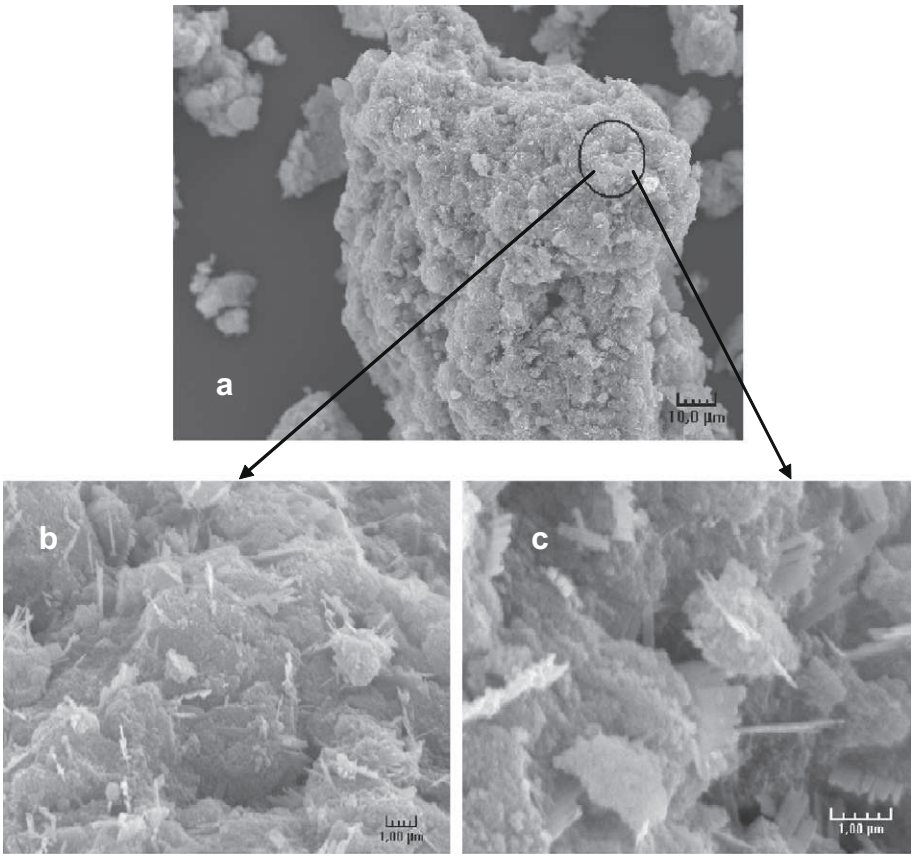

Fig. 5. SEM images of VTiS-773 catalysts at different magnifications: (a) 1000×, (b) 10,000× and (c) 20,000×.

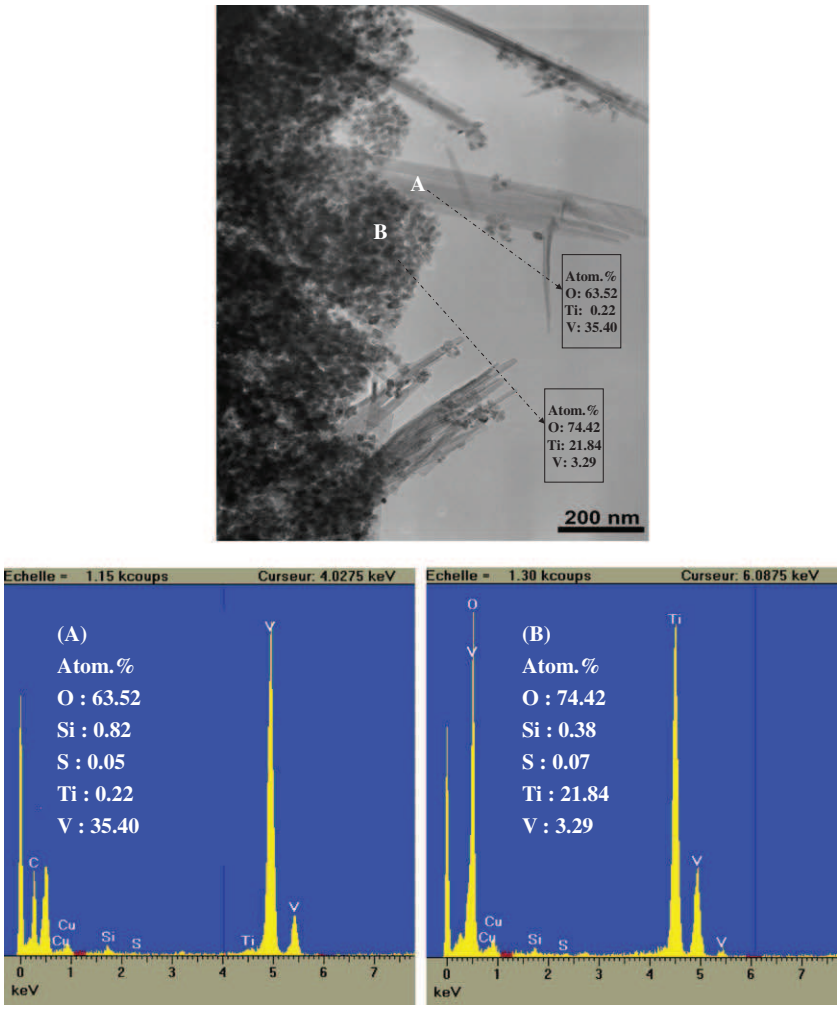

Fig. 6. TEM image and EDS spectra of VTiS-773 catalyst at the magnification of 50,000×.

Table 3
Calorimetric data for ammonia adsorption at 423 K on VTiS and VTiSw catalysts.

Sample	V_{total}[a] (μmol g^{-1})	V_{total}[a] (μmol m^{-2})	V_{irrev}[b] (μmol g^{-1})	V_{irrev}[b] (μmol m^{-2})	Q_{init}[c] (kJ mol^{-1})
VTiS-573	578	1.4	264	0.7	185
VTiS-623	591	1.6	358	1.0	241
VTiS-673	608	2.1	374	1.3	112
VTiSw50-673	568	2.0	319	1.1	253
VTiSw300-673	551	1.9	275	1.0	198
VTiS-723	268	2.7	131	1.3	190
VTiS-773	163	2.9	69	1.2	135

[a] Amount of NH_3 adsorbed under an equilibrium pressure of 27 Pa.
[b] Amount of irreversible chemisorbed NH_3.
[c] Heat evolved from the first ammonia dose.

could significantly modify only the relatively strong acidity of VTi catalysts.

In Table 3, the amount of irreversibly adsorbed ammonia, corresponding to chemisorption, decreased upon increasing calcination temperature, while the density of strong acid sites became similar when V_{irrev} is expressed per unit surface area, which confirms the role played by surface area in determining the acidity.

Fig. 8 displays the acid site strength distribution of the studied catalysts, calculated from the differential heats of NH_3 adsorption. In order to correlate with the pyridine adsorption FTIR data, this figure gives the number of acidic sites expressed in μmol g^{-1} instead of μmol m^{-2}. The strong acid sites with $Q_{diff} > 120$ kJ mol^{-1} can be ascribed to strong Lewis acid sites, while medium acid sites with $90 < Q_{diff} < 120$ kJ mol^{-1} could be assigned to Brönsted acid sites. The weak sites with $55 < Q_{diff} < 90$ kJ mol^{-1} can be considered as the physisorption sites on the catalysts surface [50]. The strange phenomenon of low initial heats of adsorption at low ammonia coverage for sample VTiS-673 makes it very difficult to calculate the number of strong acid sites ($Q_{diff} > 120$ kJ mol^{-1}). However, from the calculation on VTiSw catalysts, we can suggest that the number of strong acid sites increases with increasing calcination temperature ($T_{cal.}$) up to 673 K, then decreases when $T_{cal.} \geqslant 723$ K. In addition, the total number of acid sites including strong, medium, and weak acid sites for VTiS-723 and VTiS-773 obviously de-

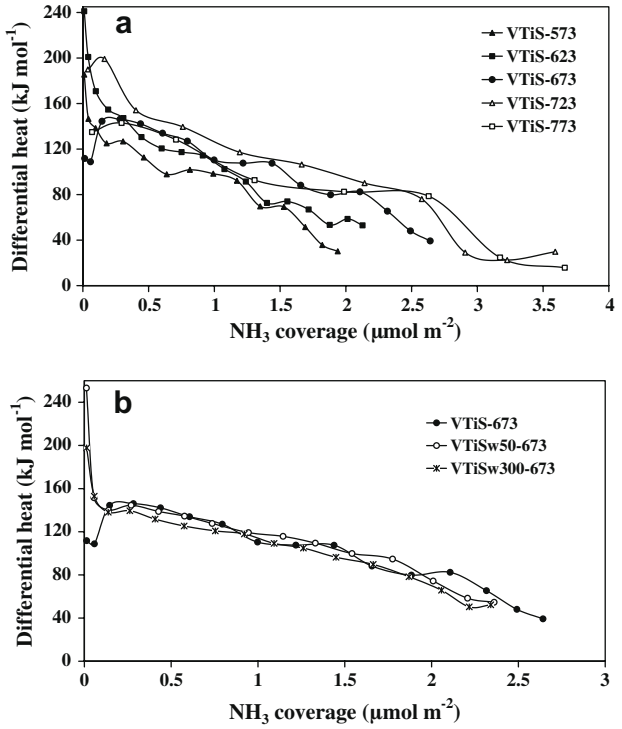

Fig. 7. Differential heats of ammonia adsorption vs. the adsorbed amount on (a) VTiS catalysts and (b) VTiSw washed catalysts.

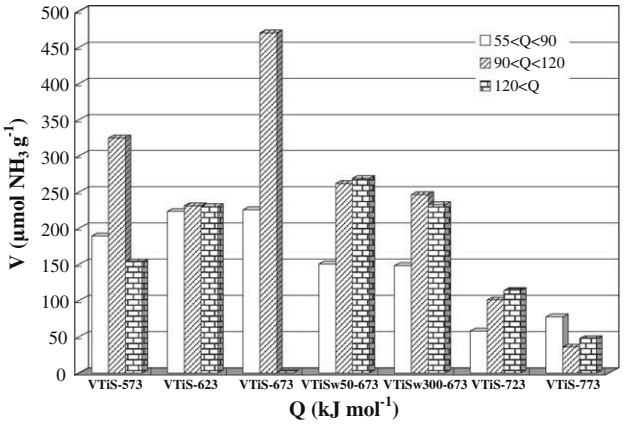

Fig. 8. Acid strength spectra of VTiS and VTiSw catalysts.

creased compared to other samples, possibly due to lower surface areas. The number of medium strength acid sites with $90 < Q_{diff} < 120$ kJ mol^{-1}, considered to be the active Brönsted acid sites as confirmed by pyridine FTIR measurements (see below), was found to be the highest for sample VTiS-673.

3.2.2. Pyridine adsorption FTIR study

Chemisorption of pyridine followed by FTIR spectroscopy is useful to probe the presence and nature of surface acid sites on catalysts [51–53]. Fig. 9 presents the FTIR spectra of pyridine adsorption on VTiS and VTiSw catalysts after desorption at 373 K for 30 min. All the spectra reported in Fig. 9 were obtained by subtracting the spectrum of the fresh catalyst (without pyridine adsorption at room temperature) from those obtained after pyridine adsorption. The bands at 1639 and 1537 cm^{-1} were attributed to Brönsted acid sites (Bpy), while the bands at 1609 and

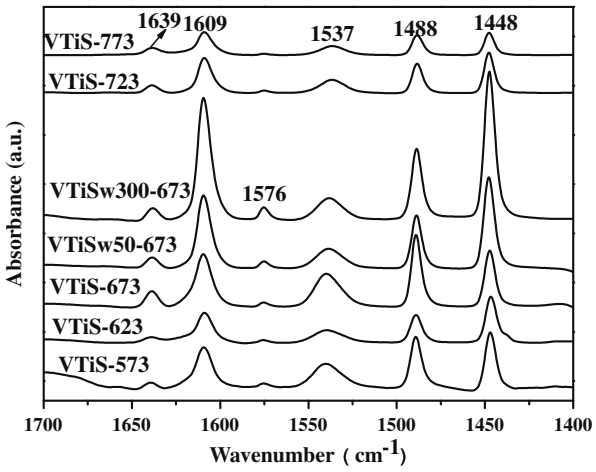

Fig. 9. FTIR spectra for pyridine adsorption and desorption at 373 K on VTiS and VTiSw catalysts.

1448 cm^{-1} corresponded to Lewis acid sites (Lpy). The bands around 1490 and 1576 cm^{-1} were associated to both Brönsted and Lewis acid sites [53].

Two Brönsted and Lewis acid site bands around ~1537 and 1448 cm^{-1}, respectively, can be used to compare the acidity by band-separation techniques of spectra [25,53,54]. The relative concentration of Brönsted and Lewis acid sites was deduced from measuring the area under the BPy and LPy peaks. In this work, the quantitative comparison of Brönsted and Lewis acid sites' population was estimated by using the same analysis method.

Fig. 10a and b show the integrated intensities of the BPy (1537 cm^{-1}) and LPy (1448 cm^{-1}) bands for VTiS and VTiSw cata-

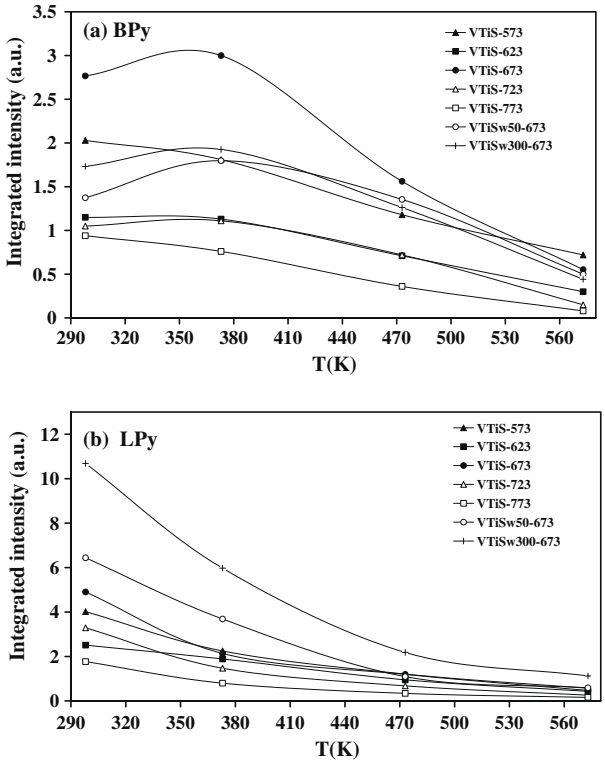

Fig. 10. Integrated intensities relative to (a) BPy band (1537 cm^{-1}) and (b) LPy band (1448 cm^{-1}) vs. evacuation temperature, after pyridine adsorption at room temperature.

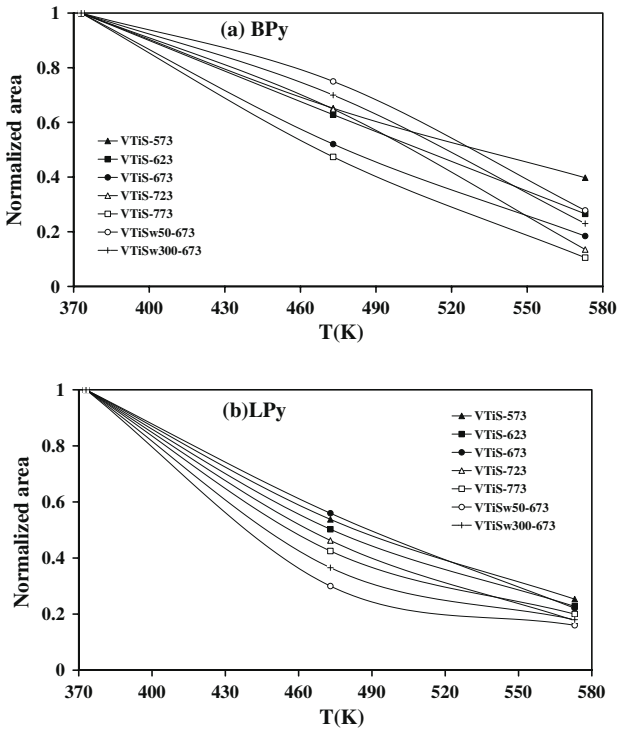

Fig. 11. Normalized area (see text) relative to: (a) BPy band (1537 cm^{-1}) and (b) LPy band (1448 cm^{-1}) vs. evacuation temperature, after pyridine adsorption at room temperature.

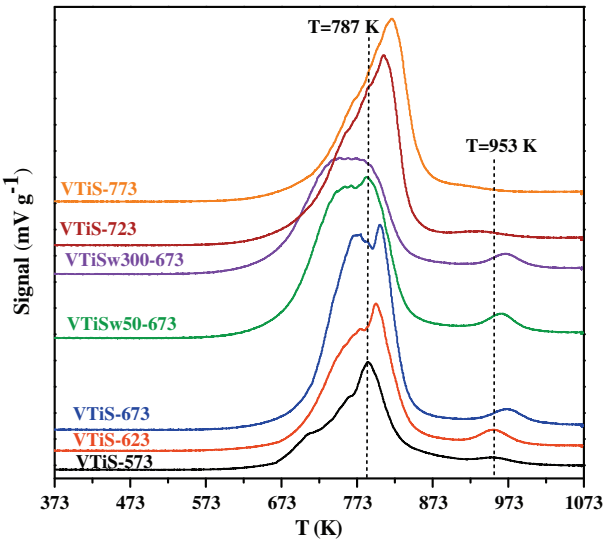

Fig. 13. TPR profiles of the VTiS and VTiSw catalysts (VTiS-573: black; VTiS-623: red; VTiS-673: blue; VTiSw50-673: olive green; VTiSw300-673: violet; VTiS-723: purple; VTiS-773: orange). (For interpretation of the references to colors in this figure caption, the reader should refer to the web version of the article.)

lysts. Assuming the possibility of physical re-adsorption with increasing evacuation temperature, it was reasonable to compare the acid sites populations at an evacuation temperature higher than 400 K. The concentration of Brönsted acid sites was found to be higher for sample VTiS-673, which was also revealed by ammonia adsorption calorimetry as shown in Fig. 8. Moreover, the number of Brönsted acid sites varied in the order VTiS-673 > VTiSw50-673 ≈ VTiSw300-673 > VTiS-573 > VTiS-623 ≈ VTiS-723 > VTiS-773, which is in agreement (except for sample VTiS-573) with the trend of the number of medium strength acid sites ($90 < Q_{diff} < 120$ kJ mol^{-1}) presented in Fig. 8. This tendency reveals that the polymeric VO_x species present on titania favor the formation of Brönsted acid sites more than crystalline vanadia species growing away from the titania support. Comparing the intensities of these two bands for VTiS-673 and the corresponding washed samples (VTiSw50-673 and VTiSw300-673), it can be seen that the concentration of Brönsted acid sites decreased with the sulfur loss. In addition, the concentration of Lewis sites increased while the Brönsted acid sites population decreased after washing with deionized water. Indeed, the presence of Brönsted acidity on VTiS catalysts can be attributed to two factors: (a) residual SO_4^{2-} and (b) the presence of defect sites [55]. Sulfate ions impact Brönsted acid character either by polarization of the O–H bond due to inductive effects or by formation of weak O–H bonds by interaction with adsorbed water. Furthermore, based on the existing theories [55,56] of predicting Brönsted acidity in the vanadia–titania system, a hypothetical reaction for transformation of Brönsted acidity to Lewis acidity induced by washing can be proposed in Fig. 12. In this reaction, two types of Brönsted acidity are respectively associated with: (type A) polarized water molecules attracted to exposed Ti^{4+} ions, as they fill the coordination sphere, and (type B) the creation of bridging hydroxyls formed between the surface vanadia and titania species. The Lewis acidity is related to unsaturated Ti ions exposed at the surface. According to this reaction, it can be seen that a progressive dehydration of acidic solid may occur due to the sulfate species loss during washing, with consequent transformation of Brönsted into Lewis acid sites. The phenomenon that the intensity of skeletal FTIR spectra bands at 1135 and 1201 cm^{-1}

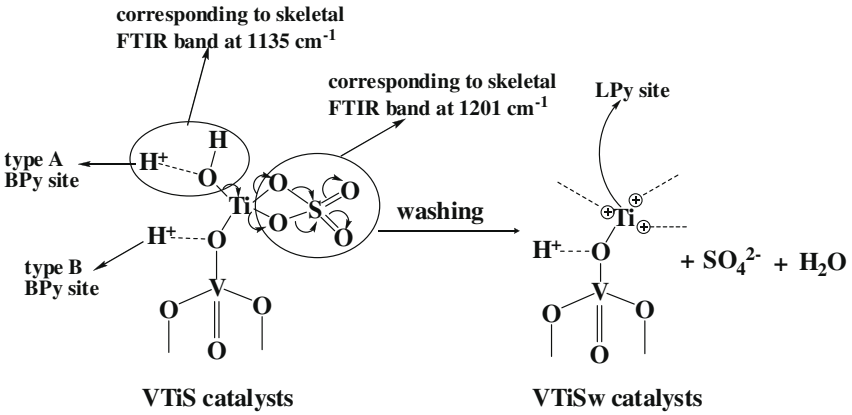

Fig. 12. Hypothetical reaction for the transformation of Brönsted acid sites to Lewis sites.

decreased after washing with water, as shown in Fig. 3b, supported this hypothetical reaction.

Meanwhile, a semiquantitative study of the strength of acid sites was carried out. To evaluate this parameter, normalized area at temperature T was defined as the ratio of the (Brönsted or Lewis) adsorption band area, measured after pyridine adsorption followed by evacuation at temperature T, to the area of the same band, measured after adsorption followed by evacuation of the probe at 373 K [57]. This quantity, calculated for Brönsted (1537 cm^{-1}) and Lewis (1448 cm^{-1}) sites adsorption bands, has been plotted as a function of evacuation temperature, as shown in Fig. 11a and b, respectively. Note that in Fig. 11a, samples VTiSw50-673 and VTiSw300-673 exhibited stronger Brönsted acidity than sample VTiS-673, which possessed the highest concentration of Brönsted acidity of unwashed samples, indicating that a high content of sulfur favored the formation of weak Brönsted acid sites (type A in Fig. 12) and thus to some extent inhibited the creation of strong acid sites. In addition, for Lewis acidity, sample VTiSw300-673 showed the highest concentration of Lewis acid sites but the lowest strength as observed in Figs. 10b and 11b, indicating that removal of sulfate from the surface weakened the Lewis acidity [58].

3.3. Reducibility of surface vanadia species by hydrogen

TPR is frequently used to study the redox properties. It is possible to correlate the redox properties with the presence of different VO_x surface species [59,60]. Normalized TPR profiles of the VTiS and VTiSw catalysts are shown in Fig. 13. The maximum reduction temperatures (T_{m1} and T_{m2}), the hydrogen consumption (expressed in μmol g^{-1}), and the theoretical surface vanadium loading (V nm^{-2}) are presented in Table 4.

The calculated surface vanadium loading, to some extent, indicates the nature of VO_x species. At low loadings (up to 2–3 V nm^{-2}), strongly bound monomeric VO_x groups with three V–O bonds to the support and a terminal partly hydrated V=O bond are formed at ambient conditions [61]. At V coverage greater than about 3 V nm^{-2}, some V–O-support bridges rearrange themselves into V–O–V bridges [16,19,62] increasing the degree of polymerization. These still-amorphous vanadia species turn into crystalline ones when the V coverage exceeds about 8 V nm^{-2} [16].

The TPR profiles of the samples with low surface vanadium loading, around 3–5 V nm^{-2}, exhibited two distinct peaks, indicating the presence of several types of oxygen-containing vanadium species on the titania surface. One peak is in the low-temperature region (T_{m1} < 873 K), while the other peak is in the high-temperature region (873 K < T_{m2} < 1023 K). Since the temperature programmed reduction treatment up to 1073 K may induce structural changes in the catalysts, the high temperature peak at 873–1023 K is most probably due to bulk V_2O_5 issued from monomeric or polymeric VO_x species at such high temperature [26]. Therefore, only the low temperature reduction peaks (T_{m1} < 873 K) were used to estimate the different surface VO_x species possibly present on the catalyst. For sample, VTiS-573, a peak (T_{m1} = 787 K) with two small shoulders at lower temperatures (708 and 763 K) was observed. With increasing calcination temperature, the surface vanadium coverage increased and the maximum temperature of the reduction peak (T_{m1}) shifted to higher values, indicating that the amount of surface vanadia species increased and more polymeric vanadia species might be formed. For example, the TPR profile of sample VTiS-623 showed a main peak centered at 798 K with a shoulder at 777 K, while the TPR profile of sample VTiS-673 exhibited a peak with two maxima at 775 and 805 K. The intensity of the left-hand shoulder maximizing around 763–775 K increased obviously by rising the calcination temperature, most possibly due to an increased amount of reducible VO_x species, i.e., an increased percentage of V^{5+} oxidation state and/or an increased amount of vanadium centers in strong interaction with the support. Additionally, from the comparison of the TPR profiles of catalysts VTiS-673 and VTiSw-673 (washed), it is noteworthy to see that the intensity of the main TPR peak decreased and that the maximum temperature of this peak slightly shifted to lower values after washing with water. These results reveal that the addition of sulfate might slightly inhibit the reduction of vanadia species and the main TPR peak, presenting either a shoulder or two maxima, is probably due to the overlapping reduction of sulfate species and monomeric and/or polymeric VO_x species. With increasing calcination temperature, the left-hand shoulder nearly vanished and only one single reduction peak shifted to higher temperatures was observed for samples VTiS-723 (T_{m1} = 809 K) and VTiS-773 (T_{m1} = 820 K). At this high surface vanadium loading, the majority of the vanadia species were obviously present as crystalline V_2O_5 species, as confirmed by Raman spectroscopy. The monomeric and polymeric VO_x species are more easily reduced than crystalline V_2O_5 particles since the reduction peak maxima shifted to higher temperatures for crystalline V_2O_5 particles.

Furthermore, the H_2 consumption was found to be the highest for sample VTiS-673, suggesting stronger redox properties for this sample. This higher reducibility is possibly coming from a strong interaction with support. In addition, the lower H_2 consumption for samples VTiS-573 and VTiS-673 also indicated that the vanadium species were not fully oxidized at lower calcination temperatures. The percentage of V^{5+} species increased with increasing calcination temperatures.

3.4. Isopropanol probe reaction

The results of isopropanol (IPA) probe reaction over the samples in flowing air are presented in Table 5. The IPA probe reaction has been extensively used to characterize the surface acid/base proper-

Table 4
Reducibility of the catalysts as revealed by the H2-TPR measurements.

Catalyst	Surface V loading (V nm^{-2})[a]	T_{max}[b] (K)			H_2 consumption (mmol g^{-1})
			Peak 1 (T_{m1})	Peak 2 (T_{m2})	
VTiS-573	3.1	763	787	952	1.2
VTiS-623	3.5	777	798	953	1.7
VTiS-673	5.2	775	805	973	2.3
VTiSw50-673	5.3	754	786	965	2.2
VTiSw300-673	5.2	752	775	969	1.8
VTiS-723	15.1	760	809	n.d.[c]	2.1
VTiS-773	27.7	770	820	n.d.[c]	2.0

[a] Supposing that all vanadium atoms are located on the surface and calculated from Table 1.
[b] Maximum temperature of the TPR peaks.
[c] Not determined.

Table 5
Catalytic activities of VTiS catalysts in the isopropanol probe reaction at 393 K in air.

Sample	Conversion of IPA (%)	Selectivity (%)		
		PPE	ACE	DIPE
VTiS-573	3	16	65	19
VTiS-623	4	26	42	32
VTiS-673	7	22	51	27
VTiSw50-673	13	10	68	22
VTiSw300-673	11	6	80	14
VTiS-723	8	8	79	13
VTiS-773	3	11	77	12

IPA, isopropanol; PPE, propylene; DIPE, diisopropyl ether; ACE, acetone.

ties under N_2 flow [63] and probe the surface redox properties in an oxidative atmosphere [27]. Thus, the conversion of IPA and selectivity to propylene (PPE), diisopropyl ether (DIPE) and acetone (ACE) in air flow can be used to probe the strength of both surface acidic and redox properties.

Results in Table 5 showed that all the studied VTiS catalysts exhibited both surface acidic and redox properties since the dehydration products (PPE and DIPE) and oxidation product (ACE) formed. Sample VTiS-573 presented a low IPA conversion. Raising the calcination temperature increased the catalytic activity since the enhanced redox properties. For example, the conversion of IPA on VTiS-573 was only 3% while that on the VTiS-673 sample was 7%. The activity in the IPA conversion reaction reached a maximum value for the washed catalysts (VTiSw50-673 and VTiSw300-673), suggesting that the high content of sulfate poisoned the active species present on the surface. In addition, the conversion of IPA decreased when the calcination temperature increased from 723 K to 773 K, probably due to the a higher formation of less active crystalline V_2O_5 particles.

It can be seen from Table 5 that samples with high sulfur content seemed more acidic than oxidative since the dehydration products (PPE and DIPE) were enhanced, while the oxidation product ACE was inhibited. The comparison of acidity detected by IPA probe reaction and ammonia adsorption calorimetry was not completely consistent, probably because the IPA probe reaction provided relative information about acidic properties linked to redox properties while ammonia adsorption calorimetry measured absolute acidic properties independently of redox properties.

3.5. The selective oxidation of methanol to DMM

Catalysts consisting of pure vanadium pentoxide with coprecipitated titanium dioxide are recognized as suitable systems for partial oxidation of methanol [64,65]. Specially, sulfated vanadia–titania catalysts are starting to have new applications in the selective oxidation of methanol to dimethoxymethane (DMM) [10,25], which can undergo further steam reforming to produce hydrogen.

Table 6 presents the whole catalytic performances of VTiS and VTiSw catalysts calcined at different temperatures. In addition, Table 7 gives the turnover frequency (TOF) of catalysts, which is defined as the number of reactant molecules converted to products over one active catalyst site per second [66]. Fig. 14a and b show the effect of reaction temperature on methanol conversion and

Table 6
Catalytic activities of the VT and VTiS catalysts in the methanol oxidation reaction.

Sample	Temp. (K)	Conversion of methanol (%)	Selectivity (%)				
			DMM	FA	MF	DME	CO_x
VTiS-573	393	4	97	0	1	2	0
	403	6	96	0	2	2	0
	413	9	94	0	4	2	0
	423	12	89	3	5	2	0
	473	51	2	56	39	3	0
VTiS-623	393	4	98	0	0	2	0
	403	6	97	0	0	3	0
	413	10	96	0	1	3	0
	423	13	91	3	1	5	0
	473	63	1	61	27	11	0
VTiS-673	393	12	98	0	1	1	0
	403	18	98	0	1	1	0
	413	29	96	0	2	2	0
	423	43	92	1	5	2	0
	453	81	6	40	44	9	1
VTiSw50-673	393	47	95	1	4	0	0
	403	74	83	4	13	1	0
	413	87	38	19	42	1	0
	423	89	3	15	38	2	42
VTiSw300-673	393	41	91	3	5	1	0
	403	52	74	10	15	1	0
	413	82	5	12	83	5	0
	423	91	0	3	72	2	23
VTiS-723	393	10	98	0	1	1	0
	403	19	97	0	2	1	0
	413	30	95	0	4	1	0
	423	49	88	1	10	1	0
	443	92	1	2	79	2	16
VTiS-773	393	6	98	0	1	1	0
	403	10	98	0	1	1	0
	413	16	93	3	3	1	0
	423	19	80	12	7	1	0
	453	71	1	11	76	2	10

DMM: dimethoxymethane; FA: formaldehyde; MF: methyl formate; DME: dimethyl ether; CO_x: CO_2 (or CO).

Table 7
The turnover frequencies (TOFs) and characteristics of VTiS catalysts.[a]

Sample	N_s[b] (V nm^{-2})	Conversion of methanol (%) at 393 K	TOF[d] $\times 10^3$ (s^{-1})
VTiS-573	3.1	4	0.1
VTiS-623	3.5	4	0.1
VTiS-673	5.2	12	0.4
VTiSw50-673	5.3	47	1.4
VTiSw300-673	5.2	41	1.2
VTiS-723	7.9[c]	10	0.6
VTiS-773	7.9[c]	6	0.6

[a] Feed conditions: methanol:O_2:N_2 = 2:6:30 mL min^{-1}, catalyst loading 0.2 g.
[b] N_s is the number of exposed catalytic active vanadium atoms per square meter.
[c] The theoretical number of exposed vanadium atoms per square meter on TiO_2 for the monolayer coverage.
[d] TOF of methanol conversion at 393 K.

DMM selectivity for all the catalysts. As presented in Table 6 and Fig. 14a and b, high reaction temperature adversely affects selectivity to DMM while it enhances the methanol conversion and selectivity to formic acid (FA) and carbon oxides. DMM remained the predominant product in the temperature range used (393–423 K). Beyond this value ($T_{react} \geqslant 425$ K), a sudden drop in the DMM selectivity was observed for all the studied catalysts. This behavior is possibly as a result of thermodynamic constraints for DMM synthesis [11]. As shown in Fig. 14a, the tendency of catalytic activity of VTiS catalysts for methanol oxidation reaction is in consistence with the order obtained from isopropanol conversion. Moreover, it was confirmed that enhanced redox properties increased catalytic activity. Among all the VTiS catalysts, the best catalytic performances were observed for samples VTiS-673 (423 K: $Con_{methanol}$ = 43%; S_{DMM} = 92%) and VTiS-723 (423 K: $Con_{methanol}$ = 49%; S_{DMM} = 88%), which displayed completely different structures of surface vanadium oxide phase. Amorphous polymeric VO_x species with terminal V=O bonds were observed only on sample VTiS-673, as indicated by Raman spectroscopy and TPR experiments, while separated phases of crystalline vanadia and titania were revealed by SEM and TEM experiments for sample VTiS-723. As reported in literature [13–15,17,18], surface structures constituted by terminal V=O are more active for DMM formation compared to crystalline V_2O_5. Further, the amorphous character of catalyst is also an important parameter since the methanol conversion to DMM requires the cooperative work of two types of sites (acid and redox) [67]. Accordingly, sample VTiS-673 should present better catalytic ability than VTiS-723.

Nevertheless, the difference between samples VTiS-673 and VTiS-723 resides not only in the surface structure but also in the sulfur concentration as presented in Table 1 (VTiS-673: *S*% = 2.6%; VTiS-723: *S*% = 0.7%). Thus, the effects of sulfur content on catalytic performance were investigated by the comparison of reactivity between VTiS-673 and VTiSw-673 catalysts, as shown in Fig. 14b. With decreasing sulfur content, obtained by washing with water, an increase in methanol conversion and a decrease in DMM selectivity were simultaneously observed. An excellent catalytic behavior with high DMM yield at the very low reaction temperature of 403 K was obtained for sample VTiSw50-673 (methanol conversion = 74%; S_{DMM} = 83%), which contained a proper amount of sulfur (*S* = 0.8%). The data show that the catalytic activity can be deeply influenced by the VO_x species nature and sulfur content. Moreover, the TOFs calculated from the number of exposed active vanadium sites for each catalyst can help in providing the intrinsic activity of the catalysts. The number of exposed surface vanadium active sites was referenced to the N_s (surface vanadium sites per square meter) value of the theoretical vanadia monolayer surface (7.9 V nm^{-2}) [66]. Below monolayer coverage, N_s was simply taken as the number of surface vanadium atoms in the catalysts (shown in Table 4, column 1). Above monolayer coverage, the N_s was taken as the theoretical value of 7.9 V nm^{-2}. As shown in Table 7, similar TOFs of the surface vanadium sites in the sub-monolayer region were obtained for VTiS-573, -623, and -673 catalysts containing increasing vanadium contents and similar sulfur contents. This is in agreement with previous observations [68,69] that the methanol oxidation activity is independent of the concentration of vanadium sites below the monolayer coverage. Deo and Wachs [69] also concluded that this selective oxidation reaction involves only one surface VO_4 site. Oppositely, TOF values vary by one order of magnitude from 4×10^{-4} s^{-1} (VTiS-673) to $\sim 1.2 \times 10^{-3}$ s^{-1} (VTiSw-673) for both samples calcined at 673 K but with different amounts of sulfur, thus revealing that sulfur would poison surface

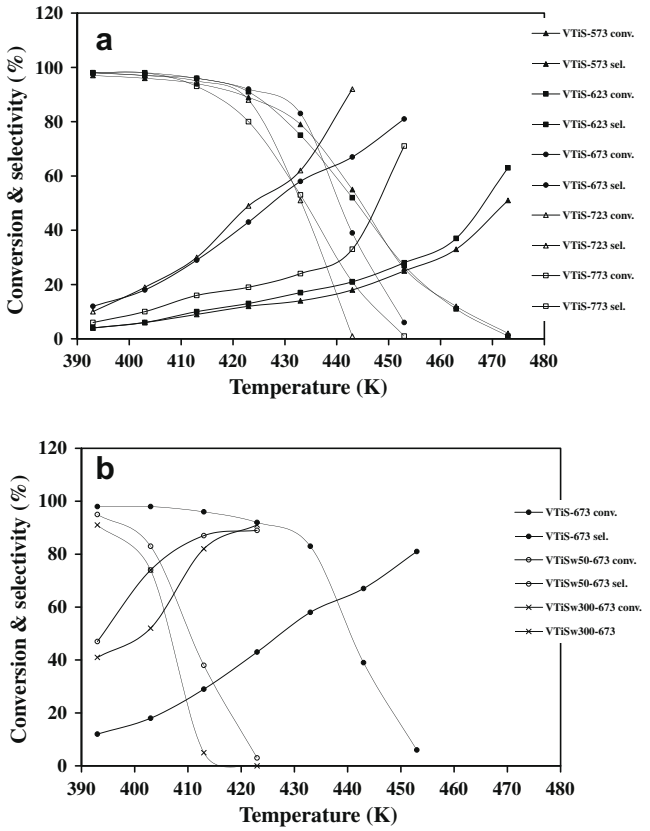

Fig. 14. DMM selectivity and methanol conversion vs. reaction temperatures over: (a) VTiS catalysts and (b) VTiSw catalysts.

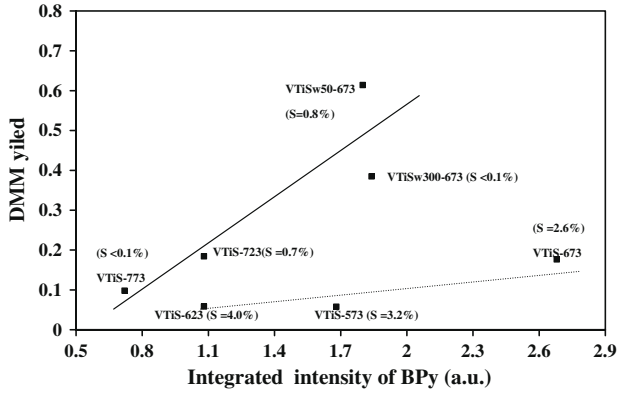

Fig. 15. Correlation between the integrated intensity relative to Brönsted acid sites (FTIR) and DMM yield.

active vanadium sites and thus decrease the catalytic activity. For samples VTiS-723 and VTiS-773 above monolayer coverage (>7.9 V nm^{-2}), the surface vanadium atoms correspond to a mixture of surface VO_4 sites and crystalline V_2O_5 sites. Thus, the relatively decreased TOF values, compared with VTiSw-673 samples, suggest that crystalline V_2O_5 phase did not contribute to the catalytic activity.

In addition, according to the above investigation by pyridine adsorption FTIR, the relative concentrations of Brönsted and Lewis acid sites were influenced by the sulfur content. In particular, the Brönsted acidity at 403 K was compared with the DMM yield at the same reaction temperature. Fig. 15 shows interesting correlations between the relative concentration of Brönsted acid sites and the DMM yield. For the VTiSw50-673, VTiSw300-673, VTiS-723, and VTiS-773 samples containing low sulfur content, the DMM yield increased quasi linearly with increasing concentration of Brönsted acid sites, suggesting that Brönsted acid sites promoted the catalytic activity. However, for VTiS-573, VTiS-623, and VTiS-673 samples with high content of sulfur, although possessing an appreciable number of Brönsted acid sites, the DMM yield did not increase remarkably with increasing concentration of Brönsted acid sites. This suggests that the high content of sulfur increased the number of Brönsted acid sites but poisoned the catalyst, which is consistent with the TOF values shown in Table 7. No evident correlation was found between the concentration of Lewis acid sites of catalysts and the DMM yield. The relationship proposed here offers a reasonable explanation of the catalytic performances shown in Table 6 and Fig. 14.

Therefore, the Brönsted acid sites and amorphous polymeric VO_x species with terminal V=O bonds of the samples possessing low sulfur content as well as redox properties are confirmed to be responsible for optimal DMM synthesis.

4. Conclusion

In the present study, sulfated vanadia–titania catalysts (S_{BET}: 57–402 $m^2\,g^{-1}$) containing different amounts of sulfur (0.1–4.0 wt.%) were prepared by co-precipitation. The influence of calcination temperature and washing with water, which determine the nature of VO_x species (polymeric and crystalline) and acidic sites, on the partial oxidation of methanol to DMM was investigated. The Raman spectra and TPR profiles of the VTiS and VTiSw catalysts provided complementary information about the nature of the vanadia species: (1) highly amorphous VO_x species were formed at the calcination temperatures of 573 and 623 K, (2) terminal V=O bonds and V–O–V linkages were obtained for samples calcined at 673 K, and (3) crystalline V_2O_5 species were observed when the calcination temperature was higher than 723 K. Additionally, as shown by SEM and TEM images, needle-like crystalline V_2O_5 species grew away from the TiO_2 surface, suggesting separated phases of V_2O_5 and TiO_2. The skeletal FTIR spectra of VTiS catalysts before and after catalytic test of methanol conversion revealed that appropriate surface hydroxyl groups and sulfate species could be the active sites in catalysts. The ammonia adsorption calorimetry study showed that the number of medium strength acid sites with $90 < Q_{diff} < 120$ kJ mol^{-1}, considered to be the active Brönsted acid sites as confirmed by pyridine FTIR measurements, is highest for sample VTiS-673. The comparison of Brönsted and Lewis acidities between VTiS-673 and VTiSw-673 samples, performed by pyridine adsorption FTIR, indicated a transformation reaction of Brönsted acid sites to Lewis acid sites after removal of some sulfate species from the surface by washing the sample with deionized water. In addition, a high concentration of sulfur can favor the formation of weak Brönsted acid sites and to some extent inhibit the creation of strong acid sites. The comparison of TOF values between washed (VTiSw-673) and unwashed (VTiS-673) samples for oxidation of methanol revealed that a high content of sulfate species would poison catalytically active sites, as confirmed by the isopropanol probe reaction. The best catalytic performance was observed for sample VTiSw50-673 with the highest DMM yield (methanol conversion:74%; S_{DMM}:83%) at the very low reaction temperature of 403 K. Consequently, an appropriate calcination temperature of 673 K with proper concentration of sulfur (~0.8 wt.%) generated polymeric VO_x species with terminal V=O bonds, high Brönsted acidity, and enhanced reducibility. These are critical parameters for optimizing DMM production.

Acknowledgments

The authors are thankful to the scientific services of Ircelyon, particularly to Mimoun Aouine and Laurence Burel for providing SEM and TEM measurements.

Hongying Zhao gratefully acknowledges the China Scholarship Council for the financial support of her PhD grant.

Financial supports from NSFC (20673055) and MSTC (2005CB221400 and 2004DFB02900) are acknowledged.

References

[1] K. Fuji, S. Nakano, E. Fujita, Synthesis 4 (1975) 276–277.
[2] Q. Sun, A. Auroux, J. Shen, J. Catal. 244 (2006) 1–9.
[3] H. Friedrich, W. Neugebauer, US Patent 3 843 562 (1974).
[4] S. Satoh, Y. Tanigawa, US Patent 6 379 507 (2002).
[5] Y. Yuan, H. Liu, H. Imoto, T. Shido, Y. Iwasawa, J. Catal. 195 (2000) 51–61.
[6] Y. Yuan, Y. Iwasawa, J. Phys. Chem. B 106 (2002) 4441–4449.
[7] H. Liu, N. Bayat, E. Iglesia, Angew. Chem. Int. Ed. 42 (2003) 5072–5075.
[8] H. Liu, E. Iglesia, J. Phys. Chem. B 109 (2005) 2155–2163.
[9] Y. Zhang, I.J. Drake, D.N. Briggs, A.T. Bell, J. Catal. 244 (2006) 219–229.
[10] Y. Fu, J. Shen, Chem. Commun. 21 (2007) 2172–2174.
[11] H. Liu, E. Iglesia, J. Catal. 223 (2004) 161–169.
[12] I.E. Wachs, T. Kim, in: D. Jackson, J. Hargreaves (Eds.), Metal Oxide Catalysis, vol. 2, Wiley-VCH, 2009, pp. 487–497.
[13] G.C. Bond, J. Chem. Technol. Biotechnol. 68 (1997) 6–13.
[14] C.R. Dias, M.F. Portela, G.C. Bond, J. Catal. 157 (1995) 344–352.
[15] G. Centi, Appl. Catal. A: Gen. 147 (1996) 267–298.
[16] B. Grzybowska-Swierkosz, Appl. Catal. A: Gen. 157 (1997) 263–310.
[17] J.M. Tatibouët, Appl. Catal. A: Gen. 148 (1997) 213–252.
[18] J.M. Tatibouët, J.E. Germain, J. Catal. 72 (1981) 375–378.
[19] A. Gervasini, P. Carniti, J. Keränen, L. Niinistö, A. Auroux, Catal. Today 96 (2004) 187–194.
[20] A.J. Van Hengstum, J.G. Van Ommen, H. Bosch, P.J. Gellings, Appl. Catal. 8 (1983) 369–382.
[21] B.M. Weckhuysen, D.E. Keller, Catal. Today 78 (2003) 25–46.
[22] M. Calatayud, C. Minot, Top. Catal. 40 (2006) 17–26.
[23] I.E. Wachs, B.M. Weckhuysen, Appl. Catal. A: Gen. 157 (1997) 67–90.
[24] D.A. Bulushev, F. Rainone, L. Kiwi-Minsker, Catal. Today 96 (2004) 195–203.
[25] H. Zhao, S. Bennici, J. Shen, A. Auroux, J. Mol. Catal. A: Chem. 309 (2009) 28–34.
[26] H. Zhao, S. Bennici, J. Cai, J. Shen, A. Auroux, Catal. Today, (2009), in press, doi:10.1016/j.cattod.2009.08.005.
[27] H. Zhao, S. Bennici, J. Shen, A. Auroux, Appl. Catal. A: Gen. 356 (2009) 121–128.
[28] P. Malet, A. Caballero, J. Chem. Soc., Faraday Trans. I 84 (1988) 2369–2375.
[29] D.A.M. Monti, A. Baiker, J. Catal. 83 (1983) 323–335.
[30] S.L.T. Andersson, J. Chem. Soc., Faraday Trans. I 75 (1979) 1356–1370.
[31] J.A. Odriozola, J. Soria, G.A. Somorjai, H. Heinemann, J.F. Garcia de la Banda, M. Lopez Granados, J.C. Conesa, J. Phys. Chem. 95 (1991) 240–246.
[32] M.H. Kim, I.S. Nam, Y.G. Kim, J. Catal. 179 (1998) 350–360.
[33] J.P. Chen, R.T. Yang, J. Catal. 139 (1993) 277–288.
[34] F.D. Hardcastle, I.E. Wachs, J. Phys. Chem. 95 (1991) 5031–5041.
[35] J. Twu, P.K. Dutta, J. Phys. Chem. 93 (1989) 7863–7868.
[36] J. Twu, P.K. Dutta, J. Catal. 124 (1990) 503–510.
[37] J.P. Dunn, J.M. Jehng, D.S. Kim, L.E. Briand, H.G. Stenger, I.E. Wachs, J. Phys. Chem. B 102 (1998) 6212–6218.
[38] N. Kausar, R. Howe, M. Skyllas-Kazacos, J. Appl. Electrochem. 31 (2001) 1327–1332.
[39] I. Giakoumelou, R.M. Caraba, V.I. Parvulescu, S. Boghosian, Catal. Lett. 78 (2002) 209–214.
[40] I.R. Beattie, T.R. Gilson, J. Chem. Soc. A (1969) 2322–2327.
[41] F. Roozeboom, M.C. Mittelmeijer-Hazeleger, J.A. Moulljn, J. Medema, V.H.J. De Beer, P.J. Gellings, J. Phys. Chem. 84 (1980) 2783–2791.
[42] I.E. Wachs, Catal. Today 27 (1996) 437–455.
[43] G. Socrates, Infrared Characteristic Group Frequencies, second ed., pp. 168–169.
[44] O. Saur, M. Bensitel, A.B. Mohammed Saad, J.C. Lavalley, C.P. Tripp, B.A. Marrow, J. Catal. 99 (1986) 104–110.

[45] M.A. Fox, M.T. Dulay, Chem. Rev. 93 (1993) 341–357.
[46] L. Nalbandian, A.A. Lemonidou, Thermochim. Acta 419 (2004) 149–159.
[47] A. Auroux, Top. Catal. 4 (1997) 71–89.
[48] A. Desmartin-Chomel, J.L. Flores, A. Bourane, J. M Clacens, F. Figueras, G. Delahay, A. Giroir-Fendler, C. Lehaut-Burnouf, J. Phys. Chem. B 110 (2006) 858–863.
[49] A. Gervasini, J. Fenyvesi, A. Auroux, Langmuir 12 (1996) 5356–5364.
[50] S. Bennici, A. Auroux, in: D. Jackson, J. Hargreaves (Eds.), Metal Oxide Catalysis, vol. 1, Wiley-VCH, 2009, pp. 391–436.
[51] H. Miyata, Y. Nakagawa, S. Miyagawa, Y. Kubokawa, J. Chem. Soc., Faraday Trans. 1 (84) (1988) 2129–2134.
[52] J. Datka, A.M. Turek, J.M. Jehng, I.E. Wachs, J. Catal. 135 (1992) 186–199.
[53] J. Keränen, A. Auroux, L. Niinistö, Appl. Catal. A 228 (2002) 213–225.
[54] H. Miyata, K. Fujii, S. Inui, Y. Kubokawa, Appl. Spectrosc. 40 (1986) 1177–1180.
[55] G. Connell, J.A. Dumesic, J. Catal. 105 (1987) 285–298.
[56] E. Ortiz-Islas, T. Lopez, J. Navarrete, X. Bokhimi, R. Gomez, J. Mol. Catal. A: Chem. 228 (2005) 345–350.
[57] T. Barzetti, E. Selli, D. Moscotti, L. Forni, J. Chem. Soc., Faraday Trans. 92 (1996) 1401–1407.
[58] B.Q. Xu, W.M.H. Sachtler, J. Catal. 167 (1997) 224–233.
[59] G.C. Bond, S.F. Tahir, Appl. Catal. 71 (1991) 1–31.
[60] G.Y. Popova, T.V. Andrushkevich, E.V. Semionova, Y.A. Chesalov, L.S. Dovlitova, V.A. Rogov, V.N. Parmon, J. Mol. Catal. A: Chem. 283 (2008) 146–152.
[61] D.A. Bulushev, L. Kiwi-Minsker, F. Rainone, A. Renken, J. Catal. 205 (2002) 115–122.
[62] G. Deo, I.E. Wachs, J. Haber, Crit. Rev. Surf. Chem. 4 (1994) 141–187.
[63] A. Gervasini, J. Fenyvesi, A. Auroux, Catal. Lett. 43 (1997) 219–228.
[64] F. Roozeboom, P.D. Cordingley, P.J. Gellings, J. Catal. 68 (1981) 464–472.
[65] A. Baiker, D. Monti, J. Catal. 91 (1985) 361–365.
[66] T. Kim, I.E. Wachs, J. Catal. 255 (2008) 197–205.
[67] S. Royer, X. Sécordel, M. Brandhorst, F. Dumeignil, S. Cristol, C. Dujardin, M. Capron, E. Payen, J.L. Dubois, Chem. Commun. 7 (2008) 865–867.
[68] C.M. Sorensen, R.S. Weber, J. Catal. 142 (1993) 1–17.
[69] G. Deo, I.E. Wachs, J. Catal. 146 (1994) 323–334.

Publication VII

Submitted to Journal of Catalysis

Influence of the metal oxide support on the surface and catalytic properties of sulfated vanadia catalysts for selective oxidation of methanol

Hongying Zhao[1], Simona Bennici[1], Jingxuan Cai[2], Jianyi Shen[2], Aline Auroux[1]*

[1]Université Lyon 1, CNRS, UMR 5256, IRCELYON, Institut de recherches sur la catalyse et l'environnement de Lyon, 2 avenue Albert Einstein, F-69626 Villeurbanne, France

[2]Laboratory of Mesoscopic Chemistry, School of Chemistry and Chemical Engineering, Nanjing University, Nanjing 210093, China

[*]Corresponding author. Fax: +33 472445399

E-mail address: aline.auroux@ircelyon.univ-lyon1.fr (A. Auroux)

Abstract

The selective oxidation of methanol to dimethoxymethane (DMM) was performed over a series of binary vanadia-based oxides (V_2O_5–TiO_2, V_2O_5–ZrO_2, V_2O_5–Al_2O_3 and V_2O_5–CeO_2) and the corresponding sulfated catalysts. The physicochemical properties of catalysts were characterized by BET, XRD, Raman, XPS, TPR–MS, ammonia adsorption calorimetry and ammonia TPD–MS techniques. The strength of the sulfate-support interaction depends on the nature of the oxide support and increases in the following order $CeO_2 > Al_2O_3 > ZrO_2 > TiO_2$. The catalytic reactivity was correlated with the nature of V–O-support bonds. Sample V_2O_5–TiO_2 exhibits the highest intrinsic activity of methanol oxidation. With the addition of sulfate, the selectivity to DMM was enhanced whereas the turnover frequency (TOF) value of vanadium sites decreased, with a rate depending on the strength of sulfate-support bonds. The best catalyst (V_2O_5–TiO_2–SO_4^{2-}) with higher DMM yield presented higher

reducibility, proper acidity and moderate strength of sulfate species.

Keywords: Supported-vanadia catalysts; Acidity; Redox character; Ammonia adsorption calorimetry; Methanol selective oxidation; Dimethoxymethane.

1. Introduction

Supported vanadia catalysts constitute a very important class of catalytic materials as they have started as model catalytic systems for fundamental studies of supported metal oxides and are extensively employed as commercial catalysts (selective catalytic reduction of NO_x with NH_3 to N_2 and H_2O, oxidative destruction of chlorinated hydrocarbons, oxidation of o-xylene to phthalic anhydride and selective oxidation and ammoxidation of C_1–C_4 hydrocarbons for olefins, oxygenates, and nitriles) [1–6]. Supporting a metal oxide on the surface of another oxide was initially proposed to improve the catalytic activity of the active metal oxide phase due to a gain in surface area and mechanical strength. The support was first considered as an inert substance that provided a high surface to carry the active metal oxide component or to improve the mechanical strength of the catalyst material [7,8], but it can also behave as active phase if partly uncovered. Generally, supported-vanadia catalysts may exhibit different catalytic properties since the metal oxide-support interaction affects both redox properties and dispersion of the active phase [9,10]. This is known as the metal oxide-support effect, although its exact origin and mechanism of operation is still unclear. The fundamental basis for the catalytic performances of supported vanadium oxides lies in the variability in geometric and electronic structure of surface vanadium oxides. Fundamental knowledge about the nature of supported vanadium oxides is of key importance in heterogeneous catalysis and spectroscopic tools are necessary to built up this knowledge.

Supported V_2O_5 catalysts are also widely studied in the reaction of methanol oxidation [11,12], which can be used as a probe reaction to characterize the activity of oxide catalysts [11,13] and further interpret it in terms of both structural and chemical (acidic and redox) properties. It appears from the literature that methanol can lead to different products by varying the nature of the catalyst and the reaction conditions

(Scheme 1) [14–16]. Redox sites enable the production of partially oxidation species such as formaldehyde (HCHO, FA) or totally oxidized species (CO_2). Acidic sites enable condensation reactions, which can give dimethyl ether (CH_3OCH_3, DME), dimethoxymethane ($CH_3OCH_2OCH_3$, DMM) and methyl formate ($HCOOCH_3$, MF). Among the aforementioned products, DMM is especially interesting for industrial applications, since it is suitable as a fuel additive with a high stability. Further, it has been shown that the addition of SO_4^{2-} species to TiO_2 enhances the acidity and can lead to improving selectivity to DMM [17].

Therefore, in this work, as a sequel to study the activity of methanol oxidation to DMM, sulfated vanadia based oxides were evaluated by this reaction. The objective of the present investigation was to examine the influence of the host metal oxide on the acidic, redox and catalytic properties of vanadia and sulfated vanadia. Moreover, the effect of the host metal oxide on the nature of active VO_x phase and sulfate species was also investigated. The structural properties were characterized by X-ray diffraction (XRD), Brunauer-Emmertt-Teller (BET), inductively coupled plasma optical emission spectroscopy (ICP-OES), X-ray photoelectron spectroscopy (XPS) and Raman spectroscopy. The redox properties were examined by temperature-programmed reduction (TPR) coupled with mass spectrometer (MS) as a detector. In addition to this, the differences obtained in the determination of acidity of these catalysts using ammonia adsorption calorimetry and ammonia temperature-programmed desorption (TPD), are also discussed.

2. Experimental

2.1 Catalyst preparation

The theoretical amount of vanadium pentoxide was fixed at 25 wt% whatever the host metal oxide used.

2.1.1 Prepared in two steps: co-precipitation of mixed oxides followed by ammonia sulfate impregnation

Binary vanadia-based oxides (denoted by VM(c1); M=Ti, Zr, Al and Ce) were prepared by modifying a previous by reported co-precipitation method [18]. The vanadia, titania, zirconia, alumina and ceria precursors were $VOCl_3$, $TiCl_4$, $ZrOCl_2$,

$Al(NO_3)_3$ and $Ce(NO_3)_3$, respectively. Briefly, $VOCl_3$ was dissolved into deionized water (1mL $VOCl_3$ in 250 mL H_2O) mixed with 5–8 mL diluted HNO_3 (38 wt% HNO_3) with vigorous stirring to form a vanadium-containing solution (S1). The oxide support precursor was dissolved into a limited deionized water to form the metal ion containing solution (S2), while $TiCl_4$ was dissolved in C_2H_5OH (1 mL $TiCl_4$ in 30 mL C_2H_5OH) in an ice bath. S2 was slowly dropped into S1 with continuous stirring to form a mixed solution (S3). Then S3 solution was slowly dropped into diluted $NH_3.H_2O$ placed in an ice bath to form the precipitate. The precipitate was first aged for 1 h at room temperature, then filtered, washed several times with deionized water until free from chloride ions, and the filtrate cake dried as reported in [18]. The samples were all calcined at 673 K in air for 5 h, except for sample VAl(c1) which calcination temperature was increased up to 773 K for a better decomposition of the precursor.

The corresponding sulfated catalysts (denoted by VMS(c1-i); M=Ti, Zr, Al and Ce) were prepared by incipient wetness impregnation of the above mentioned supported-vanadia catalysts with an aqueous solution containing the theoretical percentage of $(NH_4)_2SO_4$ to achieve a theoretical amount of 5 wt% SO_4^{2-} (1.7 wt% S). The resulting solids were then dried at 373 K overnight and then calcined at 673 K in air for 5 h.

2.1.2 Prepared directly by co-precipitation from sulfated precursors

Sulfated binary vanadia-based oxides (denoted by VMS(c2); M=Ti, Zr, Al and Ce) were also prepared by co-precipitation. The precursors were $VOSO_4$, $TiOSO_4$, $Zr(SO_4)_2$, $Al_2(SO_4)_3$ and $Ce(SO_4)_2$, respectively. The details of such preparation method have been previously described in [18]. Specially, $Ce(SO_4)_2$ was dissolved in deionized water and then the pH was adjusted to around zero by adding dilute HNO_3 (38 wt% HNO_3) in order to complete the dissolution. Then the aqueous solution of $VOSO_4$ was added dropwise to $Ce(SO_4)_2$ solution with vigorous stirring to form the mixed aqueous solution for precipitation with ammonia. At last, the samples were all calcined at 673 K in air for 5 h, except sample VAlS(c2) which calcination temperature was increased up to 773 K.

2.2 Catalyst characterization

Elemental analysis was performed using ICP optical emission spectroscopy (ICP–OES) with an ACTIVA spectrometer from Horiba JOBIN YVON.

The surface areas and pore sizes were measured by nitrogen adsorption at 77 K on a Micromeritics 2010 apparatus after heat pretreatment under vacuum for 3 h at a temperature 100 K lower than the calcination temperature.

The X-ray diffraction (XRD) measurements were carried out on a Bruker D5005 powder diffractometer scanning from 3° to 80° (2θ) at a rate of 0.02 degree.s^{-1} using a Cu Kα radiation (λ=0.15418nm) source. The applied voltage and current were 50 kV and 35 mA, respectively.

The X-ray photoelectron spectra were measured on a KRATOS AXIS Ultra DLD spectrometer equipped with a hemispherical electron analyzer and an Al anode (Al Kα=1486.6 eV) powered at 150 W, a pass energy of 20 eV, and a hybrid lens mode. The detection area analyzed was 700 × 300 μm. Charge neutralization was required for all samples. The peaks were referenced to the C–(C, H) components of the C1s band at 284.6 eV. Shirley background subtraction and peak fitting to theoretical Gaussian-Lorentzian functions were performed using an XPS processing program (vision 2.2.6 KRATOS). The residual pressure in the spectrometer chamber was 5×10^{-9} mbar during data acquisition.

Raman spectroscopy measurements were performed using a LabRAM HR (Jobin Yvon) spectrometer. The excitation was provided by the 514.5 nm line of an Ar^{+} ion laser (Spectra physics) employing a laser power of 100 μW. The laser beam was focused through microscope objective lenses (×100) down to a 1 micrometer spot on the sample.

H_2–TPR measurements were performed using a TPD/R/O–1100 instrument (ThermoFisher). Prior to each TPR run, the fresh sample was treated in a stream of O_2/He (0.998% v/v, flowing at 20 mL min^{-1}), ramping the temperature at 10 K min^{-1} from RT to 623 K and maintaining it for 60 min, and then cooled to 313 K. The TPR measurement was carried out using H_2/Ar (4.98% v/v) as reducing gas mixture, flowing at 20 mL min^{-1}. The heating rate was 5 K min^{-1} from 313 K to 1073 K. The

H_2 consumption was detected by a thermal conductivity detector (TCD). The sample size used was adjusted in order to have around 69 μmol of V_2O_5 independently of the vanadia loading of the sample. This allowed us to maintain a K value of 100 s. The characteristic number, K, can be defined to facilitate the selection of appropriate operating parameters; a fixed K value between 60 and 140 s guarantees optimal conditions to obtain good TPR profiles [19,20]. The peak areas were calibrated with given H_2/Ar (4.98% v/v) mixture injections for TPR.

Gases evolving from the TPR reactor were analyzed by a mass spectrometer (Omnistar, Pfeiffer) with a heated capillary. The signals for m/e=34 (H_2S) and 64 (SO_2) were recorded.

Temperature-programmed desorption (TPD) of ammonia was performed on a Setaram TG–DSC 111 device coupled with a mass spectrometer (Thermostar, Pfeiffer) as a detector. A capillary-coupling system was used. The TPD experiments were carried out in the range 298-923 K under helium flow as the carrier gas (10 mL min^{-1}). For each experiment, about 20 mg of sample with ammonia absorbed in previous microcalorimetric experiments was used. Initially, the samples were purged with helium at room temperature for 15 min and then heated with 5 K min^{-1} up to 373 K. The temperature was kept constant at 373 K for 30 min and then was linearly increased up to 923 K with same ramp of 5 K min^{-1}. During this temperature increase, the mass spectrometer was set at m/e=15 in order to avoid the interference of m/e peaks of water fragmentation.

The microcalorimetric studies of ammonia adsorption were performed at 423 K in a heat flow calorimeter (C80 from Setaram) linked to a conventional volumetric apparatus equipped with a Barocel capacitance manometer for pressure measurements. Ammonia used for measurements (Air Liquide, purity > 99.9%) was purified by successive freeze-pump-thaw cycles. About 100 mg of sample was pretreated in a quartz cell under evacuation overnight at a temperature 100 K lower than the calcination temperatures. The differential heats of adsorption were measured as a function of coverage by repeatedly introducing small doses of ammonia gas onto the catalyst until an equilibrium pressure of about 66 Pa was reached. The sample was

then outgassed for 30 min at the same temperature, and a second adsorption was performed at 423 K until an equilibrium pressure of about 27 Pa was attained in order to calculate the irreversibly chemisorbed amount of ammonia at this pressure.

2.3 *Catalytic reaction*

The oxidation of methanol was carried out in a fixed-bed micro-reactor made of glass with an inner diameter of 6 mm. The methanol was introduced into the reaction zone by bubbling O_2/N_2 (1/5) through a glass saturator filled with methanol (99.9%) maintained at 278 K. In each test, 0.2 g of catalyst was loaded, and the gas hourly space velocity (GHSV) was 11400 $ml.g^{-1}.h^{-1}$. The feed composition was maintained as methanol:O_2:N_2=1:3:15 (v/v). The tail gas out of the reactor was analyzed by an on-line gas chromatograph (GC) equipped with a Flame Ionization Detector (FID) detector and a thermal conductivity detector (TCD). The column used was PORAPAK N for the separation of methanol, DMM and other organic compounds. The gas lines were kept at 373 K to prevent condensation of the reactant and products. The reaction was carried out at atmospheric pressure. Prior to the test, each catalyst was pretreated by heating in air at the same temperature as that used for calcination for 1 h and then cooled in the air flow to the reaction temperature.

3. Results and discussion

3.1 Structure properties

Table 1 shows the bulk composition, pore characteristics and surface vanadium density (V/nm^2) values of the prepared materials. The sulfur content for all the VMS(c1-i) samples was similar, around 1.2–1.9 wt%, while the concentration of sulfur for VMS(c2) samples varied greatly and remained difficult to control since the different sulfated precursors. Samples VTi(c1), VZr(c1), VAl(c1) and VCe(c1) exhibited high surface area of 281, 334, 560 and 116 $m^2 g^{-1}$, respectively. Doping the VM(c1) samples with sulfate, a steady decrease of surface area can be seen for VMS(c1-i) samples, which might be due to the collapse of some pores during the second calcination. As example the N_2 adsorption-desorption isotherms and pore size distribution of VMS(c1-i) samples are depicted in Fig.2. The adsorption-desorption isotherms are similar to type IV and show type H1 or H3 hysteresis loop (mesoporous

solid in which capillary condensation takes place at higher pressures of adsorbate in addition to multilayer adsorption at lower pressures), according to IUPAC classification [21] . Mean pores wideness of the oxides is centered around 11-20 nm of pore radius (Figures 2 and Table 1). Quite often a mesoporous material contains also different amounts of micropores which result in larger adsorption at low adsorbate pressure followed by an adsorption profile resembling to type IV isotherm. The micropore surface area and the micropore volume were measured by using DeBoer's t-plot analysis. Most of the catalysts show some microporosity, especially for VAl(c1) and VAlS(c1-i) samples. VMS(c2) samples, simply prepared by co-precipitation, display similar surface area and porosity data as VMS(c1-i) samples.

The XRD patterns of vanadia-based bimetallic oxide catalysts and corresponding sulfated catalysts are presented in Figure 1. Powder XRD patterns of the mixed-vanadia-titania (zirconia and alumina) samples with or without sulfate revealed only the existence of the amorphous phase of the supports (TiO_2, Al_2O_3, and ZrO_2), while no peak of V-containing species were detected. The absence of V_2O_5 peaks is due to the very fine dispersion of V on the surface. The intensity of support peaks increased only for sample VTiS(c1-i) after the second calcination, suggesting the aggregation of TiO_2.

However, on the CeO_2 support, along with the prominent diffraction lines of cubic CeO_2, new diffraction peaks that can be attributed to the crystalline $CeVO_4$ compound are also observed for all samples before and after calcination. The preferential formation of the $CeVO_4$ compound indicated that the dispersed vanadium oxide selectively interacted with a portion of ceria and formed this stable mixed oxide [22]. In addition, the presence of sulfate species promoted the formation of $CeVO_4$.

The Raman spectra of binary vanadia-based catalysts and corresponding sulfated catalysts are shown in Fig. 3. As presented in Fig.3a, pronounced Raman bands at 1027 cm^{-1} assigned to terminal V=O bond and at 933 cm^{-1} due to V–O–V linkage for polymeric vanadate species were detected for all samples, regardless of whether SO_4^{2-} was added or not and whatever the preparation method used [23–25]. No V–O-support bridging bonds were observed probably because of the formation of

V–O–V bridges of polymeric vanadia species by breaking V–O–Ti bonds of the monomeric vanadyl species, $(Ti–O)_3V=O$ [26], which implies a weak strength V–O–Ti bond. The bands at 639, 517 and 404 cm^{-1} are corresponding to Ti–O groups [27]. A similar phenomenon was observed for VZr and VZrS samples, as shown in Fig.3b. A weak Raman band present at 1024 cm^{-1} can be associated to the terminal monoxo V=O bond of surface VO_4 species [28]. Broad Raman bands and 918 cm^{-1} with a small left-hand shoulder at ~801 cm^{-1} are corresponding to the ν_{as} vibration of bridging V–O-zirconia bonds [29] and bridging V–O–V bonds [1–3], respectively. No Raman bands corresponding to zirconium oxide were detected. The Raman spectra for VAl and VAlS samples are presented in Fig.3c. This high surface area VAl(c1) sample does not give rise to any Raman active bands for alumina support in agreement with the literature [30], and consequently all the observed Raman bands originate from the supported vanadia phase. The Raman bands at ~517 and 351 cm^{-1} have previously been assigned to the bridging V–O–V bonds of the monomeric and polymeric surface VO_4 species [28,31]. The broad band at ~950 cm^{-1} has recently been assigned to bridging V–O-alumina based on density functional theoretical (DFT) calculation [29]. Doping with SO_4^{2-} species seems to perturb the molecular structure of the surface vanadia species by broadening Raman bands for sample VAlS(c1-i). Additionally, no Raman band was observed for sample VAlS(c2) containing higher content of sulfur, suggesting that the vanadia species are totally coated by alumina or sulfate species.

As shown in Fig.3d, the Raman bands at 456 and 239 cm^{-1} are due to CeO_2 [32]. In addition to the CeO_2 features, VCe(c1) and VCeS(c1-i) samples show similar Raman band to VTiS samples at 1035 and 950 cm^{-1}. The bands at 867, 804, 759, 456, 382 and 264 cm^{-1} are characteristic of bulk $CeVO_4$ [33]. The formation of CeVO4 compound somehow reflects the presence of V–O–Ce bonds. The XPS measurements presented in the latter paragraphs provide more information about the formation of Ce^{3+} ions, supporting this observation. Trace feature of crystalline V_2O_5 species is present only in sample VCeS(c2) at 999 cm^{-1}, possibly due to the relatively low surface area.

To understand the nature of interactions between ceria and dispersed surface

vanadia species, samples of VCe and VCeS have been investigated by XPS technique. The photoelectron peaks of O 1s and Ce 3d pertaining to these VCe and VCeS samples are depicted in Figs.4 and 5, respectively. The results of surface elemental analysis, binding energies of V $2p_{3/2}$, Ce $3d_{5/2}$, O 1s and S $2p_{1/2}$, as well as the relative components from the decomposition of the O 1s lines are presented in Table 2. As can be noted from Table 2, the XPS results of surface vanadium, cerium and sulfur composition are consistent with chemical analysis results. Additionally, the lower vanadium composition for sample VCeS(c2) is possibly due to the higher concentration of $CeVO_4$ (confirmed by the intensity of XRD patterns), since surface vanadia may diffuse into the ceria lattice. The binding energies of V $2p_{3/2}$ for all the VCe and VCeS samples were ~517.2 eV, indicating that the vanadia surface species were fully oxidized (oxidation state V^{5+}) [34]. The S $2p_{1/2}$ line at the binding energy of about 169.0 eV is typical of sulfur in S^{6+} oxidation state in the form of SO_4^{2-} species on the surface of metal oxides [35,36].

As shown in Fig.4, the O 1s peaks are, in general, broad and complicated because of the overlapping contribution of oxygen from the various component oxides, which could be divided into three bands. The quantitative results acquired from the theoretical Gaussian-Lorentzian functional peak fitting are presented in Table 2 and agree with the value reported in a previous paper [18]. In addition, the peak centered at 532.0–532.2 eV in this work can be attributed both to $CeVO_4$ compound [37] and sulfate species.

The XPS core-level spectra of Ce 3d are generally characterized by complex but distinct features that are related to the final-state occupation of the Ce 4f level [38]. According to the literature [39,40], the Ce 3d spectrum can be assigned as follows: the peaks labeled u are due to $3d_{3/2}$ spin-orbit states, and those labeled v are corresponding to $3d_{5/2}$ states. Specially, the u’’’/v’’’ doublet is due to the primary photoemission from Ce(IV)-O_2. The u/v and u’’/v’’ doublets are shakedown features generating from the transfer of one or two electrons from a filled O 2p orbital to an empty Ce 4f orbital. The u’/v’ doublet is due to photoemission from Ce(III) cations. Therefore, the Ce 3d spectra of all VCe and VCeS samples shown in Fig.4 revealed a

mixture of Ce^{3+} and Ce^{4+} oxidation states. In fact, cerium in $CeVO_4$ was in the valence +3. Thus, the XPS results concerning the formation of $CeVO_4$ compound support the conclusions drawn from XRD and Raman results fairly well.

3.2 Surface acidity

Among the surface properties of vanadia catalysts of some importance for their catalytic activity in selective oxidation, acidity is one of the most significant [41]. The acidity measurements were performed by means of NH_3 adsorption experiments monitored by calorimetry coupled to volumetry. Table 3 summarizes the main results obtained. Fig. 6 shows the plots of the differential heats of NH_3 adsorption as a function of NH_3 coverage and Fig.7 presents the ammonia adsorption isotherms for the series of binary vanadia-based catalysts and corresponding sulfated catalysts.

The Q_{diff} values as exhibited in Fig.6 are all similar with a sharp decrease at the beginning except for sample VTiS(c1-i) due to sulfate species which can increase or decrease the acidity at low coverage. The surfaces of these catalysts appear as heterogeneous with a continuous slowly decrease of the acidity as a function of the coverage.

Doping SO_4^{2-} increases the acidity as can be easily seen on the isotherms (Fig.7) for VTi and VAl samples, while there is very little influence with the addition of SO_4^{2-} on VZr sample. For VCe sample, the addition of sulfate regardless the preparation method decreases the acidity (Fig.7) due to the decreased surface area, since the surface coverage by ammonia varies in the order of VCeS(c2)>VCeS(c1-i)>VCe(c1) when expressed per unit surface area (Table 3). In addition, the content of $CeVO_4$ is the highest for sample VCeS(c2) as investigated by XRD measurement. These observations confirmed that the formation of $CeVO_4$ increases the acidity of VCe samples, CeO_2 being mainly a basic support. Additionally, the number of acid sites of these catalysts (both the total population, $V_{NH3,\ total}$, and that of strong sites, $V_{NH3,\ irrev}$) reported in Table 3 follows the same trend.

To obtain more detailed information on the acidity and thermal stability of catalysts, simultaneous TPD–MS–TG–DSC profiles of sulfated binary vanadia-based catalysts are shown in Fig.8. As presented in TG curves, the first weight loss step, in

all cases, is mostly caused by ammonia desorption. Another remarkable weight loss in the higher temperature range corresponding to liberation of SO_4^{2-} is observed simultaneously with endothermic feature especially for VTiS and VZrS samples. Moreover, the weak endothermic peaks are possibly the overlay of the endothermic peak of sulfate desorption and exothermic crystallization peak.

The maximum temperatures the desorbed ammonia and sulfate TPD peaks are summarized in Table 3. Usually, it is not accurate to rank the acid strength by simply comparing the ammonia desorption maxima because of the complex diffusion effect, especially for the porous materials. However, all the samples exhibited a broad desorption ammonia peak spanned in the range of 483–780 K, suggesting the heterogeneous strength distribution of the acid sites in these samples. The change in the TPD profiles can be explained by the progressive transformation of the surface acidity. As exhibited in Table 3, the ammonia desorption maxima were similar at ~530 K for samples VTi(c1) and VTiS(c1-i) with 1.5wt% sulfur, but 20 K higher for sample VTiS(c2) with 1.8 wt% sulfur. This result suggests that strongly bonded ammonia species can be formed on sample containing high content of sulfur and/or prepared by co-precipitation. In case of VZrS and VCeS systems, the higher maximum temperature was obtained for sample VZrS(c1-i) and VCeS(c1-i) possessing higher concentration of sulfur. Furthermore, trace crystalline V_2O_5 species in sample VCeS(c2), investigated by Raman spectroscopy, also induce a decreased ammonia desorption $T_{max.}$ Therefore, the highly dispersed sulfur certainly plays an important role in determining the average strength of catalyst acidity. Besides VAlS(c1-i) and VAlS(c2) samples display similar ammonia desorption peaks with a maximum at ~ 567 K, in spite of sample VAlS(c2) containing much higher content of sulfur compared to sample VAlS(c1-i). This can be explained by a complex diffusion effect since VAlS samples show much more microporosity.

In a previous paper [42] a strange phenomenon of low initial heat of adsorption was observed by ammonia calorimetry on few sulfated-vanadia-titania samples. This phenomenon, interpreted by an endothermic reaction associated to an exothermic adsorption, was also obtained in this work but only for VTiS(c1-i) sample. Although

the low heats of adsorption were explained well as the contribution of the interaction of dissociated ammonia with sulfates [43], the desorption behavior of sulfate species obtained from NH_3–TPD indicates a reasonable explanation for what kinds of sulfate materials could favor the low initial heat of adsorption.

By using TG–TPD–MS, we have determined that the primary products of sulfated metal oxides thermal decomposition are SO_2 and O_2, which is consistent with previously reported mass spectrometry results [44]. As shown in Fig.8 and Table 3, sample VTiS(c1-i) exhibited a main peak centered at 676 K with a small shoulder at 767 K, while sample VTiS(c2) presented a peak with two maxima at 687 and 765 K. This behavior suggests the existence of different structures of sulfate species, expecting that one desorption profile could be pertained to one sulfate structure only. Besides, as proposed before by Waqif et al [45] based on IR studies, only one sulfate type of $(–O)_3S=O$ was found on TiO_2. Therefore, we attempt to say that the sulfate desorption peak centered at 676 K could possibly be assigned to bisulfate and/or lowly polymerized species while the shoulder at 767 K corresponded to highly polymerized species. In addition, the intensity of the peak centered around 767 K is much higher for sample VTiS(c1-i) compared to VTiS(c2), implying a higher content of weak sulfate species for sample VTiS(c1-i).

In the case of VZrS, VAlS and VCeS systems, similar sulfate desorption peaks were observed for each system regardless the preparation method and sulfate density. For VZrS samples, the first small peak is placed at relatively low temperature (~741 K) corresponding to lowly polymerized species, while the second peak centered at ~867 K is assigned to highly polymerized species. Additionally, samples VAlS and VCeS exhibited only one desorption sulfate peak at higher temperatures of ~960 K and >973 K, respectively, possibly due to the highly polymerized sulfate species. In conclusion, the maximum temperature of releasing sulfate species varied in the order of VTiS < VZrS < VAlS < VCeS, implying that the strength of sulfate-support interaction strongly depends on the oxide support (TiO_2, ZrO_2, Al_2O_3 and CeO_2).

It is noteworthy that VTiS(c1-i) sample which presented low initial heat of adsorption simultaneously contained higher concentration of weak sulfate species.

These results confirmed that not all the sulfated materials can induce this strange phenomenon of low initial heat of adsorption at low ammonia coverage, but only samples possessing enough weak sulfate species, such as bisulfate and low polymerized sulfate species.

3.3 Redox properties

To investigate the effect of oxide support (TiO_2, ZrO_2, Al_2O_3 and CeO_2) on the redox properties of the studied catalysts, the TPR technique was employed and the reduction process was monitored by mass spectrometry.

Figs. 9(a-d) shows the TPR profiles in the temperature range of 350–1050 K for all the samples. As shown in Fig.9a, sample VTi(c1) displays a peak centered at ~708 K with a right-hand shoulder maximizing around 758 K. The TPR profile of sample VTi(c1) indicates that the majority of vanadia species are present as polymeric VO_x species (T_{m1}<760K) [46,47], as evidenced by Raman spectra. With the addition of SO_4^{2-}, samples VTiS(c1-i) and VTiS(c2) exhibit a peak maximizing around 760 K with a left-hand shoulder at 728 K. As already reported by other authors [48,49], the reduction of S(VI) species could affect the shape of H_2 consumption profile, which was checked by mass spectrometry as reported in the following paragraphs. There is another small peak at much higher temperature, in the range of 900–1030 K, possibly assigned to bulk V_2O_5 issued from the same polymeric VO_x species.

The reduction behavior of VZr and VZrS samples is illustrated by Fig.9b. Only one peak with a maximum at 742 K was observed for sample VZr(c1), whereas samples VZrS(c1-i) and VZrS(c2) present a sharp peak centered at ~762 K and superimposed with a small left-hand shoulder (~738 K). By analogy with VTiS samples, most vanadia species render as polymeric VO_x phase. As shown in Fig.9c for VAl and VAlS samples, the maximum temperature of the reduction peak (T_{m1}) shifts to higher values and the intensity of TPR peak increases by adding sulfate species, especially for sample VAlS(c2) possessing 5.6 wt% S.

The TPR profiles of VCe and VCeS (c1-i and c2) samples are shown in Fig.9d. Two distinct reduction peaks can be observed for these three samples (see Table 4). As reported in the literature [32], pure CeO_2 shows two reduction peaks at 795 and 981K,

indicative of the reduction of Ce^{4+} to Ce^{3+}. The reduction peak for VCe(c1) is at 790 K, suggesting that the addition of vanadium oxide to ceria obscures the low temperature peak. This is consistent with the stabilization of Ce^{3+} sites at the vanadia-titania interface [50]. Upon the addition of sulfate, the maximum temperature of TPR peak shifts to 837 K for VCeS(c1-i) and to 843 K for VCeS(c2). There is some Ce^{3+} ($CeVO_4$) at the vanadia-ceria interface, confirmed by the XRD, Raman and XPS measurements. The formation of $CeVO_4$ out of surface vanadium oxide on CeO_2 reveals that V enters the ceria lattice or that ceria ions migrate to surround vanadia, in a strong metal-suport-interaction-like behavior. Thus the first reduction peak (~790 K) would be indicative of the reduction of $V^{5+}O_x/Ce^{4+}O_2$ to $Ce^{3+}V^{5+}O_4/Ce^{4+}O_2$ (the reductive formation of $CeVO_4$) and not of the reduction of surface vanadia species [51]. Bulk $CeVO_4$ exhibits a reduction peak at 954 K due to $V5^+ \rightarrow V^{3+}$ transformation and bulk CeO_2 exhibits an intense second reduction maximum at 981 K. Therefore, the second peak of mixed vanadia-ceria samples (~948 K) must be a linear combination of the reduction maxima of CeO_2 and of the transformation of V^{5+} to V^{3+} in the $CeVO_4$ phase.

The T_{m1} value of the studied samples increases in the order of VTi (708 K) < VZr (742 K)< VCe (790 K) < VAl (796 K), suggesting that the most reducible nature of TiO_2 and ZrO_2 surfaces typically leads to more reducible oxide domains than the refractory Al_2O_3 and CeO_2 supports.

The mass spectrometry (MS) data for VMS(c1-i) systems (M=Ti, Zr, Al and Ce), obtained after the TPR runs, are exhibited in Figs.10(a-d). Mass data show that twin reduction peaks correspond to the reduction of S^{6+} species (SO_4^{2-}) to S^{4+} (SO_2) and to S^{2-} (H_2S) species, respectively. In case of sample VTiS(c1-i), no formation of H_2S was detected, whereas the other samples show the presence of both H_2S and SO_2. The major SO_2 peak for sample VTiS(c1-i) is observed between 604–779 K with a maximum at 700 K. Together with H_2 consumption profile as shown in Fig.9a and Fig.10a (m/e=2), the small shoulder obtained at 724 K for sample VTiS(c1-i) (Fig. 9a) can be attributed to the reducing of sulfate species since it matches the SO_2 evolution very well. In another word, the main peak at 754 K is mostly assigned to dispersed

VO_x species. These results reflect that the addition of sulfate inhibits the reduction of vanadia since the reduction peak maxima slightly shift from 708 K for VTi(c1) to 754 K for VTiS(c1-i).

For sample VZrS(c1-i), two sulfate reduction products (H_2S and SO_2) were detected but did not evolve in parallel in the whole temperature range. The first peak is in the temperature range of 628–780 K with maximum yield at ~730 K and is due to SO_2. Beyond 751 K, H_2S evolution is observed, but this peak is very small. A similar phenomenon was observed for VAlS(c1-i) and VCeS(c1-i) samples. MS analysis shows two distinct features: a low-temperature peak related to SO_2 formation (a peak centered at 762 K for VAlS(c1-i) and 815 K for VCeS(c1-i)), followed by a higher temperature peak related to H_2S formation. Specially for sample VCeS(c1-i), two peaks for H_2S release with maxima at 836 K and 974 K were observed (see Table 4). All the SO_2 and H_2S evolutions matched that of H_2 consumption.

The sulfate reduction temperature for liberating SO_2 and H_2S is in respect with the nature of oxide support and decreases in the order of VTiS < VZrS < VAlS < VCeS. Again, the different observed maxima and relative intensity of these two distinct SO_2 and H_2S peaks indicate different types of sulfate species conforming to different sulfate structures [52,53]. The sulfate species reduced at low temperature could correspond to those not strongly bonded to the surface and consequently should be readily reduced to SO_2, while the sulfate species reduced at higher temperature are interacting strongly with the surface, and thus should be more prone to be reduced to H_2S, since SO_2 can not be formed without breakage of a M–O bond (M=Ti, Zr, Al and Ce). This observation is consistent with the thermal stability of sulfate species present on different oxide supports, as indicated by TPD–MS measurements.

As reported in Table 4. VCe and VCeS samples exhibit the highest H_2 consumption implying higher concentration of redox sites since both V and Ce oxides possess redox sites. Moreover, H_2 consumption increased upon addition of sulfate, especially for sample VAlS(c2) with 5.6 wt% S.

3.4 Methanol oxidation reaction

It is now well admitted that the partial oxidation of methanol is strongly sensitive

to the nature of the active sites, which can be employed to provide information about the surface acidity and redox properties simultaneously [11,14]. Figs.11(A–D) show the whole catalytic performance of samples, while Table 5 presents the turnover frequency of catalysts, which is defined as the number of methanol molecules converted per surface vanadium oxide site per second [54].

As shown in Fig.11A, sample VTi(c1) exhibited high activity. For example, the conversion of methanol was 58% at 393 K, with selectivies to DMM, FA, MF and DME of 64%, 15%, 21% and 0%, respectively. Moreover, the distribution of products indicates that the surface acidity was not strong enough to effectively catalyze the reaction of FA condensation with methanol to produce DMM, leading to the production of oxidation products (MF and FA). With increasing reaction temperature, the selectivity to DMM decreased while the selectivity to FA and MF increased, with a rapid increase in the total conversion of methanol. The sudden drop in DMM selectivity is possibly as a result of thermodynamic constrains for DMM synthesis [14]. At 413 K, the conversion of methanol dramatically increased to 95%, and only oxidation products could be observed, with selectivities to FA, MF and CO_x of 10%, 61% and 28%, respectively. This suggests that VTi catalyst mainly possessed strong redox sites, while activities were enhanced with the temperature increase. Upon doping VTi samples with SO_4^{2-}, the selectivity to DMM was greatly improved apparently due to the enhancement of surface acidity with the addition of SO_4^{2-}, while the selectivity to the relative oxidation products (MF and FA) decreased especially for sample VTiS(c2). Moreover, the improved acidity must be mainly due to some medium strength acid sites, since the selectivity to DME (created on the strong acid sites) still remained at a very low level.

With VZr(c1) sample (Fig.11B), low methanol conversion with high selectivity to DMM was observed up to 423 K. Above this temperature, the selectivity to DMM gradually decreased, whereas the selectivity to MF increased rapidly and became the main product. This observed trend, similar with VTi(c1) sample, can be explained by assuming that a slight increase in quantity of active redox site, and/or the deactivation of a part of medium acidic sites occurred when increasing the reaction temperature.

For VZrS samples, the selectivity to DMM was improved by SO_4^{2-} doping but not as much as VTiS samples. In addition, a small amount of DME was also obtained for VZrS samples, suggesting the existence of strong acid sites.

Fig.11C presents the catalytic performance for VAl and VAlS samples. In the low temperature range of 393–423 K, sample VAl(c1) yielded mainly DMM with much lower methanol conversion (1–8%) compared to VTi(c1) and VZr(c1) samples. The other possible products (FA, MF, and DME) were formed in low amount. The formation of DME is possibly created by the uncovered acidic Al_2O_3 support since pure Al_2O_3 carrier possesses a high activity for dehydration of methanol to DME [55]. With the addition of SO_4^{2-}, the selectivity to DME was obviously increased while the formation of DMM was slightly enhanced, again indicating that the sulfate species located on alumina support favor the dehydration of methanol to DME.

Sample VCe(c1), shown in Fig.11D, exhibits up to 423 K low conversion of methanol (4–13%) with very high selectivity to DMM (94–99%) and a light selectivity to FA (0–7%). From 423 K, DMM production decreases, again in favor of a high activity and selectivity of oxidation products (FA and MF). Note that the main oxidation products for VCe(c1) sample were FA and not MF. This can be attributed to the high concentration of redox sites and to a lack of acidic sites. Indeed acid sites may enable condensation reactions (Scheme 1) based on the results from H_2–TPR and ammonia adsorption calorimetry measurements.

In summary, we can demonstrate that sample VTiS(c2) prepared by simply straightforward co-precipitation is recognized as the best sample for partial oxidation of methanol to DMM, which in agreement with a previous paper [56].

As known, there are varieties of factors by which the host metal oxide may affect the activity of the catalyst. The relatively independent turnover frequency (TOF) values can help in providing the intrinsic activity of these catalysts. The number of exposed surface vanadium active sites was referenced to the N_s (surface vanadium sites per square meter) value of monolayer surface vanadia catalysts (7.9 V nm^{-2}) [10,22,57]. Below monolayer coverage, N_s was simply taken as the number of surface vanadium atoms (see Table 5, column 1). Above monolayer coverage, Ns was taken

as the theoretical value of 7.9 V nm^{-2}. Note that for VCe and VCeS samples, the exposed surface vanadium sites originate from highly dispersed VO_x species (confirmed by Raman spectroscopy) and $CeVO_4$ compound.

As presented in Table 5, the methanol oxidation turnover frequency (TOF) of the surface vanadium sites varied dramatically when the metal oxide support changed. The TOF value of surface vanadium sites on TiO_2, ZrO_2, Al_2O_3 and CeO_2 are 15.9×10^{-4}, 4.2×10^{-4}, 0.4×10^{-4} and 2.0×10^{-4}, respectively. Thus, the significant variation of the TOF values for monomeric and/or polymeric VO_x species with different oxide supports strongly implicates that the nature of V–O-support bond is the key parameter involved in the relevant rate-determining-step (Scheme 1) [58].

Another method often used to cast light on the mechanism of catalytic action is to search for correlations between the catalyst reactivity and some other property of its surface. Fig.12 shows a correlation of the TOFs values and the T_{max} data obtained from TPR experiments.

For VM(c1) (M=Ti, Zr, Al and Ce) samples, the T_{max} increases in the order of VAl (796 K) > VCe (790 K) > VZr (742 K) > VTi (708 K), whereas the TOF value presents an opposite trend. This observation reveals that a decrease in the T_{max} temperature would result in an increase in TOF. Furthermore, the T_{max} is related to the reducibility of samples. Although a correlation between catalytic activity in oxidation reaction and reducibility of catalysts has already existed [59,60], the factors determining the reducibility of vanadium species are still unclear. The results of a study [58,61], concluded by TPR, on the reducibility of vanadium oxide catalyst led to the assumption that the reducibility of a catalyst is mainly influenced by vanadia-support interactions. These interactions can be related to the parameter *z/a*, i.e., the ratio of the carrier charge to the sum of ionic radii of carrier cation and oxide anion [55,62]. As reported in the literature [62], the *z/a* value of carrier cation increases in the order of V/TiO_2 (1.99) > V/ZrO_2 (1.79) > V/CeO_2 (1.69) > V/Al_2O_3 (1.55). This trend was found to be consistency with the reducibility: higher *z/a* values correspond to larger reducibility.

Upon the addition of SO_4^{2-} to VM(c1) (M=Ti, Zr, Al and Ce) samples, the

corresponding maximum temperature of TPR peaks (T_{m1} in Table 4) shifted to higher value. Additionally, the T_{m1} value of VMS(c2) samples prepared by simply straightforward co-precipitation is always higher than those of the corresponding VMS(c1-i) samples regardless the concentration of sulfate. Comparing each VMS system, we can found that a higher T_{m1} value is correlated to a lower TOF value except for sample VAlS(c2). As yet no conclusive explanation can be given for this discrepancy. In order to investigate the effect of the strength of sulfate-support interactions on TOFs values, the comparison of systems VM(c1) and VMS(c1-i) was examined. The TOF value of sample VTiS(c1) decreased of 24% compared with sample VTi(c1), while the TOF value of VZrS(c1-i) decreased of 17% compared to VZr(c1). Further, no decrease in TOF values was observed by doping VAl(c1) and VCe(c1) samples with SO_4^{2-}. The decreasing rate of TOF value upon the addition of sulfate species is strongly related to the nature of the metal oxide which controls the type and strength of sulfate species (investigated by TPD–MS and TPR–MS). It has been reported for vanadia-titania samples that the presence of sulfate species could poison the catalytically active sites and then decrease the TOF value [56]. Indeed, the strength of sulfate species determines the number of active sulfate sites on the support. For example, as the strength of the Ti–S bond is weaker (low SO_4^{2-} desorption temperature in Table 3) than the Al–S bond (high SO_4^{2-} desorption temperature), the corresponding SO_4^{2-} sites are in larger number and more poisoning, thus giving rise to a higher decreasing of TOF.

4. Conclusion

The mixed vanadia-based oxides (V_2O_5–TiO_2, V_2O_5–ZrO_2, V_2O_5–Al_2O_3 and V_2O_5–CeO_2) and the corresponding sulfated catalysts were prepared by co-precipitation. Another series of sulfated catalysts was also synthesized by typical incipient wetness impregnation to investigate the effect of preparation method on the strength of sulfate-support interaction. All the studied catalysts with high surface area (73–560 $m^2\ g^{-1}$) and good active phase dispersion were evaluated in partial oxidation of methanol to DMM.

The Raman spectra provided detailed information about the nature of surface

metal oxide species: (1) terminal V=O and bridging V–O–V bonds were obtained for all samples except for VAl and VAlS which have no terminal V=O bonds; (2) no V–O-support bridging bond was observed on VTi and VTiS samples due to the incorporation of vanadium in V–O–V bridges; (3) a metal vanadate compound (i.e., $CeVO_4$) formed only on VCe and VCeS samples. The XPS measurements support the stabilization of Ce(III) by $CeVO_4$ formation and reveal no changes in the oxidation state of V(+V). The ammonia adsorption calorimetry study showed a special behavior with weaker adsorption heats at low coverage only for sample VTiS(c1-i), that containing weak sulfate species (bisulfate and/or low polymerized sulfate species) based on the results from ammonia TPD–MS. The strength of sulfate-support interactions depends on the nature of the oxide support and increases in the order of VCeS > VAlS > VZrS > VTiS, as indicated by TPD–MS and TPR–MS techniques. Additionally independently of the sulfate concentration, the strength of the sulfate species present on VMS (M=Ti, Zr, Al and Ce) catalysts prepared directly by co-precipitation are stronger than the corresponding samples prepared by impregnation.

The combination of the results obtained from TPR–MS and catalytic test indicates that the reducibility of catalyst determines its catalytic activity. Sample VTi(c1) exhibits the highest TOF value of vanadium site, reflecting the highest activity in methanol oxidation. With the addition of sulfate, the selectivity to DMM was enhanced whereas the TOF value decreased; the decreasing rate of TOF value depending on the strength of sulfate-support interaction. Consequently, sample VTiS(c2) prepared by a simply straightforward co-precipitation exhibited the best catalytic activity for DMM producing, because of the higher reducibility, proper acidity and moderate strength of sulfate species.

Acknowledgements

The authors are thankful to the scientific services of IRCELYON, particularly to Laurence Massin for providing XPS measurements.

Hongying Zhao gratefully acknowledges the China Scholarship Council for the financial support of her PhD grant.

Financial supports from NSFC (20673055) and MSTC (2005CB221400 and 2004DFB02900) are acknowledged.

References

[1] G. Deo, I.E. Wachs, J. Haber, J. Crit. Rev. Surf. Chem. 4 (1994) 141–183.
[2] I.E. Wachs, B.M. Weckhuysen, Appl. Catal. A: Gen. 157 (1997) 67–90.
[3] B.M. Weckhuysen, D.E. Keller, Catal. Today (78) 2003 25–46.
[4] M.A. Bañares, Catal. Today 51 (1991) 319–348.
[5] V.V. Guliants, Catal. Today 51 (1999) 255–268.
[6] J.N. Al-Saeedi, V.V. Guliants, O. Guerrero-Pérez, M.A. Bañares, J. Catal. 215 (2003) 108–115.
[7] F. Trifiro, B. Grzybowska, Appl. Catal. A: Gen. 157 (1997) 1–2.
[8] C.N. Satterfield, Heterogeneous Catalysis in Practice, McGraw-Hill, New York, 1980.
[9] L. Owens, H.H. Kung, J. Catal. 144 (1993) 202–213.
[10] F. Arena, F. Frusteri, A. Parmaliana, Appl. Catal. A: Gen. 176 (1999) 189–199.
[11] J.M. Tatibouët, Appl. Catal. A: Gen. 148 (1997) 213−252.
[12] P. Forzatti, E. Tronconi, A.S. Elmi, G. Busca, Appl. Catal A: Gen. 157 (1997) 387–408..
[13] M.D. Amiridis, I.E. Wachs, G. Deo, J.M. Jehng, D.S. Kim, J. Catal. 161 (1996) 247–253.
[14] H. Liu, E. Iglesia, J. Catal. 223 (2004) 161–169.
[15] H. Liu, P. Cheung, E. Iglesia, J. Catal. 217 (2003) 222–232.
[16] J.M. Tatibouët, H. Lauron-Pernot, J. Mol. Catal. A: Chem.171 (2001) 205–216.
[17] Y. Fu, J. Shen, Chem. Commun. 21 (2007) 2172−2174.
[18] H. Zhao, S. Bennici, J. Shen, A. Auroux, Appl. Catal. A: Gen. 356 (2009) 121–128.
[19] P. Malet, A. Caballero, J. Chem. Soc., Faraday Trans. I 84 (1988) 2369–2375.
[20] D.A.M. Monti, A. Baiker, J. Catal. 83 (1983) 323–335.
[21] P. Schneider, Appl. Catal. A: Gen. 129 (1995) 157–165.
[22] B.M. Reddy, A. Khan, Y. Yamada, T. Kobayashi, S. Loridant, J.C Volta, J. Phys. Chem. B 107 (2003) 5162–5167.
[23] F.D. Hardcastle, I.E. Wachs, J. Phys. Chem. 95 (1991) 5031–5041.
[24] J.P. Dunn, J-M. Jehng, D.S. Kim, L.E. Briand, H.G. Stenger, I.E. Wachs, J. Phys. Chem. B 102 (1998) 6212–6218.
[25] J. Twu, P.K. Dutta, J. Catal. 124 (1990) 503–510.
[26] S.T. Choo, Y.G. Lee, I.S. Nam, S.W. Ham, J.B. Lee, Appl. Catal. A: Gen. 200 (2000) 177–188.
[27] I.E. Wachs, Catal. Today 27 (1996) 437–455.
[28] X. Gao, M.A. Bañares, I.E. Wachs, J. Catal. 1999 (188) 325–331.
[29] N. Magg, B. Immaraporn, J.B. Giorgi, T. Schroeder, M. Bäumer, J. Döbler, Z. Wu, E. Kondratenko, M. Cherian, M. Baerns, P.C. Stair, J. Sauer, H.J. Freund, J. Catal. 2004 (226) 88–100.
[30] H. Tian, E.I. Ross, I.E. Wachs, J. Phys. Chem. B 2006 (110) 9593–9600.
[31] M.A. Vuurman, I.E. Wachs, J. Phys. Chem. 1992 (96) 5008–5016.
[32] M.V. Martinez-Huerta, G. Deo, J.L.G. Fierro, M.A. Bañares, J. Phys. Chem. C 2007 (111) 18708–18714.

[33] J. Matta, D. Courcot, E. Abi-Aad, A. Aboukaïs, Chem. Mater. 14 (2002) 4118–4125.
[34] V.I. Bukhtiyarov, Catal. Today 56 (2000) 403–413.
[35] M.H. Kim, I.S. Nam, Y.G. Kim, J. Catal. 179 (1998) 350–360.
[36] J.P. Chen, R.T. Yang, J. Catal. 139 (1993) 277–288.
[37] B.M. Reddy, A. Khan, Y. Yamada, T. Kobayashi, S. Loridant, J.C. Volta, J. Phys. Chem. B 2002 (106) 10964–10972.
[38] D.R. Mullins, S.H. Overbury, D.R. Huntley, Surf. Sci. 1998 (409) 307–319.
[39] D.A. Creaser, P.G. Harrison, M.A. Morris, B.A. Wolfindale, Catal. Lett. 23 (1994) 13–24.
[40] J.Z. Shyu, W.H. Weber, H.S. Gandhi, J. Phys. Chem. 1988 (92) 4964–4970.
[41] A. Auroux, Top. Catal. 4 (1997) 71–89.
[42] H. Zhao, S. Bennici, J. Shen, A. Auroux, J. Therm. Anal. Calorim. 99 (2010) 843–847.
[43] A. Desmartin-Chomel, J.L. Flores, A. Bourane, J.M Clacens, F. Figueras, G. Delahay, A. Giroir Fendler, C. Lehaut-Burnouf, J. Phys. Chem. B 110 (2006) 858–863.
[44] R.L. White, E.C. Sikabwe, M.A. Coelho, D.E. Resasco, J. Catal. 157 (1995) 755–758.
[45] M. Waqif, O. Saur, J.C. Lavelley, Y. Wang, B.A. Morrow, Appl. Catal. 71 (1991) 319–331.
[46] I.E. Wachs, J. Catal. 124 (1990) 570–573.
[47] G.Y. Popova, T.V. Andrushkevich, E.V. Semionova, Y.A. Chesalov, L.S. Dovlitova, V.A. Rogov, V.N. Parmon, J. Mol. Catal. A: Chem. 283 (2008) 146–152.
[48] B.Q. Xu, W.M.H. Sachtler, J. Catal. 167 (1997) 224–233.
[49] E. Ghedini, M. Signoretto, F Pinna, G. Cerrato, C. Morterra, Appl. Catal B: Environ. 67 (2006) 24–33.
[50] E.A. Mamedov, V. Cortes Corberan, Appl. Catal A: General 157 (1997) 117–142.
[51] M.V. Martínez-Huerta, J,M. Coronádo, M. Fernandez-García, A. Iglesias-Juez, G. Deo, J.L.F. Fierro, M.A. Bañares, J. Catal. 225 (2004) 240–248.
[52] C.M.S. Polato, C.A. Henriques, A.A. Neto, J.L.F. Monteiro, J. Mol. Catal. A: Chem. 241 (2005) 184–193.
[53] J.B. Laizet, A.K. Soiland, J. Leglise, J.C. Duchet, Top. Catal. 10 (2000) 89–97.
[54] T. Kim, I.E. Wachs, J. Catal. 255 (2008) 197–205.
[55] F. Roozeboom, P.D. Cordingley, P.J. Gellings, J. Catal 68 (1981) 464–472.
[56] H. Zhao, S. Bennici, J. Shen, A. Auroux, J. Catal. In press (2010). DOI: 10.1016/j.jcat.2010.02.028.
[57] A.A. Lemonidou, L. Nalbandian, I.A. Vasalos, Catal. Today 61 (2000) 333–341.
[58] I.E. Wachs, Catal. Today 100 (2005) 79–94.
[59] J. Haber, A. Kozlowska, R. Kozlowski, J. Catal. 102 (1986) 52–63.
[60] G. Deo, I.E. Wachs, J. Catal 129 (1991) 307–312.
[61] F. Roozeboom, M.C. Mlttelmeijer-Hazeleger, J.A. Moulijn, J. Medema, V.H.J. de Beer, P.J. Gellngs, J. Phys. Chem. 84 (1980) 2783–2791.
[62] F. Roozeboom, T. Fransen, P. Mars, P.J. Gellngs, Z. Anorg. Allg. Chem. 449

(1979) 25.

Figure Captions

Fig.1. X-ray powder diffractions of vanadia supported catalysts: (●) TiO_2, (■) ZrO_2, (o) $CeVO_4$ and (*) CeO_2.

Fig.2. N_2 adsorption-desorption isotherms of sulfated supported vanadia catalysts. (Inset: pore radius distribution curve from the desorption branch of the isotherms).

Fig.3. Raman spectra of (a) VTiS samples, (b) VZrS samples, (c) VAlS samples and (d) VCeS samples.

Fig.4. O 1s XPS spectra of VCe and VCeS samples (experimental O 1s spectrum: black straight line, simulated O 1s spectrum by the contribution of oxygen from various component oxides: black dotted line, O1s spectrum of V_2O_5 and CeO_2 oxides: violet, O1s spectrum of surface hydroxyl groups: red, O1s spectrum of SO_4^{2-} species and $CeVO_4$ compound: blue). (For interpretation of the references to colours in this figure caption, the reader should refer to the web version of the article.).

Fig.5. Ce 3d XPS spectra of VCe and VCeS samples.

Fig.6. Differential heats of ammonia adsorption versus the adsorbed amount on (a) VTiS samples, (b) VZrS samples, (c) VAlS samples and (d) VCeS samples.

Fig.7. Volumetric isotherms of NH_3 adsorption at 423K for (a) VTiS samples, (b) VZrS samples, (c) VAlS samples and (d) VCeS samples.

Fig.8. Simultaneous TPD–MS–TG–DSC profiles (TG: green, DSC: blue, m/e=15: purple, m/e=64: orange) of adsorbed NH_3 for supported vanadia catalysts. (For interpretation of the references to colours in this figure caption, the reader should refer to the web version of the article)

Fig.9. TPR profiles of (a) VTiS samples, (b) VZrS samples, (c) VAlS samples and (d) VCeS samples.

Fig.10. Mass spectra of the gases evolved during the TPR analysis for (a)VTiS(c1-i), (b)VZrS(c1-i), (c)VAlS(c1-i) and (d)VCeS(c1-i) samples (m/e=64: red; m/e=34: violet; m/e=2: blue; temperature: black). (For interpretation of the references to colours in this figure caption, the reader should refer to the web version of the article).

Fig.11. Selective oxidation of methanol over (A) VTiS samples, (B) VZrS samples, (C) VAlS samples and (D) VCeS samples.

Scheme1. Reaction pathways for the reaction of catalytic partial oxidation of methanol (adapted from Ref.[11, 14])

Table 1
Chemical analysis and pore characteristics of supported vanadia catalysts[a]

Sample	$T_{calcination.}$ (K)	C.A(wt%)			Surface area ($m^2\ g^{-1}$)		Pore volume ($cm^3\ g^{-1}$)		Pore diameter (nm)
		V	Ti/Zr/Al/Ce	S	S_{BET}	S_{micro}	V_{BJH}	V_{micro}	d_{BJH}
VTi(c1)	673	13.7	41.8	---	281	3.6	1.02	1.02	11.3
VTiS(c1-i)	673	13.1	40.5	1.5	204	5.5	0.82	0.82	11.9
VTiS(c2)	673	12.3	38.2	1.8	282	---	0.75	---	9.0
VZr(c1)	673	10.0	49.9	---	334	---	0.85	---	9.8
VZrS(c1-i)	673	9.9	49.1	1.9	277	4	0.75	---	10.2
VZrS(c2)	673	14.4	48.7	0.8	321	14	1.13	0.003	14.2
VAl(c1)	773	9.9	33.8	---	560	28	3.21	0.01	20.4
VAlS(c1-i)	673	9.9	33.5	1.2	392	26	1.23	0.01	10.4
VAlS(c2)	773	8.8	27.4	5.6	405	17	1.91	0.004	18.9
VCe(c1)	673	14.0	59.4	---	116	0.8	0.44	---	13.8
VCeS(c1-i)	673	13.4	55.9	1.9	86	6	0.37	---	15.1
VCeS(c2)	673	14.5	55.2	1.2	73	14	0.24	0.005	18.2

[a] S_{BET} is the surface area calculated by the BET method; V_{BJH} and d_{BJH} are the cumulative adsorption pore volume and pore diameter respectively (1.7 <pore diameter< 300 nm) calculated by the BJH method; S_{micro} and V_{micro} are respectively the surface area and pore volume in the micropore range (pore diameter < 2 nm) calculated by the deBoer's *t*-plot method.

Table 2
X-ray photoelectron spectroscopy analysis, binding energies of surface species and O1s concentration (in atomic %) for different oxygen species (V_2O_5+CeO_2; -OH; SO_4^{2-}+$CeVO_4$) present on the VCe and VCeS catalysts surfaces.

Sample	XPS (wt%)			Binding energy (ev)					
	V	Ce	S	V $2p_{3/2}$	Ce $3d_{5/2}$-satellite	O 1s			S $2p_{3/2}$
VCe(c1)	14.9	57.6	---	517.2	882.5–916.9	529.8(82%)[a]	530.9(11%)[b]	532.2(7%)[c]	168.5
VCeS(c1-i)	14.1	53.0	1.8	517.1	882.4–916.8	529.9(72%)[a]	531.2(15%)[b]	532.1(13%)[c]	----
VCeS(c2)	11.7	59.8	1.4	517.2	882.3–916.3	529.8(69%)[a]	531.0(15%)[b]	532.0(16%)[c]	168.8

[a] Binding energies (BEs) between 529.8 and 529.9 eV correspond to O in CeO_2 and V_2O_5.
[b] Binding energies (BEs) between 530.9 and 531.2 eV correspond to O in –OH.
[c] Binding energies (BEs) between 532.0 and 531.2 eV correspond to O in SO_4^{2-} and $CeVO_4$.

Table 3
Calorimetric data for ammonia adsorption at 423 K and corresponding NH_3-TPD data on VM and VMS catalysts.

Sample	V_{total}[a] (μmol g^{-1})	V_{total}[a] (μmol m^{-2})	V_{irrev}[b] (μmol g^{-1})	V_{irrev}[b] (μmol m^{-2})	Q_{init}[c] (kJ mol^{-1})	T_{max}[d] NH_3 (K)	T_{max}[e] SO_4^{2-} (K)	
							Peak1	Peak2
VTi(c1)	461	1.64	210	0.75	180	530	n.d.[f]	n.d.[f]
VTiS(c1-i)	501	2.46	311	1.52	7	534	676	767
VTiS(c2)	549	1.95	292	1.04	210	552	687	765
VZr(c1)	555	1.66	310	0.93	204	555	n.d.[f]	n.d.[f]
VZrS(c1-i)	530	1.91	288	1.04	194	576	741	867
VZrS(c2)	573	1.79	319	0.99	257	557	765	852
VAl(c1)	420	0.75	188	0.34	195	n.d.[f]	n.d.[f]	n.d.[f]
VAlS(c1-i)	461	1.17	232	0.59	207	567	966	n.d.[f]
VAlS(c2)	591	1.46	318	0.79	174	562	964	n.d.[f]
VCe(c1)	205	1.77	64	0.55	187	524	n.d.[f]	n.d.[f]
VCeS(c1-i)	165	1.92	55	0.64	159	589	>973	n.d.[f]
VCeS(c2)	183	2.51	82	1.12	151	559	>973	n.d.[f]

Notes: [a] Amount of NH_3 adsorbed under an equilibrium pressure of 27 Pa.
[b] Amount of irreversible chemisorbed NH_3.
[c] Heat evolved from the first ammonia dose.
[d] Maximum temperature of NH_3 decomposition peak from TPD-MS.
[e] Maximum temperature of SO_4^{2-}decomposition peak from TPD-MS.
[f] Not determined.

Table 4
Reducibility of the catalysts as revealed by the H_2–TPR measurements.

Catalyst	T_{max}[a] (K)			Consumption H_2 (mmol g^{-1})	T_{max}[b] (K)		
		Peak1 (T_{m1})	Peak 2 (T_{m2})		SO_2	H_2S	
VTi(c1)	758	708	963	2.0	--	--	
VTiS(c1-i)	724	754	965	2.3	700	n.d.[d]	
VTiS(c2)	728	760	950	2.3	--	--	
VZr(c1)		742	n.d.[c]	1.4	--	--	
VZrS(c1-i)	738	762	n.d.[c]	1.9	732	767	
VZrS(c2)	738	766	n.d.[c]	2.2	--	--	
VAl(c1)		796	n.d.[c]	1.4	--	--	
VAlS(c1-i)	781	805	n.d.[c]	2.0	761	802	
VAlS(c2)	843	865	n.d.[c]	4.0	--	--	
VCe(c1)		790	948	3.0	--	--	
VCeS(c1-i)		837	980	3.5	817	836	974
VCeS(c2)		843	1012	3.4	--	--	

[a] Maximum temperature of the H_2–TPR peaks.
[b] Maximum temperature of SO_4^{2-} reduction peaks from TPR–MS.
[c] Not determined.

Table 5
The turn-over frequencies (TOFs) and characteristics of supported vanadia and sulfated supported vanadia catalysts[a]

Sample	Ns [b] ($V\ nm^{-2}$)	Monolayer surface V loading ($V\ nm^{-2}$)	Conversion of methanol (%) at 393 K	TOF [d] $\times 10^4$ (s^{-1})
VTi(c1)	5.8		58	15.9
VTiS(c1-i)	7.6	7.9	42	12.1
VTiS(c2)	5.2		37	11.3
VZr(c1)	3.5		11	4.2
VZrS(c1-i)	4.2	7.9	9	3.5
VZrS(c2)	5.3		8	2.1
VAl(c1)	2.1		1	0.4
VAlS(c1-i)	3.0	7.9	1	0.4
VAlS(c2)	2.6		2	0.9
VCe(c1)	14.3		4	2.0
VCeS(c1-i)	18.4	7.9	3	2.0
VCeS(c2)	23.5		2	1.6

[a] Feed conditions : methanol : O_2 : N_2 = 2 : 6 : 30 mL min^{-1}, catalyst loading 0.2 g
[b] Ns is the number of exposed catalytic active vanadium atoms per square meter supposing that all vanadium atoms are located on the surface and calculated from Table 1..
[c] The theoretical number of exposed vanadium atoms per square meter on TiO_2, ZrO_2, Al_2O_3 and CeO_2 for the monolayer coverage.
[d] TOF of methanol conversion at 393 K.

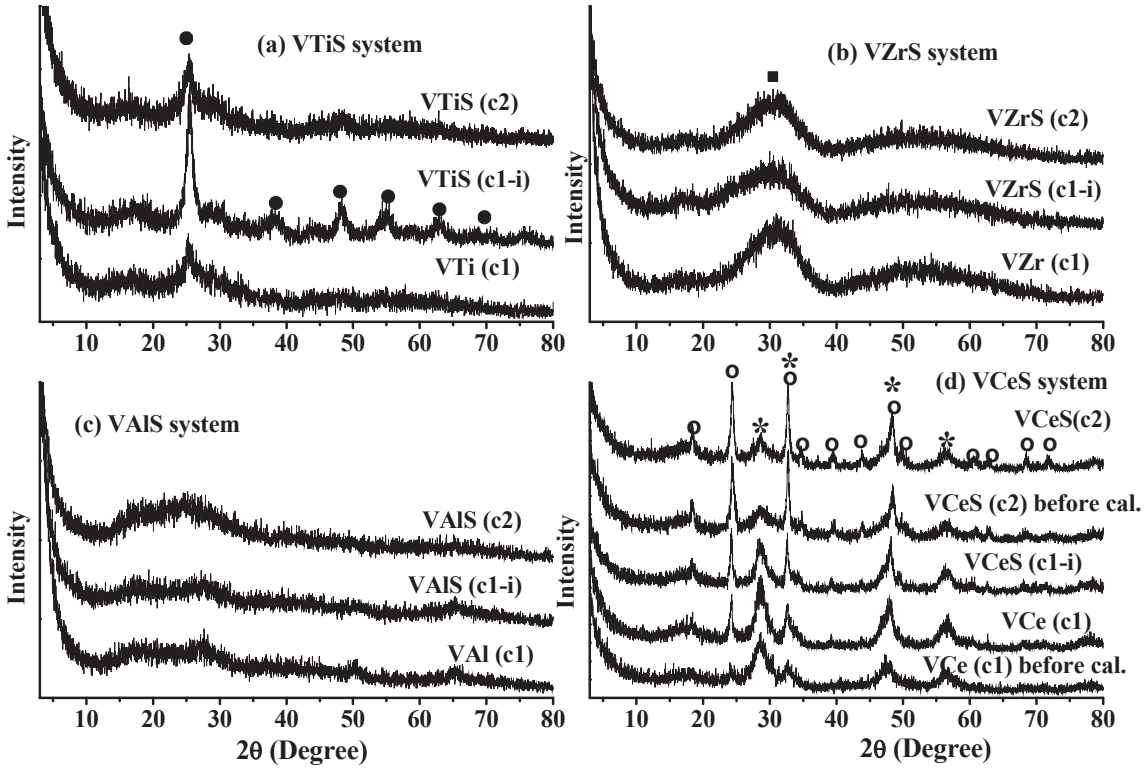

Fig.1. X-ray powder diffraction patterns of vanadia supported catalysts: (●) TiO_2, (■) ZrO_2, (o) $CeVO_4$ and (*) CeO_2.

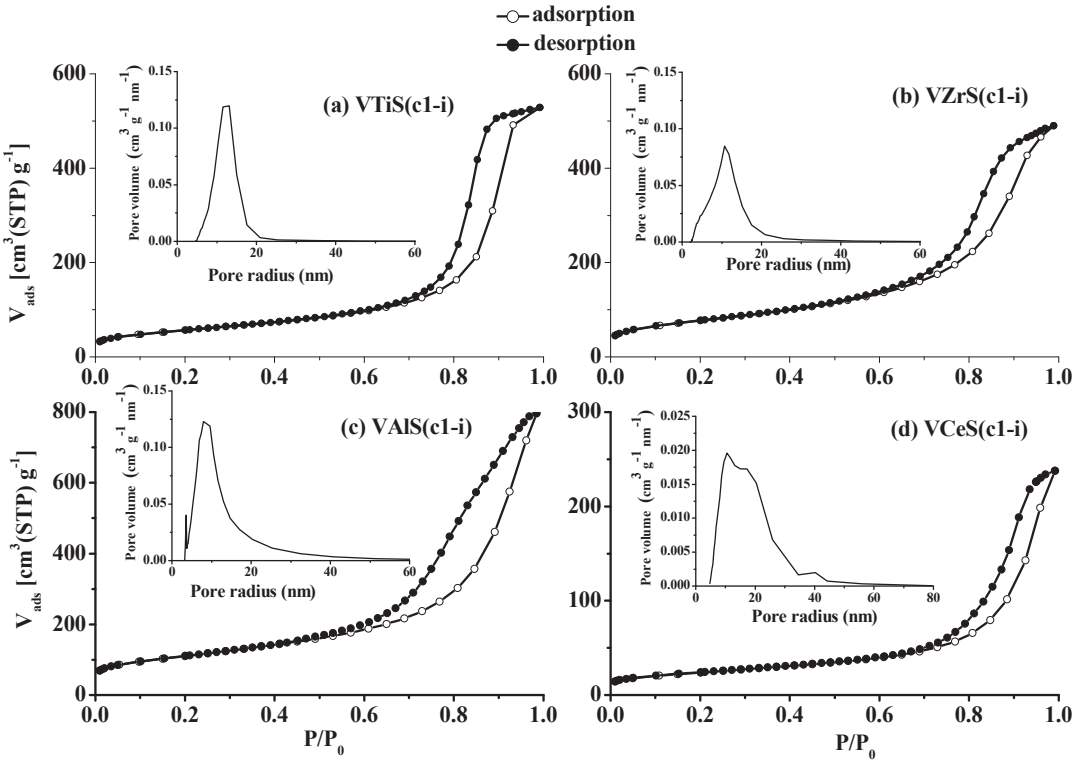

Fig.2. N_2 adsorption-desorption isotherms of sulfated supported vanadia catalysts. (Inset: pore radius distribution curve from the desorption branch of the isotherms)

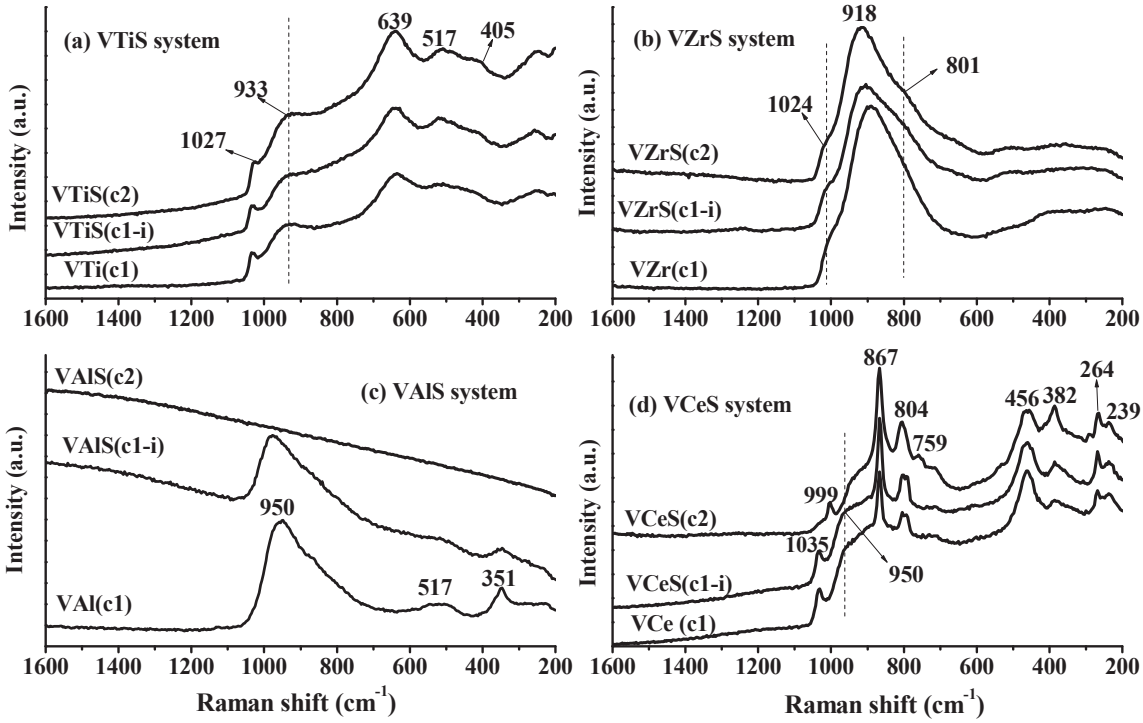

Fig.3. Raman spectra of (a) VTiS samples, (b) VZrS samples, (c) VAlS samples and (d) VCeS samples

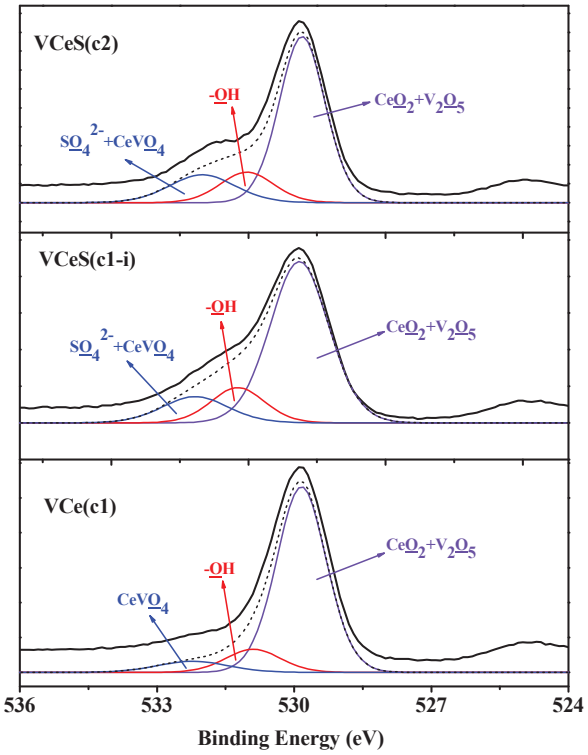

Fig.4. O 1s XPS spectra of VCe and VCeS samples (experimental O 1s spectrum: black straight line, simulated O 1s spectrum by the contribution of oxygen from various component oxides: black dotted line, O1s spectrum of V_2O_5 and CeO_2 oxides: violet, O1s spectrum of surface hydroxyl groups: red, O1s spectrum of SO_4^{2-} species and $CeVO_4$ compound: blue). (For interpretation of the references to colours in this figure caption, the reader should refer to the web version of the article.)

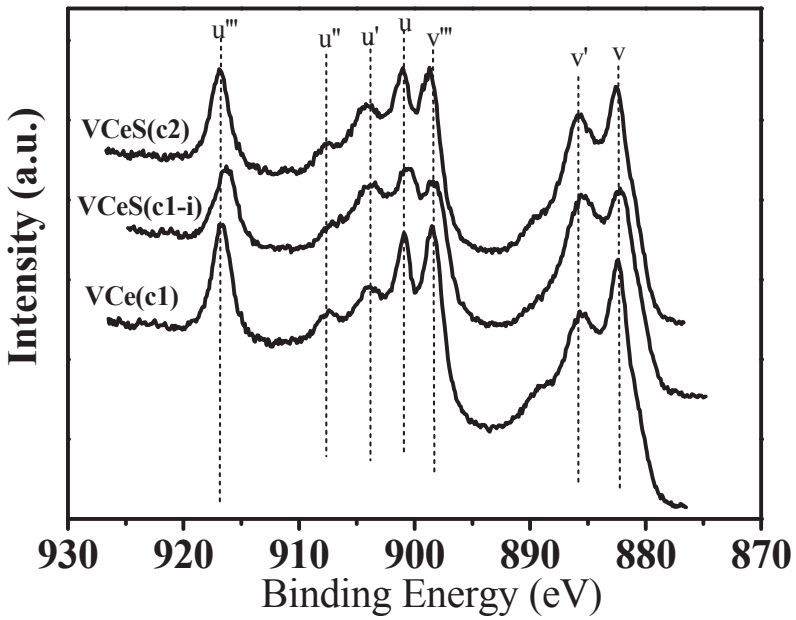

Fig.5. Ce 3d XPS spectra of VCe and VCeS samples.

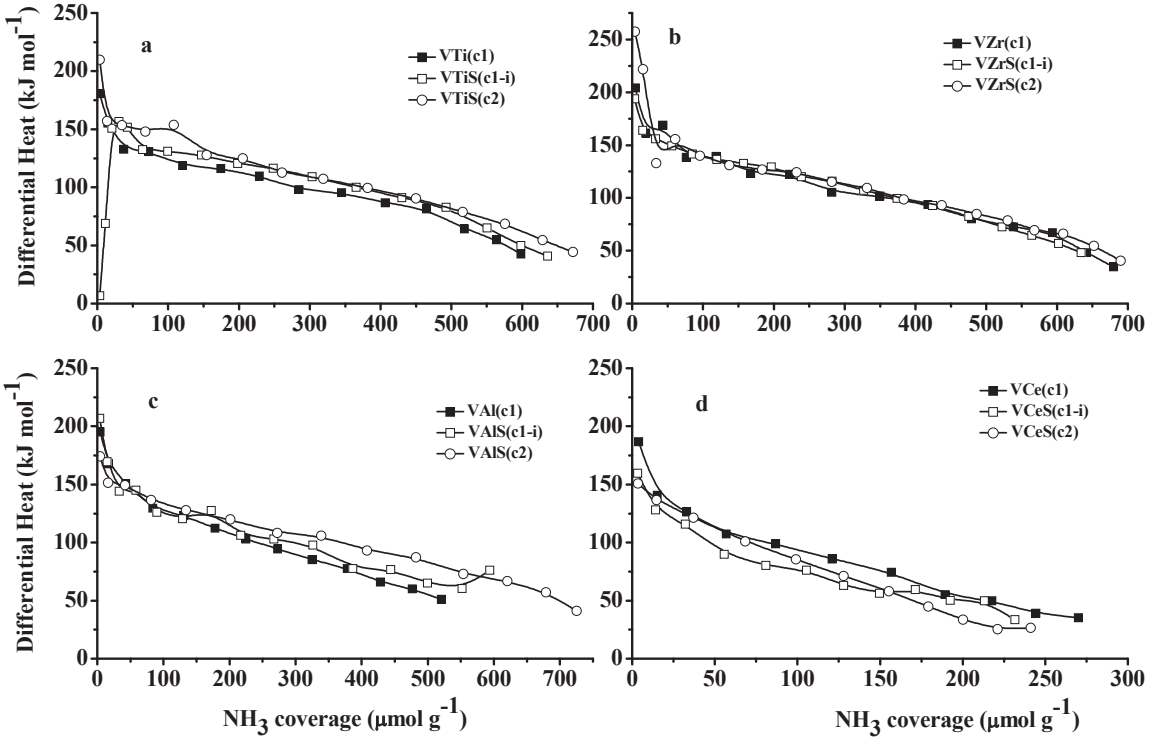

Fig.6. Differential heats of ammonia adsorption versus the adsorbed amount on (a) VTiS samples, (b) VZrS samples, (c) VAlS samples and (d) VCeS samples.

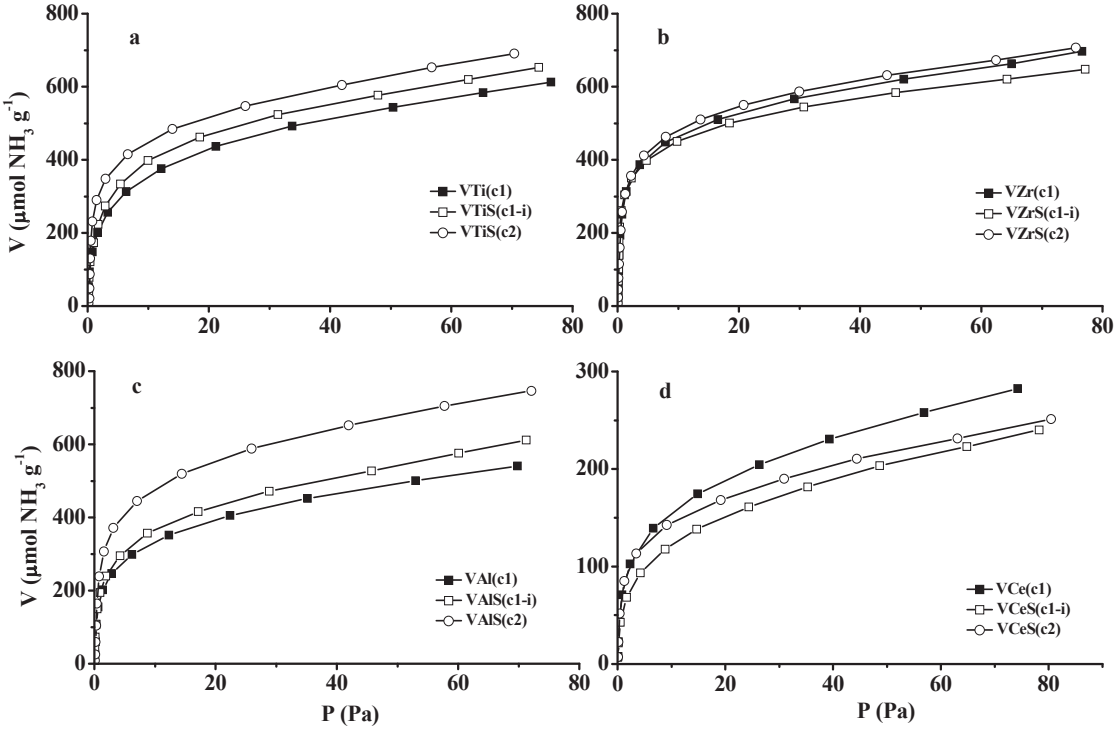

Fig.7. Volumetric isotherms of NH_3 adsorption at 423K for (a) VTiS samples, (b) VZrS samples, (c) VAlS samples and (d) VCeS samples.

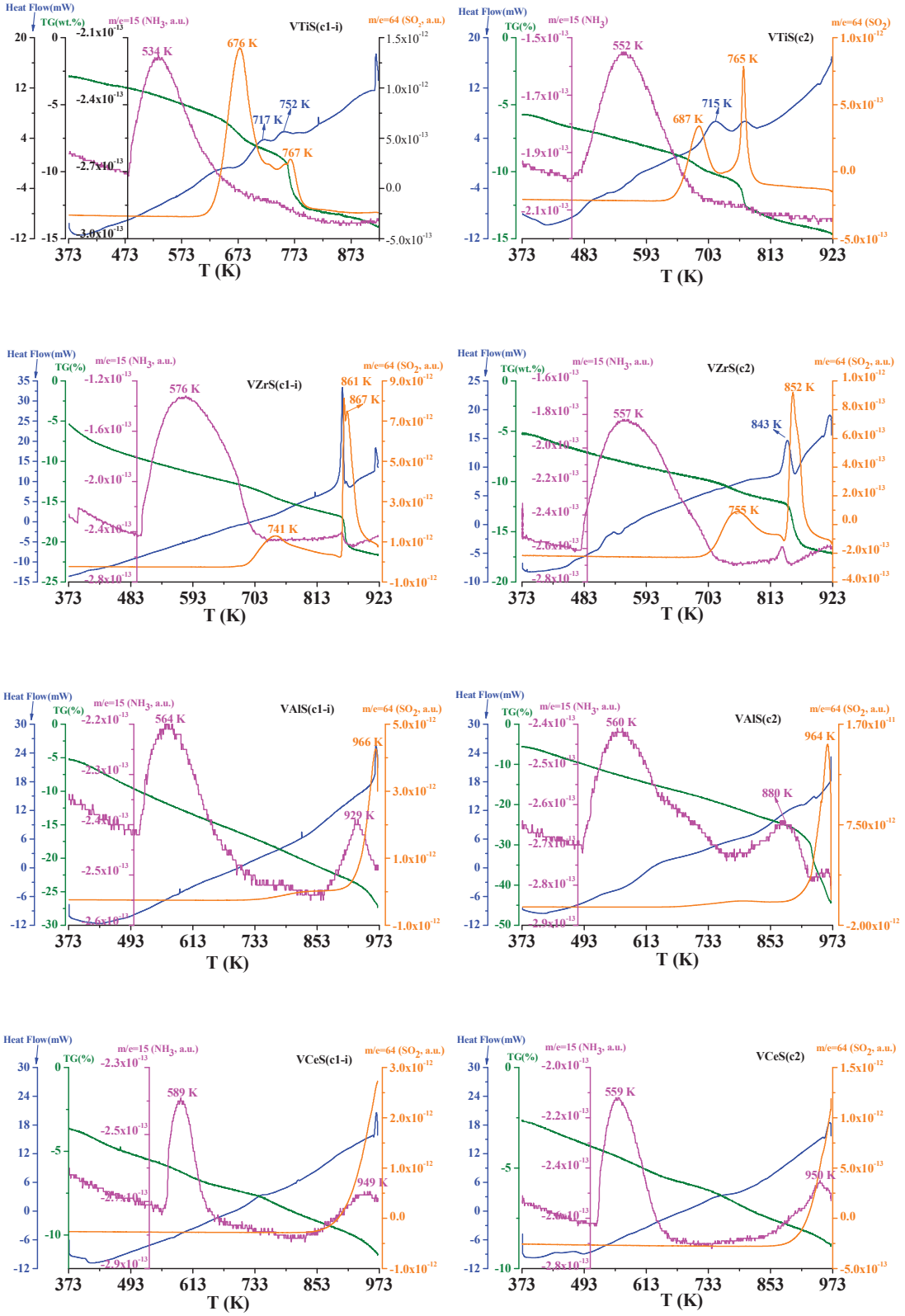

Fig.8. Simultaneous TPD–MS–TG–DSC profiles (TG: green, DSC: blue, m/e=15: purple, m/e=64: orange) of adsorbed NH_3 for supported vanadia catalysts. (For interpretation of the references to colours in this figure caption, the reader should refer to the web version of the article)

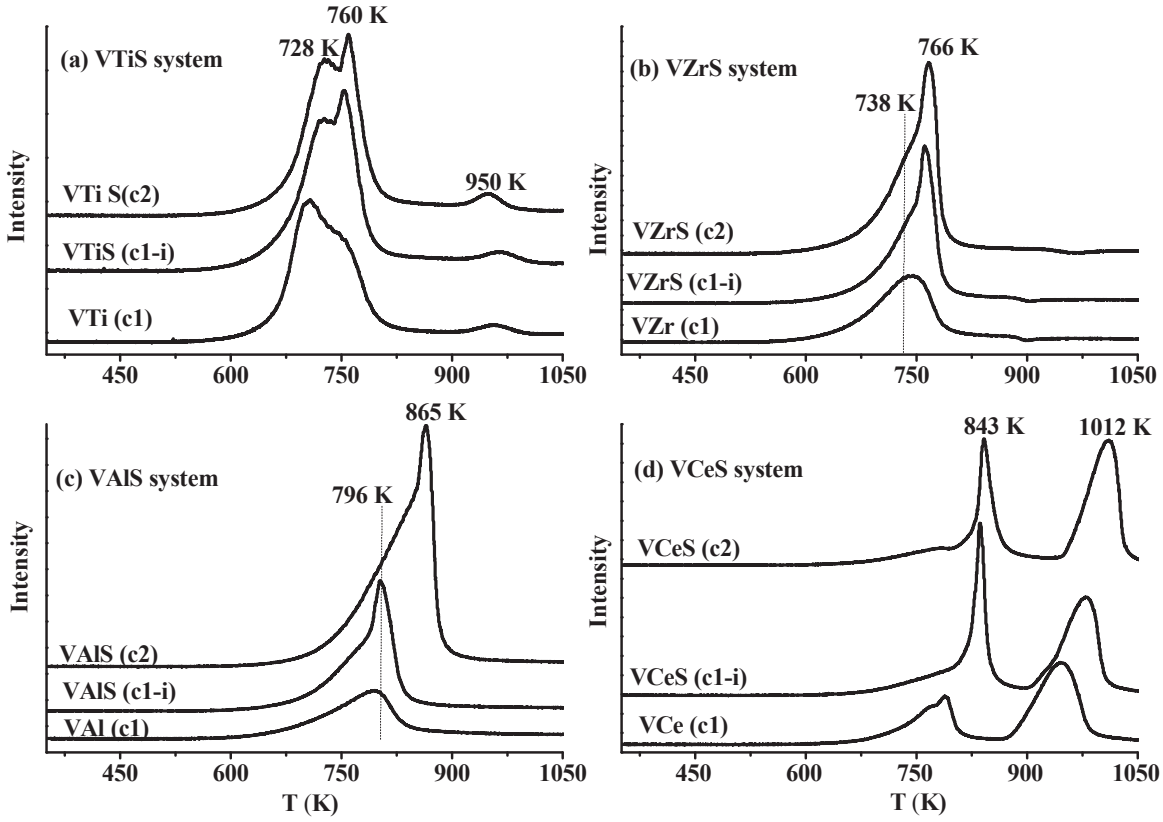

Fig.9. TPR profiles of (a) VTiS samples, (b) VZrS samples, (c) VAlS samples and (d) VCeS samples.

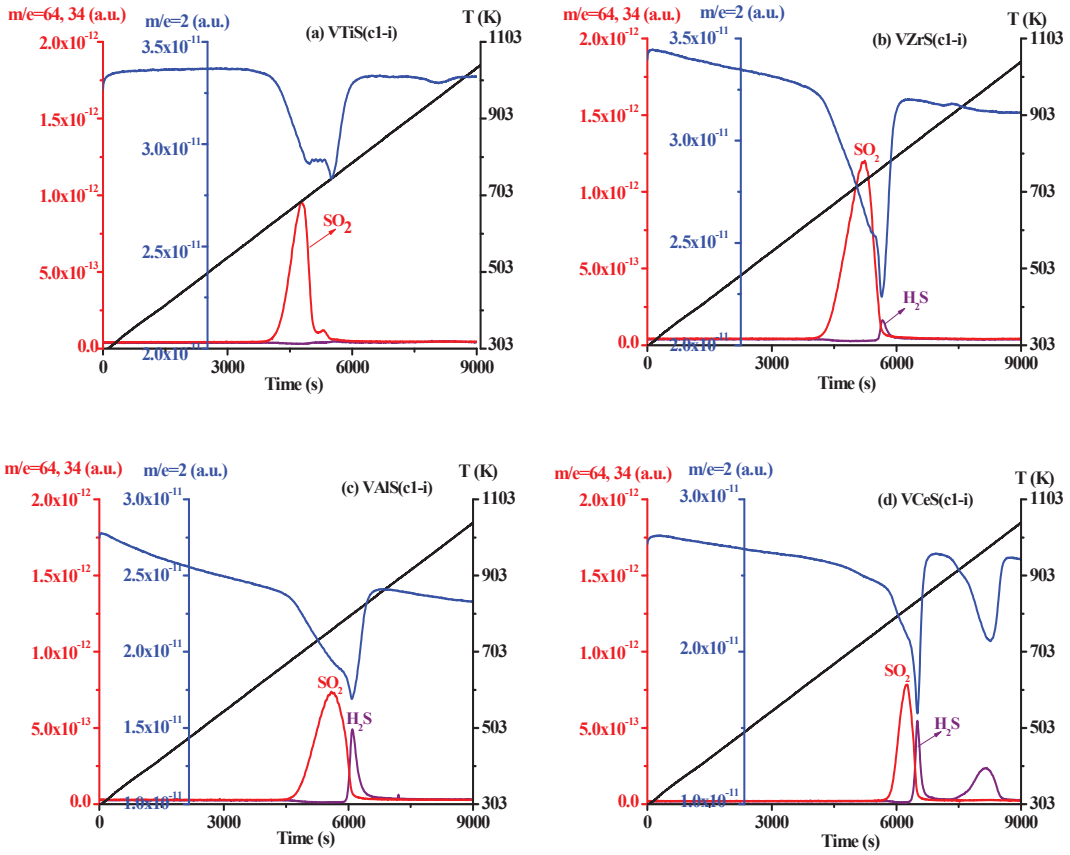

Fig.10. Mass spectra of the gases evolved during the TPR analysis for (a)VTiS(c1-i), (b)VZrS(c1-i), (c)VAlS(c1-i) and (d)VCeS(c1-i) samples (m/e=64: red; m/e=34: violet; m/e=2: blue; temperature: black). (For interpretation of the references to colours in this figure caption, the reader should refer to the web version of the article).

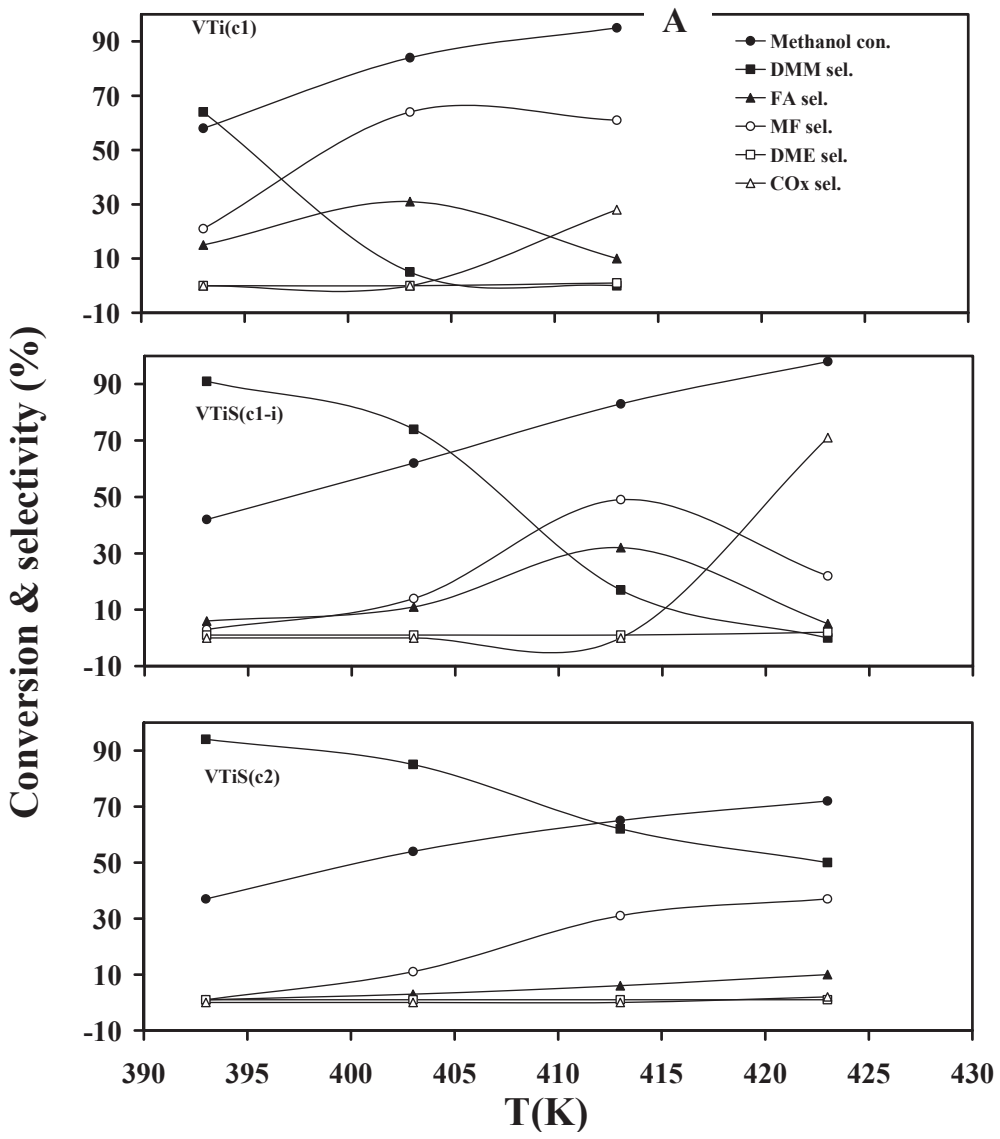
A
VTi(c1)
VTiS(c1-i)
VTiS(c2)
Methanol con.
DMM sel.
FA sel.
MF sel.
DME sel.
COx sel.
Conversion & selectivity (%)
T(K)
90
70
50
30
10
-10
390
395
400
405
410
415
420
425
430

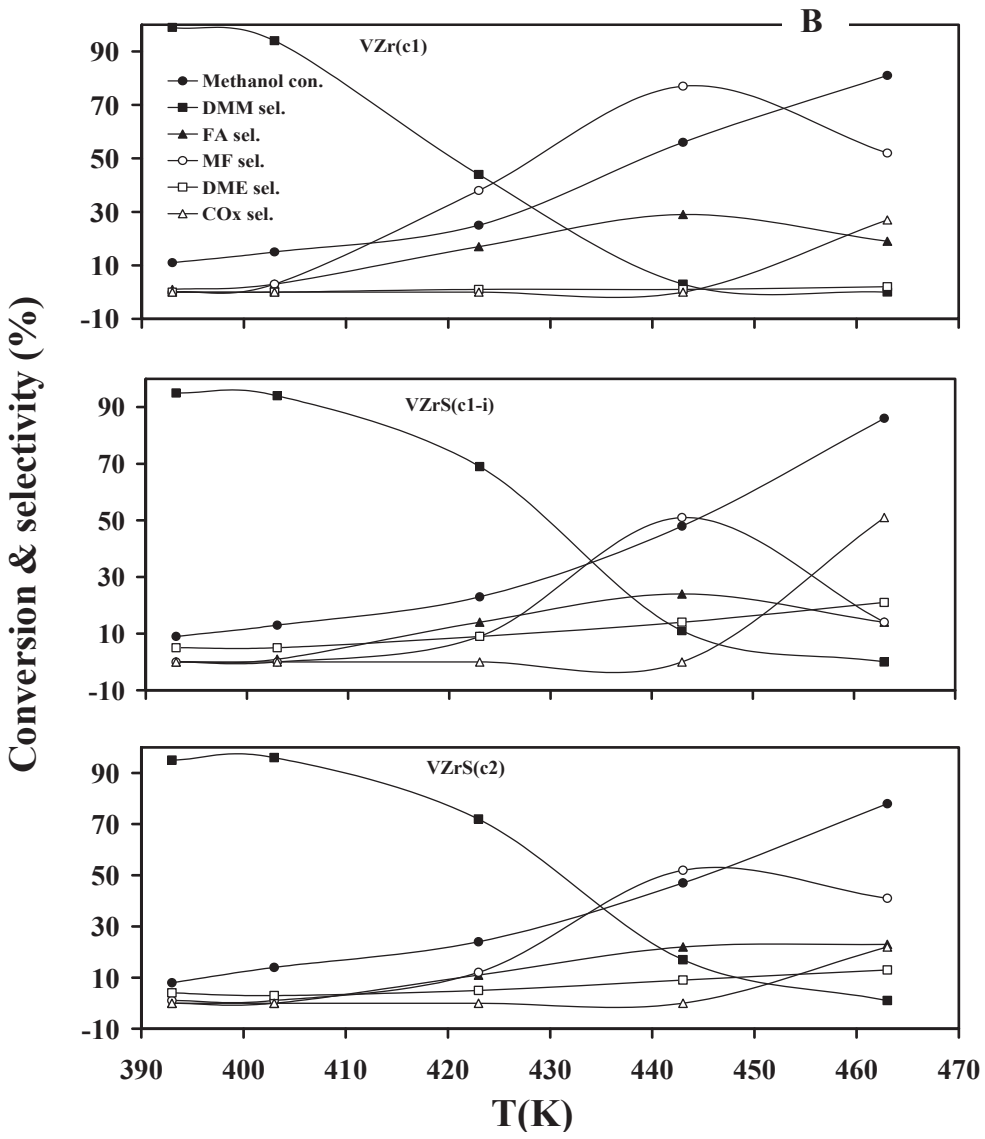
B
VZr(c1)
Methanol con.
DMM sel.
FA sel.
MF sel.
DME sel.
COx sel.
VZrS(c1-i)
VZrS(c2)
Conversion & selectivity (%)
T(K)
90
70
50
30
10
-10
390
400
410
420
430
440
450
460
470

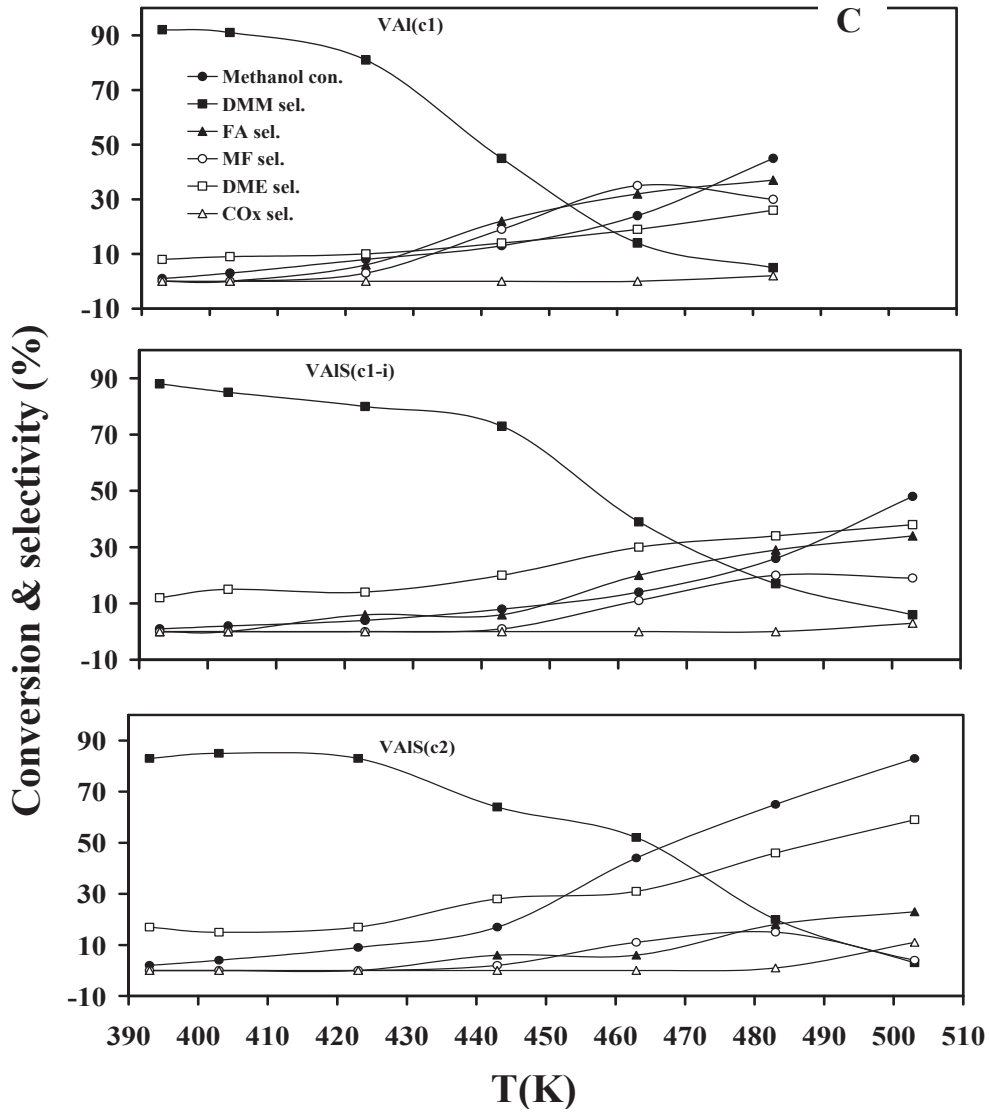
C
VAl(c1)
Methanol con.
DMM sel.
FA sel.
MF sel.
DME sel.
COx sel.
VAlS(c1-i)
VAlS(c2)
Conversion & selectivity (%)
T(K)
90
70
50
30
10
-10
390
400
410
420
430
440
450
460
470
480
490
500
510

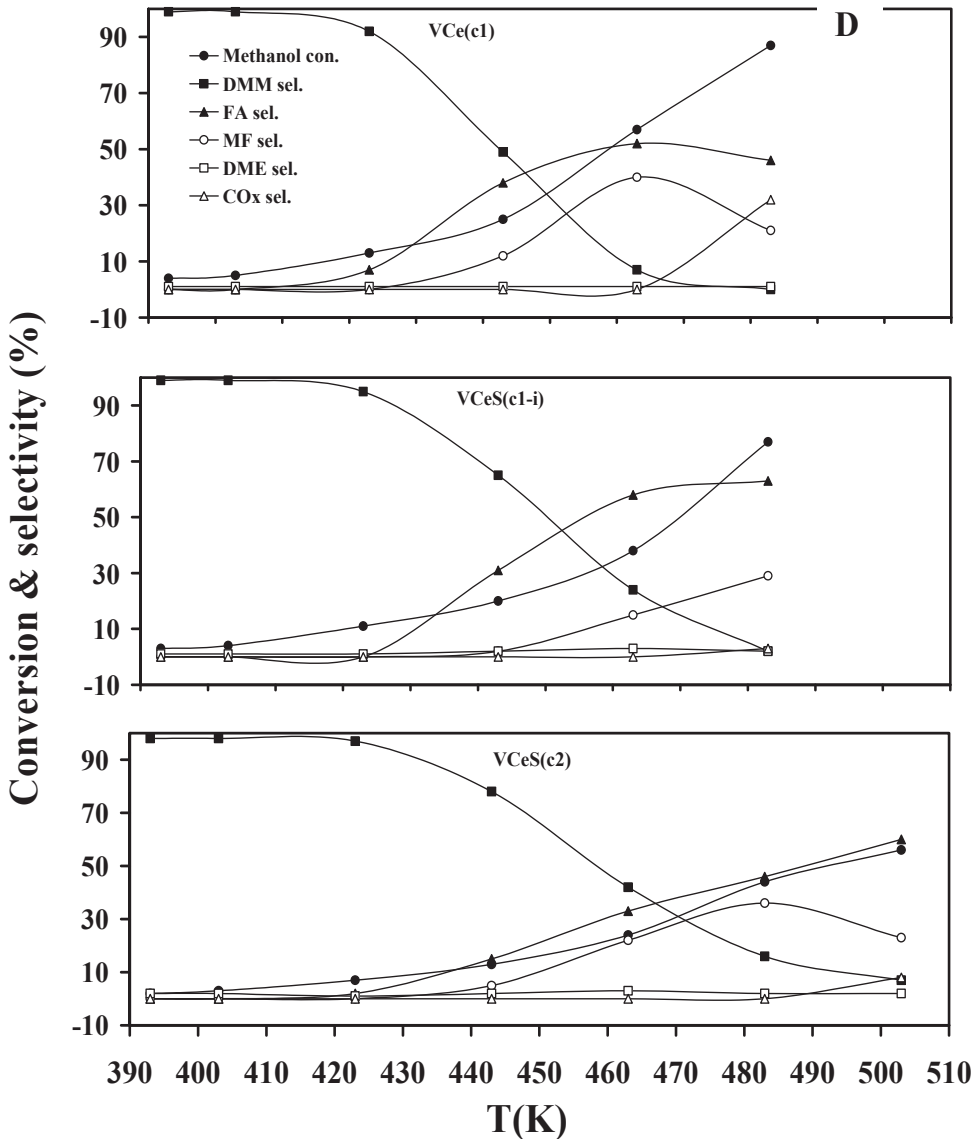

Fig.11. Selective oxidation of methanol over (A) VTiS samples, (B) VZrS samples, (C) VAlS samples and (D) VCeS samples.

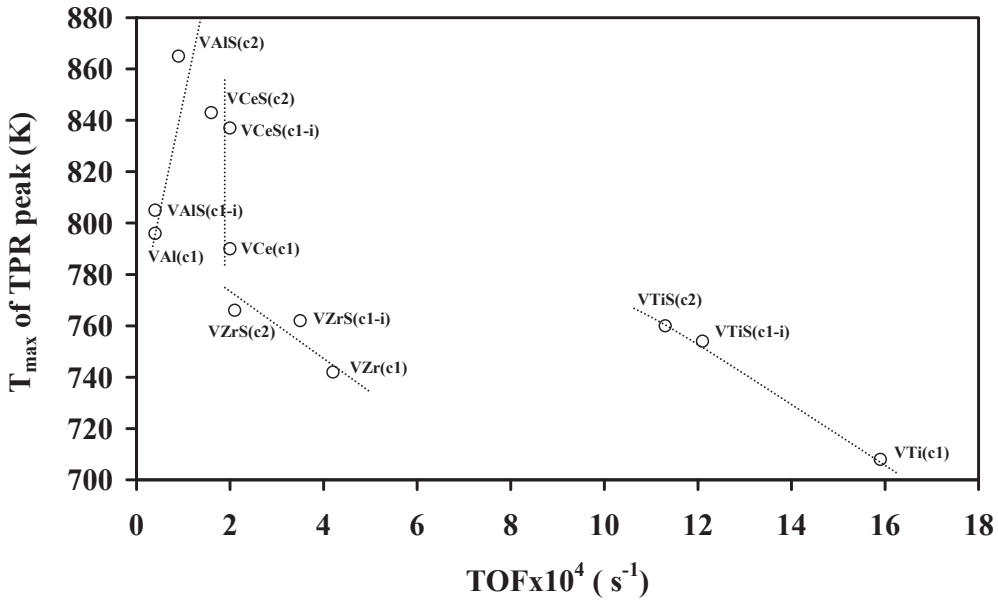

Fig.12. Correlation between the intrinsic activity of the catalysts relative to TOF value and the maximum temperature of the reduction peak.

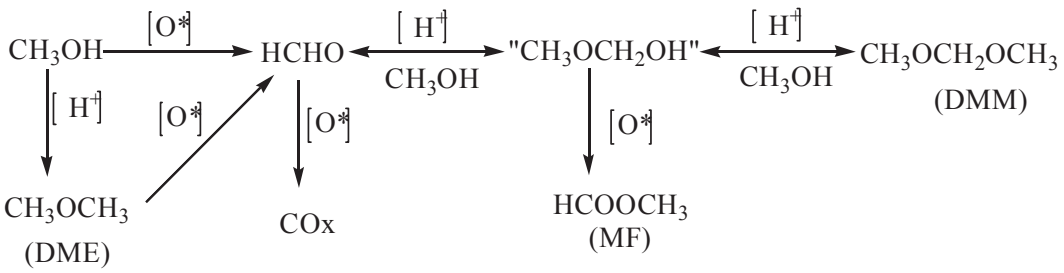

Scheme1. Reaction pathways for the reaction of catalytic partial oxidation of methanol (adapted from Ref.[11, 14])

Publication VIII

Applied Catalysis A: General, under revison

Influence of the host oxide of sulfated-titania catalysts on partial oxidation methanol reaction.

Hongying Zhao[1], Simona Bennici[1], Jianyi Shen[2], Aline Auroux[1]*

[1]Université Lyon 1, CNRS, UMR 5256, IRCELYON, Institut de recherches sur la catalyse et l'environnement de Lyon, 2 avenue Albert Einstein, F-69626 Villeurbanne, France

[2]Laboratory of Mesoscopic Chemistry, School of Chemistry and Chemical Engineering, Nanjing University, Nanjing 210093, China

[*]Corresponding author. Fax : +33 472445399.

E-mail address: aline.auroux@ircelyon.univ-lyon1.fr (A. Auroux)

Abstract

A series of sulfated binary titania-based (M_xO_y–TiO_2–SO_4^{2-}, M_x= Cr, Mn, Fe, Co or Mo) catalysts were prepared by co-precipitation and tested in methanol oxidation reaction. The structural properties were characterized by X-ray diffraction (XRD), X-ray photoelectron spectroscopy (XPS), Raman spectroscopy, scanning electron microscopy (SEM) and transmission electron microscopy (TEM). The acidic and redox properties were examined using ammonia adsorption calorimetry and temperature-programmed reduction coupled with mass spectrometer (TPR–MS) techniques, respectively. The surface M_x species were essentially 100% dispersed on catalysts, as confirmed by XRD and Raman spectroscopy characterization. XPS results indicated the oxidation state of surface M_x species. In addition, Ti and S species were present in their fully oxidization state for all the samples. The results of ammonia adsorption calorimetry showed a surface reaction between chromium oxide and ammonia. Addition of host oxide M_xO_y not only enhanced the redox properties of sample TiS but also brought changes in the sulfate reduction process, as investigated

by TPR–MS. The best catalytic performance was obtained for sample MoO_3–TiO_2–SO_4^{2-} with high activity. Furthermore, the distribution of reaction products was employed to provide information about the surface acidity and redox property simultaneously.

Keywords: Supported-titania catalysts; Acidity; Redox character; Ammonia adsorption calorimetry; TPR–MS, Methanol selective oxidation

1. Introduction

Methanol is one of the most important chemical intermediates used in the chemical industry. Furthermore, with the rapid growth of methanol production from coal-derived syngas, the research and development of new processes to transform methanol to valuable down stream products has attracted extensive attention [1–4]. Through oxidation and/or dehydration, methanol can be converted to formaldehyde (FA), dimethyl ether (DME), dimethoxymethane (DMM), methyl formate (MF), and so on [5]. Among them, DMM is an excellent solvent and chemical intermediate in industry [6,7]; moreover, it was found recently that DMM can be effectively steam-reformed to produce H_2 for fuel cell [8] because of its high content of hydrogen, extremely low toxicity and environmentally benign. As reviewed by Tatibouët [5], the various products of methanol reaction on oxides surfaces are very sensitive to the nature of surface active sites. Methanol oxidation reaction can be divided in two principal pathways: (1) reactions of oxidation that need oxygen and (2) reactions of dehydration that do not need oxygen [9]. Except for dimethyl ether (DME) the formation for all products needs at least one oxidation step. The selectivity to dimethyl ether is attributed to the dehydration ability of the catalyst which in turn is related to its acidic character. Thus, the catalytic oxidation of methanol is informative of the surface structure and behavior of the catalyst, and in fact it has been widely used as a probe reaction [10–12]. In previous papers [13–14], an extensive study of the preparation and catalytic behavior of sulfated vanadia-titania catalysts has been performed for such reaction.

In this work, a series of sulfated titania-based catalysts (M_xO_y–TiO_2–SO_4^{2-};

where M= Cr, Mn, Fe, Co or Mo) with high surface area and similar concentration of sulfur were prepared by co-precipiation in the aim to study the influence of varying the host oxide as compared to the vanadia active phase. The structural properties of prepared catalysts were characterized by XRD, BET, ICP, XPS, SEM, TEM and Raman spectroscopy measurements. The acidic and redox properties were examined by TPR–MS and ammonia adsorption calorimetry, respectively. The studied catalysts were tested in partial oxidation of methanol and the effect of host oxide M_xO_y was analyzed and compared with vanadia [14].

2. Experimental

2.1 Catalyst preparation

The theoretical amount of each metal oxide (CrO_x, Mn_2O_3, Fe_2O_3, Co_3O_4 and MoO_3) was fixed at 25 wt%.

Sulfated binary titania-based oxides (denoted by M_xTiS; M_x=Cr, Mn, Fe, Co and Mo) were prepared by a previous reported co-precipitation method [13]. In order to obtain a similar content of sulfate for each sample, the same titania precursor was used for all samples: $TiOSO_4 \cdot xH_2SO_4 \cdot xH_2O$. The other precursors were $Cr(NO_3)_3 \cdot 9H_2O$, $Fe(NO_3)_3 \cdot 9H_2O$, $Co(NO_3)_2 \cdot 6H_2O$, $Mn(NO_3)_2 \cdot xH_2O$, $(NH_4)_6Mo_7O_{24} \cdot 4H_2O$. The details of the preparation method have been previously described in [13]. Specially for sample $MoO_3/TiO_2\text{-}SO_4^{2-}$, theoretical required amount of $(NH_4)_6Mo_7O_{24} \cdot 4H_2O$ was dissolved into a limited amount of deionized water and then added to filtrated precipitate cake containing Ti. At last the mixed cake containing Mo and Ti was dried as reported in [13]. All the samples were calcined at a given temperature of 673 K in air for 5 h.

2.2 Catalyst characterization

Elemental analysis was performed using ICP optical emission spectroscopy (ICP–OES) with an ACTIVA spectrometer from Horiba JOBIN YVON.

The surface areas and pore sizes were measured by nitrogen adsorption at 77 K on a Micromeritics 2010 apparatus after heat pretreatment under vacuum for 3 h at a temperature 100 K lower than the calcination temperature.

The X-ray diffraction (XRD) measurements were carried out on a Bruker D5005

powder diffractometer scanning from 3° to 80° (2θ) at a rate of 0.02 degree.s^{-1} using a Cu Kα radiation (λ=0.15418nm) source. The applied voltage and current were 50 kV and 35 mA, respectively.

The X-ray photoelectron spectra (XPS) were measured on a KRATOS AXIS Ultra DLD spectrometer equipped with a hemispherical electron analyzer and an Al anode (Al Kα=1486.6 eV) powered at 150 W, a pass energy of 20 eV, and a hybrid lens mode. The detection area analyzed was 700 x 300 μm. Charge neutralization was required for all samples. The peaks were referenced to the C–(C, H) components of the C1s band at 284.6 eV. Shirley background subtraction and peak fitting to theoretical Gaussian-Lorentzian functions were performed using an XPS processing program (vision 2.2.6 KRATOS). The residual pressure in the spectrometer chamber was 5×10^{-9} mbar during data acquisition.

Raman spectroscopy measurements were performed using a LabRAM HR (Jobin Yvon) spectrometer. The excitation was provided by the 514.5 nm line of an Ar^{+} ion laser (Spectra physics) employing a laser power of 100 μW. The laser beam was focused through microscope objective lenses (×100) down to a 1 micrometer spot on the sample.

Scanning electron microscopy (SEM) was performed using a Philips 5800 SEM electron microscrope. The samples were deposited onto scotch carbon and metallized by sputtering. The gold film ensures a good conductivity for the observation.

Scanning electron microscopy (SEM) was performed using a Philips 5800 SEM electron microscrope. The samples were deposited onto scotch carbon and metallized by sputtering. A gold film ensures a good conductivity for the observation.

The recording of transmission electron micrographs was carried out using a JEOL 2010 equipment operating at 200 kV with a high resolution pole piece and an energy dispersive X-ray spectrometer (EDS) (Link Isis from Oxford Instruments). The samples were dispersed in ethanol using a sonicator and a drop of the suspension was dripped onto a carbon film supported on a copper grid and then ethanol was evaporated. EDS study was carried out using a probe size of 15 nm to analyze borders and centers of the particles and the small particles. Standard deviations were evaluated

for atomic ratio from at least 10 analyzes.

H_2–TPR measurements were performed using a TPD/R/O–1100 instrument (ThermoFisher). Prior to each TPR run, the fresh sample was treated in a stream of O_2/He (0.998% v/v, flowing at 20 mL min^{-1}), ramping the temperature at 10 K min^{-1} from RT to 623 K and maintaining it for 60 min, and then cooled to 313 K. The TPR measurement was carried out using H_2/Ar (4.98% v/v) as reducing gas mixture, flowing at 20 mL min^{-1}. The heating rate was 5 K min^{-1} from 313 K to 1073 K. The H_2 consumption was detected by a thermal conductivity detector (TCD). The sample size used was adjusted in order to have around 69 μmol of M_xO_y independently of the M_xO_y loading of the sample. This allowed us to maintain a K value of 100 s. The characteristic number, K, can be defined to facilitate the selection of appropriate operating parameters; a fixed K value between 60 and 140 s guarantees optimal conditions to obtain good TPR profiles [15,16]. The peak areas were calibrated with given H_2/Ar (4.98% v/v) mixture injections for TPR.

Gases evolving from the TPR reactor were analyzed by a mass spectrometer (Omnistar, Pfeiffer) with a heated capillary. The signals for m/e=34 (H_2S) and 64 (SO_2) were recorded.

The microcalorimetric studies of ammonia adsorption were performed at 423 K in a heat flow calorimeter (C80 from Setaram) linked to a conventional volumetric apparatus equipped with a Barocel capacitance manometer for pressure measurements. Ammonia used for measurements (Air Liquide, purity > 99.9%) was purified by successive freeze-pump-thaw cycles. About 100 mg of sample was pretreated in a quartz cell under evacuation overnight at a temperature 373 K lower than the calcination temperatures. The differential heats of adsorption were measured as a function of coverage by repeatedly introducing small doses of ammonia gas onto the catalyst until an equilibrium pressure of about 66 Pa was reached. The sample was then outgassed for 30 min at the same temperature, and a second adsorption was performed at 423 K until an equilibrium pressure of about 27 Pa was attained in order to calculate the irreversibly chemisorbed amount of ammonia at this pressure.

2.3 *Catalytic reaction*

The oxidation of methanol was carried out in a fixed-bed micro-reactor made of glass with an inner diameter of 6 mm. The methanol was introduced into the reaction zone by bubbling O_2/N_2 (1/5) through a glass saturator filled with methanol (99.9%) maintained at 278 K. In each test, 0.2 g of catalyst was loaded, and the gas hourly space velocity (GHSV) was 11400 mL g^{-1} h^{-1}. The feed composition was maintained as methanol:O_2:N_2 = 1:3:15 (v/v). The tail gas out of the reactor was analyzed by an on-line GC equipped with an FID detector and a TCD detector. The column used was PORAPAK N for the separation of methanol, DMM and other organic compounds. The gas lines were kept at 373 K to prevent condensation of the reactant and products. The reaction was carried out at atmospheric pressure.

3. Results and discussion

3.1 Structure properties

Table 1 shows the BET surface area, porosity data, bulk (ICP) and surface (XPS) analysis for the prepared materials. Due to the same sulfate titania precursor and calcination temperature, both bulk and surface sulfur contents of the samples were in the range of 1.5–2.8 wt%. In addition, all the catalysts displayed high surface area of 340–407 m^2 g^{-1} along with similar pore volume (1.1–1.5 cm^3 g^{-1}) and average pore sizes (11.4–14.3 nm).

The XRD patterns of sulfated titania-based catalysts are presented in Fig.1. It can be seen from the figure that typical diffraction peaks characteristic of anatase TiO_2 were observed for TiS and 25CoTiS samples whereas, samples 25CoTiS, 25FeTiS, 25MnTiS and 25CrTiS exhibited much broader diffraction patterns indicating more amorphous nature of their TiO_2 species. No diffraction peaks of M_x-containing species (where M_x=Cr, Mn, Fe, Co or Mo) were detected, indicating the very fine dispersion of M_x on the surface.

In Table 2, the results in terms of binding energies of surface species and M_x/(S+Ti) atomic ratio, as obtained from XPS quantitative analysis, are reported for all samples. In Fig.2 experimental and fitted XPS spectra of Cr2p, Mn2p, Fe2p, Co2p and Mo3d are presented.

For sample 25CrTiS, two peaks, obtained by applying a peak-fitting program,

occurred for $Cr2p_{3/2}$ spectra: one at ~576 eV and the other at ~579 eV. These two species can be assigned to Cr^{3+} (Cr_2O_3) and Cr^{6+} (CrO_3), respectively [17]. Generally, the Cr^{6+} ion is more stable in air between 1073–1273 K, whereas the Cr^{3+} ion is more stable near room temperature. One possible reason for the formation of Cr^{6+} compounds is due to the reaction of Cr_2O_3 with anatase TiO_2 during air calcination [18]. Note that during storage, Cr^{6+} to Cr^{3+} reduction could occur. This process is fully reversible [18]. The $Mn2p_{3/2}$ peak position at 641.5 eV and the $Mn2p_{1/2}$ satellite structure are characteristic of Mn_2O_3 [19]. For sample 25FeTiS, the binding energies of $Fe2p_{3/2}$ and $Fe2p_{1/2}$ appeared respectively at 710.7 and 724.1 eV, which confirmed the presence of Fe_2O_3 as chemical component [20]. The spectra of Co2p were fitted with Co^{2+} and Co^{3+} components, characterized by binding energies at about 781.7 and 780.4, respectively [21]. The presence of satellite peaks at about 6 eV from the high energy component is a further evidence for Co^{2+} species. With the uncertainty of the fitting procedure, the binding energies of $Co2p_{3/2}$ are typical of pure Co_3O_4. In case of sample 25MoTiS, special attention has to be given to the absolute peak position in each $Mo3d_{5/2}$–$Mo3d_{3/2}$ doublet. Binding energy of the doublet A at 232.4 eV for $Mo3d_{5/2}$ and 235.6 eV for $Mo3d_{3/2}$ (see Table 2) was ascribed to Mo^{6+} being in reasonable agreement with literature [22] whereas the doublet B at lower binding energies was attributed to reduced Mo ions (Mo^{5+}).

The Ti $2p_{3/2}$ binding energy clustered around a value of about 458.4 eV is again in reasonable agreement with literature for Ti^{4+} [23]. In addition, the $S2p_{1/2}$ line at the binding energy of about 168.5 eV is typical of sulfur in S^{6+} oxidation state, such as in Na_2SO_4 or $Fe_2(SO_4)_3$ [24,25].

It is worth noticing, in Table 2, that the atomic ratio of M_x/(Ti+S) (M_x= Cr, Mn, Fe, Co or Mo) for all samples is close to 0.2–0.4, indicating a similar surface concentration of metal M_x species.

The surface structure of metal oxide species was examined by Raman spectra, from 1200 to 250 cm^{-1}, as shown in Fig. 3. From the literature [26,27], Raman spectra of binary titania-based catalysts display bands between 980 and 1030 cm^{-1}, which are assigned to terminal M=O vibrations (where M= Cr or Mo) of the surface metal oxide

species. In addition, bands characteristic of bridging M–O–M bonds, 860–940 cm^{-1}, associated with polymerized surface species can also be found in the spectra of the high surface coverage chromium and molybdenum oxide supported catalysts [26,27]. However, in this work, all the observed Raman bands are below 800cm^{-1}, possibly corresponding to anatase TiO_2 [27]. For example, samples 25CrTiS, 25MnTiS and 25FeTiS exhibited Raman bands at 609, 412 and 274 cm^{-1}, while sample 25CoTiS presented Raman bands at 715 and 427 cm^{-1}. No Raman band was observed for TiS and 25MoTiS samples. The absence of M=O and M–O–M Raman vibrations (where M_x= Cr, Mn, Fe, Co or Mo) indicates that the surface species are highly amorphous, as confirmed by XRD measurement.

As example, the surface morphology of sample 25MoTiS examined by electron microscopy is presented in Fig.4. The SEM image shows cauliflower-shaped species, constituted by homogeneous quasi-spherical particles. However, the dimensions of these particles are very difficult to estimate from SEM analysis. Therefore, the morphology of sample 25MoTiS was deeply analyzed by TEM, and its composition (EDS) is also given, as shown in Fig.5. An overview of TEM image indicates that there is no separated phase of TiO_2 and MoO_3 for sample 25MoTiS which was obtained by addition of ammonia molybdate after formation of the $Ti(OH)_4$ gel. Moreover, the EDS analysis, which in consistence with XPS and ICP data, suggests that molybdenum oxide is highly dispersed on the surface of titania support.

3.2 Surface acidity

Surface acidity, in terms of number of acid sites, sites strength and strength distribution, was determined by ammonia adsorption microcalorimetry [28]. Table 3 summarizes the main results obtained. Fig.6 shows the plots of the differential heats of ammonia adsorption as a function of ammonia coverage and Fig.7 presents the ammonia adsorption isotherms for the series of sulfated binary titania-based catalysts.

The initial heats of ammonia adsorption (Table 3) on all the studied samples were found to be about 160–190 kJ mol^{-1}, suggesting their quite acidic character. In addition, the differential heats (Q_{diff}) as exhibited in Fig.6 display a similar shape with a continuous decrease as a function of the ammonia coverage, revealing the

heterogeneous strength distribution of these catalysts. For comparison sulfated vanadia-titania catalyst 25VTiS has been added on Figs.6 and 7 [14].

The effect of host oxide M_xO_y (where M_x= Cr, Mn, Fe, Co or Mo) on the acidity of binary titania-based catalysts can be seen on the isotherms (Fig.7). Note that a strange phenomenon for ammonia adsorption isotherm was observed for sample 25 CrTiS which clearly shows that equilibrium was not reached at low ammonia coverage. This phenomenon is due to a surface reaction between Cr-containing compound and ammonia. However, Fig.6, which represents the differential heats of ammonia adsorption, did not reflect so clearly this particular behavior of sample 25CrTiS, except by a much higher ammonia adsorption capacity. The acidity of the studied catalysts varied in the order of 25CrTiS > 25FeTiS > 25CoTiS ≈ 25MnTiS ≈TiS > 25VTiS > 25MoTiS. Additionally when the ammonia coverage was expressed per unit surface area, the total number of acid sites density (Table 3, column 3) of samples 25FeTiS, 25CoTiS, 25MnTiS and TiS became similar. The data in Table 3 also indicate that 50–70% of the adsorbed ammonia is strongly chemisorbed on the samples.

3.3 Redox properties

In order to investigate the effect of host oxide M_xO_y (where M_x= Cr, Mn, Fe, Co or Mo) on the redox properties of sulfated binary titania-based catalysts, the TPR technique was employed and the reduction process was monitored by mass spectrometry. Fig. 8 shows the reduction profiles of all the studied catalysts, while Fig.9 exhibited the mass spectra obtained after the TPR runs. Table 4 summarizes the most important results, in terms of maximum temperatures of the reduction peaks and of the integrated H_2 consumptions.

For sample TiS, only a very weak H_2 consumption peak around 804 K was observed, which might be due to a slight reduction of surface Ti species and the reduction of surface SO_4^{2-} species (confirmed by mass spectroscopy), which reveals the low reducibility of TiO_2. Therefore, the reducibility of the catalysts is strongly affected by the presence of surface metal oxides such as MoO_3, Co_3O_4, Fe_2O_3, Mn_2O_3 and CrO_x.

In the case of 25MoTiS system, two distinct peaks were observed and the TPR profile was a little different from the TPR profile of MoO_3 [29], due to the interaction between TiO_2 and Mo species. The major peak in the low-temperature region (T_{m1}=735 K) may be assigned to the reduction of dispersed polymolybdates (Mo^{6+} and Mo^{5+}) linked to TiO_2 [30]. The other peak in the high-temperature region (T_{m2}=1005 K) could be assigned to reduction of poorly crystalline MoO_2 generated from the reduction of MoO_3 phase [31]. Sample 25CoTiS shows a TPR peak centered at 510 K with a left-hand shoulder around 482 K, which can be assigned to the overlap of the two-step reduction of Co_3O_4 to CoO and then to Co^{0+} [32,33]. On sample 25FeTiS, a reduction peak with a maximum at 686 K (T_{m1}) was observed. According to the literature [34], this peak was attributed to the reduction of Fe_2O_3 to Fe_3O_4 (magnetite). Additionally, it is note worthing that another minor TPR peak appears at high temperature (T_{m2}=791 K) possibly due to the further transformation of magnetite to FeO [34]. Sample 25MnTiS presents two main TPR peaks at 635 and 815 K, respectively. The first peak (635 K) is assigned to the reduction of Ti^{4+} to Ti^{3+} and Mn_2O_3 to Mn_3O_4 because of the interaction between titania and manganese oxide. The second reduction peak (815 K) with a left-hand shoulder at 795 K may be assigned to the overlap of the reduction of free Mn_2O_3 to Mn_3O_4, and then Mn_3O_4 to MnO. For thermodynamic reasons further reduction of MnO does not occur under the applied experimental conditions [35]. Similar TPR profiles have been also obtained by other authors [35,36] for both unsupported and titania supported manganese oxides, even though the peak temperatures were slightly different, which can be due to different experimental conditions and different size of the manganese oxide particle. Sample 25CrTiS also displays two distinctive TPR peaks. The first reduction peak at 544 K is due to the reduction of Ti^{4+} to Ti^{3+} and Cr^{6+} to Cr^{5+} because of the titania-chromia interaction [37]. The second peak at 724 K could correspond to the reduction of Cr^{6+} and/or Cr^{5+} free of any interaction with Ti^{4+} [37].

As reported in Table 4, the H_2 consumption of the studied catalysts, indicating the total number of redox sites, increased in the order of 25MnTiS ≈ 25CoTiS ≈ 25MoTiS > 25CrTiS > 25FeTiS >> TiS.

The mass spectrometry (MS) data of Fig.9 presented for all samples except 25CrTiS only one product resulting from sulfate reduction namely SO_2. In case of sample 25CrTiS, two sulfate reduction products (SO_2 and H_2S) were detected but did not evolve in parallel in the whole temperature range [38]. The first peak due to SO_2 is in the temperature range of 644–737 K with maximum yield at ~686 K. Beyond 696 K, H_2S evolution began to be observed. The TPR–MS results indicate that the presence of the M_xO_y host oxide brings about some important changes in the sulfate reduction process, and this is particularly evident in the case of 25CrTiS sample. It should also be mentioned that no decomposition of the sulfate species was observed under inert atmosphere. Moreover, all the SO_2 and H_2S evolutions matched that of H_2 consumption.

3.4 Methanol oxidation reaction

As already known, the partial oxidation of methanol is strongly sensitive to the nature of the active sites, and can be employed to provide information about the surface acidity and redox properties simultaneously [5,10]. Methanol is converted to formaldehyde (FA) and methyl formate (MF) on redox sites, to dimethyl ether (DME) on acidic sites, and to DMM on acidic and redox bi-functional sites. Table 5 presents the whole catalytic performances of sulfated binary titania-based catalysts.

Sample TiS exhibited a high selectivity only to DME due to its acidic character and the lack of redox activity of TiO_2, in good agreement with the results from NH_3 adsorption calorimetry and TPR. It possessed a low activity for methanol conversion. Even at 463 K, the highest temperature employed in this work, the conversion of methanol was only 3% on TiS sample. Addition of host oxide M_xO_y did not improve the catalytic activity significantly except for sample 25MoTiS. All samples but 25MoTiS displayed a very low conversion level of methanol (Table 5). Sample TiS exhibited high selectivity only to DME and the addition of host oxide M_xO_y did not improve significantly the catalytic activity except for sample 25MoTiS. For example, at the same reaction temperature of 463 K, the conversion of methanol for samples 25CrTiS, 25MnTiS, 25FeTiS and 25CoTiS was 7%, 4%, 6% and 1%, respectively, while for sample 25MoTiS it was 79%. Apparently, MoO_3 is much more active than

other host oxides studied in this work for methanol oxidation reaction.

For sample 25MoTiS, the conversion of methanol was 5% at 393 K, with selectivities to DMM, FA, MF and DME of 79%, 0%, 0% and 21%, respectively. The distribution of products indicates that sample 25MoTiS possessed more acidic (medium and strong) sites than redox sites. With increasing the reaction temperature, the selectivity to DMM suddenly dropped, whereas the selectivity to MF and FA increased rapidly, those becoming the main products, and the selectivity to DME remained at the same lever. This observed trend can be explained by assuming that an increase in quantity of active redox sites, and/or the deactivation of medium acidic sites occurred when increasing the reaction temperature [39].

Moreover, sample 25CrTiS and 25MnTiS yielded mainly DMM in the whole temperature range of 393–463 K. The other possible products (FA, MF and DME) were formed in very low amount. For samples 25FeTiS and 25CoTiS, the main product of methanol oxidation was DME, which was created on strong acid sites. As reported in [14], 25VTiS exhibited much more activity and selectivity to DMM than all reported samples in this paper.

These observations are supported by the work of G. Busca [40] who reported a summary of the acid-base properties of various metal oxides. MoO_3 and V_2O_5 display medium-strong acid strength of both Brönsted and Lewis character while CoO, Fe_2O_3 and Cr_2O_3 show only Lewis acidity of medium and weak strength associated with some basicity. The higher methanol conversion of V_2O_5 and MoO_3 could be explained by the presence of Brönsted acid sites as already shown in ref.[14] for sample 25VTiS. Moreover the better catalytic performance of vanadia containing catalysts is probably due to the higher Brönsted/Lewis ratio as observed by I.E. Wachs [41] comparing alumina supported vanadia and molybdena catalysts.

Conclusion

A series of sulfated binary titania-based oxides (M_xO_y–TiO_2–SO_4^{2-}, M_x= Cr, Mn, Fe, Co or Mo) with high surface area (340–407 $m^2\ g^{-1}$) were prepared by modified co-precipitation. The XRD and Raman results suggest that all the surface M_x species were highly dispersed on the catalysts. The bulk (ICP) and surface (XPS) analysis

revealed that the sulfur content of all studied catalysts was similar, in the range of 1.5–2.8wt%. The XPS measurements showed that Ti and S species were present in their fully oxidized state for all samples, while the oxidation states of Cr were +6 and +3 and +6 and +5 for Mo. Meanwhile, Mn, Fe and Co species exhibited the presence of Mn_2O_3, Fe_2O_3 and Co_3O_4 as chemical component, respectively. The ammonia adsorption calorimetry study presented a special behavior of surface reaction between ammonia and Cr-containing compound. The results obtained from TPR–MS indicate that the addition of host oxide M_xO_y enhanced the redox properties of sample TiS and brought about some important changes in the sulfate reduction process. In addition, the total number of redox sites increased in the order of 25MnTiS ≈ 25CoTiS ≈ 25MoTiS > 25CrTiS > 25FeTiS >> TiS. Samples FeTiS and CoTiS produced mainly DME from dehydration of methanol owing to its lack of active redox sites, while samples 25CrTiS and 25MnTiS yielded mainly DMM due to their bi-functional character. The best catalytic performance was observed for sample 25MoTiS even if lower than that observed previously on 25VTiS. Therefore, the distribution of methanol oxidation products successfully investigated the relative surface acidity and redox property.

Acknowledgements

The authors are thankful to the scientific services of IRCELYON, particularly to Laurence Massin for providing XPS measurements.

Hongying Zhao gratefully acknowledges the China Scholarship Council for the financial support of her PhD grant.

Financial supports from NSFC (20673055) and MSTC (2005CB221400 and 2004DFB02900) are acknowledged.

References

[1] F. Roozeboom, P.D. Cordingley, P.J. Gellings, J. Catal. 68 (1981) 464–472.
[2] C.R. Anthony, L. Mcelwee-White, J. Mol. Catal. A: Chem. 227 (2005) 113–117.
[3] S. Damyanova, M.L. Cubeiro, J.L.G. Fierro, J. Mol. Catal. A: Chem. 142 (1999) 85–100.
[4] A. Baiker, D. Monti, J. Catal. 91 (1985) 361–365.
[5] J.M. Tatibouët, Appl. Catal. A 148 (1997) 213–252.
[6] K. Fuji, S. Nakano, E. Fujita, Synthesis 4 (1975) 276–277.
[7] J. Masamoto, T. Iwaisako, M. Chohno, M. Kawamura, J. Ohtake, K. Matsuzaki, J. Appl. Polymer Sci. 50 (1993) 1299–1305.
[8] Q. Sun, A. Auroux, J. Shen, J. Catal. 244 (2006) 1–9.
[9] P. Forzatti, E. Tronconi, A.S. Elmi, G. Busca, Appl. Catal. A 157 (1997) 387–408.
[10] M. Badlani, I.E. Wachs, Catal. Lett. 75 (2001) 137–149.
[11] H. Liu, E. Iglesia, J. Phys. Chem, B 109 (2005) 2155–163.
[12] Q. Sun, Y. Fu, J. Liu, A. Auroux, J. Shen, Appl. Catal. A 334 (2008) 26–34.
[13] H. Zhao, S. Bennici, J. Shen, A. Auroux, Appl. Catal. A 356 (2009) 121–128.
[14] H. Zhao, S. Bennici, J. Shen, A. Auroux, J. Catal. 272 (2010) 176–189.
[15] P. Malet, A. Caballero, J. Chem. Soc., Faraday Trans. I 84 (1988) 2369–2375.
[16] D.A.M. Monti, A. Baiker, J. Catal. 83 (1983) 323–335.
[17] S. Wang, K. Murata, T. Hayakawa, K. Suzuki, Appl. Catal. A 196 (2000) 1–8.
[18] E.A. Belaya, V.V. Viktorov, Inorg. Mater. 43 (2007) 1323–1325.
[19] B.R. Strohmeier, D.M. Hercules, J. Phys. Chem. 88 (1984) 4922–4929.
[20] R.C. Chikate, K.W. Jun, C.V. Rode, Polyhedron 27 (2008) 933–938.
[21] L.F. Liotta, G. Di Carlo, G. Pantaleo, A.M. Venezia, G. Deganello, Appl. Catal. B 66 (2006) 217–227.
[22] Y.V. Plyuto, I.V. Babich, I.V. Plyuto, A.D. Van Langeveld, J.A. Moulijn, Appl. Surf. Sci. 119 (1997) 11–18.
[23] J. Keränen, C. Guimon, E.I. Iiskola, A. Auroux, L. Niinistö, Catal. Today 78 (2003) 149–157.
[24] M.H. Kim, I-S. Nam, Y.G. Kim, J. Catal. 179 (1998) 350–360.
[25] J.P. Chen, R.T. Yang, J. Catal. 139 (1993) 277–288.
[26] J.P. Dunn, H.G. Stenger, I.E. Wachs, Catal. Today 53 (1999) 543–556.
[27] J.P. Dunn, H.G. Stenger, I.E. Wachs, J. Catal. 181 (1999) 233–243.
[28] A. Auroux, Top. Catal. 4 (1997) 71–89.
[29] F. Arena, N. Giordano, A. Parmaliana, J. Catal. 167 (1997) 66–76.
[30] X. Zhang, D. He, Q. Zhang, Q. Ye, B. Xu, Q. Zhu, Appl. Catal. A 249 (2003) 107–117.
[31] A. Calafat, L. Avilán, J. Aldana, Appl. Catal. A 201 (2000) 215–223.
[32] B. Jongsomjit, T. Wongsalee, P. Praserthdam, Catal. Commun. 6 (2005) 705–710.
[33] K. Takanabe, K. Nagaoka, K. Nariai, K. Aika, J. Catal. 230 (2005) 75–85.
[34] S. Minicò, S. Scirè, C. Crisafulli, R. Maggiore, S. Galvagno, Appl. Catal. B 28 (2000) 245–251.
[35] I.R. Leith, M.G. Howden, Appl. Catal. 37 (1988) 75–92.

[36] A. Wöllner, F. Lange, H. Schmelz, H. knozinger, Appl. Catal. A 94 (1993) 181–203.
[37] B. Sun, E.P. Reddy, P.G. Smirniotis, Appl. Catal. B 57 (2005) 139–149.
[38] J.B. Laizet, A.K. Soiland, J. Leglise, J.C. Duchet, Top. Catal. 10 (2000) 89–97.
[39] S. Royer, X. Sécordel, M. Brandhorst, F. Dumeignil, S. Cristol, C. Dujardin, M. Capron, E. Payen, J.L. Dubois, Chem. Commun. 7 (2008) 865–867.
[40] G. Busca, Phys. Chem. Chem. Phys. 1 (1999) 723–736.
[41] I.E. Wachs, Catal. Today 27 (1996) 437–455.

Table 1
Chemical analysis and pore characteristics of sulfated titania-based catalysts[a]

Sample	C.A(wt%)			XPS (wt.%)			Surface area ($m^2\ g^{-1}$)	Pore volume ($cm^3\ g^{-1}$)	Pore diameter (nm)
	M_x[a]	Ti	S	M_x[a]	Ti	S			
25CrTiS	13.5	38.5	2.5	15.6	31.9	2.7	403	1.5	13.7
25MnTiS	14.1	39.0	2.1	14.1	34.8	2.4	346	1.1	11.4
25FeTiS	14.6	39.4	2.1	15.2	33.5	2.8	407	1.4	12.6
25CoTiS	14.3	38.8	2.8	15.8	34.4	2.7	343	1.3	14.1
25MoTiS	14.9	39.8	1.5	14.0	31.8	1.6	341	1.3	14.3
TiS	n.d.[b]	50.4	1.8	n.d.[b]	44.4	2.5	391	1.2	11.9

[a] M_x= Cr, Mn, Fe, Co or Mo.
[b] Not determined.

Table 2
Binding energies of surface species and M_x/(Ti+S) atomic ratios for sulfated titania-based catalysts.

Sample	Binding energy (eV)			M_x/(Ti+S)
	$Ti2p_{3/2}$	$S2p_{3/2}$	Surface M_x species [a]	
25CrTiS	458.3	168.6	$Cr2p_{3/2}$: (576.6, 578.7)	0.4
25MnTiS	458.3	168.5	$Mn2p_{3/2}$: (641.5); $Mn2p_{1/2}$: (653.4)	0.3
25FeTiS	458.4	168.5	$Fe2p_{3/2}$: (710.7); $Fe2p_{1/2}$: (724.1)	0.3
25CoTiS	458.3	168.4	$Co2p_{3/2}$: (780.4, 781.7); $Co2p_{1/2}$: (786.7)	0.3
25MoTiS	458.5	168.5	$Mo3d_{5/2}$: (231.4, 232.4); $Mo3d_{3/2}$: (234.6, 235.6)	0.2
TiS	458.5	168.5	---	---

[a] M_x= Cr, Mn, Fe, Co or Mo.

Table 3
Calorimetric data for ammonia adsorption at 423 K on sulfated titania-based catalysts.

Sample	V_{total}[a] (μmol g^{-1})	V_{total}[a] (μmol m^{-2})	V_{irrev}[b] (μmol g^{-1})	V_{irrev}[b] (μmol m^{-2})	V_{irrev}[b] / V_{total}[a]	Q_{init}[c] (kJ mol^{-1})
25CrTiS	812	2.0	533	1.3	0.66	188
25MnTiS	730	2.1	336	1.0	0.48	162
25FeTiS	817	2.0	497	1.2	0.60	196
25CoTiS	732	2.1	465	1.4	0.67	168
25MoTiS	535	1.6	260	0.8	0.50	189
TiS	750	1.9	445	1.1	0.58	184
25VTiS[14]	608	2.1	374	1.3	0.61	112

Notes: [a] Amount of NH_3 adsorbed under an equilibrium pressure of 27 Pa.
[b] Amount of irreversible chemisorbed NH_3.
[c] Heat evolved from the first ammonia dose.

Table 4
Reducibility of the catalysts as revealed by the H_2–TPR–MS measurements.

Catalyst	T_{max}[a] (K)				H_2 consumption (mmol g^{-1})	T_{max}[b] (K)	
	Peak 1 (T_{m1})			Peak 2 (T_{m2})		SO_2	H_2S
25CrTiS		544		724	2.9	686	727
25MnTiS		635	795	815	3.5	790	n.d.[c]
25FeTiS		686		791	2.0	700	n.d.[c]
25CoTiS	755	783		n.d.[c]	3.5	733	n.d.[c]
25MoTiS		735		1005	3.4	665	n.d.[c]
TiS		804		n.d.[c]	0.3	750	n.d.[c]

[a] Maximum temperature of the TPR peaks.
[b] Maximum temperature of SO_4^{2-} reduction peaks from TPR–MS.
[c] Not determined.

Table 5
Catalytic activities of sulfated titania-based catalysts in the methanol oxidation reaction.

Sample	Temp. (K)	Conversion of methanol (%)	Selectivity (%)				
			DMM	FA	MF	DME	COx
25CrTiS	393	3	99	0	0	1	0
	423	3	94	0	0	6	0
	463	7	58	4	20	18	0
25MnTiS	393	0.2	100	0	0	0	0
	423	1	97	0	0	3	0
	463	4	78	15	0	7	0
25FeTiS	393	0.1	0	0	0	100	0
	423	1	29	0	0	71	0
	463	6	39	0	0	61	0
25CoTiS	393	0.03	0	0	0	100	0
	423	0.1	0	0	0	100	0
	463	1	28	0	0	72	0
25MoTiS	393	5	79	0	0	21	0
	423	16	64	10	0	26	0
	463	79	1	42	27	24	6
TiS	393	0.1	0	0	0	100	0
	423	0.5	0	0	0	100	0
	463	3	8	0	0	92	0
25VTiS[14]	393	12	98	0	1	1	0
	423	43	92	1	5	2	0
	453	81	6	40	44	9	1

DMM: dimethoxymethane; FA: formaldehyde; MF: methyl formate; DME: dimethyl ether; CO_x: CO_2 (or CO).

Figure Captions

Fig.1 X-ray powder diffraction patterns of sulfated titania-based catalysts.

Fig.2. Mo 3d, Co 2p, Fe 2p, Mn 2p and Cr 2p XPS spectra for the sulfated titania-based samples. (experimental specta: black straight line, simulated spectra: red dotted and straight line). (A and B: $Mo3d_{5/2}$–$Mo3d_{3/2}$ doublets of 25MoTiS system). (For interpretation of the references to colours in this figure caption, the reader should refer to the web version of the article)

Fig.3 Raman spectra of sulfated titania-based catalysts

Fig.4. SEM image of sample 25MoTiS at the magnification of 30,000×.

Fig.5. TEM image of sample 25MoTiS at the magnification of 800,000×.

Fig.6. Differential heats of ammonia adsorption versus the adsorbed amount on sulfated titania-based samples and sulfated vanadia-titania sample as reference. (TiS: black, 25VTiS: orange, 25MoTiS: purple, 25CoTiS: red, 25FeTiS: blue, 25MnTiS: pink, 25CrTiS: green) (For interpretation of the references to colours in this figure caption, the reader should refer to the web version of the article)

Fig.7. Volumetric isotherms of NH_3 adsorption at 423K for sulfated titania-based samples and sulfated vanadia-titania sample as reference. (TiS: black, 25VTiS: orange, 25MoTiS: purple, 25CoTiS: red, 25FeTiS: blue, 25MnTiS: pink, 25CrTiS: green) (For interpretation of the references to colours in this figure caption, the reader should refer to the web version of the article)

Fig.8. TPR profiles of sulfated titania-based catalysts as a function of temperature and time (10 K min^{-1}). (TiS: black, 25MoTiS: purple, 25CoTiS: red, 25FeTiS: blue, 25MnTiS: pink, 25CrTiS: green) (For interpretation of the references to colours in this figure caption, the reader should refer to the web version of the article)

Fig.9. Mass spectra of the gases evolved during the TPR analysis. (TiS: black, 25MoTiS: purple, 25CoTiS: red, 25FeTiS: blue, 25MnTiS: pink, 25CrTiS: green) (For interpretation of the references to colours in this figure caption, the reader should refer to the web version of the article)

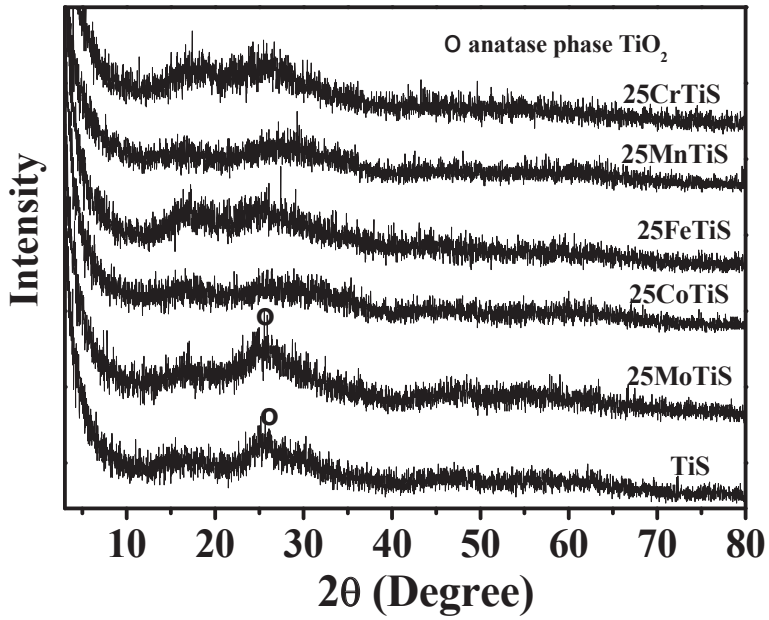

Fig.1 X-ray powder diffraction patterns of sulfated titania-based catalysts.

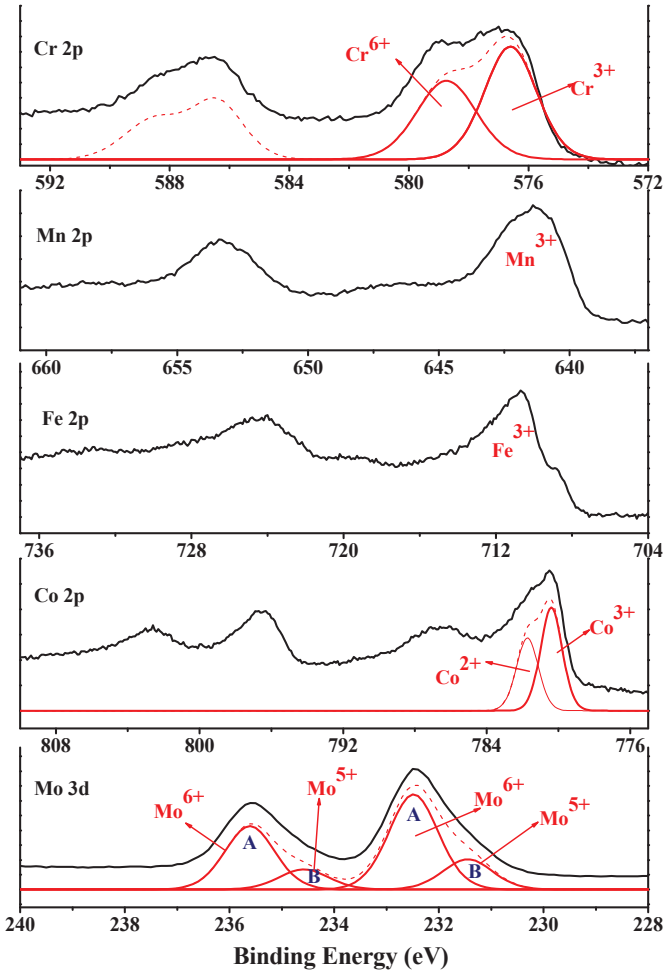

Fig.2. Mo 3d, Co 2p, Fe 2p, Mn 2p and Cr 2p XPS spectra for the sulfated titania-based samples. (experimental specta: black straight line, simulated spectra: red dotted and straight line). (A and B: $Mo3d_{5/2}$–$Mo3d_{3/2}$ doublets of 25MoTiS system). (For interpretation of the references to colours in this figure caption, the reader should refer to the web version of the article)

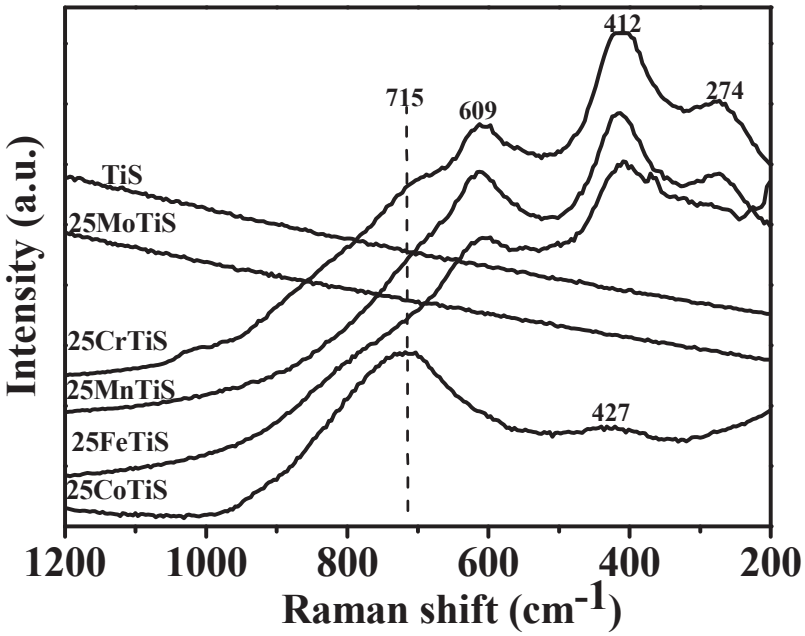

Fig.3 Raman spectra of sulfated titania-based catalysts.

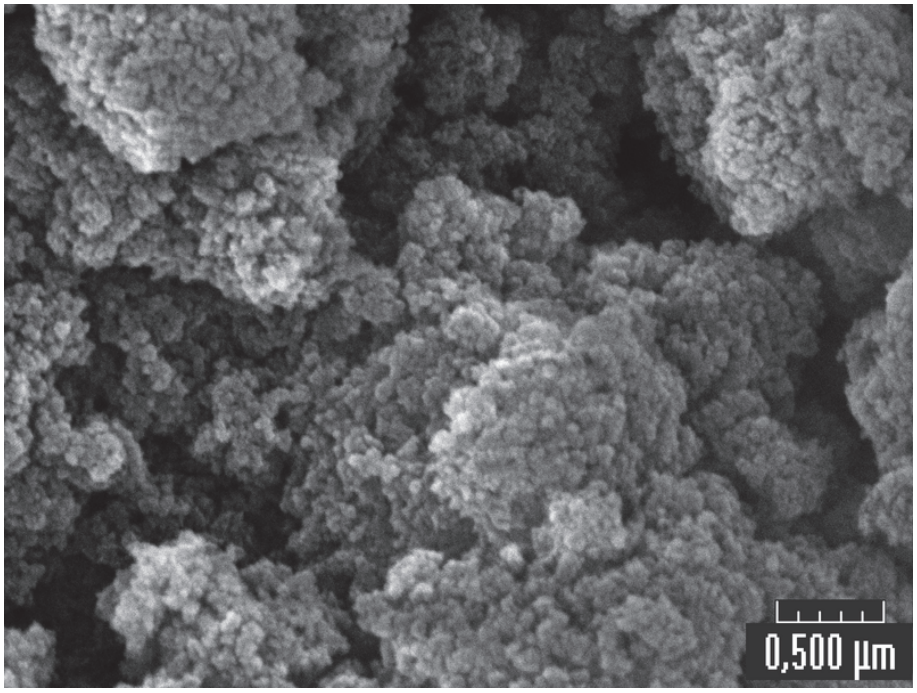

Fig.4. SEM image of sample 25MoTiS at the magnification of 30,000×.

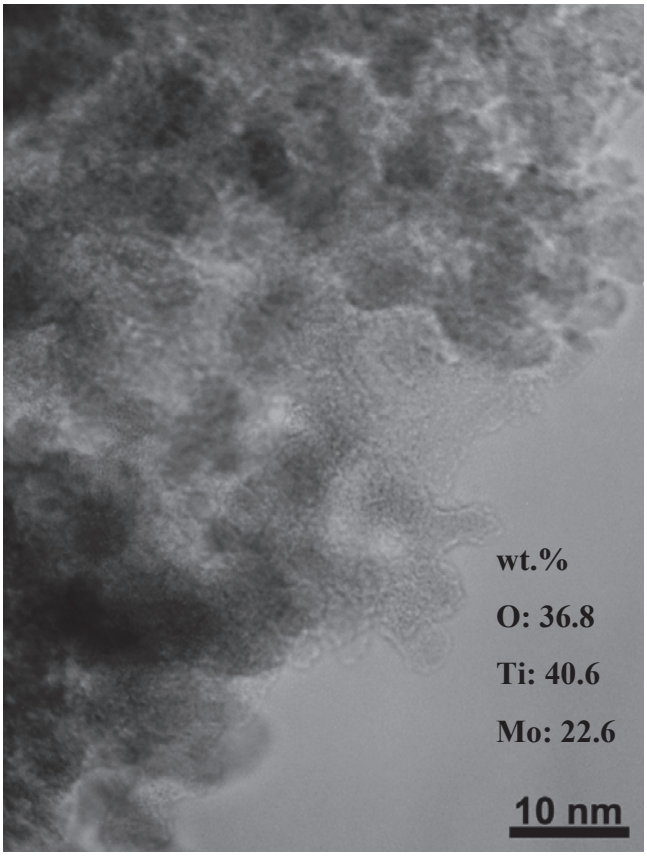

Fig.5. TEM image of sample 25MoTiS at the magnification of 800,000×.

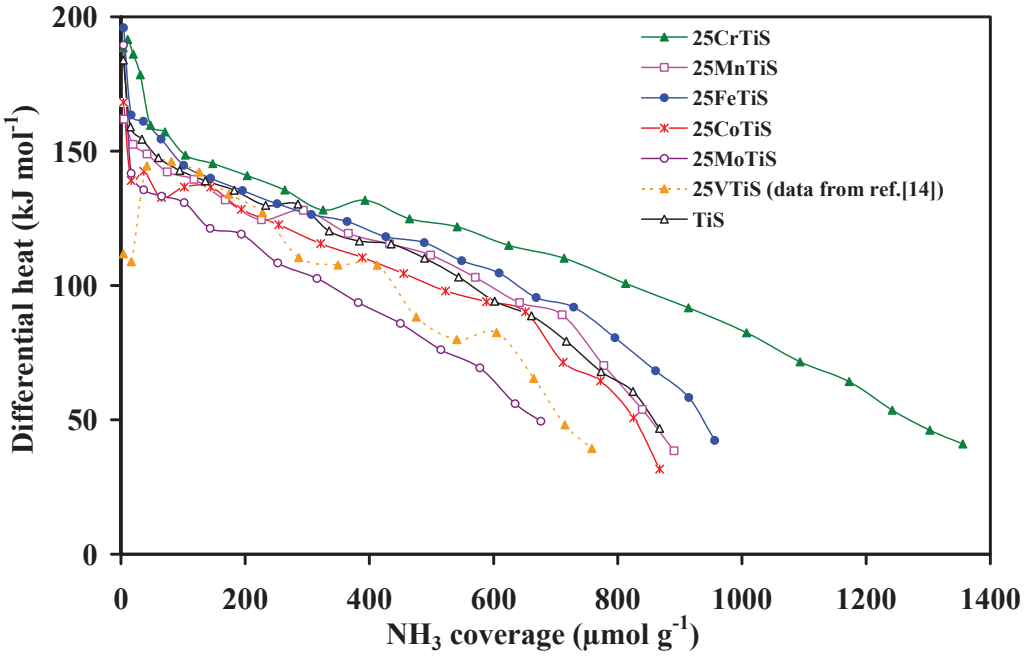

Fig.6. Differential heats of ammonia adsorption versus the adsorbed amount on sulfated titania-based samples and sulfated vanadia-titania sample as reference. (TiS: black, 25VTiS: orange, 25MoTiS: purple, 25CoTiS: red, 25FeTiS: blue, 25MnTiS: pink, 25CrTiS: green) (For interpretation of the references to colours in this figure caption, the reader should refer to the web version of the article)

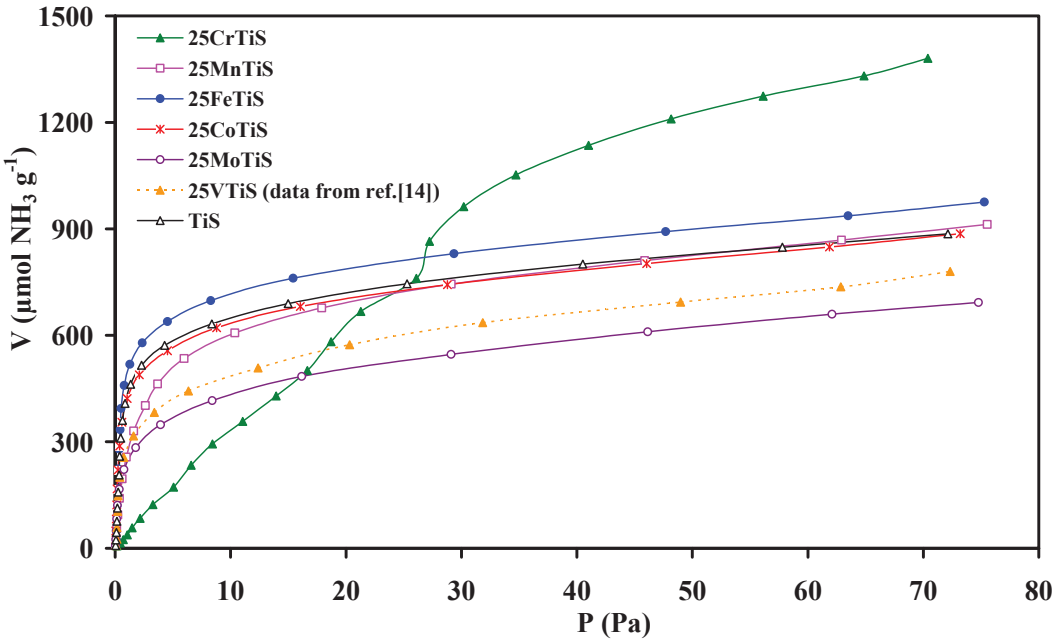

Fig.7. Volumetric isotherms of NH_3 adsorption at 423K for sulfated titania-based samples and sulfated vanadia-titania sample as reference. (TiS: black, 25VTiS: orange, 25MoTiS: purple, 25CoTiS: red, 25FeTiS: blue, 25MnTiS: pink, 25CrTiS: green) (For interpretation of the references to colours in this figure caption, the reader should refer to the web version of the article)

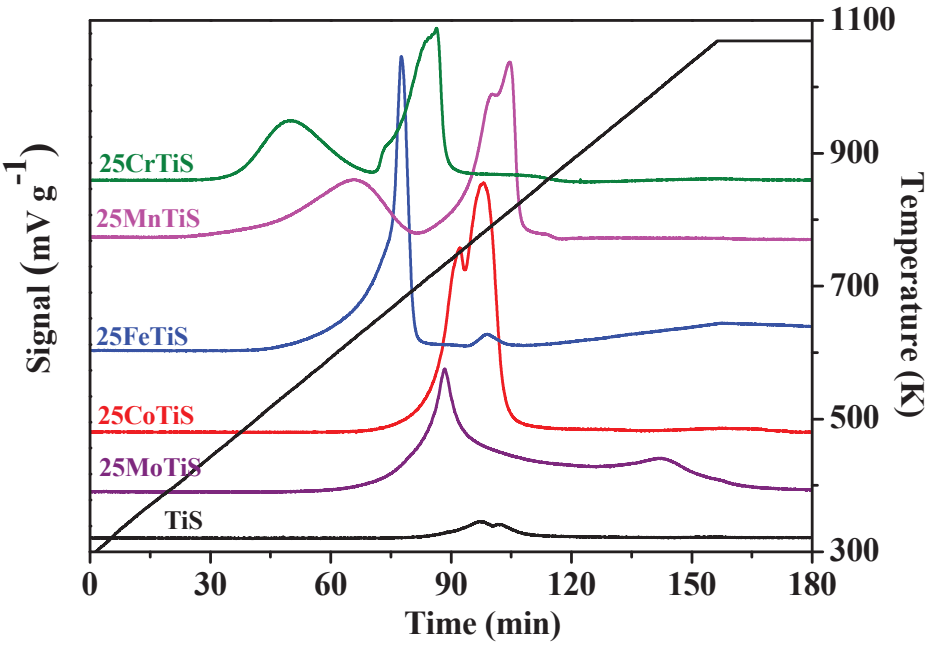

Fig.8. TPR profiles of sulfated titania-based catalysts as a function of temperature and time (10 K min^{-1}). (TiS: black, 25MoTiS: purple, 25CoTiS: red, 25FeTiS: blue, 25MnTiS: pink, 25CrTiS: green) (For interpretation of the references to colours in this figure caption, the reader should refer to the web version of the article)

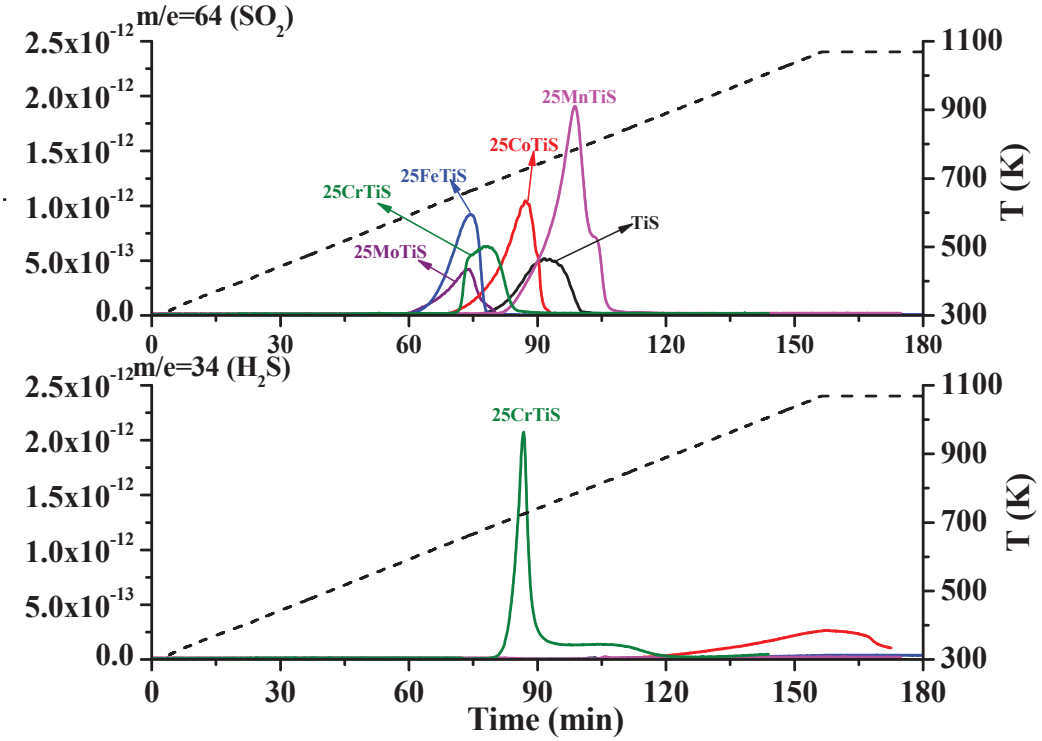

Fig.9. Mass spectra of the gases evolved during the TPR analysis. (TiS: black, 25MoTiS: purple, 25CoTiS: red, 25FeTiS: blue, 25MnTiS: pink, 25CrTiS: green) (For interpretation of the references to colours in this figure caption, the reader should refer to the web version of the article)

Conclusion

5. Conclusion

This work is related to the topic “Clean Energy”. The application of fuel cells based on hydrogen energy for electric power generation has immense potential since they offer efficiency, environmental and operational benefits better than those obtained from conventional technologies such as internal combustion engines.

DMM (dimethoxymethane) is a hydrogen containing fuel which has the advantages of high content of hydrogen, non toxicity and to be environmentally benign and easy for storage and transportation at ambient conditions (as a liquid). Therefore, it can be used as preferred material for mobile H_2 storage and transportation. DMM is industrially produced via the condensation of methanol and formaldehyde. In this work, we studied a new process of selective oxidation of methanol to produce DMM on a redox-acidic bi-functional catalyst on which methanol was first oxidized on the redox sites to produce formaldehyde, and formaldehyde was subsequently condensed with additional methanol on the acidic sites to form DMM.

In this work, bi-functional catalysts of V_2O_5–TiO_2–SO_4^{2-}; binary vanadia-based oxides (V_2O_5–TiO_2, V_2O_5–ZrO_2, V_2O_5–Al_2O_3 and V_2O_5–CeO_2) and the corresponding sulfated catalysts; and sulfated binary titania-based oxides (M_xO_y–TiO_2–SO_4^{2-}, M_x= Cr, Mn, Fe, Co or Mo) were prepared, characterized and evaluated as catalysts for the reaction of selective oxidation of methanol to DMM. Additionally, we demonstrated the possibility of new catalysts to improve the DMM production through methanol oxidation reaction. The catalysts were thoroughly characterized in terms of their acidic and redox properties in order to find correlations between the identified active sites and the catalytic properties. The structural characteristics of all investigated systems have been acquired by means of XRD, BET, chemical analysis, XPS, Raman and FTIR. The acidity was characterized by ammonia adsorption microcalorimetry, adsorption-desorption of pyridine studied by FTIR and TPD of ammonia; while reducibility and redox properties in general were achieved by TPR/TPO measurements.

5. Conclusion

The following is a summary of the general conclusions:

It has been proven by the results obtained in this work that catalytic oxidation of methanol is a structure-sensitive reaction. The distribution of catalytic products reflects the nature of the surface active sites: methanol is converted to formaldehyde (FA) and methyl formate (MF) on redox sites, to dimethyl ether (DME) on acidic sites, and to DMM on acidic and redox bi-functional sites. Therefore, the DMM production is strongly determined by the balance of acidic and redox properties.

Among the applied preparation methods (co-precipitation with and without 1wt% PEG-400, sol-gel and mechanical grinding), co-precipitation without PEG-400 was the best preparation method in terms of maximizing the surface area (250 m^2 g^{-1}) and in catalytic performances for V_2O_5–TiO_2–SO_4^{2-} catalysts. With the addition of SO_4^{2-} species, the DMM selectivity was enhanced. In this work, it has been shown that critical parameters for DMM generation are the amount of Brönsted acid sites, high reducibility of vanadia, and the presence of active polymeric VO_x species at the surface. It has been observed that the sulfur content is important: if it is too high, the catalytic activity is lowered, since the sulfate species could poison the catalytically active sites. Thus, it can be concluded that the proper concentration of sulfur is the key parameter to optimize the DMM production. The results obtained in this work revealed that it is possible to tune the SO_4^{2-} amount by choosing the right calcination temperature and proper amount of washing water (an appropriate calcination temperature of 673 K with 50 mL washing water generated the proper concentration of sulfur of about 0.8 wt%). Moreover at 673 K, the active polymeric VO_x species with terminal V=O bonds are produced, the Brönsted acidity is pronounced and a higher reducibility is detected. All these features are related with the high DMM yield.

In the sulfated mixed vanadia-based oxide systems, the combination of results obtained from TPR–MS and catalytic test indicates that the strength of (V–O)-support and sulfate-support interactions determine the catalytic activity and the DMM

selectivity, respectively. The (V–O)-support bond is the key parameter involved in the relevant rate-determining step. The strength of (V–O)-support bonds decreases in the order of TiO_2 < ZrO_2 < Al_2O_3 < CeO_2, whereas the catalytic activity presented an opposite trend. Consequently, sample V_2O_5–TiO_2–SO_4^{2-} exhibited the highest catalytic activity and DMM yield comparing to zirconia, alumina and ceria supported catalysts.

In the case of sulfated binary titania-based oxide systems, it has been shown that the addition of host oxide M_xO_y (M_x = Cr, Mn, Fe, Co or Mo) to TiO_2–SO_4^{2-} did not improve significantly the methanol conversion, except for sample MoO_3–TiO_2–SO_4^{2-}. However, methanol conversion obtained using MoO_3–TiO_2–SO_4^{2-} was lower than that previously observed on V_2O_5–TiO_2–SO_4^{2-} catalyst. The higher methanol conversion observed on the samples containing V_2O_5 and MoO_3 in comparison with other catalysts investigated in this work could be explained by the presence of medium-strong acid sites of Brönsted character. Moreover, the better catalytic performances of vanadia containing catalysts are probably due to the higher Brönsted/Lewis ratio. Samples Fe_2O_3–TiO_2–SO_4^{2-} and Co_3O_4–TiO_2–SO_4^{2-} produced mainly DME from dehydration of methanol owing to their lack of active redox sites, while samples CrO_x–TiO_2–SO_4^{2-} and Mn_2O_3–TiO_2–SO_4^{2-} yielded mainly DMM due to their bi-functional character.

It could be concluded that sulfated catalysts containing both vanadia and titania are recognized as the best systems for partial oxidation of methanol to DMM among all the studied samples in this thesis. Furthermore, the sample VTiSw50–673 exhibited the best catalytic performance with the highest DMM yield (methanol conversion:74%; S_{DMM}:83%) at the very low reaction temperature of 403 K.

Abbreviations

DMM Dimethoxymethane

DME Dimethyl ether

MF Methyl formate

FA Formaldehyde

IPA Isopropanol

PPE Propylene

DIPE diisopropyl ether

ACE Acetone

XRD X-ray diffraction

BET Brunauer, Emmett, Teller

XPS X-ray photoelectron spectroscopy

ICP-OES Inductively coupled plasma optical emission spectroscopy

FTIR Fourier transformed infrared spectroscopy

TEM Transmission electron microscopy

SEM Scanning electron microscopy

TPR/O Temperature-programmed reduction/oxidation

TPD Temperature-programmed desorption

Abstract (English, French)

TITLE

Sulfated vanadia-based and titania-based catalysts for selective oxidation of methanol to dimethoxymethane (DMM)

ABSTRACT

This work is related to the subject "Clean Energy". Dimethoxymethane (DMM) is a suitable H_2 storage material for mobile application because of its high content of hydrogen, extremely low toxicity and environmentally benign. Therefore, sulfated vanadia-titania, sulfated binary vanadia-based and titania-based catalysts were prepared and evaluated in the reaction of selective oxidation of methanol to DMM and further production of hydrogen. The surface acidic and redox properties of the studied catalysts were correlated to their catalytic performance. In addition, the reaction mechanisms and the identification of factors limiting the activity and selectivity of catalysts were also studied.

KEY WORDS

Dimethoxymethane, Methanol selective oxidation, Acidic and redox properties, Ammonia adsorption microcalorimetry, Pyridine FTIR

Abstract (English, French)

TITRE

Etude de catalyseurs à base d'oxyde de titane et d'oxyde de vanadium sulfatés pour l'oxydation sélective du méthanol en diméthoxyméthane (DMM)

RESUME

Ce travail est en relation avec la thématique "Energies Propres". Le diméthoxyméthane est un composé adapté au stockage de l'hydrogène pour des applications mobiles, de par sa forte teneur en hydrogène, sa très faible toxicité et son faible impact sur l'environnement. De ce fait, des catalyseurs mixtes, à base d'oxyde de vanadium et d'oxyde de titane sulfatés ont été préparés et testés dans la réaction d'oxydation sélective du méthanol en DMM, en vue de la production d'hydrogène. Les propriétés acides et redox de surface ont été corrélées aux performances catalytiques. Les mécanismes de réaction et l'identification des facteurs limitant l'activité et la sélectivité des catalyseurs ont été aussi étudiés.

DISCIPLINE

Chimie, Catalyse

MOTS-CLES

Diméthoxyméthane, Oxydation sélective du méthanol, Propriétés acides et redox, microcalorimétrie d'adsorption d'ammoniac, IRTF de pyridine

---

INTITULE ET ADRESSE DU LABORATOIRE

Institut de Recherches sur la Catalyse et l'Environnement de Lyon,

UMR 5256 CNRS/Université Lyon 1,

2 avenue Albert Einstein, 69626 Villeurbanne Cedex, France